Dissertation zur Erlangung des Doktorgrades
der Naturwissenschaften an der Fakultät Biologie
der Ludwig-Maximilians-Universität München

In vitro reconstitution of the primary chromatin architecture of *Saccharomyces cerevisiae*

Christian Johannes Wippo

München
Juli 2011

Dissertation eingereicht am: 19. April 2011

Mündliche Prüfung am: 26. Juli 2011

1. Gutachter: Prof. Dr. Peter Becker

2. Gutachter: Prof. Dr. Stefan Jentsch

3. Gutachter: Prof. Dr. Heinrich Leonhardt

4. Gutachter: Prof. Dr. Michael Boshart

5. Gutachter: Prof. Dr. Dirk Eick

6. Gutachter: Prof. Dr. Kirsten Jung

Ehrenwörtliche Versicherung

Ich versichere hiermit ehrenwörtlich, dass die vorgelegte Dissertation von mir selbständig und ohne unerlaubte Hilfe angefertigt wurde.

München, den ....

(Christian Wippo)

Erklärung

Hiermit erkläre ich, dass ich mich nicht anderweitig einer Doktorprüfung ohne Erfolg unterzogen habe.

München, den ....

(Christian Wippo)

Wesentliche Teile dieser Arbeit sind in folgenden Publikationen veröffentlicht:

Zhang Z*, **Wippo CJ***, Wal M, Ward E, Korber P, Pugh BF (2011). A packing mechanism for nucleosome organization reconstituted across a eukaryotic genome. Science, 2011. 332 (6032): p. 977-80.
* These authors contributed equally to the manuscript

Wippo CJ, Israel L, Watanabe S, Hochheimer A, Peterson CL, Korber P (2011). The RSC chromatin remodelling enzyme has a unique role in directing the accurate positioning of nucleosomes. EMBO Journal. 30(7): 1277-88

Wippo CJ and Korber P (2011). *In vitro* reconstitution of *in vivo*-like nucleosome positioning on yeast DNA. Methods in Molecular Biology [accepted for publication]

Wippo CJ, Krstulovic BS, Ertel F, Musladin S, Blaschke D, Stürzl S, Yuan GC, Hörz W, Korber P, Barbaric S (2009). Differential cofactor requirements for histone eviction from two nucleosomes at the yeast PHO84 promoter are determined by intrinsic nucleosome stability. Molecular and Cellular Biology. 29(11): 2960-81

Diese Arbeit ist Beate, Wolfgang und Andreas gewidmet.

I. Table of contents

II. Summary

The primary chromatin structure of eukaryotes consists of nucleosomes, which are mostly well positioned, especially at promoter regions. Here, the positioning architecture shows two major features: short (~140 bp) nucleosome depleted regions (NDRs) and regular nucleosomal arrays that emanate from these NDRs. As nucleosomes impede access to the DNA that is wrapped around the histone octamer, these evolutionarily conserved structures have major regulatory impact on all DNA-templated processes such as transcription. However, the understanding of how this primary chromatin structure is established, i.e. what determines nucleosome positioning, is still limited. So far the main limitation to study nucleosome positioning mechanisms was the lack of an *in vitro* approach that allowed to directly identify factors and to test models.

This study provides the first comprehensive approach to biochemically characterize nucleosome positioning factors and their mode of action. For one, nucleosome positioning was faithfully reconstituted *in vitro* across the entire yeast genome. As this reconstitution required a yeast whole cell extract and ATP, our results immediately highlight the major contribution of *trans* factors to nucleosome positioning and thus argue very definitively against the "genomic code for nucleosome positioning" hypothesis . Genome-wide reconstitution at subsaturating nucleosome density (half the complement) generated localized arrays with the same internucleosomal distance (spacing) as for fully assembled chromatin. This argues against the widely referenced statistical positioning model and suggests a new, remodeling enzyme-based mechanism for generating the regular nucleosomal arrays: active and directional packing against 5' NDRs. This packing mechanism might be directed from the 5' NDRs, which would amount to "5' organising centres" that orchestrate the positioning of most nucleosomes.

Beyond these global mechanistic features, we initiated the biochemical dissection of the involved factors by extract fractionation. We independently identified the RSC nucleosome remodeling complex as a key player and show for the first time that the RSC complex is specifically and directly required for establishing NDRs *in vitro*. Nonetheless, in most cases RSC is not sufficient but requires other factors to do so.

In addition, our detailed study of *PHO84* promoter chromatin in the context of *PHO84* gene regulation highlighted two interesting and fundamental aspects of both nucleosome positioning and remodeling. First, even nucleosomes that can be properly positioned by DNA intrinsic sequence cues may still require *trans* factors to protect or re-establish the right positioning in the presence of other disrupting activities. Second, the DNA-sequence mediated intrinsic stability of a nucleosome can determine the type of remodeling enzymes required for nucleosome remodeling.

Overall, our results provide major insight into the general mechanistic principles of nucleosome positioning and into the specific role of the RSC remodeling complex. Importantly, the successful genome-wide reconstitution of the primary chromatin architecture opens the gates for future whole-genome biochemical studies of chromatin assembly, nucleosome positioning and chromatin-templated processes, e.g. transcription, in the context of an *in vivo*-like chromatin architecture.

III. Zusammenfassung

Die Chromatinstruktur in Eukaryoten besteht primär aus Nukleosomen, die wiederum mehrheitlich genau positioniert sind, insbesondere in Promotorregionen. In diesen Regionen wird die Chromatinstruktur durch zwei Hauptmerkmale charakterisiert: kurze (~140 bp) nukleosomarme Regionen (NDRs) und von diesen NDRs ausgehende regelmäßig aneinander gereihte Nukleosomen-Anordnungen. Da Nukleosomen den Zugang zu der um das Histonoktamer gewundenen DNA behindern, haben diese evolutionär konservierten Strukturen großen Einfluss auf die Regulation aller Prozesse mit DNA-Matrizen wie zum Beispiel der Transkription. Jedoch verstehen wir noch kaum, wie diese grundlegende Chromatinstruktur etabliert wird, also was die Nukleosomen-Positionierung bestimmt. Entsprechende Untersuchen wurden bisher v.a. dadurch beschränkt, dass kein *in vitro* Ansatz zur Verfügung stand, der die biochemische Identifizierung der beteiligten Faktoren und das direkte Testen von Positionierungs-Modellen erlauben würde.

Diese Arbeit stellt den ersten umfassenden Ansatz zur biochemischen Charakterisierung von Nukleosomen-Positionierungs-Faktoren und ihrer Wirkungsweise bereit. Zum einen wurde die Nukleosomen-Positionierung für das ganze Hefegenom *in vitro* rekonstituiert und zwar mit *in vivo*-ähnlichen Positionen. Da diese Rekonstitution Ganzzell-Hefeextrakt und ATP benötigte, betonen unsere Ergebnisse sofort den überwiegenden Beitrag von *trans*-Faktoren für die Nukleosomen-Positionierung und argumentieren deshalb sehr deutlich gegen die "Genomischer Nukleosomen-Positionierungs-Code" Hypothese. Zum anderen zeigte eine genomweite Rekonstitution bei limitierender Nukleosomen-Dichte (halbe Besetzung) lokale Nukleosomen-Reihungen mit den selben internukleosomalen Abständen wie mit dem voll-assemblierten Chromatin. Das spricht gegen das häufig zitierte „statistische Positionierungs-Modell“ und für einen neuen Remodulierungs-Enzym-basierten Mechanismus für die Generierung der Nukleosomen-Reihungen: aktives und gerichtetes „Packen“ der Nukleosomen gegen die 5'NDRs. Dieser „Packen“ oder „Schieben“ könnte von den 5'NDRs gesteuert werden, was der Existenz von "5' Organisationszentren", welche dann die Positionierung der meisten Nukleosomen organisieren, entspräche.

Über die globalen Positionierungs-Mechanismen hinaus, haben wir die biochemische Aufreinigung der beteiligten Faktoren mithilfe einer Extrakt-Fraktionierung begonnen. Wir konnten unabhängig die zentrale Rolle des RSC Remodulierungs-Komplexes bestätigen und zum ersten mal zeigen, dass der RSC Komplex direkt und spezifisch für die Etablierung von NDRs *in vitro* notwendig ist. Nichtsdestotrotz war RSC alleine in den meisten Fällen nicht hinreichend, sonder benötigte zusätzliche Faktoren.

Des Weiteren ergab unsere detaillierte Untersuchung des *PHO84* Promoter Chromatins im Kontext der *PHO84* Genregulation zwei interessante und fundamentale Aspekte sowohl der Nukleosomen-Positionierung als auch -Remodulierung. Erstens, selbst Nukleosomen die durch DNA-intrinsische Sequenzpräferenzen korrekt positioniert werden, können trotzdem *trans*-Faktoren benötigen, um die richtige Positionierung in Gegenwart anderer störender Aktivitäten zu schützen oder wieder zu etablieren. Zweitens, DNA-Sequenz-bedingte intrinsische Stabilität eines Nukleosomes kann bestimmen, welches Remodulierungs-Enzym zur Nukleosomen-Remodulierung benötigt wird.

Insgesamt liefern unsere Ergebnisse wichtige Erkenntnisse über die generellen mechanistischen Prinzipien der Nukleosomen-Positionierung und über die spezifische Rolle des RSC Remodulierungs-Komplexes. Für die Zukunft eröffnet die erfolgreiche Genom-weite Rekonstitution der Nukleosomen-Positionierung die Möglichkeit, Genom-weite biochemische Untersuchungen der Chromatin-

Assemblierung, Nukleosomen-Positionierung und anderer Chromatin-basierender Prozesse, z.B. Transkription, im Kontext einer *in vivo*-ähnlichen Chromatin-Architektur durchzuführen.

1. Introduction

1.1. Chromatin

Despite the known complexity of biological systems it has often come as a surprise how factors originally identified to be part of one biological function later turned out to impact on different other functions as well. Whether this strong interconnectivity of different biological functions is a mere consequence of evolutionary pressure towards efficiency or whether it is a necessary consequence of functioning complexity or both remains a question to be answered. However this may be, many aspects of biology are originally studied by reductionist approaches before they can be realized in the wider context. Chromatin biology is an example for such a field that has emerged from the initial study of isolated aspects and is now an area of research that integrates these individual components on a genome-wide and cross-species level.

"Chromatin" is the term for the complex and dynamic structure found in eukaryotes that is formed and maintained by the interaction of the genomic DNA with a large range of different proteins and RNA. Most simply chromatin can be understood functionally as the mechanisms by which eukaryotes achieve both the necessary packaging of, as well as regulating the access to, their genomic DNA. The necessity for compaction is a consequence of the length of the genomic DNA vastly exceeding the diameter of the nucleus and the required high degree of compaction is achieved by several hierarchical packaging steps (Fig. 1).

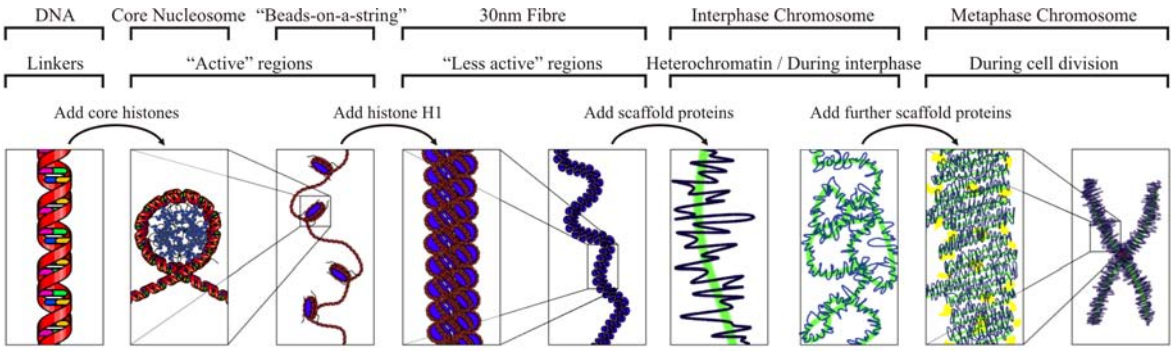

Figure 1. Packaging of a eukaryotic genome
Images represent the intermediate packaging states from naked DNA to a condensed mitotic chromosome. The names of the packing states are indicated on top and their location or functional association below. Arrows indicate transitions from lower to higher packing orders together with required factors. The figure simplifies the packaging of eukaryotic genomes and not all indicated components are present in all eukaryotes (adapted from an image by Richard Wheeler).

At the most basic level chromatin consists of DNA wound around an octamer of two copies each of the histones H2A, H2B, H3 and H4 forming the nucleosome core [1-3]. Such a nucleosome core incorporates around 147 bp of DNA [2-4]. The nucleosome cores are separated from each other by a short stretch of "free" DNA called the linker. The size of the linker varies from species to species and, in multicellular organisms, from tissue to tissue covering a known total range of 7 bp (*S. pombe* [5]) to 87 bp (*Thyone briareus* sperm [6]). For *S. cerevisiae* the average linker size is 18 bp and the sum of the core nucleosomal DNA and the linker length, referred to as the nucleosome repeat length, comes to 165 bp. Consequently, the *S. cerevisiae* genome (12.5 Mbp) is packaged in around 60,000 [7] to 70,000 [8] nucleosomes. The next packing step is generally believed to be the formation of the 30 nm fibre for the structure of which two major models were proposed [9-11]. Which of these structures is

actually adopted *in vivo*, or whether both are formed (in the same or different organisms) is still under debate [12-14]. The existence of the 30 nm fibre *in vivo* as such was recently even called into question [15]. While a reasonable understanding of the nucleosomal structure and the 30 nm fibre is available, the details of the higher packaging orders are sparse. Incorporation of the non-canonical histone H1 at a ratio of close to one H1 per nucleosome core is typically associated with higher-order chromatin condensation [16]. Notably, *S.cerevisiae* only possesses a distantly related orthologoue of H1 (Hho1) that is, like in many/most other eukaryotes, present only at substoichiometric amounts (ratios of 1 Hho1 molecule per 37 nucleosomes [17] or per 11 nucleosomes [18] were reported) and removal of Hho1 does not change the repeat length of bulk chromatin [19] contrary to the removal of H1 in mice [20]. In addition to H1, a range of other non-histone scaffold proteins play a role in higher-order packing [21]. Conceptually it is important that the degree of compaction for any given locus can be variable. While almost all DNA is packaged to the level of the mitotic chromosome (Fig. 1) during cell division, the compaction status during interphase will often correlate with the "activity" of that locus, which itself is affected by the chromosomal location, outside signals, tissue type and epigenetic memory [22, 23]. In general, the higher condensed a genomic region, the less accessible it becomes for processes such as transcription. Consequently, untranscribed / inactive regions of the genome often remain in a highly condensed state during interphase (referred to as heterochromatin), whereas the active regions adopt a more open structure (euchromatin). Heterochromatin formation plays a major role in genome regulation of higher eukaryotes where intergenic regions make up most of the genome and expression of many genes is tissue specific [24, 25]. The budding yeast *S.cerevisiae* in contrast only has a rudimentary form of heterochromatin that is mostly restricted to the telomeric regions, silent rDNA repeats, and the silent mating type locus [26].

1.2. "Epigenetic" chromatin marks

Incorporation of the DNA into nucleosomes and higher order structures not only serves to compact the DNA but is also used as means of regulating various, if not all, DNA-based processes such as transcription, replication, recombination and repair [27-31]. In some instances the information stored in chromatin beyond the primary sequence of the DNA may even be heritable. This heritable and non-heritable information is included in chromatin as posttranslational covalent modification of histones, incorporation of variants of the canonical core histones, methylation of the DNA and association/interaction of various factors with such specific modifications [28, 32-34]. Cells encode a diverse set of different classes of enzymes that catalyse the addition and the removal of these chromatin "marks" ("writers" and “erasers”). In turn, particular marks or their combinations can be recognised by proteins (the "readers") via specific binding domains. The interaction between the chromatin marks, the "writers", the "readers" and proteins specific for cellular functions make up the regulatory network that help to regulate and orchestrate the aforementioned processes [29, 33].

1.2.1. Posttranslational histone modifications

All core histones are subject to posttranslational modifications with histones H3 and H4 being the major targets [32]. Most of these modifications localize to the N-terminal "tails" of the histones that protrude from the nucleosome core. Nine different classes of modifications have been identified to date [32] of which lysine acetylation, lysine methylation and serine phosphorylation are the most well studied. Establishment of these covalent mark requires enzymes (acetyltransferases,

methyltransferases and kinases, respectively) that catalyze the modification of specific sites. These covalent modifications impact on the function of their associated DNA by two different mechanisms. For one, they can alter the interactions between neighbouring nucleosomes or of the histones with the DNA itself, such that the accessibility of the nucleosomal DNA, or the formation of higher order structures are altered. For example, acetylation of lysine 16 on histone H4 (H4K16ac) negatively affects formation of the 30 nm fibre *in vitro* [35]. Second, histone modifications are specifically bound by other non-histone proteins via specialized domains. Methylation is recognised by chromo-like (chromo, tudor and MBT) as well as by PHD domains. Recognition of acetylation and phosphorylation requires a bromodomain or a domain within 14-3-3 proteins, respectively. Acetylation is generally associated with active transcription, whereas methylation can be both an activating or a repressive mark. For example, H3K4me in budding yeast localizes to the 5' end of active genes whereas H3K36me tends to accumulate towards the 3' end of active genes and associates with the elongating form of RNA pol II [36, 37]. In contrast, H3K9me is a repressive mark involved in heterochromatin of higher eukaryotes. In line with the scarcity of heterochromatin in *S.cerevisiae*, H3K9me is absent in this yeast.

1.2.2. Histone variants

Most (especially higher) eukaryotes express variants of the canonical H3, H2A and H2B histones. These are incorporated during or outside S-phase [38] and represent yet another level of regulation as they can alter the structure and stability of the nucleosome as well as provide an altered binding platform for non-histone proteins [33, 39]. The *S.cerevisiae* genome encodes only two histone variants, the H3 variant Cse4 (homolog of the human CENP-A) and the H2A variant Htz1 (homolog of H2A.Z). Cse4/CENP-A localises to the centromeres and is important for proper centromere function [40, 41]. Htz1/H2A.Z is enriched at both active and inactive promoters in yeast [42, 43] and plays a role in gene activation [44] and repression [45], spreading of silent heterochromatin [45, 46] and chromosome stability [47]. H2A.Z containing nucleosomes were reported as intrinsically less stable [48-50] (though there is also evidence to the contrary [39, 51, 52]) and to have higher intrinsic mobility [53, 54]. These intrinsic properties likely play a role in the yet little understood mechanism by which H2A.Z affects a broad range of processes [39].

1.2.3. ATP-dependent nucleosome remodeling enzymes

Nucleosome remodeling enzymes are a family of proteins that non-covalently alter the composition, conformation and position of nucleosomes. Amongst their most prominent activities are histone removal in *cis* ("sliding") or *trans* ("disassembly"), histone variant exchange and chromatin assembly (Fig. 2). They derive energy for these processes from the hydrolysis of ATP catalysed by a Snf2-type family ATPase [55-57]. Such Snf2-type ATPases were identified in a wide range of organisms and grouped according to sequence similarity [58] (Fig. 3). The *S.cerevisiae* genome encodes 17 such ATPases but not all of these have been shown to be remodelers as such. For example, Mot1 plays a role in eviction of TBP thereby repressing transcription [59]. Nevertheless, many of the identified Snf2-type ATPases indeed use nucleosomes as substrate and catalyse one or more steps highlighted in Figure 2. Such non-covalent alterations play a major role in diverse processes such as transcriptional regulation (e.g. SWI/SNF [60, 61], RSC [62], Ino80 [63, 64]), DNA repair (e.g. Rad16 [65]), replication (e.g. Ino80 [61, 64, 66]), recombination (e.g. Rad54 [67], Ino80[68]) and incorporation (Swr1 [69]) or removal (Ino80 [70]) of the histone variant Htz1.

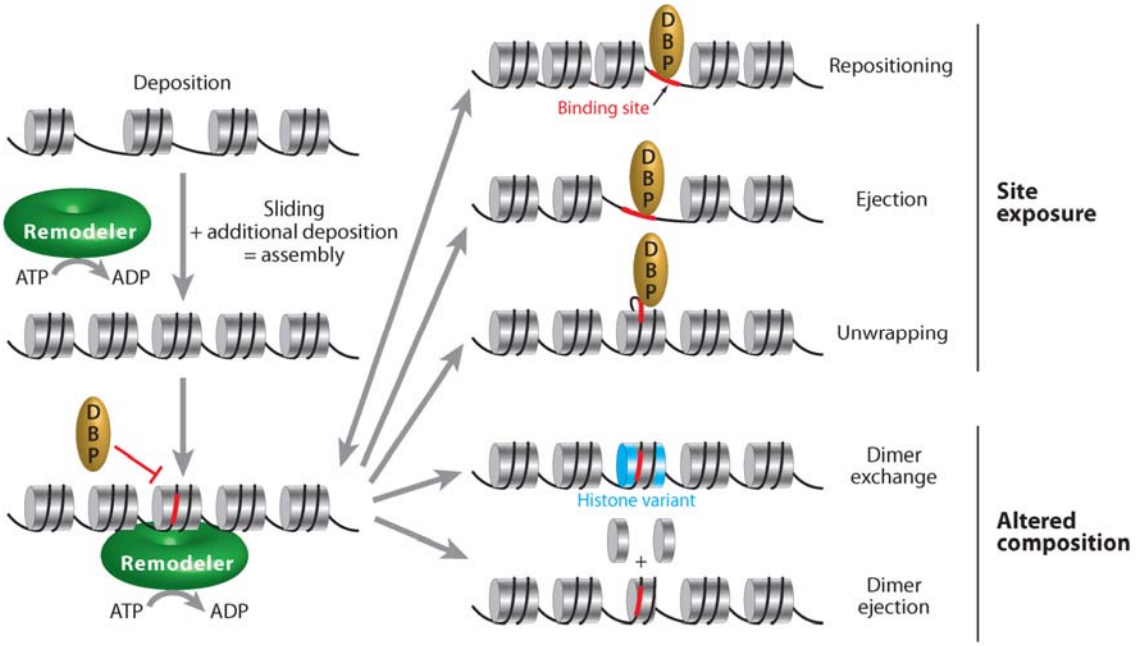

Figure 2 Functions of ATP-dependent nucleosome remodelling complexes.
Graphical representation of various chromatin alterations catalysed by ATP-dependent nucleosome remodeling enzymes (adapted from Clapier and Cairns [56]).

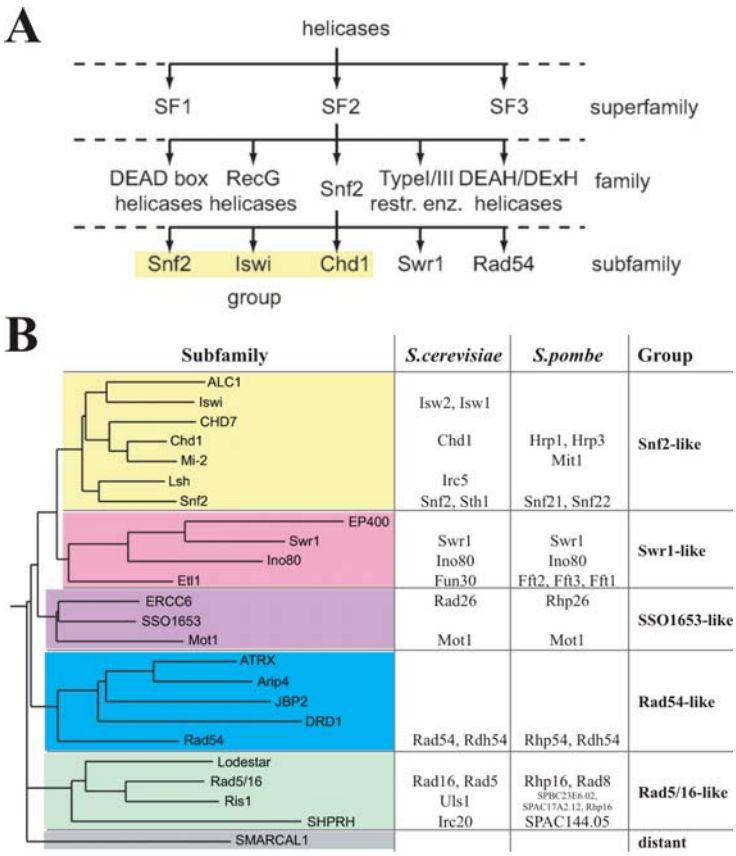

Figure 3. Family of Snf2-type nucleosome remodeler ATPases
(A) Hierarchical tree diagram of the Snf2 protein family and its closest relatives. **(B)** Rooted tree of all 24 Snf2 family subfamilies sorted into 6 groups (background colour and column on the right). Names of Snf2-type proteins identified in *S.cerevisiae* and *S.pombe* are listed. Where more than one member of a subfamily was identified the names are given in the order of sequence similarity (adapted from Flaus *et al.* [58]).

1.3. Nucleosome Positioning & Occupancy

1.3.1. Definitions

Every individual nucleosome of any given cell at any given moment in time locates to a specific stretch of DNA. However, these locations can vary with time and across the cell population leading to different nucleosomal configurations occurring at different frequencies across time or cell population (Fig. 4A) [71]. As it is experimentally very difficult to determine every individual nucleosomal configuration across a cell population, two different metrics were coined: "nucleosome occupancy" and "nucleosome positioning". Nucleosome occupancy is the probability of a certain base pair to be within a nucleosome (Fig. 4A). Occupancy thus describes the average accessibility of DNA with the limitation that differences in accessibility between sites located at the centre versus the edge of the nucleosome are not taken into consideration [72, 73]. In contrast, nucleosome positioning is the probability of a nucleosome to start at a given base pair divided by the sum of all probabilities of a nucleosome starting within a 147bp window around that given base pair (Fig. 4A). Figure 4B illustrates the independence of nucleosome occupancy and nucleosome positioning, i.e. that any region can have high occupancy and low positioning or vice versa at the same time.

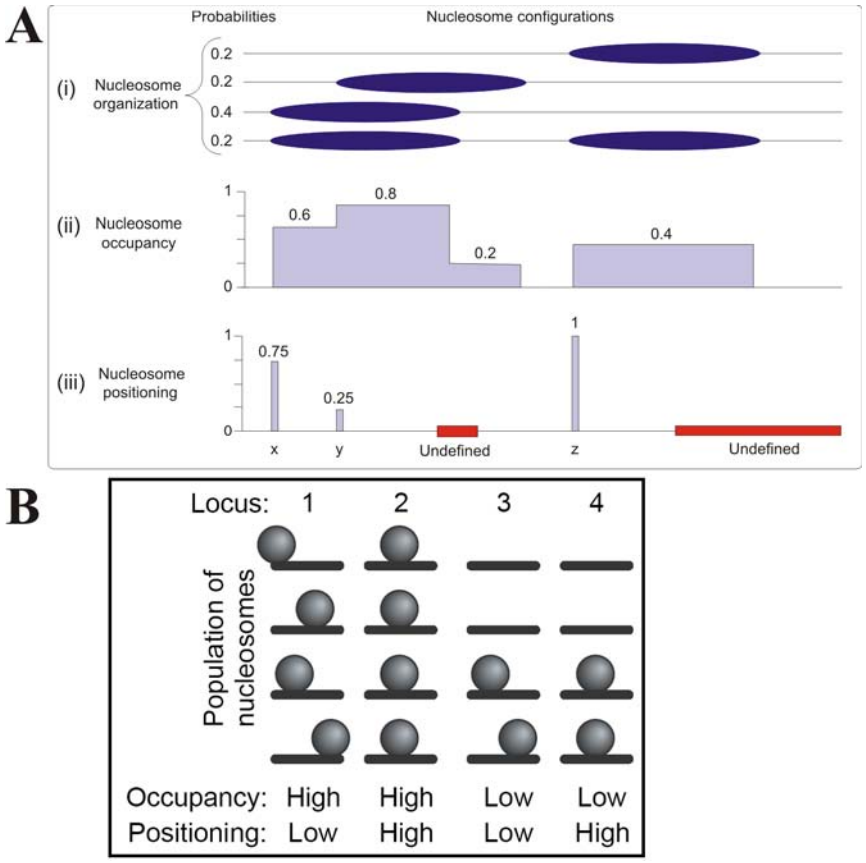

Figure 4. Nucleosome occupancy and nucleosome positioning are two different metrics to described nucleosome organization.

(A)(i) Example region with four different nucleosome configurations ("Probabilities" indicates the occurrence of each configuration). Flat ellipsoids represent nucleosomes. (ii) Nucleosome occupancy is equal to the probability of a certain base pair being located within a nucleosome (iii) nucleosome positioning is defined as the probability of a nucleosome starting at a given base pair divided by the sum of all probabilities of a nucleosome starting within a 147bp window (the red bars demark regions for which nucleosome positioning is not defined). Adapted from Kaplan *et al.* [71]. **(B)** Independence between nucleosome occupancy and nucleosome positioning. Spheres represent nucleosomes. The left and right nucleosomes in (A) corresponds roughly to loci 1 and 4, respectively. adapted from Zhang *et al.* [74].

Another important term is "spacing", which refers to the average distance between the midpoint of neighbouring nucleosomes across a region of interest (or the entire genome). The term "regular spacing" describes that several nucleosomes in a region are separated by equally/similarly sized linkers. In nucleosome occupancy maps such regular spacing manifests as a series of equally spaced peaks (for examples see [75, 76]).

1.3.2. Introduction

Originally, nucleosomes were seen as a mere packing principle or at best as a factor that generally and unspecifically reduces DNA access. Initial evidence also suggested that nucleosomes were distributed randomly along the DNA [77, 78]. The first evidence that nucleosomes can occupy specific positions came from the study of SV40 virus [79-81] and African green monkey (*Cercopithecus aethiops*) α satellite DNA [82-84]. Positioned nucleosomes were subsequently also observed at other loci such as the *Xenopus laevis* 5S rDNA promoter [85], *S. cerevisiae* TRP1ARS1 plasmid [86], chicken tRNA genes [87] or the *S.cerevisiae PHO5* locus [88, 89]. It was realized early on that nucleosome positions at certain loci correlated with certain aspects of transcriptional regulation indicating that the positioning of nucleosomes had functional consequences [90-92]. For example, the N-2 nucleosome at the *PHO5* promoter occludes a high-affinity binding site for the transactivator Pho4. Removal of this nucleosome is a pre-requisite to Pho4-binding and full induction of *PHO5* [90].

While the study of individual loci provided the proof of principle that nucleosome can be positioned, it was not until the pioneering study by Yuan *et al.* that the full genome-scale prevalence of nucleosome positioning became clear [93]. Yuan *et al.* managed to map nucleosome positions across the entire *S.cerevisiae* chromosome III at 20bp resolution and showed that a majority of nucleosomes, especially at promoter regions, are well positioned. Their experimental approach was to digested chromatin to mononucleosomes with micrococcal nuclease (MNase; an enzyme that preferentially cleaves linker DNA) and hybridised the mononucleosomal DNA to a tiling microarray. This first approach was since widely used to map nucleosomes across entire genomes of a range of species. Further advance came through replacing the hybridization step with high throughput sequencing which, in principle, allows for nucleosome maps with single base-pair resolution. By these approaches, genomic nucleosome maps were obtained for species ranging from unicellular yeasts [5, 7, 8, 43, 75, 76, 93-98] to *C.elegans* [99, 100] and other metazoans (*Drosophila* and humans) [101-103], all showing a high degree of non-random nucleosome positioning and occupancy.

These mapping studies identified a conserved stereotypical promoter architecture (Fig. 5A). A region upstream of the transcriptional start site (TSS) is strongly depleted of nucleosomes and referred to as nucleosome depleted region (NDR) or in some cases, maybe somewhat erroneously, nucleosome free region (NFR). The term NDR will be used from here on as most of these regions actually display low but non-zero nucleosome occupancy levels [7]. It was even suggested that, at least in metazoans, NDRs are actually covered by H2A.Z/H3.3 containing nucleosomes, which are intrinsically unstable [48] and were not scored previously as they were lost during mononucleosome preparation [49]. The width of such NDRs varies from promoter to promoter and even more from species to species but typically ranges from 100 to 180 bp (140 bp average in *S.cerevisiae* [75]). This NDR is flanked by two strongly positioned nucleosomes. According to the nomenclature proposed by Jiang and Pugh [7], the nucleosomes upstream of the NDR are numbered consecutively -1, -2, -3, ... and downstream +1, +2, +3, ... (Fig. 5A). Importantly, the +1 position is strongly linked to the TSS position. In a wide range

of unicellular yeasts the TSS typically resides 10-15bp inside the upstream border of the +1 nucleosome [5, 75, 93, 95, 97]. In contrast, the TSS in metazoans is located inside the NDR approximately 60 bp upstream of the +1 nucleosome border [101, 102]. In *S. cerevisiae* functional transcription factor (TF) binding sites typically localise to the accessible NDR region [8, 93, 95, 104]. This stereotypical arrangement was termed "open" as the crucial promoter region is readily accessible to transcription factors and the transcription machinery (Fig. 5A). Genes whose promoters fall into this class often belong to the housekeeping genes, their transcription level often shows little variation and is mostly independent of chromatin cofactors (such as histone acetyl transferases (HATs) or remodeling enzymes) [104, 105] (Fig. 5C).

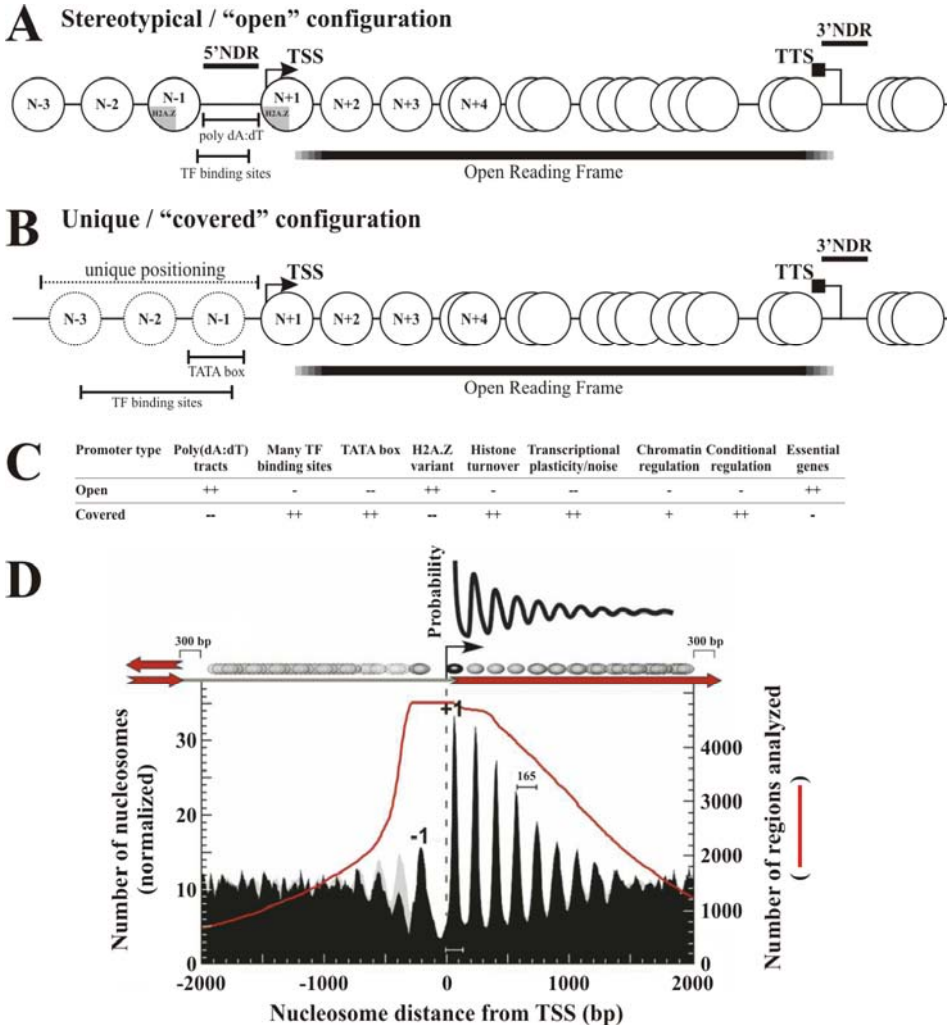

Promoter type	Poly(dA:dT) tracts	Many TF binding sites	TATA box	H2A.Z variant	Histone turnover	Transcriptional plasticity/noise	Chromatin regulation	Conditional regulation	Essential genes
Open	++	-	--	++	-	--	-	-	++
Covered	--	++	++	--	++	++	+	++	-

Figure 5. Typical chromatin configurations of *S. cerevisiae* genes.

(A) Simplified and averaged overview of the configuration of a stereotypical or "open" *S. cerevisiae* promoter. Circles represent nucleosomes and are numbered relative to the 5' nucleosome depleted region (5'NDR) upstream of the transcriptional start site (TSS). Overlapping circles indicate less well positioned nucleosomes. Enrichment of poly dA:dT stretches and transcription factor (TF) binding sites in the 5' NDR and of histone variant H2A.Z in nucleosomes N-1 and N+1 is indicated. The transcriptional termination site (TTS), the 3'NDR and the open reading frame (ORF, horizontal bar) are indicated. The range of distances between ORF borders and TSS and TTS, respectively, is indicated as shading of the horizontal bar **(B)**. Same as in **(A)** for a non-stereotypical or "covered" *S. cerevisiae* promoter. Unique positioning is highlighted by the stippled nucleosomes upstream of the TSS, which are just an example. The typical locations of the TATA box and TF sites are indicated. **(A+B)** Not all components of the figure are drawn to scale (adapted from Radman-Livaja and Rando [106] and Cairns [105]). **(C)** Correlations of various features with the "open" and "closed" promoter classes. "++"/"--" denotes strongly positive / negative correlation and "+" / "-" denote a moderately positive / negative correlation. Adapted from Cairns [105]. **(D)** Composite nucleosome profile of all *S. cerevisiae* genes aligned at their TSS. Regions closer than 300 bp from an adjacent TSS or TTS were excluded from the analysis (see red trace for number of loci included in the analysis). The trace labelled "probability" at the top of the figure gives the distribution of nucleosomes as predicted by the "statistical positioning" model [107]. Taken from Mavrich *et al.* [75].

In contrast, promoters with a non-stereotypical chromatin architecture show increased nucleosome occupancy upstream of the TSS, i.e. they lack a stereotypical NDR in terms of location and/or extent, and are referred to as "covered" (Fig. 5B). Furthermore, TF binding sites at such promoters are generally distributed more widely across the entire promoter region and often located inside nucleosomes. As the unique/covered architecture of such promoters is key in their transcriptional regulation, stress-induced and other condition-specifically expressed genes often feature this arrangement, for example the yeast *PHO5* promoter [89]. High nucleosome occupancy in the vicinity of the TSS and placement of TF sites within nucleosomes necessitates the involvement of chromatin co-factors in order to provide access for TFs and the transcription machinery. Consequently, "covered" promoters display a wider range of expression levels, are more dependent on co-factors for their expression, show higher rates of histone turnover and frequently harbour a TATA box [104, 105] (Fig. 5C). In yeasts, the majority of genes fall into the "open" class whereas, for example in humans, which have a large number of tissue specific and developmentally regulated genes, most promoters do not confine to the stereotypical arrangement [102]. Finally, the classification into "open" and "covered" is somewhat arbitrary as many promoters display features of both classes [104, 105].

Another major conserved feature of primary chromatin architecture are regular nucleosomal arrays that emanate from the 5'NDR either bidirectionally (*S. cerevisiae* [7, 75, 93]) or almost exclusively in the downstream direction (*S. pombe* [5]). Such arrays over the ORF were also seen in metazoans, but were limited to expressed genes (humans [102]) or genes with H2A.Z containing +1 nucleosome (*Drosophila* [101]). The regularity of the array decreases with distance from the NDR as seen in composite plots of all genes aligned at their TSS (Fig. 5D, 20B or [7] and references therein).

While more nucleosome maps become available and the importance of nucleosome positioning in regulating DNA based processes becomes increasingly clear the fundamental question of what determines nucleosome positioning remains open. Several factors were identified that contribute to positioning but the extent of their contribution and how they function mechanistically remains to be understood.

1.3.3. What determines nucleosome positions?

Nucleosome positioning is determined by *cis* and *trans* factors. The *cis*-factor refers to the variable affinity of different DNA sequences for the histone octamer. For example, poly dA:dT stretches strongly disfavour nucleosome formation. Such *cis*-factors are commonly referred to as "intrinsic" or "DNA-encoded". These terms can be misleading as in principle all positioning information is DNA encoded. Also *trans*-factors, i.e. any factor that acts on top of histones and DNA, are recruited via specific DNA sequence elements and/or alter the chromatin template according to their own "preferences", which in turn are defined by their amino acid composition and thus also encoded in the DNA. So the principle difference between positioning factors in *cis* or in *trans* is if only histones or something else is required in addition to the DNA template. Most prominent *trans*-factors are sequence specific binding proteins and nucleosome remodeling enzymes (see below).

1.3.3.1. DNA sequence in combination with histones only (*cis* factors)

Most of the "intrinsic" influence of the DNA sequence on nucleosome positioning stems from the differential energetic costs of wrapping DNA around the histone octamer. The histone octamer has a

diameter of about 65 Å around which ~147 bp of DNA have to be accommodated in ~1.7 turns [2, 108]. The tight wrapping around the small histone octamer consequently requires sharp "bending" of the DNA around the octamer surface, which involves major conformational deformations of the DNA helix. The energetic costs of these conformational changes are more than outweighed by the favourable electrostatic interactions between the negatively charged DNA backbone and the positive charged amino acid residues on the octamer surface. As a result, basically any DNA sequence can be packaged into a nucleosome and nucleosomes are stable structures under physiological conditions.

Nevertheless, the energetic costs of DNA deformation varies greatly for different sequences [109-111], though the differences between naturally occurring sequences are usually low. Such differences have been recognised as potential determinants of nucleosome positioning such that nucleosomes occupy favourable sequences and sequences with high deformation costs reside in linker regions. Several studies screened for DNA sequences with high histone octamer affinity by competitive salt assembly *in vitro* [109-113]. Analysis of these high affinity sequences as well as nucleosomal sequences isolated from living cells identified AA/AT/TA/TT dinucleotides to occur with a periodicity of ~10 bp together with GG/GC/CG/CC dinucleotides ~5bp out of phase [8, 75, 93, 113-116]. These dinucleotide periodicities were realised as helping with the sharp bends required every ~10 bp for wrapping of the nucleosomal DNA [114, 117, 118]. However, the amplitude of these periodicities is greater for *in vitro* selected sequences than for those isolated from *in vivo*, indicating that these dinucleotide periodicities might have less of a role in positioning nucleosomes *in vivo* [115, 119, 120]. Segal *et al.* prominently published the first *in silico* model to predict nucleosome positioning based only on these dinucleotide periodicities in combination with steric interactions of neighbouring nucleosomes ("A genomic code for nucleosome positioning" [113]). Based on their supposed ability to predict ~50% of nucleosome positions from the DNA sequence alone, they argued that much of the information needed to position nucleosomes is encoded in the DNA as intrinsic sequence preferences. However, the high prediction success (~50%) was only achieved by allowing for an error in nucleosome positions of up to 35 bp [113]. At this error margin, random predictions already "correctly" predict 35% of all nucleosome positions. While the success rate of 50% was a considerable and significant improvement to random guessing, it by no means supports the notion that "approximately half of all nucleosome positions are encoded in the DNA sequence" [113]. Cumulating evidence suggests that the major intrinsic contribution of the DNA sequence is not to encode sequences with particularly high affinity for nucleosome formation ("nucleosome positioning sequences") but rather to encode sequences with low affinity ("nucleosome excluding sequences").

Homopolymeric dA:dT stretches strongly disfavour nucleosome formation *in vitro* [118, 120-125] and such sequences are enriched in *S.cerevisiae* promoter NDRs [93, 126-128]. Moreover a poly dA:dT stretch is directly required for NDR formation at the *HIS3* promoter [127, 129]. Why such dA:dT stretches disfavour nucleosome formation has not yet been fully resolved but possibly involves cooperative interactions between adjacent bases and their unusual hydration structure ([122] and references therein). While poly dA:dT stretches are by far the most commonly employed sequence feature to exclude nucleosomes in *S. cerevisiae*, other sequences such as poly dG:dC or Z-DNA forming sequences similarly disfavour nucleosome formation [127, 130, 131]. More advanced *in silico* nucleosome prediction models incorporated both favourable and unfavourable sequence features into their algorithms. While this improved the prediction success, overall the models still came short on accurately predicting most nucleosome positions [128, 132]. In fact, several authors have stated implicitly that their results show that extrinsic factors contribute too much to nucleosome positioning as to enable the prediction of such positions from sequence alone [115, 128, 132].

Moreover, all aforementioned computational models were trained on *in vivo* positioning information. Such positions already are the net result of DNA *cis* and *trans* influences and hence the models did not make predictions exclusively based on DNA intrinsic sequence clues. One recent model was trained on *in vitro* data only and supposedly performed very well [120]. However this model was only used to predict nucleosome occupancy and suffers from the methodological caveats described below [133].

In order to establish the true extent to which intrinsic DNA sequence features direct positioning, two groups recently reconstituted the entire yeast genome by salt assembly using just sheared genomic yeast DNA and purified chicken or fly histones [119, 120]. Both studies succeeded in setting up the 5' and 3' NDRs to some degree but generally failed to reconstitute the +1 or -1 nucleosome or the regular arrays that emanate from the 5' NDRs. Zhang *et al.* interpret this data as clear evidence that intrinsic sequence preferences are unable to direct proper nucleosome positioning on a genomic scale [119]. Kaplan *et al.*, in contrast, analysed their data mainly with respect to nucleosome occupancy. They correlate the observed nucleosome occupancy per base pair (in this case the number of sequencing reads covering that base pair) *in vivo* with *in vitro* and arrived at a very high correlation coefficient of 0.74. They conclude that intrinsic DNA features dictate much of the "nucleosome organization" observed *in vivo* [120, 134].

At first these results suggest that nucleosome positioning is not defined by intrinsic DNA sequence preferences whereas general occupancy levels are. However, even the strong occupancy correlations between *in vivo* and *in vitro* observed by Kaplan *et al.* were recently questioned on technical and methodological grounds [133, 135, 136]. In short, their statistical analyses was argued to be subject to the “influential point effect” that can lead to an overestimation of correlation degrees [133, 135]. Furthermore, the correlation of Kaplan *et al.* was indicated to be sensitive to sequencing artefacts as they did not normalize their data against a genomic DNA control [133]. In line with this suspicion, the correlation of their *in vitro* occupancy levels with *in vivo* occupancy levels derived from microarray hybridization instead of high throughput sequencing was much weaker [120, 133]. Astonishingly, mock occupancy maps generated by digestion of naked genomic DNA to mononucleosomal sized fragments by MNase had correlation coefficients as great as 0.35 [137]. Moreover, an *in silico* model trained on mononucleosomal sized sequences generated by MNase digestion or even sonication of naked DNA accurately predicts nucleosome occupancy with correlation coefficients of 0.64 and 0.61 [136]. As these surprising correlations likely are driven by the coincidental enrichment of preferred MNase cleavage sites as well as "sonication fault lines" in linker DNA, they further support the notion that a significant contribution in all such correlations might be due to MNase sequence specificity and/or inadequate statistical analyses.

Nevertheless, there is no doubt that DNA intrinsic sequence preferences alone can contribute to the formation of nucleosome depleted regions. However, this depletion relative to coding regions was not as great *in vitro* as *in vivo* arguing also for an extrinsic contribution to NDR formation [119, 120]. Moreover, it remains unclear to what extent such depleted regions are stable in the context of the cellular protein environment, especially nucleosome remodeling complexes. Indeed certain proteins (nucleosome remodeling complexes and sequence specific DNA binders - see following chapters) are required to set up or maintain NDRs as in their absence nucleosome occupancy over NDRs was increased [138-140].

Since the limits of the DNA sequence contribution to nucleosome positioning becomes clearer the focus shifts to the parallel search for *trans* factors or processes that contribute to nucleosome positioning.

1.3.3.2. Proteins - *trans* factors

1.3.3.2.1. Nucleosome remodeling enzymes

Nucleosome remodeling enzymes are prime candidates for extrinsic positioning factors as they possess the ability to slide nucleosomes in *trans* along the DNA helix [55-57], which, coupled to their ATPase activity, enables them to also move nucleosomes over intrinsically unfavourable sequences [141-143]. Several *in vitro* studies using various purified remodeling enzymes showed that such remodeling enzymes indeed move nucleosomes away from positions specified by salt assembly [141, 144-146]. In some cases, the new nucleosome positions differed for different remodeling enzymes [144, 145, 147]. Apparently, remodeling enzymes can carry their own "positioning information" and thus position nucleosomes according to their own preferences [144]. To what extent such "remodeler-intrinsic" positioning information is relevant *in vivo* is unclear as only few (e.g. [148]) of the previous *in vitro* studies compared remodeler specified positioning to the *in vivo* positions.

The *S. cerevisiae* RSC complex is beginning to emerge as a major regulator of promoter chromatin architecture. RSC's role in nucleosome positioning was originally shown *in vivo* for the *CHA1* promoter where RSC positions a nucleosome upstream of the *CHA1* TSS under repressive conditions [149]. Subsequently, another *in vivo* study demonstrated that RSC is required for proper positioning at a large number of Pol II loci and affects nucleosome occupancy at Poll III promoters [140]. Recent studies elaborated that RSC has a particular role in removing nucleosomes from promoter NDRs *in vivo* as nucleosome occupancy over NDRs increased upon conditional inactivation of either the Sth1 [139] or Rsc3 [138] subunit of the RSC complex. On chromosome III, RSC was required for proper NDR formation at more than half of the pol II promoters [139]. Interestingly, the Rsc3 and Rsc30 subunits contain a sequence specific DNA binding domain [138] and the corresponding DNA motif localises to promoter NDRs that show increased nucleosome occupancy upon loss of the Rsc3 subunit [138]. To what extent this motif is necessary or even sufficient to direct NDR formation by RSC had yet to be determined.

Furthermore, both *S. cerevisiae* members of the ISWI-subfamily (Isw2 and Isw1) appear to influence nucleosome positioning, especially in genic regions. Isw2 represses transcription of the *POT1* gene by sliding of a nucleosome over an intrinsically unfavourable sequence element at the *POT1* promoter [142]. Genome-wide analysis of nucleosome positions in an *isw2* mutant identified that Isw2 shifts entire arrays of nucleosomes by 10-70 bp (typically ~15 bp) from coding regions into intergenic (promoter) regions [95]. This repositioning appears to suppress erroneous transcription by moving nucleosomes over cryptic transcriptional start sites [95]. In addition, Isw2 is also involved in setting up repressive chromatin structures at several other loci (e.g. *SUC2*) often in combination with the Tup1-Ssn6 suppressor complex [150]. Isw1, in contrast, seems to alter nucleosome positions rather in the middle of open reading frames [151]. Similar to Isw2, Isw1 appears to counteract intrinsic sequence preferences as nucleosome positions in the *isw1* mutant corresponded more closely to those seen upon nucleosome assembly *in vitro*. Again, the repositioning activity of Isw1 was linked to suppression of erroneous transcription [151].

Members of the ISWI-subfamily, such as *Drosophila* ACF, are characterized as “spacing activities”, i.e. they establish regular nucleosomal arrays with uniform linker lengths *in vitro* [152-155]. Mutations in ISWI-subfamily members lead to a loss of proper higher-order chromatin structure [156-158] suggesting that the establishment of such regular arrays might be a prerequisite for higher order compaction [14, 57, 159]. Importantly, remodeling complexes could be involved in setting up the regular arrays that emanate from promoter NDRs [5, 95, 151]. However, in *S. cerevisiae* loss of either ISWI-subfamily member did not lead to a general loss of regular spacing [95, 151]. While there could be some redundancy between Isw2 and Isw1 with respect to their spacing function, recent evidence highlighted that also members of other subfamilies might be able to set up regular arrays *in vivo*. The Ino80 complex has similar properties to Isw2 and Isw1 *in vitro*, which could enable it to act as a spacing factor [160]. The *S. pombe* Mit1 ATPases is a member of the Mi-2 subfamily and a subunit of the SHREC complex, which is required for proper positioning at the silent *mat3M* locus [161] and *mit1* mutants displayed a less regular nucleosomal array pattern downstream of promoter NDRs than the wildtype, indicating that the SHREC complex (or another complex containing Mit1) could be involved in the formation of nucleosomal arrays over gene bodies [5].

The combined evidence strongly indicates that nucleosome remodeling complexes play a role in nucleosome positioning by setting up specific nucleosome architectures upstream, downstream and within open reading frames, possibly linked to maintaining proper and regular spacing. However, the majority of studies deduce remodeler involvement from analysing nucleosome positioning in the respective mutants. On the one hand this approach cannot exclude indirect effects and on the other hand it is not clear to which extent these remodelers act as mere "sliding machines" that do not specify nucleosome positions by themselves but help to establish nucleosomes positions specified by some other factor, e.g. sequence specific DNA binding proteins.

1.3.3.2.2. Sequence specific DNA binding proteins

Sequence specific DNA binding proteins can contribute to nucleosome positioning by excluding nucleosomes from their binding site [120, 138, 139]. With the exception of a few transcription factors that can bind particularly well to their site when incorporated into a nucleosome [162-165], most binding factors render the bound DNA incompatible with wrapping around the histone octamer [166]. Conversely, wrapping of the DNA around the histone octamer distorts and/or occludes the binding motifs for sequence specific DNA binders (apart from the aforementioned exceptions).

Which factor comes out "victorious" depends on both on the kinetics and thermodynamic of the competition between histones and the DNA binding protein. For one, the binding factor needs to be able to access its binding site (kinetics). Access can be provided during replication/transcription before nucleosome re-assembly, nucleosome remodeling enzymes or spontaneous short "breathing"/unwrapping nucleosomal DNA [72, 73]. Equally, the histone octamer needs certain means by which it can "reach" the binding site since the histone octamer can neither slide along the DNA nor assemble itself into a nucleosome under physiological conditions. For the histone octamer, re-assembly after replication/transcription, histone turnover or nucleosome remodeling enzymes, are the means by which the kinetic barrier can be overcome. Given that both the factor and the histone octamer can access the binding site, the relative affinities for the particular stretch of DNA as well as the concentrations of both components (thermodynamics) determines whether the DNA binding factor or the histone octamer will primarily occupy the factor binding site. In addition,

cooperative interactions (for example between two adjacent DNA binding factor (e.g. Pho4 and Pho2 [167])) further influence the binding competition.

Both occupied and unoccupied, but conserved binding motifs tend to be nucleosome depleted [8, 43, 120]. The cause-consequence relationship between binding site location and nucleosome positions is not always clear. It seems that on one hand there are many factors with specific functions and relatively few binding sites, which may or may not influence positioning in few instances. For example, binding sites for the transactivator Pho4 are often in linker regions, but stay nucleosome free even in the absence of Pho4 [168, 169]. On the other hand there are few factors with many binding sites are probably dedicated to regulate nucleosome positioning on a global scale. These are called "general regulatory factors" (GRFs) and, in accordance with their genome-wide role in nucleosome positioning, play a role in the regulation of a wide range of processes [97, 119, 138, 139]. For example, Abf1 was original identified as "ARS-Binding factor 1" and accordingly plays a role in replication [170, 171]. However, later studies also revealed its role in DNA repair and transcriptional activation and repression of a large number of genes [172, 173]. Binding sites for Abf1 and Reb1, another GRF, are most strongly nucleosome depleted and often localise to NDRs [8, 120]. Ablation of these proteins leads to an increase in occupancy over their binding sites confirming that these proteins are indeed involved in setting up NDRs at their binding sites [138, 139]. Comparative analysis of nucleosome positioning in twelve different *Ascomycetes* yeasts revealed that the extent to which a given DNA binding factor acts as a nucleosome positioning regulator shows evolutionary plasticity. For example, Cbf1 sites in *S. cerevisiae* (and its closest relatives) were not nucleosome depleted whereas such sites in the more distantly related yeasts such as *K. lactis* and *D. hansenii* were strongly nucleosome depleted. The opposite was true for most cases of Reb1 binding sites [97].

1.3.3.3. Replication and Transcription

Disassembly of nucleosomes is a prerequisite for passage of the replication fork [30, 174]. Thus replication principally should disrupt positioned nucleosomes. However, histone chaperones that associate with the replication machine re-assemble the nucleosomes after replication [30, 174]. Consequently, such factors involved in re-assembly could affect the location of the newly assembled nucleosomes. However, up to date no involvement of replication in positioning nucleosomes has been observed and properly positioned nucleosomes can be reconstituted *in vitro* in the absence of replication [129, 169, 175, 176]. Nevertheless, it cannot be excluded that, for example, nucleosome disassembly preceding replication creates windows of opportunity for certain factors to access the DNA and subsequently affect where nucleosomes are reassembled. Furthermore, as replication is likely to remove any input of positioning information by *trans* factors, re-establishment of proper positioning could be aided by the association of certain general positioning factors with the replication bubble. Indeed several factors known to be involved in nucleosome positioning, such as Abf1 and various nucleosome remodeling complexes, are associated with replication [171, 177, 178].

Transcription is the other major process that leads to wide-spread disruption of the primary chromatin structure. Similar to replication, chaperones disassemble nucleosomes ahead of and re-assemble them after passage of the polymerase [29, 179]. Contrary to replication, there is some evidence that the process of transcription itself or some of its components might play a role in positioning. The nucleosome arrangement at a majority of yeast loci strongly correlates with the position of the transcriptional start site [7, 8, 43]. Nucleosomal arrays in *S. cerevisiae* emanate in both directions from the 5'NDR but are more prominent in the direction of the associated ORF [7],

whereas in *S. pombe* such arrays are even mostly limited to the direction of transcription [5] and in humans such arrays are only seen at actively transcribed genes [102]. While this mere correlation does not resolve the casual relationship it remains an interesting hypothesis that these arrays are set up by the passing polymerase or some other associated factor. The role of transcription in yeast was recently tested by several groups via depleting the largest RNA polymerase II subunit (Rpo21/Rpb1) *in vivo*. The Rando group noticed a decreased NDR width upon pol II depletion in addition to a small but concerted downstream shift of the nucleosomal array over the ORFs [98]. This was interpreted as a retrograde nucleosome shift due to polymerase passage, i.e. the nucleosomes are normally re-assembled further upstream of their original location such that the passage of the polymerase constitutes a sort of “conveyor belt” towards the 5’ NFR and leads to a more densely packed array. Contrary to this, two other studies reported no major changes in nucleosome positioning or occupancy after pol II depletion [137, 139]. It has to be noted that their analyses were either restricted to promoter nucleosome occupancy [137] or the employed microarray was of too low resolution to detect subtle changes in the nucleosomal arrays [139]. Noteworthy, inactive yeast genes show similarly stereotypical arrays over the ORF ([75]), which is difficult to explain by transcription unless the arrays have high intrinsic stability and can be conserved once set up by very low frequency transcription. As alternative to the process of transcription itself, the transcription factors as such, e.g. RNA polymerase II, the pre-initiation complex or other general transcription factors (all of which are enriched at many yeast loci to some extent [180, 181]), might contribute to nucleosome positioning similarly to sequence specific binding proteins (see above 1.3.3.2.2). Again, the cause-consequence relationship underlying the observation that factors of the transcription machinery are enriched in NDRs remains to be tested.

1.3.3.4. Positioning Mechanisms and Models

The main features of the primary chromatin architecture of *S. cerevisiae* (and other species) are the 5' NDRs, the adjacent well-positioned +1 and -1 nucleosomes and the regular arrays that emanate in the downstream (and to some extent upstream) direction from the NDR/+1 nucleosome. Several of the major contributors to nucleosome positioning, such as anti-nucleosomal sequences, nucleosome remodelers and GRFs, are known. But what are the mechanisms by which these factors set up the *in vivo* nucleosome architecture?

It is conceptually easy to envision how nucleosome are removed or kept away from NDRs. Either the local DNA sequence resists packaging of the DNA into a nucleosome and/or some extrinsic factors remove and/or compete with histones at that site. In line with this, there is good evidence for all three mechanisms [122, 138, 139]. The mechanism(s) by which the adjacent nucleosomes are placed and the regular arrays are generated remains a mystery though. One of the most widely discussed models was put forward by Kornberg and Stryer as early as 1988 [107]. Their model requires a fixed barrier (e.g. a bound TF or an NDR), free mobility/placement of nucleosomes on the DNA (by whatever mechanism), and treats nucleosomes as hard, non-interacting spheres. In such a system, nucleosomes will align at the barrier in regular intervals by a purely stochastic processes creating very well positioned nucleosomes next to the barrier. The degree of regularity decreases with distance from the barrier as small deviations add up over distance. This model recapitulates the same pattern as seen *in vivo* suggesting that "statistical positioning" might generate these arrays *in vivo*. Recently, the statistical positioning model was more thoroughly derived from the physics Tonks model for a one-dimensional gas and again shown to generate the same regular nucleosomal arrays seen *in vivo* [182]. Moreover, this analysis suggested different properties of the barrier for the up-

and downstream nucleosomal arrays. The shape of the upstream arrays was more consistent with a “soft” barrier, i.e. a nucleosome excluding element. The downstream arrays appeared to emanate from a “hard” barrier, i.e. a positioned +1 nucleosome against which the +2, +3 etc. nucleosomes aligned by statistical positioning.

It is important to note that for statistical positioning the nucleosome spacing within the arrays is a direct consequence of nucleosome density on the DNA. *In vivo*, this would be a consequence of the level of histone expression / incorporation. The spacing variability in different species or cell types would be the result of different histone densities and not of regulated spacing processes.

The statistical positioning model assumes, but does not explain, that nucleosomes can be freely mobile along the DNA under physiological conditions and thus assumes that all sequences can be equally well incorporated into nucleosomes, which is at odds with the well described variable affinity of different sequences (see references in chapter 1.3.3.1.). ATP-dependent nucleosome remodeling and transcription elongation are two processes that could circumvent both problems as both remodeling and transcription has the potential to overrule DNA intrinsic affinity differences as well as to allow for (free) nucleosome movement under physiological conditions. The ability of spacing activities to generate regular arrays *in vitro* [152-154] speaks for the former and the changed downstream array pattern upon inactivation of RNA pol II *in vivo* [98] speaks for the latter. Further, a transcription based mechanism could explain why regular nucleosomal arrays tend to be most pronounced downstream, i.e. in the direction of transcription. As these two processes are difficult to separate in a living cell, *in vitro* experiments might be required to identify what components play a role in array formation.

1.4. Aims of this study

Understanding the nucleosome positioning mechanisms is of considerable interest due to its major regulatory impact on all DNA-based processes. So far only limited information on the positioning mechanisms is available, especially regarding cause-consequence relationships, and the extent to which all the involved components have been identified is unclear. Our lab has previously established an *in vitro* system that reconstitutes *in vivo*-like positioning at the *PHO5* and *PHO8* promoters [175, 176]. Importantly, reconstitution of proper positioning was dependent on the presence of both a yeast whole cell extract (WCE) and ATP. Our system is unique in its ability to reconstitute proper nucleosome positioning beyond DNA-intrinsic positions. Moreover, the *PHO5* and *PHO8* promoter serve as ideal models as they each represent the two different promoter architectures: "open" (*PHO8*) and "covered" (*PHO5*) (see 1.3.3, Fig. 4) [89, 105, 183]. The "open" promoter architecture of *PHO8* promoter harbours an NDR of about 120 bp just upstream of its TSS which is flanked by two positioned nucleosomes (Fig. 6A) [7, 183]. The divergently transcribed *KRE2* gene (about 900 bp upstream of *PHO8*) has a promoter with similarly stereotypical architecture. The "*KRE2-PHO8*" promoter region is from here on referred to as the "*PHO8* promoter". The *PHO5* promoter in contrast is “covered” as it displays high nucleosome occupancy upstream of the TSS and lacks a stereotypical NDR (Fig. 6B,[89]). As mechanistic aspects of nucleosome positioning can principally best be tackled by *in vitro* approaches I used our previously established reconstitution system in connection with the exemplary *PHO8* and *PHO5* promoters to advance our understanding of how nucleosomes are positioned.

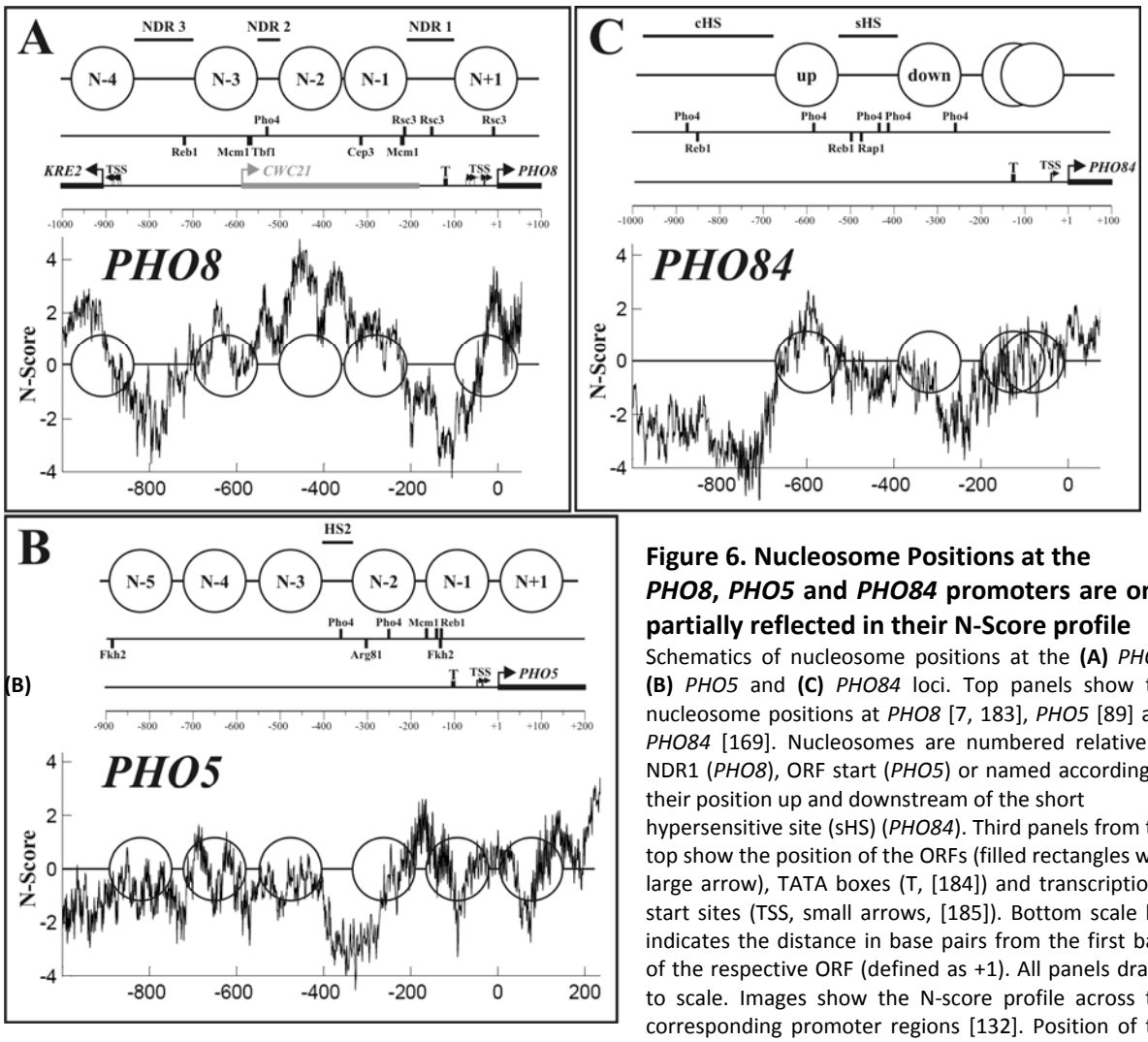

Figure 6. Nucleosome Positions at the *PHO8*, *PHO5* and *PHO84* promoters are only partially reflected in their N-Score profile

Schematics of nucleosome positions at the **(A)** *PHO8*, **(B)** *PHO5* and **(C)** *PHO84* loci. Top panels show the nucleosome positions at *PHO8* [7, 183], *PHO5* [89] and *PHO84* [169]. Nucleosomes are numbered relative to NDR1 (*PHO8*), ORF start (*PHO5*) or named according to their position up and downstream of the short hypersensitive site (sHS) (*PHO84*). Third panels from the top show the position of the ORFs (filled rectangles with large arrow), TATA boxes (T, [184]) and transcriptional start sites (TSS, small arrows, [185]). Bottom scale bar indicates the distance in base pairs from the first base of the respective ORF (defined as +1). All panels drawn to scale. Images show the N-score profile across the corresponding promoter regions [132]. Position of the nucleosomes drawn in for comparison. Second panel indicates the mapped **(A)** Pho4 [183], Rsc3 [186]; **(B)** Pho4 [187], Fkh2 and Arg81 [188], Mcm1 [189]; **(C)** Pho4 [169, 190], and predicted binding sites **(A)** all others, [138]; **(B)** Reb1 [138]; **(C)** Reb1 and Rap1 [138].

1.4.1. Identification of the *PHO5* and *PHO8* positioning factors

The major aim of my study was to identify the (*trans*) factors involved in determining nucleosome positioning at the *PHO5* and *PHO8* promoters. For this, I initially tested a number of candidate factors that were previously implicated in nucleosome positioning and/or play a role in chromatin based processes at the *PHO5* and *PHO8* loci. In addition, a different approach was needed to identify so far unknown positioning determinants for the *PHO5*/*PHO8* promoters. Here we employed our *in vitro* system. Assembly of the *PHO5* and *PHO8* promoter by salt dialysis alone does not yield *in vivo*-like positioning, but further incubation with WCE and ATP does generate the proper pattern [175, 176]. Therefore the WCE must contain an ATP-dependent positioning activity that carries the positioning information for the nucleosomes at the *PHO5* and *PHO8* promoter. Fractionation of this whole cell extract and testing the subsequent fractions in our reconstitution assay provided us with an unbiased approach to identify the components that contribute to the "nucleosome positioning activity".

Initially, we improved the reconstitution system and tested it at more loci beyond the *PHO* promoters. The extent to which the *in vitro* system could reconstitute proper positioning at other loci came as a surprise and allowed us in the end to carry out pioneering experiments on genome-wide positioning mechanisms.

2. Results

2.1. Refining the *in vitro* reconstitution system

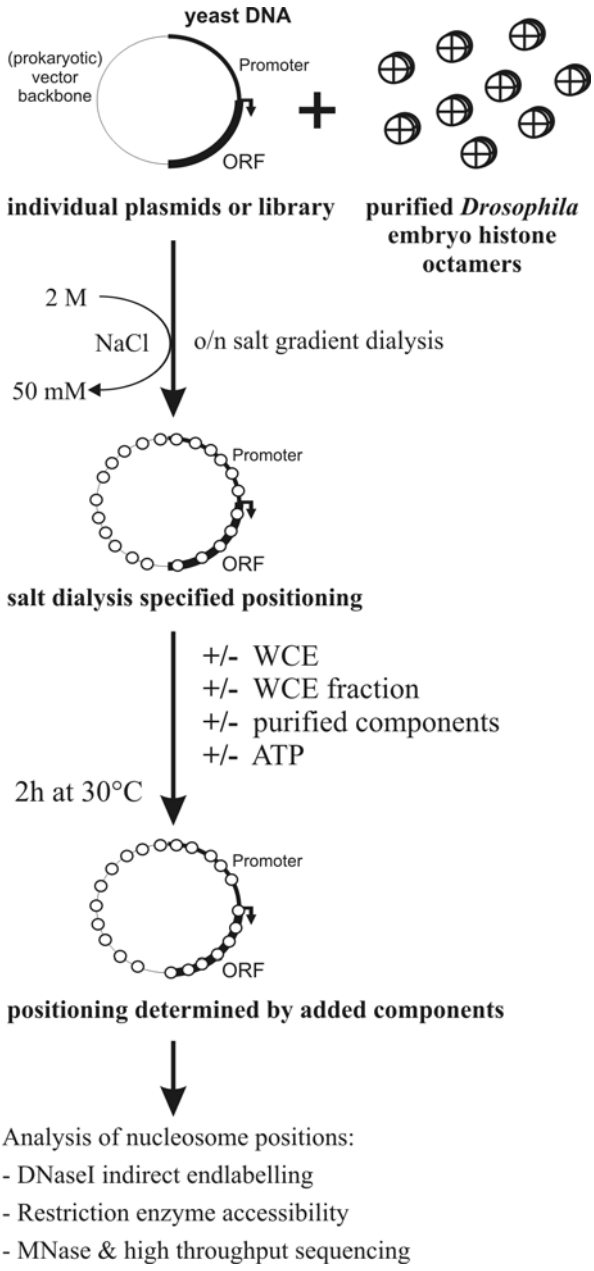

Figure 7. The *in vitro* reconstitution system
Schematic overview. Individual plasmids or a plasmid based genomic library are assembled into chromatin with purified *Drosophila* embryo histone octamers by salt gradient dialysis. This yields positions that are specified by the intrinsic DNA preferences under these conditions. Next, the preassembled plasmids are incubated with WCE, WCE sub-fractions and/or purified components in the presence or absence of ATP for 2 hours at 30°C. In the presence of ATP, components may alter nucleosome positions according to their own preferences. Nucleosome positions can be analyzed by DNaseI indirect endlabelling, by restriction enzyme accessibilities or by MNase digestion followed by high-throughput sequencing.

Central to this study was the *in vitro* reconstitution assay that was previously shown to establish *in vivo*-like nucleosome positioning at the *PHO5* and *PHO8* loci [175, 176] (Fig. 7). First, supercoiled plasmid DNA is assembled into chromatin by salt gradient dialysis using purified *Drosophila* embryo histone octamers. This does not generate *in vivo*-like positioning at the *PHO5* and *PHO8* loci [175, 176] and, on linear DNA fragments, also not genome-wide [119, 120]. Second, in the actual positioning assay, the improperly positioned nucleosomes are moved to their *in vivo* positions by incubation with an *S. cerevisiae* WCE. In the absence of ATP, nucleosome positions remain unchanged but in the presence of ATP some unknown activity within the extract alters the positioning at the *PHO5* and *PHO8* promoters such that it closely resembles the *in vivo* positioning [175, 176]. Furthermore, any components alone or in addition to the *S. cerevisiae* WCE can be tested with this system for their influence on positioning.

I refined and extended the original protocol [175, 176] of this *in vitro* reconstitution system. To counteract chromatin aggregation, the concentration of histones and DNA during salt assembly was lowered and the total reaction volume increased to reduce the effect of the small volume changes that occurred during dialysis. Originally, the assay buffer contained 1.5 mM $MgCl_2$ on top of 3 mM ATP/$MgCl_2$ [175], which promoted chromatin aggregation in many instances (data not shown). This extra 1.5 mM $MgCl_2$ was omitted from the buffer, which greatly reduced aggregation without impact on the nucleosome positioning activity (data not shown). Finally, as we wished to include a number of new loci, we constructed a series of new plasmid templates for the *in vitro* system. Originally, the shuttle vectors C-leu (*PHO5*) and

pP8apin (*PHO8*) were used as templates to allow *in vitro* versus *in vivo* comparisons on the very same template. Since *in vivo* positioning looked virtually indistinguishable on these plasmids and on the chromosomal locus we chose to make further *in vivo* comparisons directly with the corresponding chromosomal loci. So we did not need the rather larger shuttle vectors (~ 10kb) but could use a smaller backbone, and make more efficient use of material in assembly reactions with template mixtures as less DNA was required to include the same number of templates. All new vectors contained an about 3.5 kb yeast PCR fragment cloned into the ~2.6 kb pUC19 vector. For the new *PHO8* locus template, we initially sub-cloned a pP8apin fragment into pUC19 resulting in plasmid pUC19-*PHO8*-short (Fig. 8A). Sequencing of this insert revealed a number of sequence differences relative to the SGD data base that were already present in the original pP8apain plasmid (data not shown). Apparently, the *PHO8* sequence in pP8apain was based on a different allele. In order to use yeast DNA templates that were all based on the reference genome sequence, we used genomic DNA of strain BY4741 to also create plasmid pUC19-*PHO8*-long (Fig. 8A), as well as to create all other new plasmids (chapter 4.4.1.). Reconstitution of *in vivo*-like positioning worked equally well with these three *PHO8* templates (Fig. 8B).

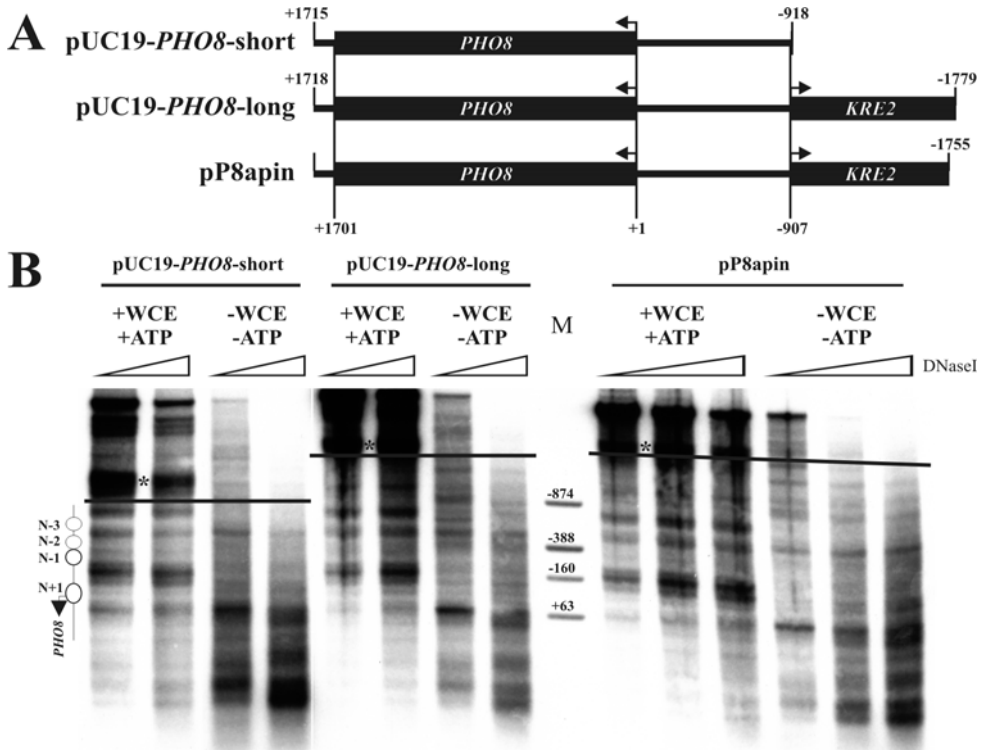

Figure 8. Nucleosome positioning at the *PHO8* promoter could be reconstituted independent of the vector backbone, insert size or the *PHO8* allele.

(A) Schematic overview of different inserts in the pUC19-*PHO8*-short, pUC19-*PHO8*-long and pP8apin plasmids. Numbers indicate positions relative to the *PHO8* ATG (in bp). **(B)** *In vitro* reconstitution of nucleosome positioning at the *PHO8* promoter on plasmids described in **(A)**. Pre-assembled plasmids pUC19-*PHO8*-short, pUC19-*PHO8*-long and pP8apin were incubated with ("+WCE +ATP") or without ("-WCE -ATP") WCE and ATP, and analyzed by DNaseI indirect endlabelling. Asterisks mark the position of a hypersensitive site that is generated at a site within the lacZ ORF of the bacterial vector backbone. The horizontal line indicates the approximate location of the insert-backbone border. Schematics of the *PHO8* promoter are shown on the left. Ramps indicate increasing DNaseI concentrations. The numbers above the marker bands refer to the position (in base pairs) relative to the *PHO8* ATG.

Successful reconstitution of nucleosome positioning at the *PHO5* promoter critically depends on near maximal assembly degrees (histone:DNA mass ratio of ~1)[175]. We controlled for high assembly degrees also in the refined system by analysing plasmid superhelicity after salt assembly. Plasmids

purified from *E. coli* are heavily negatively supercoiled. Nucleosome formation itself introduces about one negative supercoil [191], or, in the case of *in vitro* assembly of supercoiled templates, stabilizes one pre-existing negative supercoil against relaxation by topoisomerase I. As pre-existing supercoils might help nucleosome formation, salt assembly works better with negatively supercoiled templates [192]. The number of negative supercoils in *E. coli*-purified plasmids roughly matches the number seen in fully assembled plasmids [193]. To identify the number of nucleosome-constrained supercoils, the assembled plasmids were treated with topoisomerase I (Topo I).

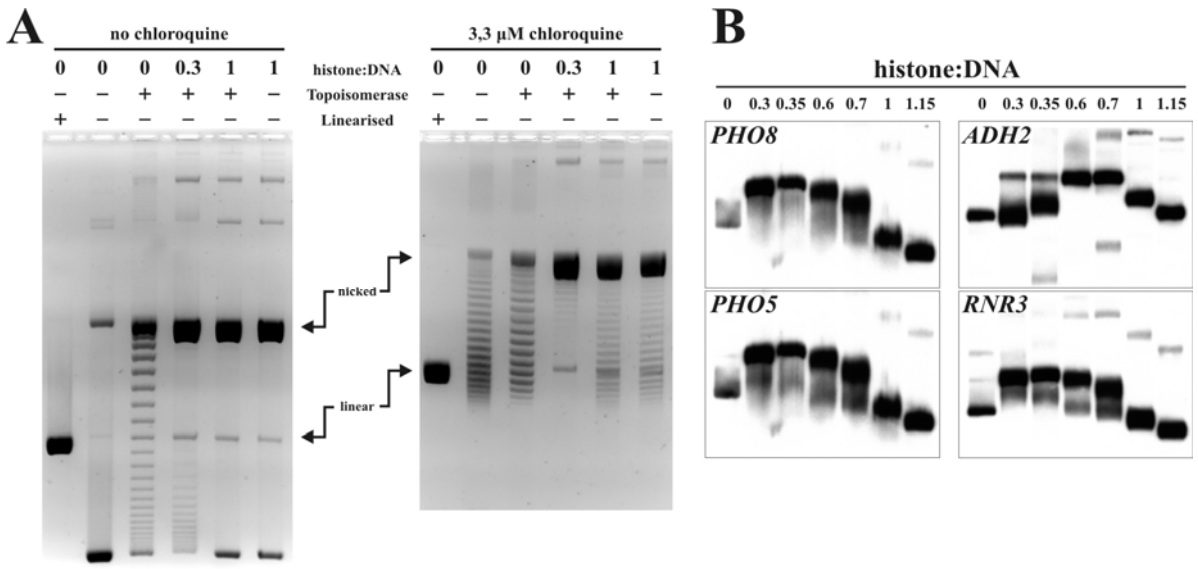

Figure 9. Salt gradient dialysis yielded a homogenous chromatin populations even for underassembled plasmids.

(A) Supercoil analysis in pUC19-*PHO8*-long plasmids assembled at various degrees and treated with topoisomerase I . pUC19-*PHO8*-long plasmids were assembled at the indicated histone:DNA mass ratios and incubated with (+) or without (-) topoisomerase I. pUC19-*PHO8*-long was linearized with PstI. Number of topoisomerase I resistant supercoils were resolved by gel electrophoresis in the presence or absence of 3.3 µM chloroquine and detected by ethidium bromide. **(B)** Equimolar mixtures of plasmids pUC19-*PHO8*-long, pUC19-*PHO5*, pUC19-*RNR3* and pUC19-*ADH2* were assembled by salt gradient dialysis at different histone:DNA mass ratios as indicated, separated on a native 0.35X TBE 0.9% agarose gel and analyzed by Southern blotting and hybridization with probes specific for the respective locus.

Assembly with a histone:DNA ratio of about 1:1 indeed fully protected the same number of supercoils from removal by Topo I as the number generated in *E. coli*, i.e. the plasmids migrated at a similar position as the untreated plasmids (Fig. 9A "no chloroquine" gel - Note that plasmids with more supercoils migrate faster). Moreover, in samples with a histone:DNA ratio of 0.3, plasmids contained much fewer supercoils than the samples with a 1:1 ratio. To further resolve the topoisomers of the highly assembled plasmids we electrophoresed the same samples in the presence of chloroquine, which intercalates into the DNA, introduces positive supercoils, and thereby reduces the number negative supercoils towards the resolution range of the gel. Plasmids assembled with a 1:1 ratio had a very similar supercoil distribution as the untreated plasmids, confirming the high assembly degree (Fig. 9A - panel on the right). Noteworthy, most of the plasmid population was nicked due to the sheering forces (pipetting etc.) during handling of the large (~6.1 kb) assembled templates. Such nicking was previously reported for even smaller plasmids [194], is promoted by nucleosome assembly (Fig. 9A - compare unassembled with assembled plasmids), and precludes direct analysis of the majority of templates by this technique. However, the un-nicked subpopulation should be a good proxy for the assembly degree estimation of the whole population.

As described above, we cloned ~3.5 kb fragments each of another ten loci of interest (*ADH2*, *CHA1*, *GCY1*, *HIS3*, *HO*, *PHO84*, *POT1*, *RNR3*, *SNT1*, *SUC2*) into pUC19 vectors. Positioned nucleosomes at these loci had been described and mapped, and for several loci positioning factors were previously identified or implicated (e.g. RSC for *CHA1* [149] or Reb1/Abf1 for *SNT1* [42]). For direct comparisons, we assembled several plasmids together in one tube as previously done for the *PHO5*/*PHO8* loci [175]. In case of limiting histones per total DNA, different histone affinities of the plasmid inserts could lead to uneven assembly degrees within such plasmid mixtures. Even with only one plasmid type it was unclear to what extent assembly with limiting amounts of histones could give rise to sub-populations of different assembly degrees. Such uneven assembly could lead to biased results when comparing the reconstitution at different loci. To check for such uneven assemblies, we assembled an equimolar mixture of pUC19-*PHO8*-long/pUC19-*PHO5*/pUC19-*ADH2*/pUC19-*RNR3* with varying amounts of histones (approximate histone:DNA ratio from 0.3 to 1.15) followed by native agarose gel, Southern blot and differential hybridization (Fig. 9B). For each of the six histone:DNA mass ratios there was only one major band, but its position varied between assembly degrees, even between rather similar ratios (Fig. 9B, compare 0.3 with 0.35 or 0.6 with 0.7). Thus, all of each of the different plasmids were assembled into rather homogeneous chromatin populations, i.e. acquired a similar number of nucleosomes. Furthermore, the highly similar migration behaviour of the *PHO8*, *PHO5* and *RNR3* containing plasmids for each assembly degree also suggested that even different plasmids were assembled to the same degree. The uniform assembly degree across different plasmids was later also confirmed by an MNase protection assay (data not shown). It was later realised that plasmid pUC19-*ADH2* was actually a dimer of ~12 kb (data not shown), which likely explains its different migration behaviour.

2.2. *In vitro* reconstitution of nucleosome positioning at 10 new loci

The ten plasmids containing the *PHO84*, *ADH2*, *RNR3*, *CHA1*, *SNT1*, *SUC2*, *HIS3*, *HO*, *GCY1* and *POT1* loci were salt assembled at a ~1:1 histone:DNA mass ratio and incubated in the positioning assay without WCE, with WCE but without ATP, and with both WCE and ATP. Positioning was analysed by DNaseI indirect endlabelling. Unassembled plasmids ("Free DNA") and isolated yeast nuclei ("*in vivo*") were analyzed in parallel (Fig. 10).

The DNaseI pattern for all "-WCE / -ATP" samples was different from that of free DNA, i.e. salt assembly led to a non-random nucleosome distribution. However, in most cases these DNaseI patterns did not match those seen *in vivo* (Fig. 10, compare "-WCE/-ATP" with "*in vivo*"). Merely at the *PHO84* and *HIS3* locus, the salt assembly chromatin pattern resembled somewhat the *in vivo* pattern, especially the position of a major NDR. Incubation with WCE in the absence of ATP did not change the DNaseI patterns, apart from slight changes at the *RNR3* and *PHO84* promoters. Most importantly, incubation with WCE and ATP reconstituted *in vivo*-like positioning at almost all loci (Fig. 10, Compare "+WCE/+ATP" with "*in vivo*"). Reconstitution of promoter NDRs was particularly good, especially at the *ADH2*, *CHA1*, *SNT1* and *HIS3* loci. In sole contrast, at *POT1* the WCE generated a very strong band that had no matching NDR *in vivo*. Therefore also the new loci mostly behaved as previously shown for the *PHO5* and *PHO8* loci [175]. First, salt assembly was insufficient to reconstitute proper positioning indicating that the DNA sequence alone could not properly position the nucleosomes. Second, the WCE in the presence of ATP and in the context of the reconstitution assay provided the necessary and sufficient *trans* factors for proper positioning at most loci.

Consequently, the reconstitution system that was developed for *PHO5* and *PHO8* is generally capable of reconstituting *in vivo*-like positioning *in vitro* at other yeast loci. Together, these results argue that intrinsic DNA sequence preferences are not the major determinant of nucleosome positioning.

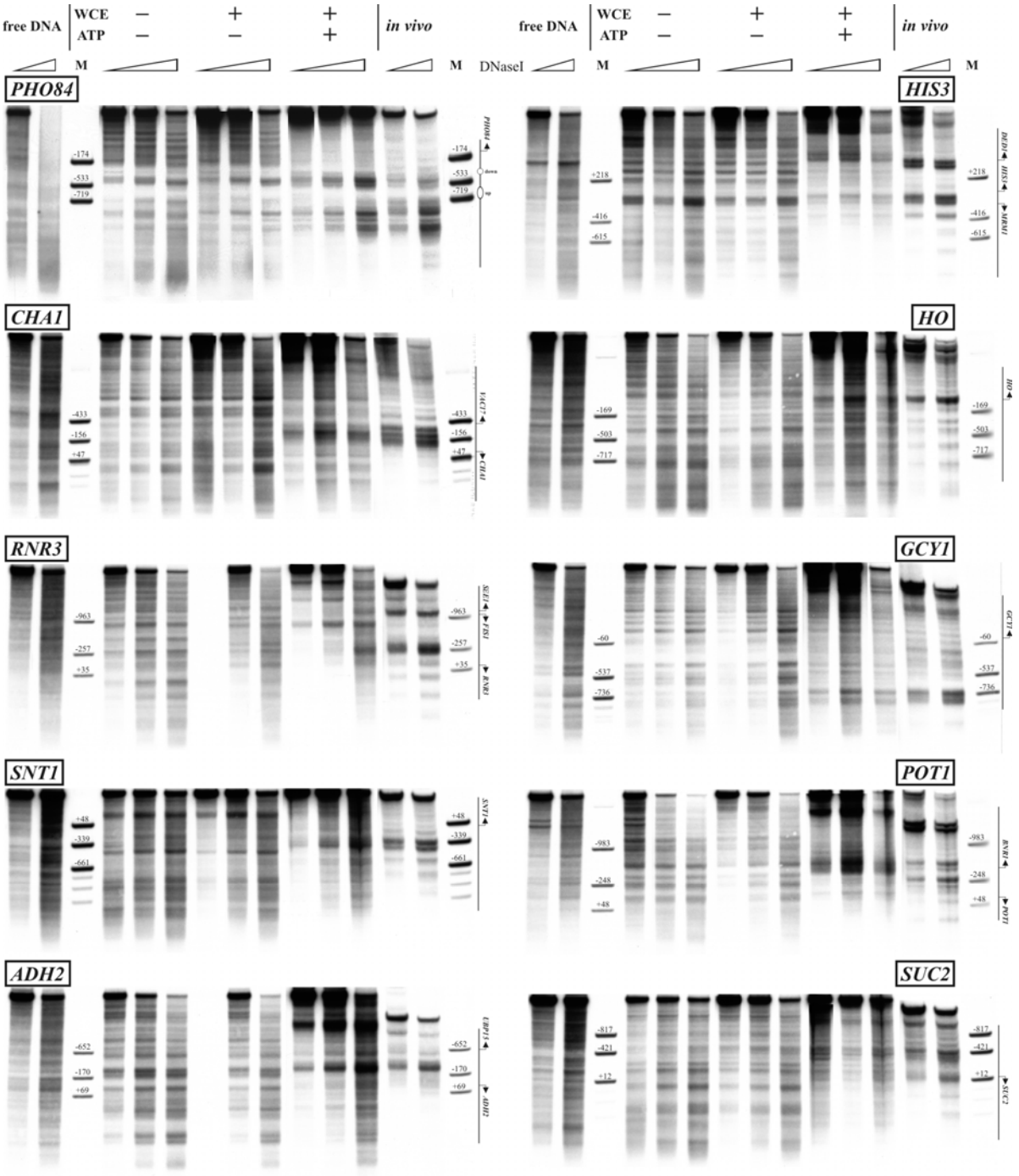

Figure 10. WCE reconstituted *in vivo*-like nucleosome positioning at many yeast loci.
pUC19 plasmids containing either one of the *PHO84*, *ADH2*, *RNR3*, *SNT1*, *GCY1*, *HIS3*, *HO*, *CHA1*, *POT1* and *SUC2* loci were assembled by salt gradient dialysis, incubated in the presence or absence of WCE and ATP, and analyzed by DNaseI indirect endlabelling. Free DNA samples were generated from non-assembled plasmids in the absence of WCE and ATP but under otherwise identical conditions. The *in vivo* samples were prepared from nuclei isolated from the wildtype strain BY4741 grown logarithmically at 30°C. Numbers above the marker bands refer to the position (in base pairs) relative to the start of the corresponding ORF. Approximate start of the respective open reading frames is indicate in the schematics on the right.

While proper reconstitution generally required WCE and ATP, the *HIS3* and *PHO84* promoter were already properly reconstituted to some degree by salt assembly alone. The NDR upstream of the *HIS3* ORF was already seen in the "-WCE/-ATP" sample and remained unchanged upon addition of extract and ATP. On the same blot, reconstitution of the NDR downstream of the *HIS3* ORF (i.e. upstream of *DED1*) in contrast was dependent on WCE and ATP. Note that the pUC19-*HIS3* plasmid contained the full length *HIS3* ORF whereas the *in vivo* sample was generated from a *his3* strain with a partial deletion of the *HIS3* ORF. Hence the band corresponding to the NDR downstream of *HIS3* migrated faster in the *in vivo* sample. At the *PHO84* promoter the results were even more striking as the entire banding pattern upstream / below the "-174" marker was very similar to the *in vivo* pattern already after salt assembly (Fig. 10, compare "-WCE/-ATP" with *in vivo*). Although addition of WCE and ATP made the pattern even more similar to *in vivo* (especially removing the strong bands located within the *PHO84* ORF) this suggested that intrinsic DNA sequence preferences were sufficient to direct proper positioning at the *PHO84* promoter.

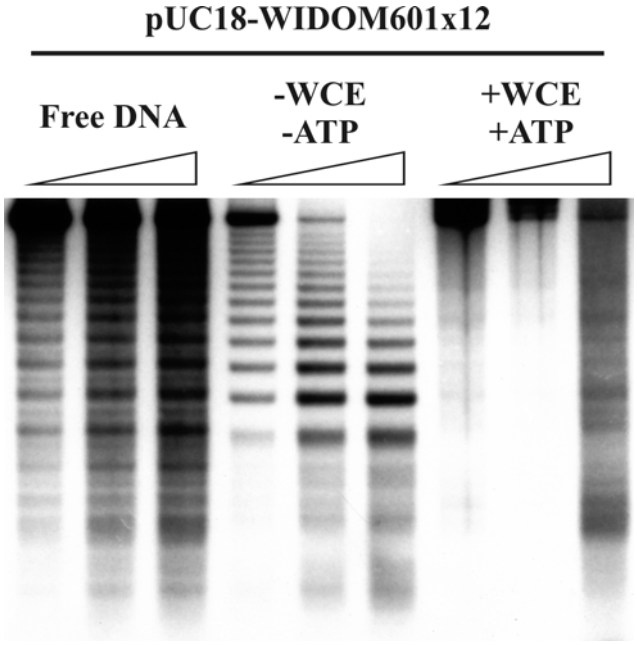

Figure 11. Activities within the WCE overrode the intrinsic sequence preferences of a 12mer WIDOM 601 array.

Analysis of the (re-)positioning power of the WCE on a template with strong artificial intrinsic positioning preferences. Pre-assembled pUC18-WIDOM601x12 plasmids were incubated with or without WCE and ATP as indicated, and analyzed by DNaseI indirect endlabelling. Free DNA sample was generated from non-assembled pUC18-WIDOM601x12 plasmids in the absence of WCE/ATP but under otherwise identical conditions.

The strong (re-)positioning activity of the WCE was further highlighted by its ability to overwrite the strong intrinsic positioning cues of the "Widom 601" sequence. This sequence was selected for its high affinity for histones during salt assembly [109]. Salt assembly of a 12mer of this Widom 601 sequence in a pUC18 backbone indeed generated an array of strongly positioned nucleosomes as indicated by the regular banding pattern with hardly any background signal (Fig. 11). Owing to the sequence preferences of DNaseI the "Free DNA" control also displayed the appearance of a regular banding pattern that could have been misinterpreted as regular nucleosomal structure highlighting the importance of a "Free DNA" control, especially for so far unprobed chromatin regions [195, 196]. WCE in the presence of ATP appeared to override the intrinsic positioning of the 12mer array as the regular DNaseI pattern became rather smeared suggesting randomised positioning.

Salt gradient dialysis assembly selects those positions that are intrinsically favoured at salt concentrations still high enough (probably 0.6 to 1 M) to allow free nucleosome sliding [117]. Consequently, the intrinsically favoured positions at low salt concentrations may be different but the nucleosomes are unable to re-equilibrate to these positions, i.e. they could be kinetically trapped at the positions favoured at relatively high salt concentration. It was therefore conceivable that the WCE itself did not provide positioning information as such, but rather that the remodeling enzymes in the extract allowed the trapped nucleosomes to slide to the positions intrinsically determined under physiological / low-salt conditions of the positioning assay. In other words, it was still possible

that nucleosome positions were more or less only determined by DNA-intrinsic sequence preferences of histone octamer assembly rather than by additional *trans*-factors. In the following, this important conceptual distinction was addressed experimentally.

2.3. Reconstitution system critically requires specific components from the *S. cerevisiae* WCE

Incubation of salt assembled nucleosomes at elevated temperatures can alter the nucleosome distribution on the template even at low salt concentration ("thermal sliding") [145, 197]. Incubation of assembled plasmid templates at 50°C (Fig. 12A) or 55°C (Fig. 12B) only lead to very marginal changes in the DNaseI pattern and in no case to the proper *in vivo*-like positioning. So thermal sliding did not free the nucleosomes from kinetically trapped positions, indicating that in our system the nucleosomes might already reside at their intrinsically preferred positions. However, the increased temperature itself, just like high salt, alters the thermodynamic conditions of the system, i.e. the preferred intrinsic positions at 55°C and low salt could be similar to those at room temperature and relatively high salt, but still be very different from the preferred positions at 30°C. So it was still possible that nucleosomes, if allowed to move freely at 30°C under low salt conditions, might redistribute to the *in vivo* positions.

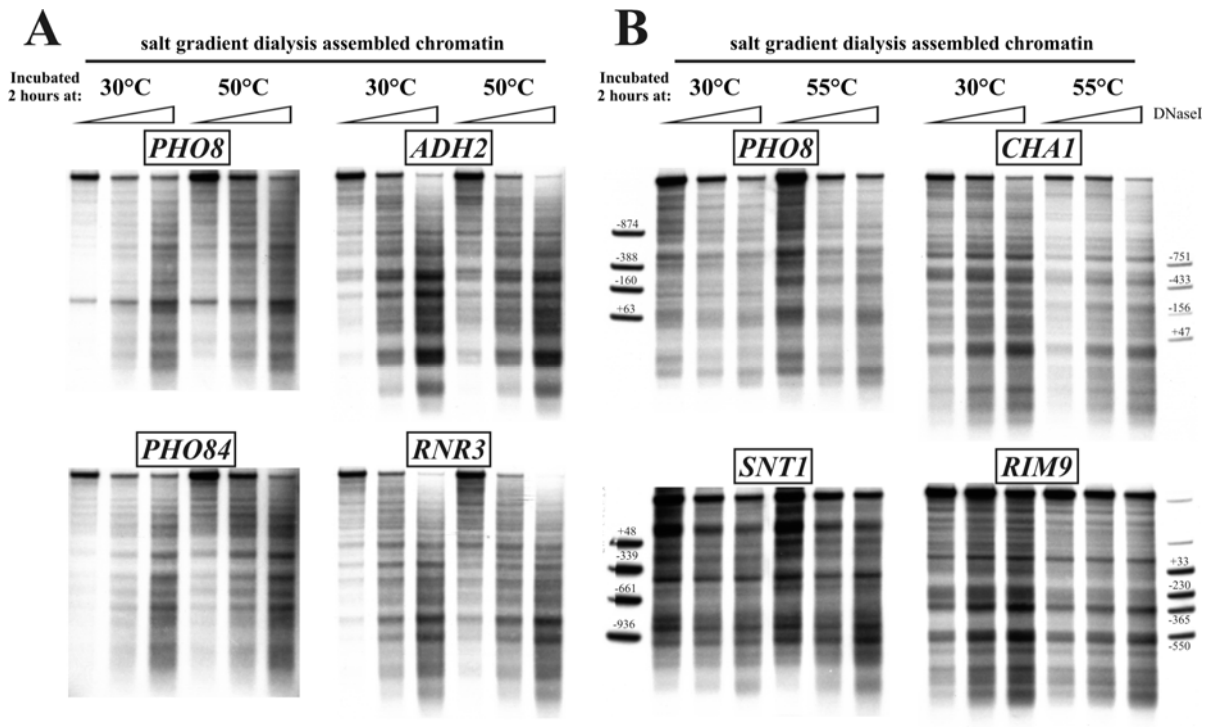

Figure 12. Thermal sliding did not generate *in vivo*-like nucleosome positioning.
(A) pUC19-*PHO8*-long, pUC19-*PHO84*, pUC19-*ADH2* and pUC19-*RNR3* plasmids pre-assembled by salt gradient dialysis were incubated as indicated and analyzed by DNaseI indirect endlabelling. **(B)** Same as **(A)** except with pUC19-*PHO8*-long, pUC19-*SNT1*, pUC19-*CHA1* and pUC19-*RIM9.* Numbers above the marker bands refer to the position (in base pairs) of the corresponding restriction site relative to the start of the respective ORF.

To test this possibility we provided nucleosome mobility by adding remodeler-containing extracts from distantly related species. *Drosophila* embryo extract (DREX) could assemble the *PHO5* and *PHO8* locus into chromatin but failed to reconstitute nucleosome positioning [175, 176]. Nonetheless, subsequent addition of WCE induced proper *in vivo*-like positioning. The major caveat of this experiment was that the early *Drosophila* extract contains high amounts of the ISWI-type remodeler ACF. ACF has spacing activity, i.e. generates extensive regularly spaced nucleosomal arrays [152, 153, 155]. The *PHO5* and *PHO8* promoters are not covered by regular arrays and thus the mechanistic properties of ACF might have prevented proper positioning. We therefore decided to test a whole cell extract from the very distantly related yeast *S. pombe* (PEX), which lacks remodelers of the ISWI-subfamily. Salt pre-assembled plasmids were incubated with ATP and either DREX or PEX and analysed for the resulting positioning (Fig. 13A). DREX failed to induce any specific or *in vivo*-like positioning confirming previous results [175]. Furthermore, also PEX was unable to achieve proper positioning at *PHO8* (and at *PHO5* (data not shown)). The *PHO8* NDR1 was reconstituted to some extent albeit the corresponding band was narrower and less intense. Subsequent addition of *S. cerevisiae* WCE "rescued" the system and reconstituted *in vivo*-like positioning.

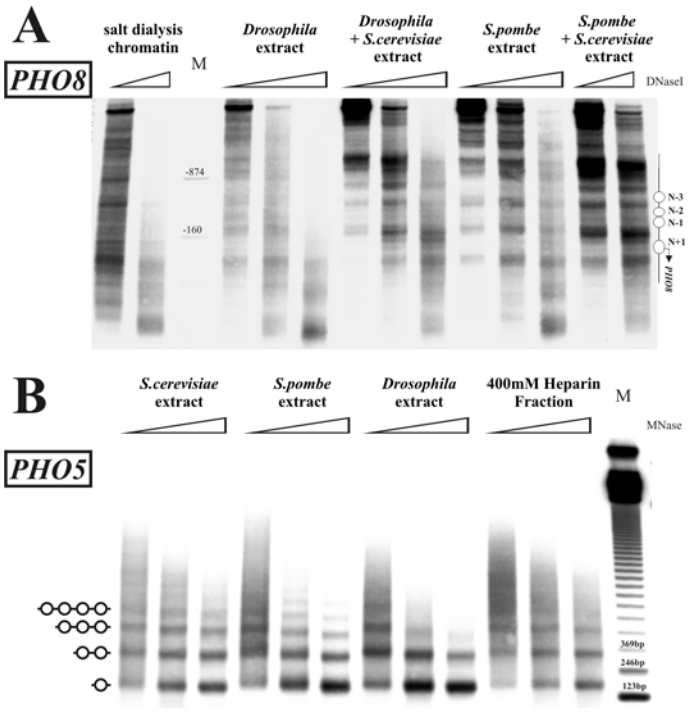

Figure 13. The activity required for reconstituting *in vivo*-like positioning at the *PHO8* promoter was specific to *S. cerevisiae* extracts.

(A) Pre-assembled pUC19-*PHO8*-short plasmids were incubated with *Drosophila* embryo extract (DREX), *S. pombe* WCE or without extract ("salt dialysis chromatin") for 1.5 hours and either analyzed directly by DNaseI indirect endlabelling or incubated for an extra 1.5h with *S. cerevisiae* WCE. Labeling as in Figure 8B. **(B)** Pre-assembled pUC19-*PHO5* plasmids were incubated with either *S. cerevisiae* WCE, *S. pombe* WCE, DREX or the 400 mM KCl Heparin fraction of the *S. cerevisiae* WCE (see Fig. 34A). Samples were digested with MNase and analyzed by Southern blotting and hybridization with a probe specific for the *PHO5* promoter. Marker (M) was the 123bp ladder. Schematics on the left indicate. mono-, di-, tri- and tetranucleosomes.

Importantly, DREX and PEX did not remove nucleosomes from the *PHO5* and *PHO8* promoters as controlled by MNase ladder analysis and specific probing for the *PHO5* and *PHO8* promoter. All three extracts generated clear MNase ladders at the *PHO5* and *PHO8* promoter regions (Fig. 13B and data not shown) with very similar, if not identical, spacing.

In summary, three different approaches that allow for nucleosome mobility (high salt during assembly, temperature induced sliding, DREX and PEX intrinsic remodelers) all failed to reconstitute *in vivo*-like nucleosome positioning on *S. cerevisiae* DNA templates. Proper positioning was only reconstituted by the *S. cerevisiae* extract. This very strongly argues for specific positioning determinants in the *S. cerevisiae* WCE that are necessary in addition to intrinsic DNA sequence preferences and are dominant over factors from heterologous extracts (see also [175]) .

Interestingly our WCE-based *in vitro* system reconstituted *in vivo*-like nucleosome positioning on yeast DNA with either *Drosophila* embryo histones or recombinant histones from *Drosophila*,

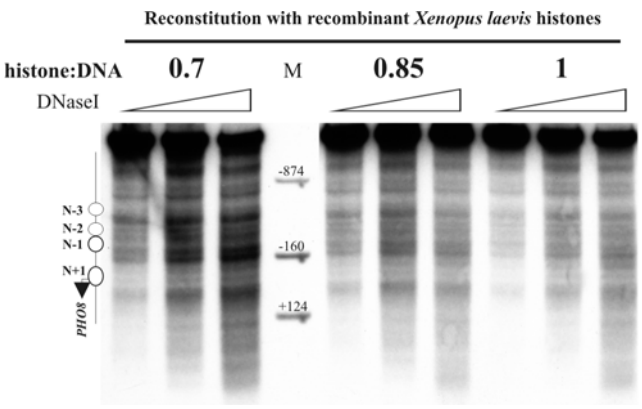

Figure 14. Reconstitution of *in vivo*-like nucleosome positioning at the *PHO8* promoter with recombinant *Xenopus laevis* histones.

pP8apin plasmids were assembled by salt gradient dialysis with recombinant *Xenopus laevis* histones, incubated with WCE and ATP and analyzed by DNaseI indirect endlabelling. Schematics, ramps and markers as in Figure 8B.

S.cerevisiae [198, 199] or *Xenopus* (Fig. 14). While histones are amongst the most well conserved proteins [200], there are still enough differences to suggest that specific interactions of components from the *S. cerevisiae* WCE with the histones were either absent or limited to the conserved regions. Furthermore, recombinant histones lacked posttranslational modifications (PTMs) and the *Drosophila* embryo histones contain PTMs not inherent to *S. cerevisiae*. Consequently, by whatever mechanism nucleosomes are positioned in our *in vitro* system, specific PTMs or histone variants were likely not involved in this process.

2.4. *PHO84*: Intrinsic nucleosomal stability is a determinant of remodeler dependency

In vitro reconstitution of nucleosome positioning at the *PHO5* and *PHO8* promoters suggested that differences in nucleosome stability may cause differentially stringent requirements for chromatin cofactors [175]. *In vitro* reconstitution of proper positioning at *PHO5* required a maximal assembly degree and maximal amount of WCE ([175]; data not shown), whereas proper positioning at the *PHO8* promoter was reconstituted even at sub-saturating concentrations of histones or WCE ([175]; Fig. 15). This differential *in vitro*-stability of the promoter architecture correlated with a differential co-factor requirement for nucleosome eviction. Both *PHO5* and *PHO8* are activated upon phosphate starvation by binding of the Pho4 transactivator, recruitment of various cofactors (such as Gcn5, SWI/SNF and Asf1) and subsequent eviction of promoter nucleosomes. Remodeling and removal of the nucleosomes at the *PHO5* promoter occurs in the absence of SWI/SNF (although kinetically delayed) whereas remodeling at the *PHO8* promoter is absolutely dependent on SWI/SNF [201]. The correlation of high *in vitro* stability and strong co-factor dependency *in vivo* previously led to the postulation of a causal link, i.e. nucleosomes with high intrinsic stability require specific "strong" remodeling/removal factors for their eviction, whereas a redundant set of co-factors exists for nucleosomes with low(er) intrinsic stability [175].

In addition to *PHO5* and *PHO8*, nucleosome positions and transcriptional regulation was also characterized for another promoter of the *PHO* regulon: the *PHO84* promoter. Here, the main feature is two positioned nucleosomes, one upstream and one downstream of a short DNaseI hypersensitive site (Figs. 6, 10 and 16) that are both remodelled and removed upon promoter induction. Interestingly, the *PHO84* promoter, with respect to remodeler dependency, behaves like a hybrid between the *PHO5* and *PHO8* promoter [169]. Remodeling of the downstream nucleosome occurred in the absence of both the SWI/SNF and Ino80 remodeling enzymes whereas the upstream nucleosome was not removed in the absence of SWI/SNF or, under sub-maximal induction conditions, also not in the absence of Ino80. Thus, the upstream nucleosome had similar remodeling

requirements as the *PHO8* promoter nucleosomes whereas the downstream nucleosome could be redundantly remodelled just like the *PHO5* promoter nucleosomes. So we tested also here if the remodeler dependency of these two nucleosomes correlated with their intrinsic stability.

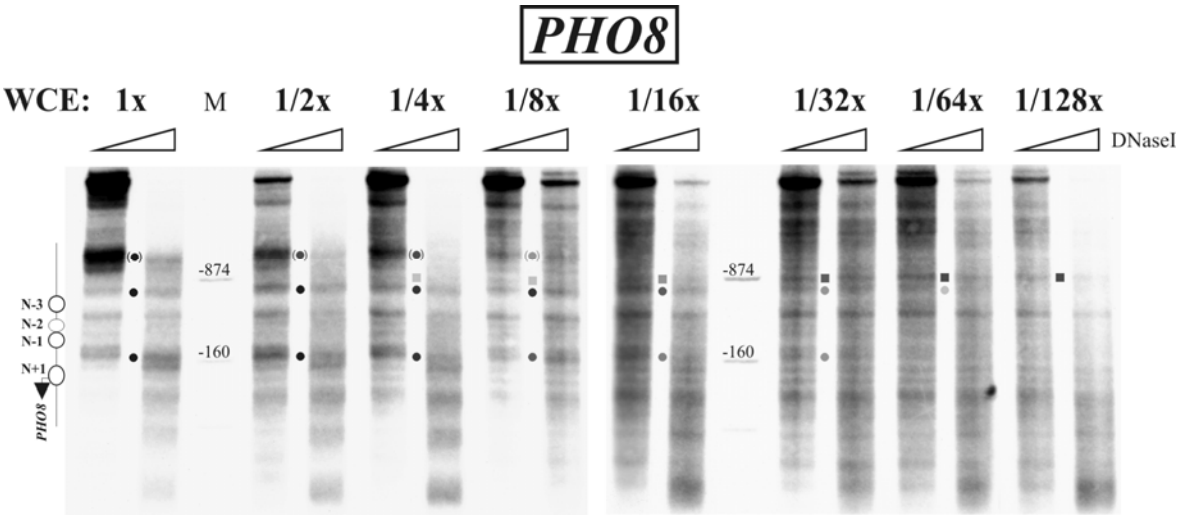

Figure 15. Reduction of the amount of WCE in the reconstitution reaction leads to a progressive decrease in the number of templates with properly positioned nucleosomes.

Titration of the WCE extract in reconstitution reactions containing pre-assembled pUC19-*PHO8*-short plasmids. Numbers above the ramps indicate the relative amount of WCE present in each reconstitution reaction. Dots mark the position of three bands set up by activities within the WCE (see "1x" lane) and the square the position of a band that is removed by the activities of the WCE (see "1/128X" lane). Intensities of the dots/squares reflects the intensity of the corresponding bands. The dot in brackets marks the position of a l band within the lacZ ORF of the bacterial vector backbone that is co-generated along with proper positioning (see Fig.8B). Schematics, ramps and markers as in Figure 8B.

As shown in Figure 10, salt assembly already correctly positioned both the upstream and downstream nucleosome indicating that both nucleosomes might be largely positioned by strong nucleosome positioning sequences (*cis* factors), which may lead to high intrinsic stability. In addition, assembly with a histone:DNA ratio of 0.6 gave the same results, i.e. both nucleosomes remained properly positioned (Fig. 16A, Lane "0.6 -WCE -ATP"). However, when we added WCE to the under-assembled chromatin, the downstream nucleosome was lost or shifted further downstream as an extra strong band appeared that overlapped with the position of the downstream nucleosome (Figure 16A; compare samples for 1:1 and 0.6:1). We confirmed this by measuring restriction enzyme accessibility at various sites across the promoter including two enzymes that cut within the position of the upstream (HhaI) and downstream nucleosome (TaqI) (Fig. 16B). Accessibilities for the 1:1 ratio chromatin were generally very low but the data for the 0.6:1 ratio chromatin was conclusive. The HhaI site remained much less accessible (36%) upon addition of WCE/ATP than the two sites that cut in the neighbouring linkers (66% and 73% for BsrBI and MfeI respectively). The TaqI site in contrast became as accessible (69%) as the neighbouring linkers (73% and 60%) arguing for lower stability of the downstream compared to the upstream nucleosome.

As further support, we carried out an *in silico* analysis of the nucleosome forming probability of the three *PHO* promoters using the N-score model developed by Yuan *et al.* [132]. This model was trained on *S. cerevisiae in vivo* nucleosome occupancy data and should therefore reflect the average nucleosome stability in the presence of all relevant factors *in vivo*. The N-Score profiles for the *PHO5*, *PHO8* and *PHO84* promoter were kindly provided by G. C. Yuan and supported the correlation between nucleosome stability and remodeler dependency (Fig. 6). The N-Score profile for the *PHO5* promoter features mostly negative values, i.e. low probability for nucleosome formation, and the

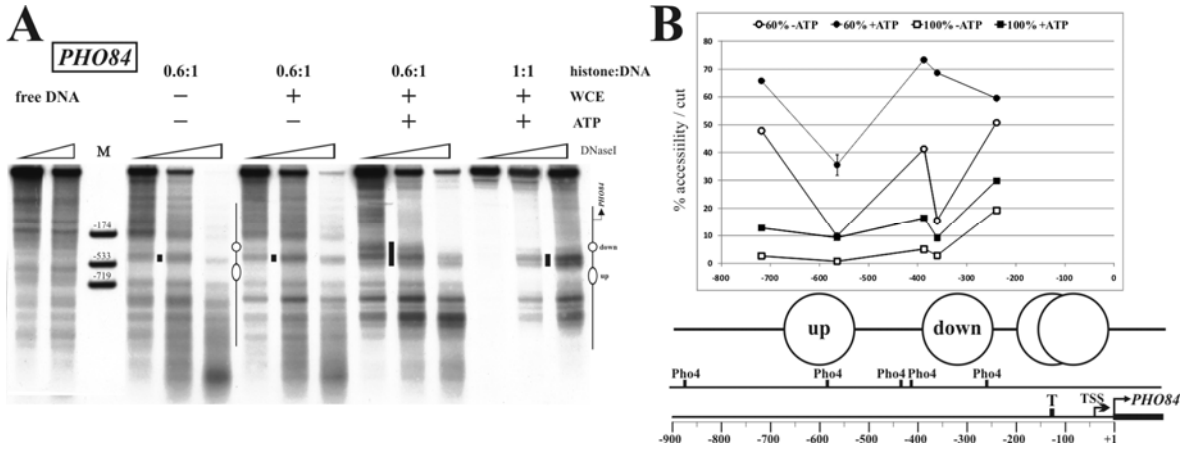

Figure 16. Downstream nucleosome at the *PHO84* promoter had a lower intrinsic stability *in vitro*.
(A) *In vitro* reconstitution of nucleosome positioning at the *PHO84* promoter with sub-maximally assembled chromatin templates. pUC19-*PHO84* plasmids were pre-assembled at the indicated histone:DNA mass ratios and incubated in the presence or absence of WCE and ATP and analyzed by DNaseI indirect endlabelling. Free DNA samples, markers and ramps as in Figure 10. Vertical bars highlight the extent of the DNaseI accessible region downstream of the upstream nucleosome. Schematics between lanes 6 and 7 and on the right indicate the approximate positions of the "up"-stream and "down"-stream nucleosome. **(B)** Same samples as in **(A)** were analyzed by restriction enzyme accessibility. Accessibility is plotted relative to the position of the restriction site (in bp from the *PHO84* ORF start): BsrBI (-718), HhaI (-564), MfeI (-387), TaqI (-360) and PacI (-239). The average and variation of two biological replicates is shown (BsrBI and PacI only one replicate). Error bars were in some cases within symbol size. Schematics below the graph show the *in vivo* positions of the nucleosomes at the *PHO84* promoter, Pho4 binding sites, TATA box and the TSS as in Figure 7.

major peaks in the profile correspond to sites that are linker regions *in vivo* indicating that the actual occupied positions *in vivo* might be at odds with average *in vivo* sequence preferences. The N-Score profile for *PHO8* displays generally very high values and the position of the two main troughs correspond to the positions of the NDRs upstream of the *PHO8* and *KRE2* ORF while the locations of the nucleosomes generally overlap with peaks in the N-Score profile. So the nucleosomes of the *PHO8* promoter occupy DNA with high nucleosome forming probability.

At the *PHO84* promoter, the upstream nucleosome is centred right over the only major N-Score peak. Upstream of this peak is a long region with extremely low N-Score values corresponding to a nucleosome depleted region, both *in vivo* and *in vitro* (Figure 10, 16, 18 and 19). Downstream of the major peak, the N-score profile is flat and displays rather average values. Evidently, the correlation between the three N-Score profiles and the actual nucleosome positions strongly support the hypothesis that remodeler-dependent nucleosomes are more stable than remodeler-independent nucleosomes. Nonetheless, all these correlations, i.e. between the remodeler-dependency *in vivo*, the stabilities *in vitro* and the predicted stabilities *in silico*, do not necessarily argue for a causal relationship between intrinsic stability and remodeler dependency of a nucleosome.

Therefore, we rationally manipulated the intrinsic stability of the upstream nucleosome in order to test if this affected its dependency on SWI/SNF for remodeling. Homopolymorphic dA:dT stretches have low intrinsic affinity for nucleosome formation ([122] and references therein). We mutated stretches of 10 or 19 residues within the upstream nucleosome to adenine in the *PHO84* locus-containing pCB84a shuttle vector. The corresponding vectors pCB84a-10A and pCB84a-19A were used for analysis of the chromatin architecture *in vivo*, and a "19A" derivative of the pUC19-*PHO84* plasmid ("pUC19-*PHO84*-19A") for analysis *in vitro*. A comparison of the N-Score profile of the wildtype promoter with its "10A" and "19A" derivatives predicted that these mutations should reduce the stability of the upstream nucleosome (Fig. 17). In order to directly measure the decreased

stability, we assembled the pUC19-PHO84-19A vector *in vitro* both with a saturating (histone:DNA mass ratio of 1:1) and sub-saturating (0.6:1) amount of histones and analysed the positioning in the presence and absence of WCE/ATP.

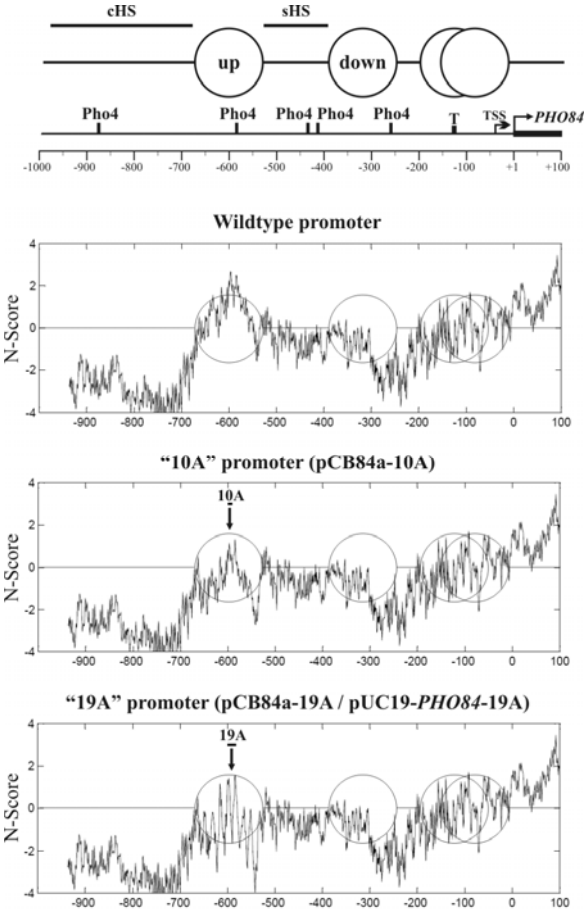

Figure 18. Insertion of polyA stretches into the upstream nucleosome leads to a local decrease in N-Score .

Top: Schematics of the *PHO84* promoter (as in Figure 7). Below: N-Score profiles [132] for the wildtype promoter and for promoters with 10 or 19 nucleotides mutated (arrows) within the upstream nucleosome to adenine. Dashed circles overlayed onto the N-Score profiles give the nucleosome positions as in the top panel.

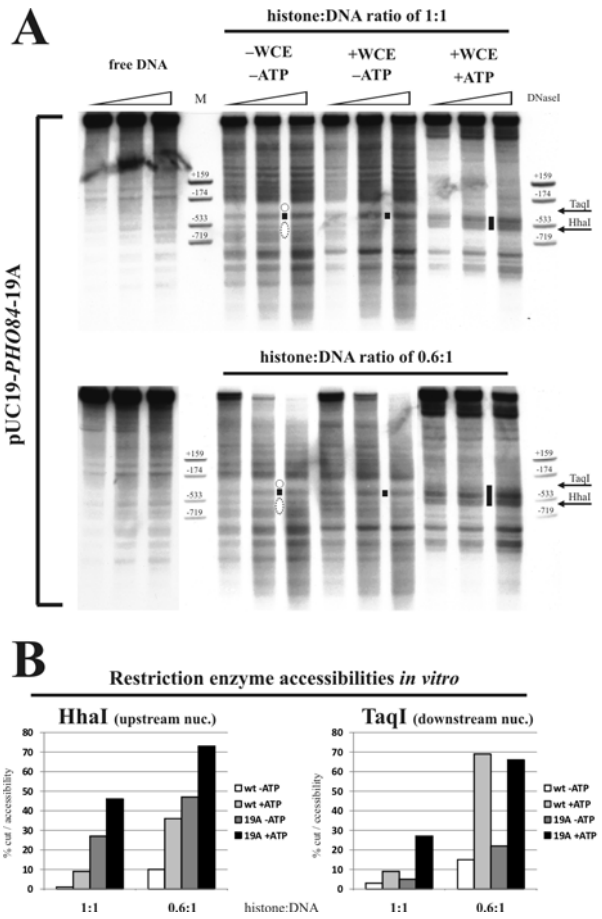

Figure 17 . A polyA stretch destabilizes the upstream nucleosome *in vitro*.

(A) *In vitro* reconstitution of nucleosome positioning at the *PHO84* promoter after mutation of a 19bp stretch to adenine (Fig. 17). pUC19-*PHO84*-19A plasmids were pre-assembled at the indicated histone:DNA mass ratios, incubated with or without WCE and ATP and analyzed by DNaseI indirect endlabelling. Free DNA samples, markers and ramps as in Figure 16. Arrows mark the approximate location of the TaqI and HhaI site. **(B)** same as **(A)** except that also pUC19-*PHO84* ("wt") was pre-assembled and samples were incubated with WCE in the presence ("+ATP") or absence ("-ATP") of ATP. Samples were analyzed by HhaI (upstream nucleosome) and TaqI (downstream nucleosome) accessibility.

Introduction of the "19A" stretch destabilised the upstream nucleosome, as the region normally protected by the upstream nucleosome became accessible to DNaseI and HhaI for both assembly degrees (Figure 18A and B). This effect was already apparent in the absence of WCE/ATP indicating that the "19A" mutation not only destabilised the nucleosome in the presence of WCE but already sufficiently lowered the intrinsic affinity of this stretch of DNA during salt assembly. The integrity of the downstream nucleosome was mostly unaffected by the altered sequence within the upstream nucleosome (Figure 18A and B, compare TaqI values of wt and 19A).

Finally, we assessed the effect of destabilizing the upstream nucleosome on its remodeling requirements *in vivo*. Positioning on the pCB84a-10A and -19A shuttle vectors was analysed in a wildtype and an *snf2* strain before and after induction by phosphate starvation. Based on the *in vitro* data, the initial concern was that the upstream nucleosome might already have been displaced under non-inducing ($+P_i$) rendering subsequent experiments inconclusive. However, the upstream nucleosome was still mostly present on both the pCB84a-10A and -19A variant promoter under repressive conditions as monitored by protection from DNaseI (Figure 19A: $+P_i$ pattern). Stability of the upstream nucleosome on the pCB84a-10A vector was confirmed by measuring HhaI accessibility. At the chromosomal locus, the HhaI accessibility was 29% and 14% (Fig. 19B) for the wt and *snf2* strain respectively and for the "10A" variant the accessibilities were even lower (15% and 9%). Together with the DNaseI data this showed that the upstream nucleosome at the “10A” variant was not already destabilised under non-inducing conditions. The HhaI accessibility for "19A" variant in contrast was elevated (Fig. 19B: 40% and 48%) in line with the high instability of this construct seen *in vitro*. This increased accessibility of the upstream nucleosome was not seen with DNaseI, probably due to the low digestion degree integral to the indirect endlabeling protocol. Nonetheless, even the elevated HhaI values were well below the values seen after removal of the nucleosome under fully inducing conditions (Fig. 19B: 78% (wt pCB84a-19A $-P_i$)).

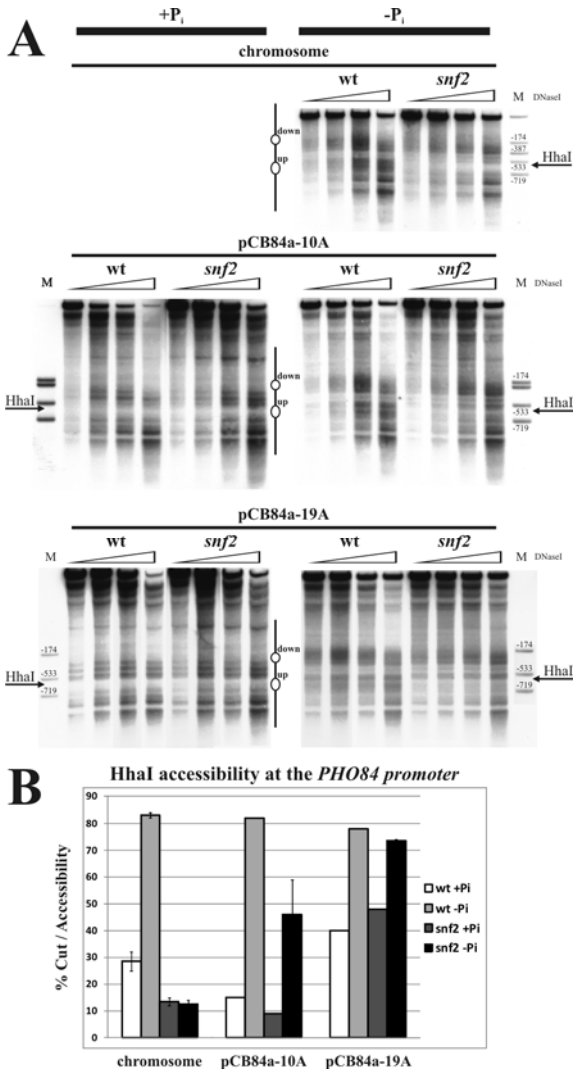

Figure 19. Lowering the intrinsic stability of the upstream nucleosome reduces the Snf2-dependency for its remodelling.

(A) *In vivo* DNaseI indirect endlabelling analysis of the *PHO84* promoter at its chromosomal locus and on pCB84a-10A and pCB84-19A plasmids in a wildtype (CY337) or an *snf2* strain (CY407). Nuclei were prepared from cells grown in $+P_i$ (repressing conditions) and $-P_i$ (inducing conditions) medium. Arrows indicate the approximate position of the HhaI site. Ramps and markers as in Figure 16. **(B)** HhaI accessibility of the strains described in **(A)**. The average and variation of two biological replicates is shown. Error bars were in some cases within symbol size.

As expected, both the upstream and downstream nucleosomes at the chromosomal locus were removed in the wildtype strain upon phosphate starvation as seen from loss of protection from DNaseI at both sites, whereas only the downstream nucleosome was removed in the *snf2* strain (Fig. 19A). This differential behaviour was well reflected by the HhaI accessibilities. While the HhaI accessibility in the wildtype increased from 29% to 83%, accessibility in the *snf2* mutant was unchanged (Fig. 19B). Stunningly, this dependency on SWI/SNF was strongly reduced for both the 10A and 19A construct. HhaI accessibility in the *snf2* mutant increased from 9% to 45% on the pCB84a-10A vector upon phosphate removal and from 48% to 73% on the pCB84-19A vector. This

increased accessibility was also reflected in the DNaseI pattern where protection of the region normally occupied by the upstream nucleosome was reduced (10A) or lost (19A) (Fig. 19A). In other words, lowering the intrinsic stability by introduction of a stretch of 10A had no impact on nucleosome integrity under non-inducing conditions but partially alleviated the Snf2-dependency of the upstream nucleosome. Similarly, the 19A variant displayed a partially impaired upstream nucleosome under non-inducing conditions that could be completely remodelled even in the absence of Snf2. In conclusion, the requirement for SWI/SNF to remove the upstream nucleosome upon induction was not just correlated but, at least in part, caused by the higher intrinsic stability of this nucleosome.

2.5. *In vitro* reconstitution of nucleosome positioning over the entire *S. cerevisiae* genome

Two prominent recent studies failed to reconstitute *in vivo*-like nucleosome positioning genome-wide by salt gradient dialysis assembly [119, 120]. Our extract-based *in vitro* reconstitution system in contrast achieved *in vivo*-like positioning at least at 11 out of 12 promoters. It thus seemed promising to attempt the reconstitution of nucleosome positioning across the entire *S. cerevisiae* genome using our extract-based *in vitro* system.

Initially we tried to assemble linear genomic DNA, either long fragments (~50 kb) or shorter sheared fragments (approximately 2-6 kb). Unfortunately, salt assembly of these fragments lead to aggregation even at the sub-saturating histone:DNA mass ratios of 0.7:1 and even at a quarter of the usual absolute concentrations. Similar problems were reported before where linear genomic DNA could only be assembled with a histone:DNA ratio of no greater than 0.4:1 [120]. Given that loci like the *PHO5* promoter required a maximum degree of assembly, such low assembly degrees were considered unsuitable to permit genome-wide reconstitution of proper positioning. To circumvent the aggregation problem, we returned to using

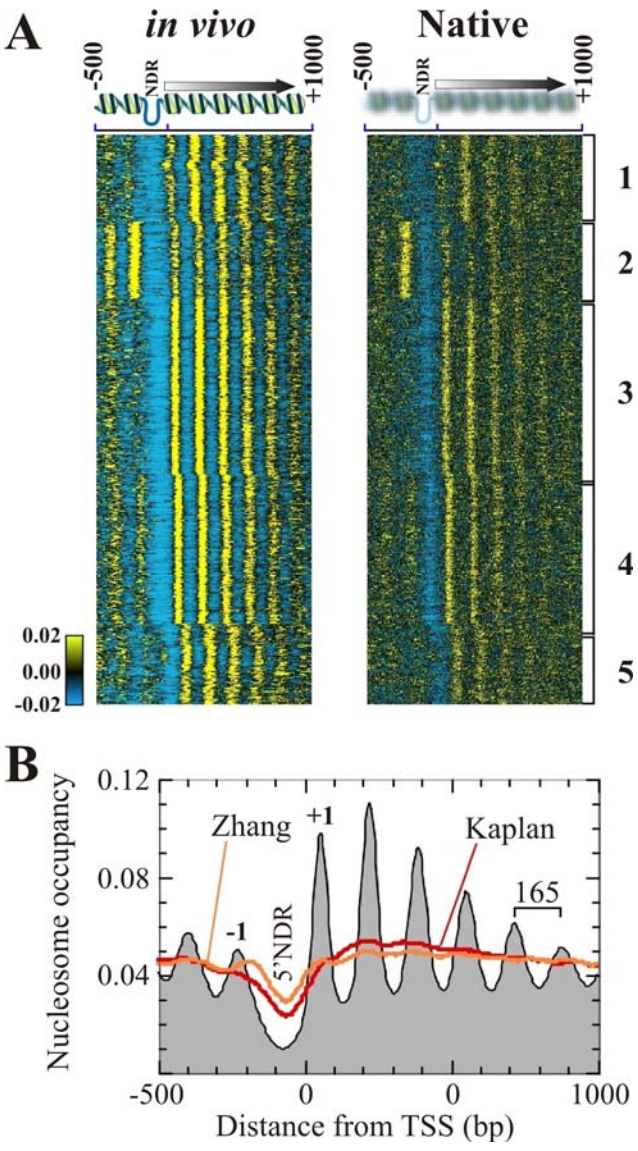

Figure 20. Salt gradient dialysis does not generate proper nucleosome positioning.
(A) Cluster view showing five patterns of nucleosome organization in the *in vivo* sample shown in **(B)** aligned by their TSS. The "Native" patterns correspond to *in vivo* chromatin that was cross-linked *in vitro* and otherwise processed as the *in vivo* sample. Yellow, black, and blue indicate a high, medium, and low occupancy level (tag counts), respectively. **(B)** Composite distribution of nucleosome midpoints centred around transcriptional start sites. Gray backdrop shows the *in vivo* pattern as in panel A [76]. Red and orange trace correspond to salt assembly patterns *in vitro* (by Kaplan et al. [120] and Zhang et al. [119], respectively). Peaks corresponding to the +1 and -1 nucleosome as well as the location of the 5'NDR is indicated.

circular supercoiled plasmid DNA in the form of a genomic plasmid library. We chose the library constructed by Rose *et al.* [202] as this library features long genomic inserts (10-30 kb) in combination with a comparatively small backbone (Ycp50: ~ 8 kb). This library was assembled with the same high histone:DNA mass ratios as the previously used individual pUC-based plasmids without showing any aggregation problems (see further below).

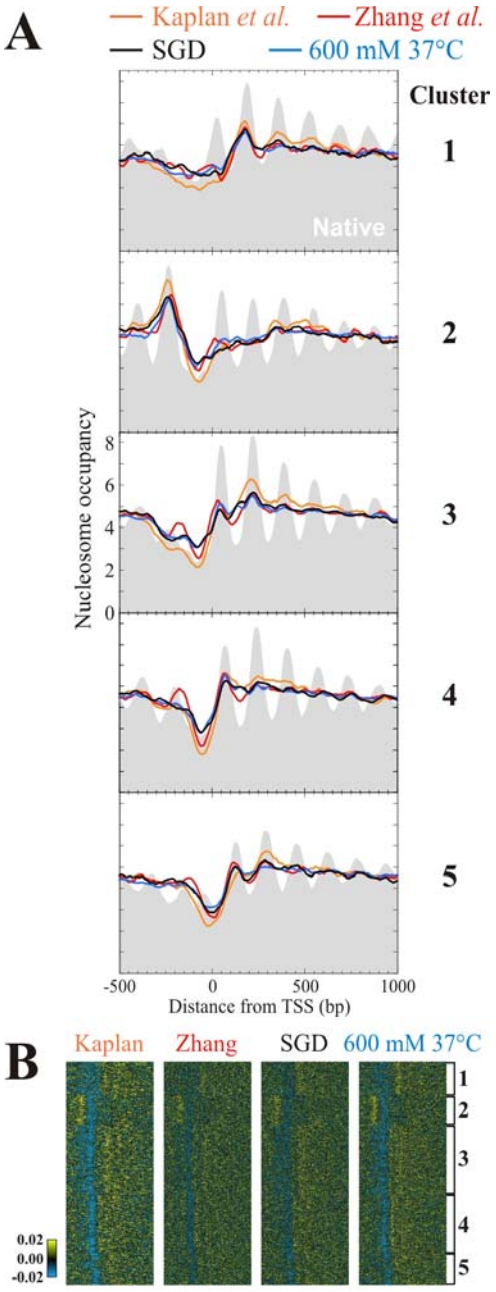

Figure 21. *Cis* factors specify only very few nucleosome positions

(A) Composite distribution of nucleosome midpoints in individual clusters for *in vitro* reconstituted or salt washed *ex vivo* nucleosomes. "SGD": supercoiled Ycp50 library assembled by salt gradient dialysis at a 1:1 histone:DNA mass ratio. "600 mM": native chromatin samples incubated with 600 mM NaCl at 37°C for 90 minutes prior to cross-linking. **(B)** Gene-by-gene representation as in Fig. 20A. Kaplan *et al.* and Zhang *et al.* from [120, 119], respectively.

The next challenge was to find a suitable method for mapping nucleosome positions in our *in vitro* system across the entire genome. DNaseI indirect endlabeling resolves positioning across only 1-2 kb of DNA, much too little for mapping the 12.5 Mbp genome. Moreover, this technique requires more material per locus than can be conveniently assembled *in vitro* as the locus of interest is "diluted" by the presence of the whole genome background. Consequently, we chose the same approach as did the other two genome-wide nucleosome reconstitution studies [119, 120] and collaborated with the group of Frank Pugh (PennState University) in order to map nucleosomes by high throughput sequencing. In contrast to our previous analyses, this approach required not a limited but an extensive digestion of chromatin with MNase to obtain mostly mononucleosomal DNA. In order to prevent nucleosome repositioning during the extensive MNase digestion the chromatin was crosslinked prior to addition of MNase. In some cases, the thus generated mononucleosomes were immunopurified using an anti-H3-C-terminal antibody. This way we selected nucleosomal DNA by two criteria: protection from MNase digestion and association with histone H3. The latter controlled against nucleosomes reassembled onto free DNA after crosslinking and against mapping repositioned nucleosomes that were not crosslinked efficiently. However, results were the same if this immunopurification step was omitted (data not shown) suggesting that either crosslinking was efficient or that no nucleosomal reassemblies or rearrangements occurred during the MNase digest.

To generate an appropriate nucleosomal map for comparison with our *in vitro* data, Elissa Ward in the Pugh lab isolated native chromatin from wildtype cells and crosslinked it after cell disruption (i.e. the material was crosslinked *in vitro* similar to our *in vitro* reconstituted samples) and prior to MNase digestion. This map was termed "native" and highly similar to

maps generated from cells that were crosslinked *in vivo* (Fig. 20A). Nonetheless, the peak-to-trough ratio was less pronounced. This "blurring" of nucleosome positions is likely an *in vitro* cross-linking artefact.

2.5.1. Histones and DNA, either in salt assembly or thermal sliding, are not sufficient to reconstitute proper nucleosome positioning genome-wide

Initially, we confirmed the findings by Kaplan *et al.* and Zhang *et al.* that reconstitution of nucleosome positioning by salt assembly alone was largely not successful. Both their *in vitro* assemblies recapitulated some of the depletion seen at the 5'NDRs *in vivo* but failed to generate the extensive nucleosomal arrays that emanate from the NDRs into the coding regions (Fig. 20B) as previously noted [119, 120, 203]. To see if salt assembly alone was able to generate proper positioning at promoter subsets, we clustered all promoters by k-means into five groups on the basis of *in vivo* similarity of their promoter architectures (Figs. 20A and 21A) [74]. We included in the comparison the mapping data from our salt assembled Ycp50 plasmid library as well as from chromatin isolated from *in vivo* where most DNA binding factors were washed away and nucleosomes were allowed to redistribute to their preferred positions by incubation at 600 mM NaCl for 90 minutes at 37°C. All four different approaches yielded maps that were very similar to each other for all 5 clusters (Fig. 21A and B) indicating that all four approaches generated a similarly true reflection of DNA intrinsic positioning under high salt conditions.

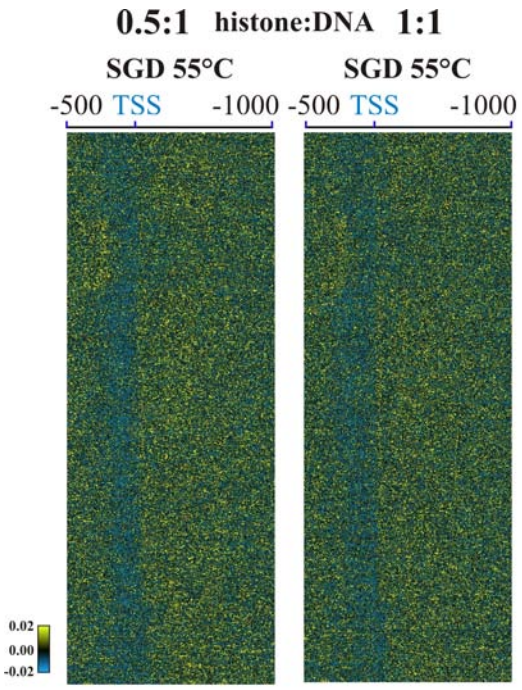

Figure 22. Heat-shifting of salt assembled chromatin does not lead to proper nucleosome positioning

TSS-aligned cluster plot of nucleosomes reconstituted on the Ycp50 genomic library by salt gradient dialysis (SGD) at the indicated histone:DNA mass ratios and subsequently incubated at 55°C for 1 h 45 min followed by 15 min at 30°C and MNase digestion without cross-linking. The region 500 bp up- to 1000 bp downstream of the TSS is shown.

Again, while *nucleosome exclusion* in the NDRs of the five clusters was reasonably well recapitulated, reconstitution of *nucleosome positioning* was much less successful and limited to individual nucleosomes in individual clusters (Fig. 21A). For example, nucleosome -1 in cluster 2 was rather well reconstituted in all four samples (Fig. 21A - see both cluster and composite plots) indicating that DNA intrinsic sequence cues have a prominent role in positioning this nucleosome. Other positions, such as nucleosome +2 in cluster 1 or nucleosome +1 in clusters 3-5, were partially reflected in the composite plots suggesting a significant, but minor role of sequence intrinsic features in helping to position these nucleosomes. Most importantly, neither of the four different approaches in neither of the cluster reconstituted the regular arrays that emanate from the 5'NDR *in vivo*. These analyses argue that nucleosome positioning determined solely by DNA intrinsic sequence cues is limited to contributing to nucleosome depletion over NDRs and to positioning of a few nucleosomes.

As discussed in chapter 2.3., salt assembly places nucleosomes according to sequence preferences under high salt conditions. We incubated the SGD at

55°C for nearly 2 hours to allow for thermal sliding and re-distribution of the nucleosomes to positions preferred under low-salt conditions (for the principle limitations of this approach see chapter 2.3.). This did not lead to any noticeable changes in the nucleosome distribution and did not make it more *in vivo*-like (Fig. 23). We also tested chromatin that was assembled at half the histone:DNA mass ratio to see if thermal sliding occurred in the presence of more freely accessible DNA. This was also not the case (Fig. 23). Apparently, the determination of nucleosome positions requires additional input from factors other than just histones and DNA alone.

2.5.2. Whole genome reconstitution of positioned nucleosomes requires WCE and ATP

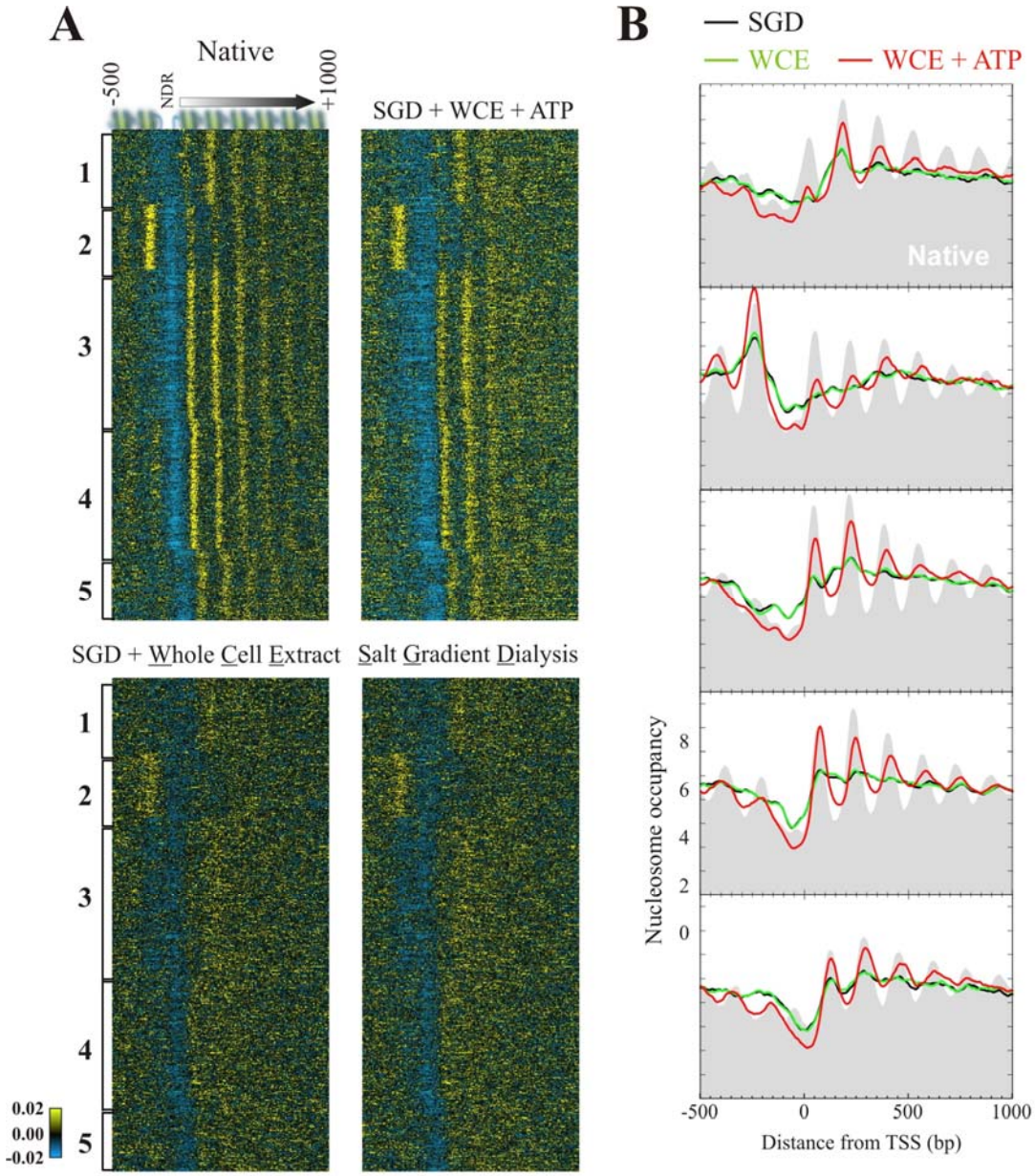

Figure 23. WCE and ATP can reconstitute proper nucleosome positioning at promoter regions.
(A) TSS-aligned cluster plot of nucleosomes reconstituted on the Ycp50 library by salt gradient dialysis and incubated alone (SGD) or with WCE (SGD+WCE) or WCE and ATP (SGD+WCE+ATP). "Native" pattern (see Fig. 20B) is shown for comparison. **(B)** Composite plots of individual clusters of the samples in **(A)**.

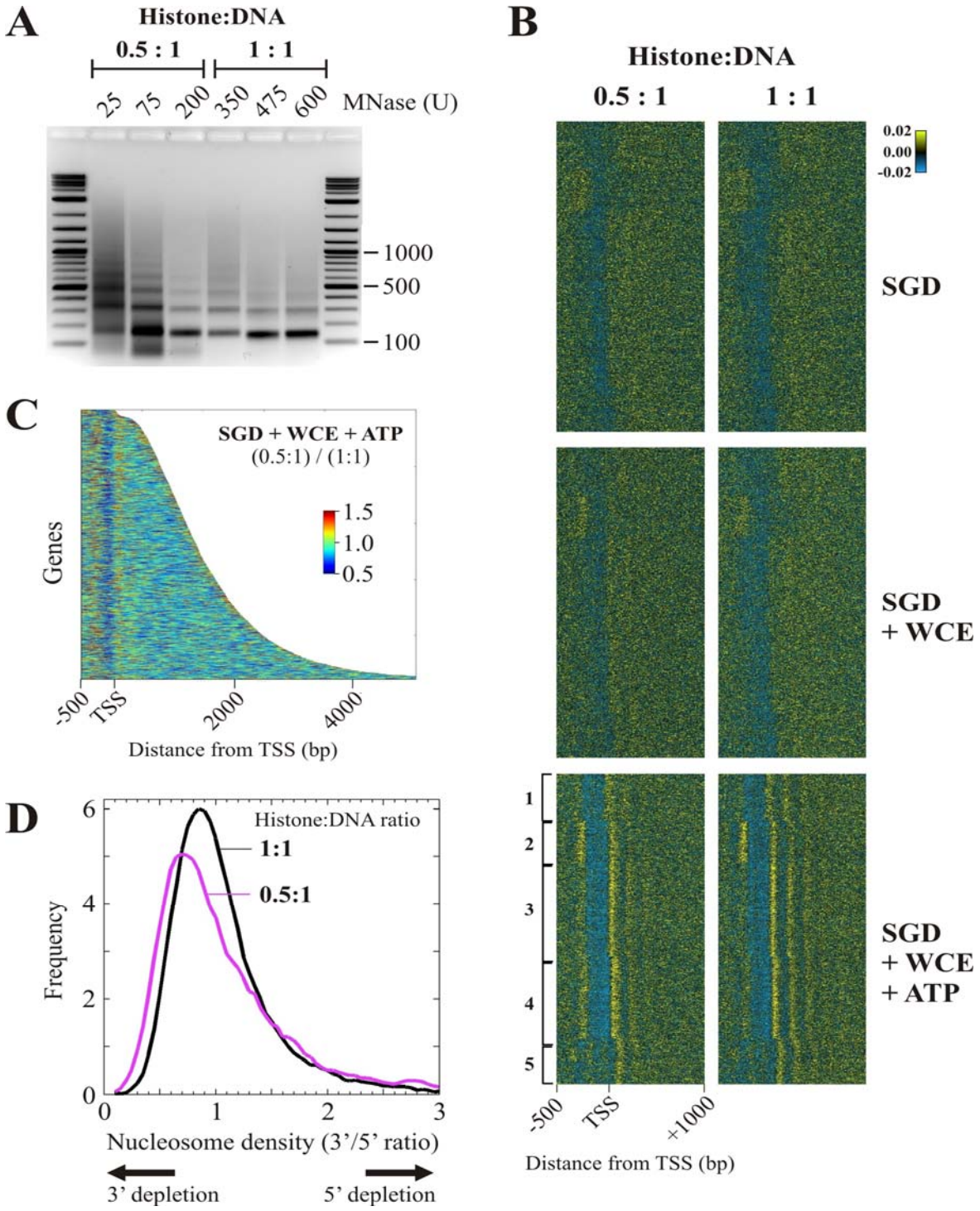

Figure 24. Nucleosomes are actively packed against a barrier.

(A) Ethidium bromide stained agarose gel (inverse image) of Ycp50 library assembled at the indicated histone:DNA ratios, then incubated with WCE and ATP and digested with the indicated amounts of MNase. Size (in bp) of some marker bands is given. **(B)** TSS-aligned cluster plots of nucleosomes reconstituted at the indicated histone:DNA mass ratios and incubated alone (SGD), with just WCE (SGD +WCE) or with WCE and ATP (SGD +WCE +ATP). **(C)** Histone density ratios of the "SGD +WCE +ATP" samples reconstituted at 0.5:1 versus 1:1 histone:DNA mass ratio. The colour scale represents the magnitude of the density ratio. Genes are aligned at the TSS, sorted by gene length and shown only up to the termination site. **(D)** Frequency distribution of the average histone density ratio between the 3' region (from +140 bp to transcript termination site) and the 5' region (from -20 to +140 bp) for the two different histone:DNA ratios.

Salt assembly failed to reconstitute proper nucleosome positioning both at individual loci (Fig. 10) as judged by DNaseI indirect end labelling as well as genome-wide as judged by MNase-ChIP-seq (Fig. 21). As the *S. cerevisiae* WCE plus ATP can recapitulate *in vivo*-like positioning at several selected loci (Fig. 10) [175, 176], we incubated our assembled Ycp50 library with WCE, with or without ATP, too. Astonishingly, incubation with WCE and ATP reconstituted the proper promoter architecture at nearly all genes (Fig. 22A and B). Particularly striking was the appearance of the regular nucleosomal arrays (Fig. 22A and B) that are characteristic of native / *in vivo* chromatin (Fig. 20A and B) and that could not be reconstituted by purely physical means (Fig. 21A and B). Moreover, nucleosome depletion at the 5'NDRs was even lower (compare Figs. 21 and 22), i.e. more *in vivo*-like, in the WCE +ATP sample, demonstrating that factors within the WCE also contribute to 5'NDR formation. Importantly, as was the case for analysis of individual promoters (Fig. 10), all changes were ATP dependent as addition of WCE in the absence of ATP did not lead to any changes in the nucleosomal pattern (Fig. 22A and B). Cluster analysis showed that the WCE and ATP dependent reconstitution was particularly good for clusters 3-5, which represent the canonical “open” promoter architecture, whereas the arrays in cluster 2 as well as nucleosome +1 in cluster 1 were less well reconstituted (Fig. 22B).

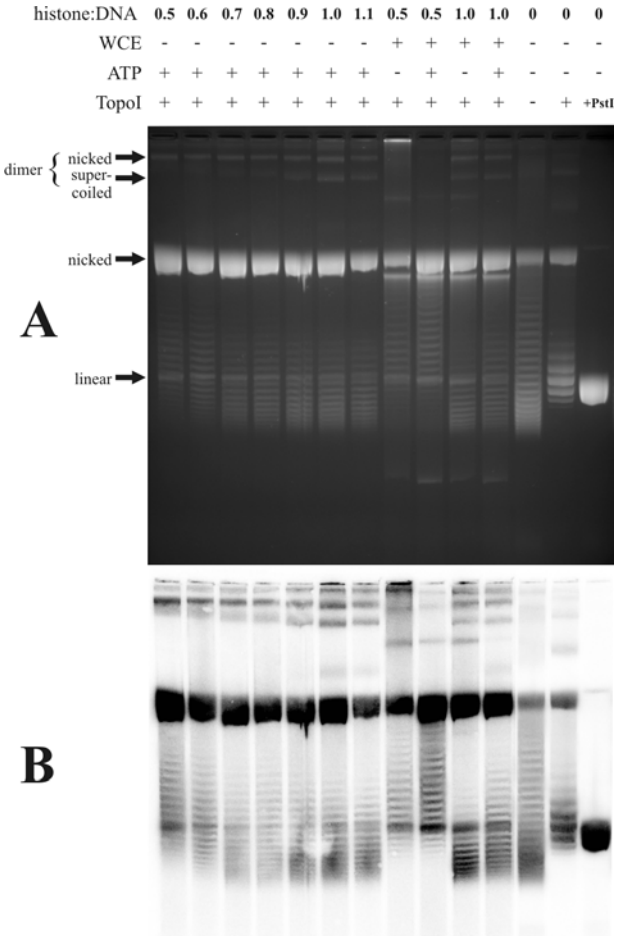

Figure 25. WCE does not increase the assembly degree of pre-assembled plasmids.

(A) Ethidium bromide stained agarose gel electrophoresis of pUC19-*PHO8*-long plasmids assembled at the indicated histone:DNA mass ratios and incubated with WCE, ATP and topoisomerase I as indicated. Electrophoresis was in the presence of 3 µM chloroquine. The positions of the linear and nicked monomeric and dimeric templates, respectively, are indicated. The lane on the very right contains pUC19-*PHO8*-long plasmid linearized via PstI digestion. **(B)** Same as panel **(A)**, but visualized after Southern blotting and hybridization with a pUC19 specific probe.

As such this is the first ever genome-wide reconstitution of nearly all aspects of nucleosomal promoter architecture in *S. cerevisiae*. These results very clearly highlight the importance of *trans*-factors and ATP in determining nucleosome positioning. Noteworthy, the (partial) reconstitution of the primary structure of an entire eukaryotic genome is both a beautiful demonstration of the self-organizing principles of complex biological sub-systems as well as the power of biochemical *in vitro* approaches.

"Statistical positioning" is the most widely discussed model to explain the generation of the regular nucleosomal arrays [107]. This model predicts that the spacing within the array is a function of the nucleosome density [107, 182]. We decided to test this prediction of "Statistical positioning" model by reconstituting nucleosome positioning *in vitro* at half the histone density (i.e. Ycp50 library assembled at half the histone:DNA mass ratio (0.5:1)). In our initial MNase titration experiments we already noticed that overall nucleosomal spacing was the same in both the 0.5:1 and 1:1 assembled chromatin

even after incubation with WCE and ATP (Fig. 24A). Reconstitution of nucleosome positioning by incubation of the 0.5:1 material with WCE and ATP worked fairly well (Fig. 24B). While the arrays over the ORFs were less clear (i.e. lower peak-to-through ratio), the distance between the peaks, i.e. the spacing, remained unchanged. This experiment might have been confounded if the WCE might contribute an endogenous histone pool such that the assembly degree was increased beyond the 0.5:1 ratio used for the salt assembly starting material. However, the high digestion degree of the 0.5:1 chromatin even at low MNase concentrations (Fig. 24A, note the MNase units indicated on top of the lanes) as well as the presence of the sub-nucleosomal sized band, which is indicative of under-assembled chromatin, already suggested that the bulk of the 0.5:1 sample had a substantially lower assembly degree than the 1:1 sample.

To really be sure that our conclusions were valid, we used a more sensitive topology-based assay to asses if and to what degree the WCE altered the assembly degree in both the 0.5:1 and 1:1 samples. We used the pUC19-*PHO8*-long plasmid as a proxy for the plasmid library since the plasmids of the Ycp50 library were too large and heterogeneous for this kind of analysis. As a "calibration" curve we assembled the pUC19-*PHO8*-long plasmid at histone:DNA mass ratios from 0.5:1 to 1.1:1. As expected, the degree of supercoiling reached its maximum in the 1:1 sample as there was no further downshift in the topoisomer band distribution beyond the 1:1 sample (Fig. 25A and B). Arguably, the band distribution for assemblies beyond 0.7:1 is not well resolved in this gel. However, the migration position of the supercoiled plasmid dimer (Fig. 25 - see labels) also shows an increase in superhelicity at histone:DNA mass ratios higher than 0.7:1. Further, our previous native gel analysis of pUC19-*PHO8*-long (Fig. 9B) clearly showed an increase in the assembly degree beyond the 0.7:1 mass ratio. Incubation of the 0.5:1 or the 1:1 sample together with WCE did not result in a downshift of the band distribution showing that the WCE did not increase the assembly degree in either of the two samples. Incubation with WCE together with ATP even resulted in a mild upshift indicating an overall slight ATP-dependent reduction of the assembly degree in both the 0.5:1 and 1:1 sample. This is not a problem with respect to the previous conclusions as the relative assembly degree between the two samples was maintained. Moreover, the maintenance of physiological spacing at even lower histone:DNA mass ratios was even more at odds with the statistical positioning model.

To detect further subtle differences between the 0.5:1 and 1:1 +WCE/+ATP patterns, Zhenhai Zhang in the Pugh group plotted the ratio between the two samples for every gene aligned at their TSS (Fig. 24C). In the 0.5:1 sample both the NDR regions as well as the interior of the ORFs were depleted relative to the nucleosome +1 position, indicating that the WCE/ATP actively "collects" or "pushes" nucleosomes towards the +1 position. This was also apparent when plotting the frequency distribution of 3' occupancy over 5'occupancy for both the 0.5:1 and 1:1 sample (Fig. 24D). In the 1:1 sample the distribution is centred near "1" indicating that most genes have a similar nucleosome occupancy towards both their 5' and 3' end. In the 0.5:1 sample however the distribution is skewed towards lower values, which highlights a depletion of the 3' relative to the 5'end and further suggest that nucleosomes are pushed or packed towards the 5'end / +1 nucleosome.

2.6. The search for *trans* factors that determine nucleosome positioning at the *PHO5* and *PHO8* promoters

Our *in vitro* reconstitution studies of *in vivo*-like nucleosome positioning, both at single loci (chapters 2.1-2.4) and genome-wide (chapter 2.5), amply suggested an ATP-dependent and specific nucleosome positioning activity in the *S. cerevisiae* WCE. We therefore thought to identify these activity/factor(s). The initial focus was on the positioning determinants for our *PHO5* and *PHO8* model promoters for which no positioning factors were known.

2.6.1. The candidate approach

Initially, we tested a number of candidate factors that were previously implicated in nucleosome positioning at other loci (though not at *PHO5* or *PHO8*). First, we tested ATP dependent nucleosome remodeling enzymes, which were shown early on to contribute to nucleosome positioning *in vivo* [149, 204, 205]. Even a "remodeler code" for nucleosome positioning was postulated recently [144]. Central to all nucleosome remodelers is their ATPase that belongs to the Snf2-type helicase family [58]. The yeast genome encodes 17 proteins that belong to this family, only two of which (Sth1 and Mot1) are essential. We tested for a role of most non-essential remodeler ATPases by monitoring the *PHO5* and *PHO8* promoter DNaseI patterns in the respective deletion mutants *in vivo*. None of the *snf2*, *isw2*, *ino80*, *swr1*, *fun30*, *irc5*, *irc20*, *rad5*, *rad16*, *rad26*, *rad54*, *rdh54* and *uls1* single mutants exhibited changes in nucleosome positioning as monitored by DNaseI indirect endlabelling (Fig. 26, [205] and data not shown). Members of the ISWI-subfamily specifically interact with the N-terminal tail of histone H4 and fail to remodel nucleosomes in its absence [206].

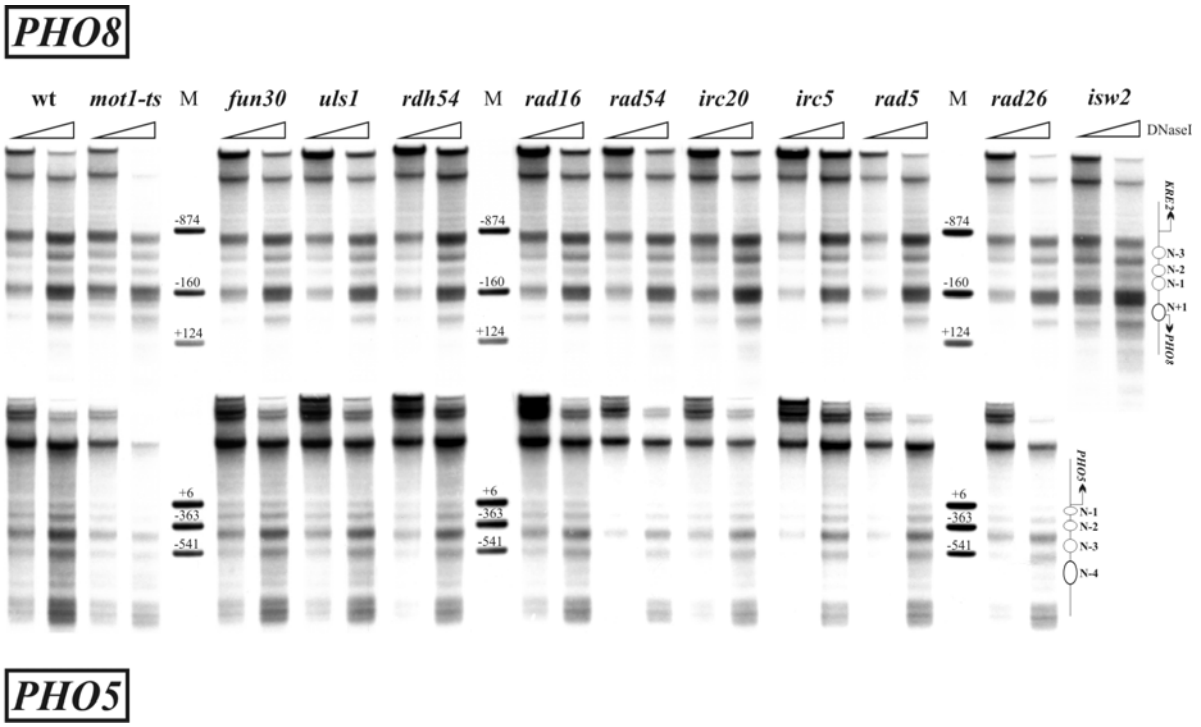

Figure 26. All non-essential Snf2-type ATPases as well as Mot1 are not necessary for proper nucleosome positioning at the *PHO8* and *PHO5* promoter *in vivo*.

DNaseI indirect endlabelling of the *PHO8* and *PHO5* promoter in a wildtype strain (BY4741) and in strains carrying deletion mutant alleles of the indicated Snf2-type ATPases or in a strain carrying a temperature sensitive allele of Mot1 (*mot1-ts*). Nuclei were prepared from cells grown logarithmically at 30°C. For the *mot1-ts* strain this corresponds to semi-permissive conditions. Schematics, ramps and markers as in Figure 8B.

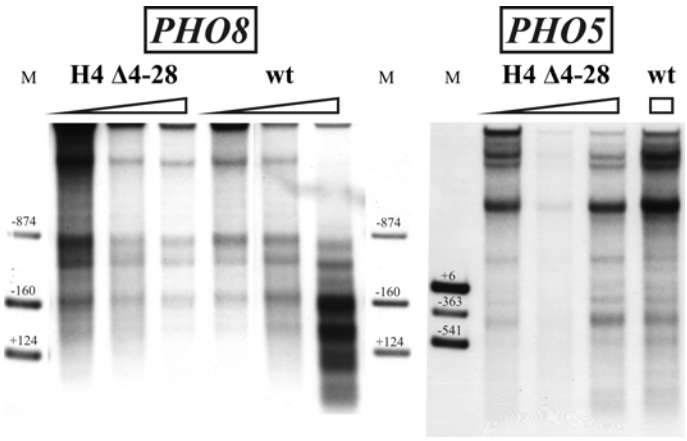

Figure 27. Histone H4 N-terminal tails are dispensable for proper nucleosome positioning at the *PHO8* and *PHO5* promoters.

DNaseI indirect endlabelling analysis of the *PHO8* and *PHO5* promoter regions in a wildtype strain (PKY899) and a strain carrying an allele that encodes an N-terminally truncated version of histone H4 (Δ4-28; PKY813). Nuclei were prepared after logarithmic growth at 30°C. Ramps, markers and schematics as in Figure 8B.

Other remodelers can act independently of the H4 N-terminal tail [160], but not all putative remodelers have been tested in this regard. We analysed positioning at *PHO5* and *PHO8* in a mutant lacking the H4 N-terminal tail (H4 Δ4-28). Positioning at both promoters was unaltered in this strain (Fig. 27). Moreover, an extract from the *isw1 isw2 chd1* triple mutant was able to generate proper nucleosome positioning *in vitro* (Hertel and Korber, unpublished observations). A mutant carrying the temperature sensitive *mot1-1* allele showed no changes at the semi-permissive temperature of 30°C (Fig. 26), even though such conditions already lead to *mot1*-specific phenotypes [207].

To test the essential RSC remodeling complex, we performed immunodepletion of a WCE prepared from a strain carrying a myc-tagged Sth1 subunit (the ATPase of the RSC complex). The first immunodepletion removed most of the RSC complex but there was still a considerable amount of residual Sth1 visible by Western analysis (Fig. 28A). This partially depleted extract reconstituted positioning at *PHO8* considerably less well than a mock-depleted wildtype extract or the non-depleted original myc-Sth1 extract (Fig. 28B). A second immunodepletion was even more efficient as judged by the disappearance of the Sth1 band in the Western blot (Fig. 28A). However, and contrary to the first experiment, this extract, though devoid of any detectable amounts of RSC, again reconstituted nucleosome positioning at *PHO8* rather well, though less clearly (Fig. 28C). So we could not pinpoint a role for RSC by immunodepletion.

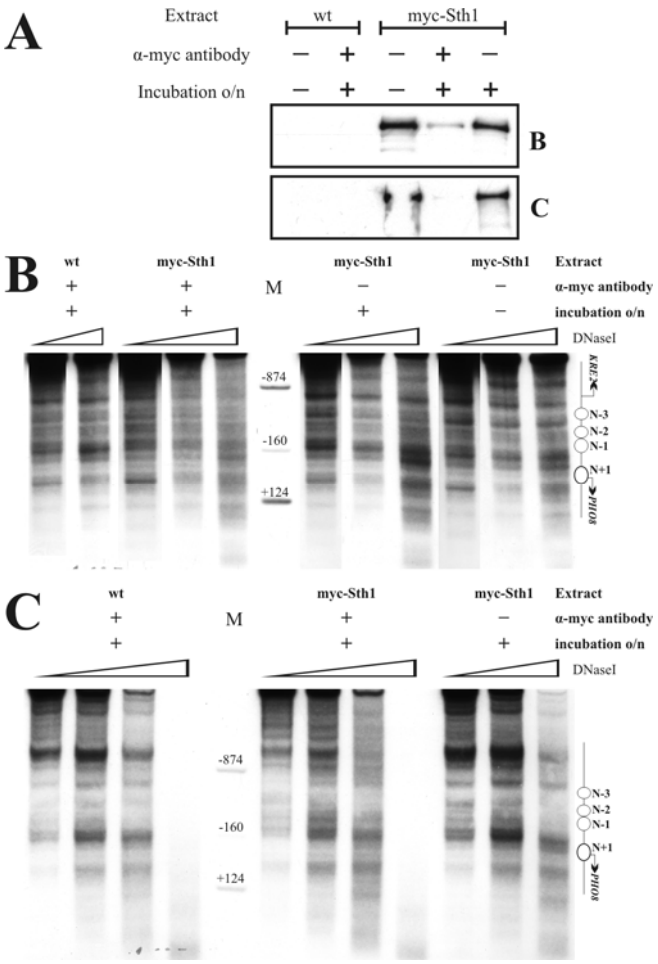

Figure 28. Immunodepletion of RSC from the WCE had variable influence on the positioning activity.

(A) Western blot analysis to detect remaining Sth1-9xmyc after immunodepletion. WCE extract from strain FT4 (wt) or from strain FT4 *STH1-9MYC::TRP* were immunodepleted with or without anti-myc antibody. Top ("B") and bottom ("C") samples were used for the experiments in panels **(B)** and **(C),** respectively. **(B+C)** DNaseI indirect endlabelling analysis of pre-assembled pP8apin **(B)** or pUC19-*PHO8*-short **(C)** plasmids incubated with the extracts described in **(A)**. Schematics, ramps and marker as in Figure 8B.

Meanwhile, Parnell *et al.* published global effects on nucleosome occupancy in an *sth1* temperature sensitive degron strain (*sth1-td*) upon growth at the non-permissive temperature using a low resolution custom microarray . There were no changes at the *PHO8* promoter, even though a moderate amount of RSC complex binding was detected via the myc-tagged Rsc3 and Rsc8 subunits [140] (Fig. S4A). In combination with our immunodepletion results, this was taken as evidence that also the RSC complex did not play an essential role in nucleosome positioning at *PHO8*. Collectively, it seemed at first that no remodeler ATPase had an essential role in nucleosome positioning at the *PHO8* promoter. Nonetheless, none of these experiments could exclude that two (or more) remodelers have redundant functions in nucleosome positioning at *PHO5*/*PHO8*.

Second, we checked the essential histone chaperone Spt6 that was shown to be required for reassembly of *PHO5* and *PHO8* promoters chromatin after transcriptional shutdown [208]. Using the *spt6-1004* allele at the published non-permissive conditions (2 h at 39°C [208]) we noticed no changes in the nucleosome pattern at the *PHO5* and *PHO8* promoters (data not shown).

Third, an *htz1* mutant, deleted for the gene encoding the histone H2A variant H2A.Z that was discussed to contribute to nucleosome positioning at the *GAL1* promoter [209] and to alter the intrinsic sequence preferences of the histone octamer [210, 211], also displayed the wild type DNaseI pattern (*PHO8*: Fig. S1; *PHO5*: data not shown).

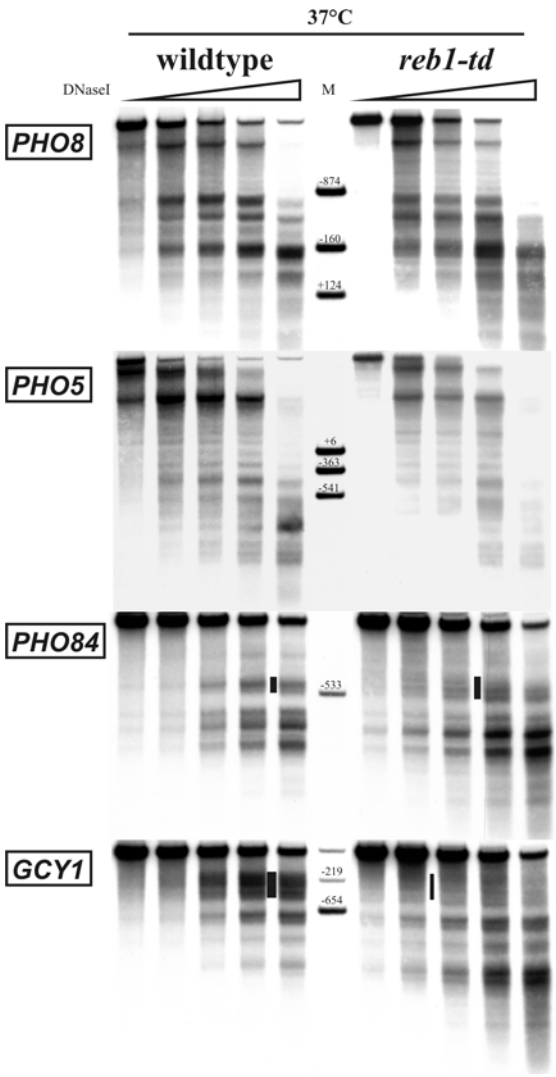

Figure 29. In contrast to *GCY1*, nucleosome positioning at the *PHO8* and *PHO5* promoter is not altered after ablation of Reb1.
DNaseI indirect endlabelling analysis of the indicated promoters in a wildtype strain (YKL200) and a strain carrying a temperature sensitive degron allele of Reb1 (*reb1-td*). Cells were grown logarithmically at 25°C in YPRaff + Gal medium and then shifted to 37°C overnight. Black bar on the *GCY1* blot marks the long NDR upstream of *GCY1* that became inaccessible (thinner bar) upon Reb1 inactivation. Other labels as in Figure 8B.

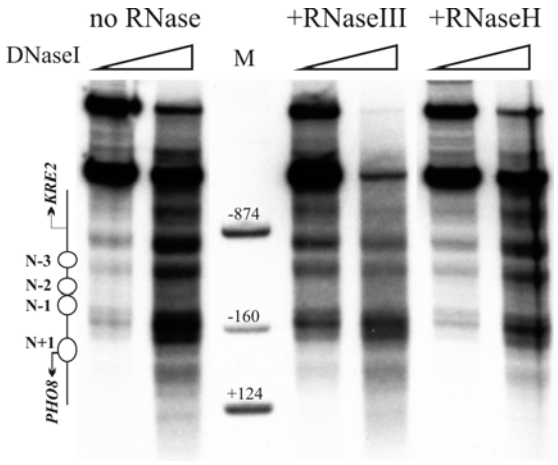

Figure 30. "The *PHO8* nucleosome positioning activity" is unlikely to have an RNA component.
DNaseI indirect endlabelling analysis of pre-assembled pUC19-*PHO8*-long plasmids incubated with WCEs that were pre-treated with RNaseIII (cleaves double-stranded RNAs) or RNaseH (cleaves RNA/DNA hybrids) for 1 h. Schematics, ramps and markers as in Figure 8B.

Fourth, we knew that an extract from the *pho4 pho2 cpf1* triple mutant also generated the proper nucleosome positioning pattern *in vitro* [175], and this mutant showed the same nucleosome positioning *in vivo* as the wildtype strain (data not shown). Further, neither Pho4/Cbf1 binding sites mutants *in vitro* (data not shown) nor *pho4* deletion mutants *in vivo* [183, 212] showed an altered positioning at the *PHO8* promoter.

Fifth, the abundant sequence specific binding factor Reb1 was previously implicated as a positioning factor at many loci [42, 138, 139]. The *PHO5* promoter lacks putative Reb1 binding sites, however the *PHO8* promoter harbours a putative Reb1 site in the NDR upstream of *KRE2*, i.e. in a position where Reb1 could act as nucleosome excluding factor. Since Reb1 is essential, we constructed a temperature sensitive degron mutant (*reb1-td*). Even after extended incubation at the non-permissive temperature positioning at *PHO8* (and *PHO5*) was unaltered (Fig. 29). As a positive control, we analysed positioning at the *GCY1* locus. This locus features a long NDR with a Reb1 binding site. Removal of this Reb1 site results in increased nucleosome occupancy over the *GCY1* NDR [213], as confirmed in our *reb1-td* mutant under repressive conditions (Fig. 29). This all together argued against an essential role for any of the factors that were show or implicated to function at the *PHO8* and *PHO5* promoters [183, 212, 214] and that could have acted as boundary factors for nucleosome positioning [107].

Finally we considered a role for a non-protein factor, like RNA, in nucleosome positioning at *PHO5* and *PHO8*. The WCE is very rich in RNAs (data not shown). Previous treatment of the WCE with RNase A, an enzyme that cleaves single stranded RNAs, did not reduce the extract's ability to reconstitute proper positioning [215]. We elaborated on this pilot experiment and treated WCE also with RNase III (cleaves double stranded RNAs) and RNase H (cleaves RNA in a RNA/DNA duplex). WCE treated with either of these RNases was able to properly reconstitute nucleosome positioning at *PHO5* and *PHO8* (*PHO8*: Fig. 30; *PHO5*: data not shown). In addition, RNAs were almost entirely removed during the fractionation described below without loss of the positioning activity for *PHO8*. These results argued against a role for RNA in determining positioning, at least at *PHO5*/*PHO8*, though these experiments could still not exclude that some inaccessible / indigestible / complex-bound RNAs were involved.

2.6.2. Fractionation of the whole cell extract

Our candidate approach failed to identify any positioning factor(s) for *PHO5* and *PHO8*. We therefore turned to an unbiased approach: fractionation of the WCE. We fractionated the WCE and tested the individual fractions in our *in vitro* system for their ability to reconstitute nucleosome positioning, chiefly at the *PHO8* promoter. In contrast to the *PHO5* promoter, where proper nucleosome positioning *in vitro* was very sensitive to perturbations of the system, *PHO8* in contrast proved to be a highly suitable test promoter since even trace amounts of the positioning activity still gave visible changes of the DNaseI pattern (Fig. 15 and data not shown). Consequently, it was possible to test many different fractionation steps on a small scale before running the final purification on a larger scale. In the end, we planned to identify the positioning factors by mass-spectrometry analysis of the final fraction positive for proper positioning.

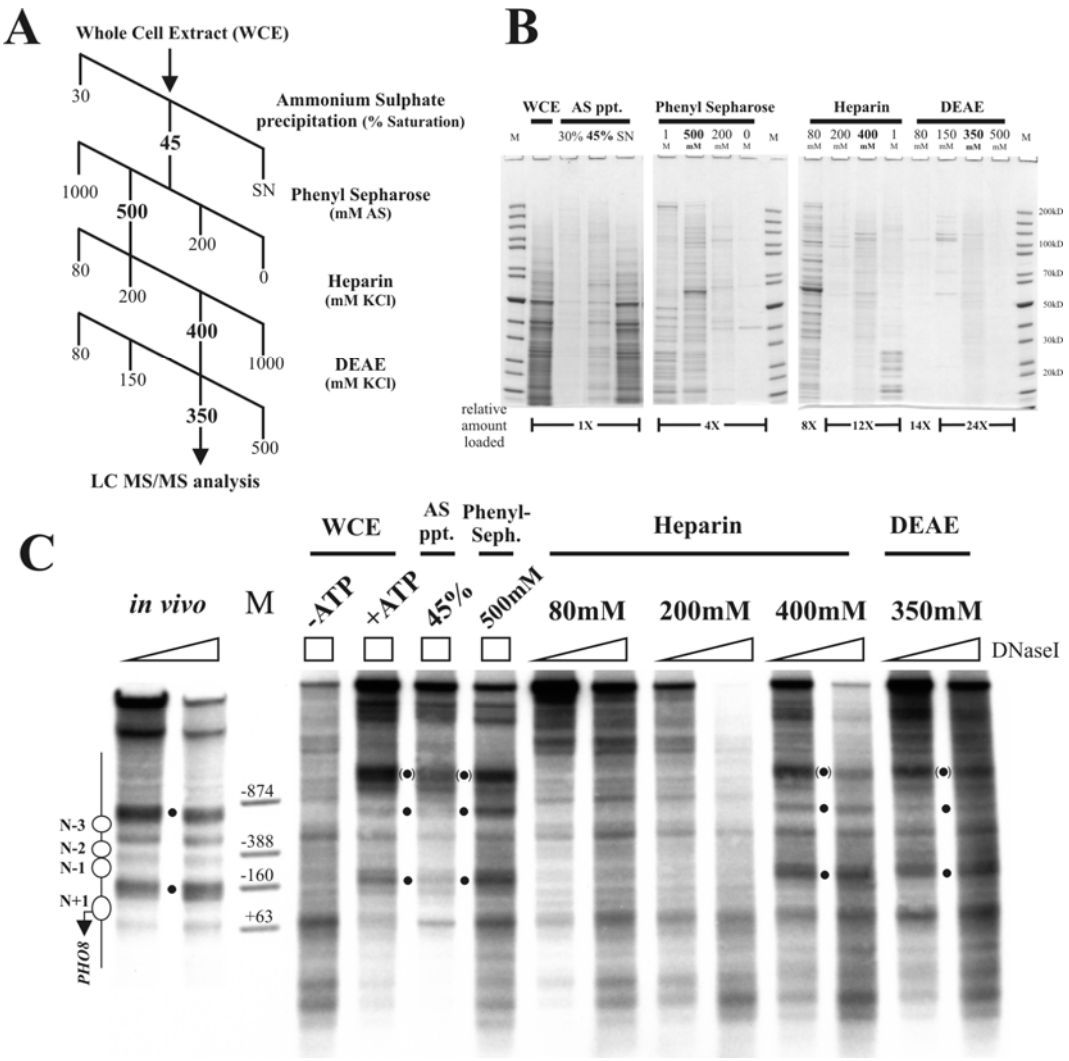

Figure 31. Enrichment of the "*PHO8* nucleosome positioning activity" over four sequential purification steps.

(A) Schematic overview of the four purification steps to enrich the nucleosome positioning activity for *PHO8*. Fractions containing the activity are highlighted in bold. Protein content of the last positive fraction (350mM KCl DEAE) was analyzed by mass-spectrometry (LC-MS/MS). SN, supernatant. **(B)** Analysis of the protein content of WCE and fractions on a 4-12% acrylamide SDS-PAGE gel stained with colloidal coomassie. 1 µl of WCE was loaded and the relative amount of the fractions as indicated below the lanes such that the total volume of each fraction in relation to the total volume of the input (WCE) sample was taken into account. Sizes of some marker bands as indicated. **(C)** Comparison of the *in vivo* (strain BY4741, 30°C log phase) DNaseI pattern with the patterns generated *in vitro* by WCE or some of the WCE fractions (see panel A) on pUC19-*PHO8*-short plasmids. ATP addition as indicated. Black dots mark the diagnostic bands of the *in vivo* pattern that are seen *in vitro* only in the presence of ATP and the nucleosome positioning activity. Black dots in brackets denote a DNaseI accessible region within the lacZ ORF of the pUC19 backbone that was co-generated by the nucleosome positioning activity for the *PHO8* promoter. Schematics, markers and ramps as in Figure 8B.

After initial screening of various column materials for affinity-chromatography we traced the positioning activity over four sequential steps (Fig. 31A and C). The first step was a sequential ammonium sulphate precipitation (Fig. 32A), which proved to be very useful. Firstly, the positioning positive fraction ("45%" saturation) contained only a minor proportion of the total protein input as most proteins did not precipitate at 45% ammonium sulphate saturation (Fig. 31B). Secondly, pelleting of the positioning activity allowed for concentrating the sample, which counteracted the overall dilution of the positioning activity during subsequent steps. Finally, the "45% pellet" was re-suspended in buffer containing 1 M ammonium sulphate, which was the starting buffer for the subsequent phenyl-sepharose column, allowing to omit one buffer exchange dialysis step.

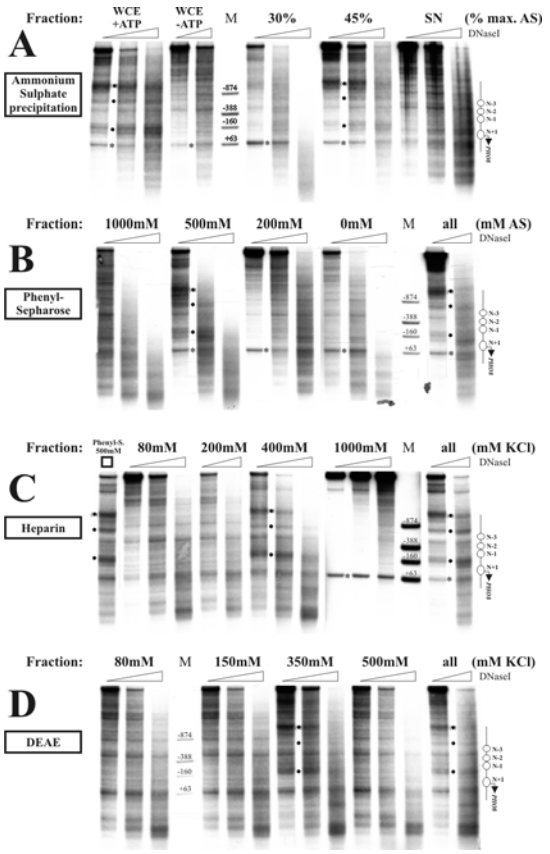

Figure 33. Positioning assays for all fractions collected during the four-step WCE fractionation.

(A-D) DNaseI indirect endlabelling analysis of pre-assembled pUC19-*PHO8*-short plasmids incubated with the indicated fractions in the presence of ATP or with WCE in the presence or absence of ATP. Asterisks mark artefact bands generated by a star activity of the BglII restriction enzyme used for secondary cleavage. Other labels as in Figure 31. **(B-C)** "all" indicates that all fractions collected during the corresponding purification step were pooled again in the same reconstitution reaction.

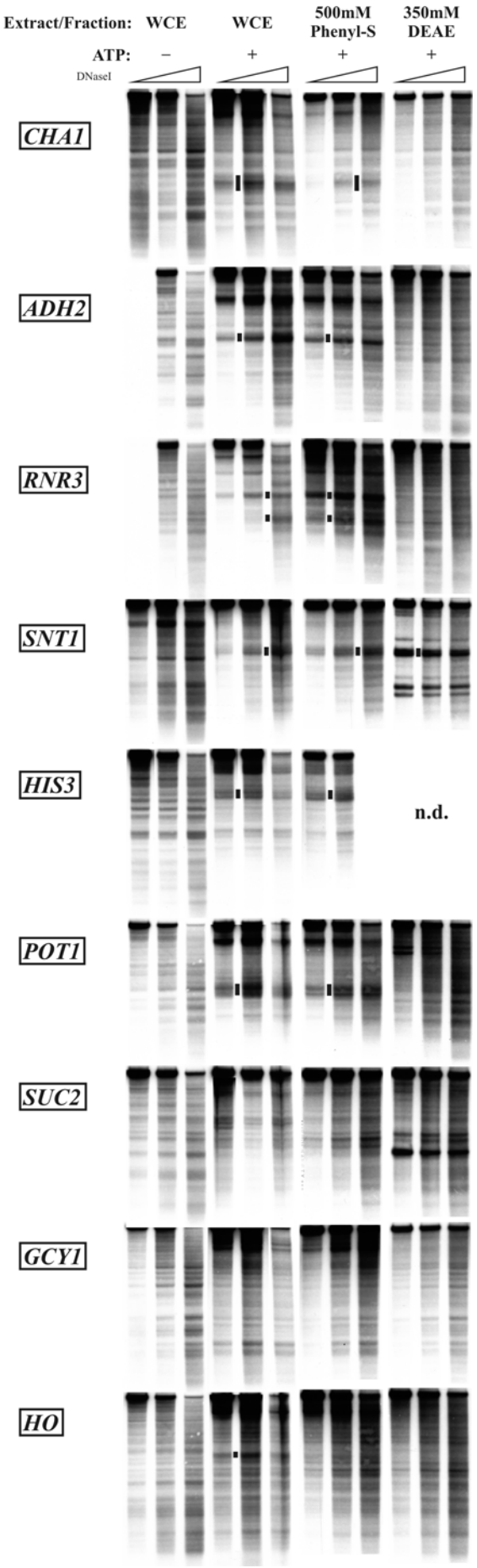

Figure 32. The "500 mM Phenyl Sepharose" fraction, but not the "350 mM DEAE" fraction, contained the positioning activity for most loci.

DNaseI indirect endlabelling analysis of pre-assembled pUC19 plasmids with the indicated loci, incubated with the WCE, fractions (Fig 31) and ATP as indicated. Labels as in Figure 32. WCE samples were run on the same, but the fraction samples on separate gels. "n.d." not done. Bars in between lanes denote strong *in vivo*-like NDRs.

The next three fractionations were carried out by column-chromatography: first based on hydrophobicity (phenyl sepharose, Fig. 32B), next by cation-exchange (Heparin, Fig. 32C) followed by anion-exchange (DEAE, Fig. 32D). Importantly, the positioning activity was only ever found in one fraction and it was never necessary to combine fractions to regain the positioning activity (Fig. 32A-D). Overall, this four step purification scheme greatly reduced the complexity of the protein mix (Fig. 31B) with only a very moderate concomitant loss of the positioning activity. Even the final positive fraction (350 mM DEAE) was able to reconstitute positioning at *PHO8* quite well (Figs. 31C and 32D).

We also tested some of the fractions that could properly position nucleosomes at *PHO8* for their positioning activity at the *ADH2*, *RNR3*, *SNT1*, *CHA1*, *GCY1*, *SUC2*, *HO*, *HIS3* and *POT1* loci. The 500 mM ammonium sulphate phenyl sepharose fraction was able to generate *in vivo*-like nucleosome positioning at almost all tested loci as well as the WCE (Fig. 33). In contrast, the final 350 mM DEAE fraction was only positive for *PHO8* (Fig. 31C, 32D), *SNT1* and possibly *GCY1* (though even the full WCE did not alter the DNaseI pattern much at *GCY1*) but not at any other tested locus (Fig. 33). This demonstrates that distinct factor(s) are required for different loci in our *in vitro* system, which could be separated by our fractionation scheme.

In a separate experiment, we also tested fractions positive for *PHO8* for their effects on *PHO84* (Fig. 34A). Addition of either the 450 mM Heparin or the 350 mM DEAE fraction disturbed the *in vivo*-like positioning set up by salt assembly (Figs. 10 and 34B). Since the full WCE did not show this effect, something must have been lost during the purification process that normally protects/improves the proper positioning set up by salt assembly. The *PHO84* locus was our best example for intrinsic DNA sequence preferences directing *in vivo*-like positioning. Nevertheless, this positioning was not stable in the presence of a sub-fraction of the WCE. This raised the question of whether even those positions that could be specified by intrinsic DNA sequence preferences alone were stable in the presence of the nuclear protein environment (remodelers, chaperones and DNA binding factors). At least for the case of *PHO84*, intrinsic proper positioning evidently required some factor in the WCE that maintained proper positioning in the presence of other "counteracting" activities.

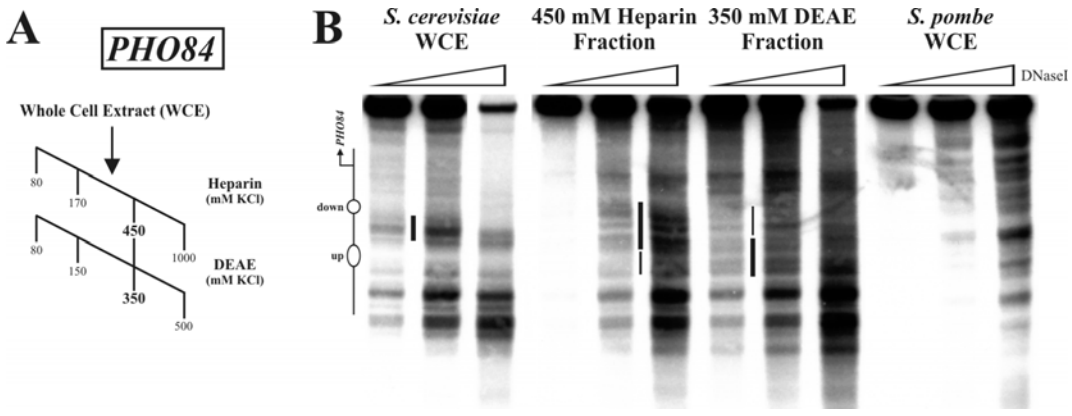

Figure 34. Fractions positive for the "*PHO8* positioning activity" disrupted the *in vivo*-like DNA-intrinsic nucleosome positioning at the *PHO84* promoter.

(A) Schematic overview of the two-step purification scheme yielding fractions used in **(B)**. **(B)** DNaseI indirect endlabelling analysis of pre-assembled pUC19-*PHO84* plasmids incubated with the indicated WCEs and fractions in the presence of ATP. Schematics on the left show the approximate positions of the upstream and the downstream nucleosome (Fig. 7) that were disrupted by the addition of either of the fractions. Bars in between lanes demark the accessible sites in the region of the up- and the downstream nucleosome. Ramps and schematics as in Figure 16.

We analyzed the protein content of the final positive fraction (350 mM DEAE) by LC-MS/MS mass spectrometry and identified 212 proteins (see Table S2 of [186]). 95 of these were localized exclusively to the cytoplasm, leaving 117 proteins of nuclear (though not necessarily exclusively) or of unknown localization [216]. Several of these (potentially) nuclear proteins were considered as candidates to contribute to the "nucleosome positioning activity" either because they were previously shown to play a role in nucleosome positioning at other loci or because of their close links to chromatin and/or transcription (Table S1). These new candidates were tested *in vivo* and/or in our *in vitro* assay.

2.6.3. Many of the new candidates identified by LC-MS/MS did not play role in positioning at the *PHO8* promoter

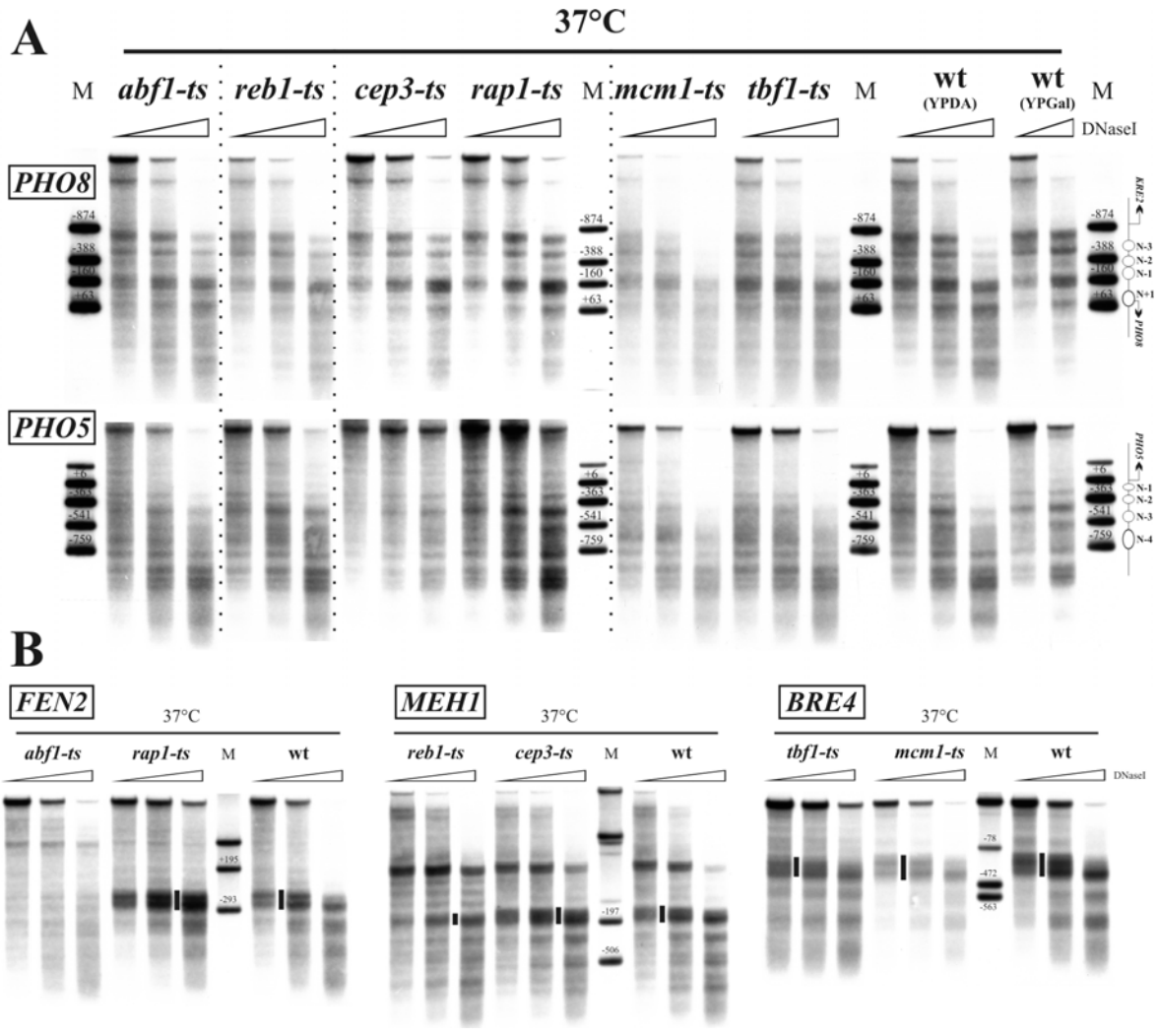

Figure 35. None of the tested essential sequence specific DNA binding proteins was required for proper positioning at the *PHO8* promoter.

(A) DNaseI indirect endlabelling analysis of the *PHO8* and *PHO5* promoter regions in a wildtype strain (wt; BY4741) or in strains carrying a temperature sensitive (*ts*) allele of the indicated genes. Strains were grown logarithmically at 25°C and then shifted to the non-permissive temperature (37°C) overnight. Wildtype strain was grown either in YPDA or YPGal. Stippled lines indicate where samples were run on separate gels. All other labels as in Figure 26. **(B)** Same as for **(A)** except for the indicated promoter regions. Bars in-between lanes mark the intensity and extent of DNaseI hypersensitive sites.

During the analysis of our mass spectrometry data Badis *et al.* published genome-wide changes of nucleosome occupancy in strains carrying temperature sensitive alleles of the genes encoding the essential DNA binding factors Abf1, Reb1, Rap1, Mcm1, Tbf1 and Cep3 [138]. They found no significant changes in nucleosome occupancy at the *PHO8* promoter in any of these strains under restrictive conditions. Since Abf1, Rap1 and Cep3 were detected in our final fraction and since the *PHO8* promoter harbours putative binding sites for Reb1, Mcm1, Tbf1 and Cep3 (Fig. 6), we analyzed the respective temperature sensitive strains from Badis *et al.* by DNaseI indirect endlabelling after extended growth at the non-permissive temperature (over night instead of 3-7h). Even at these more restrictive conditions, we found no changes in the chromatin structure at the *PHO8* promoter in all six strains (Fig. 35A) confirming the results of Badis *et al.* and our previous results for Reb1 (Fig. 29). As positive control, we analyzed loci with the greatest increase in nucleosome occupancy according to Badis *et al.*, i.e., at *FEN2*, *MEH1*, *BRE4*, *MUB1*, *MRPL49*, and *TVP38* for effects of ablating Abf1, Reb1, Tbf1, Rap1, Mcm1, and Cep3, respectively. For Abf1, Reb1, and Tbf1 we confirmed the results of Badis *et al.*, whereas for unknown reasons we saw no effects at the reported positive control loci for Rap1, Mcm1, and Cep3 (Fig. 35B and data not shown). Nevertheless, our results in combination with those of Badis *et al.* argue that these six DNA binding factors do not contribute to nucleosome positioning at the *PHO8* promoter.

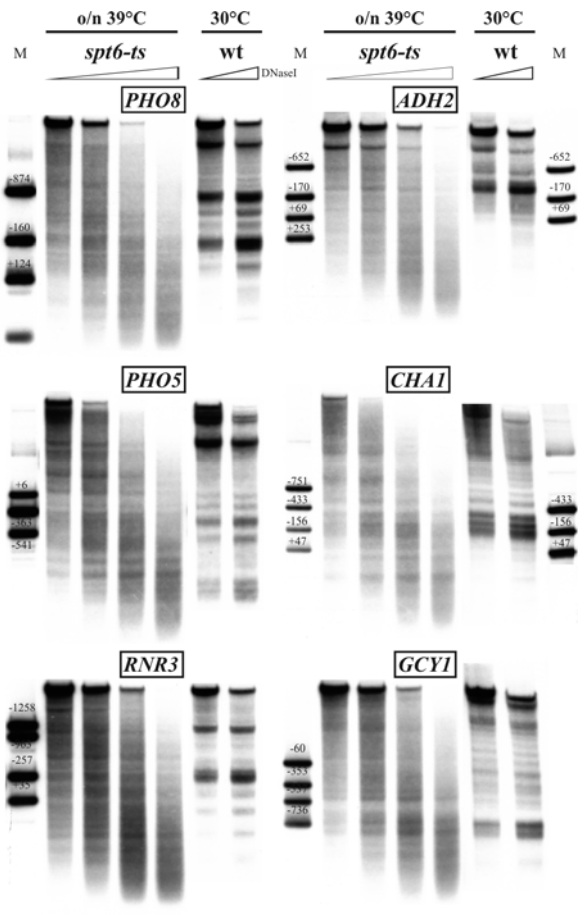

Figure 36. Incubation of the *spt6-ts* strain at the non-permissive temperature for an extended time led to a global loss of nucleosome positioning.

DNaseI indirect en labelling analysis of the indicated promoter regions in a wildtype strain (BY4741) or a strain carrying the temperature sensitive allele *spt6-1004* grown logarithmically at 25°C and then shifted to 39°C overnight (spt6-1004) or grown logarithmically at 30°C (BY4741). Ramps and markers as in Figure 10.

In addition, we excluded a role for the Hap2/3/4/5 complex and for the putative transcription factor Sef1, which were also present in our final fraction, by DNaseI indirect endlabelling analysis of the respective deletion mutants (Table S1 and Fig. S1).

Although we had previously tested Spt6 (see above chapter 3.6.1), we noticed that it came up prominently in the MS analysis of our final fraction (Table S1 and [169]) as well as in the MS analysis of earlier less pure fractions (data not shown). Furthermore, Spn1, a factor that physically interacts with Spt6 [217], was also present. We therefore analysed the temperature sensitive *spt6-1004* mutant again after extended (over night instead of 2h) growth at the non-permissive temperature (39°C). DNaseI indirect endlabelling analysis showed greatly reduced specific positioning over the entire *PHO8* promoter (Fig. 36). However, also at many other loci (*ADH2*, *CHA1*, *GCY1*, *PHO5*, *RNR3*; Fig. 36) nucleosome positioning was lost. Importantly, we did not observe such global deleterious effects on chromatin structure for

any of the other *ts* strains we analyzed. An extract prepared from an *spt6-1004* strain grown at 39°C overnight failed to reconstitute nucleosome positioning at the *PHO8* promoter (Fig. 37A). However, this extract failed to reconstitute positioning also at five other tested loci (*ADH2*/*RNR3*: Fig. 37A; *PHO5*/*CHA1*/*GCY1*: data not shown). In contrast, extracts from both the *spt6-1004* mutant as well as from the wildtype strain that were grown for only four hours at 39°C reconstituted nucleosome positioning at the *PHO8* promoter, though slightly less well than a wt extract grown at 30°C (Fig. 37B). So high temperature by itself was already slightly deleterious to the wt extract, i.e. to some of the positioning factors. In summary, nucleosome positioning was not substantially affected for the *spt6-1004* mutant after 2h (*in vivo*) or 4h (*in vitro*) incubation at the non-permissive temperature, but was globally compromised after overnight incubation (both *in vivo* and *in vitro*). Spt6 might be required for general maintenance of chromatin integrity, maybe in connection with ongoing transcription, or these effects were merely caused by the incubation at the non-permissive temperature for such an extended time. In any case, we did not find a specific role for Spt6 in determining nucleosome positioning at the *PHO8* or any other promoter.

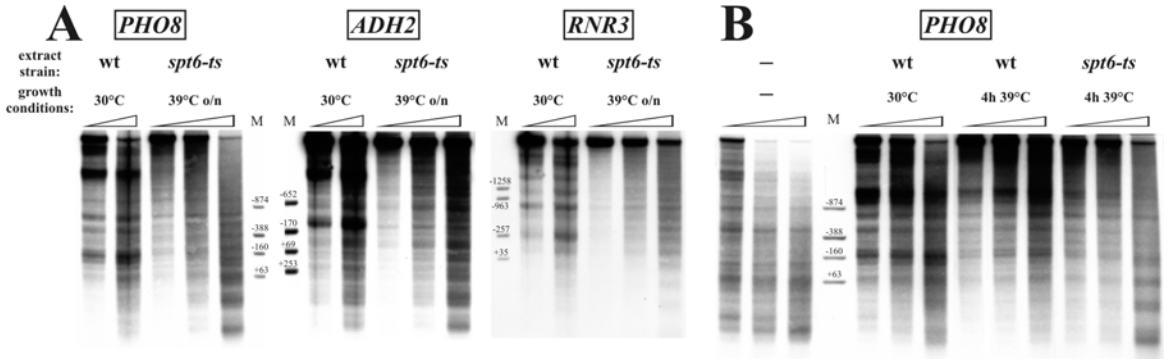

Figure 37. An extract made from the *spt6-ts* strain after overnight incubation at the non-permissive temperature failed to reconstitute proper nucleosome positioning *in vitro*.
(A) DNaseI indirect endlabelling analysis of pre-assembled pUC19-*PHO8*-long, pUC19-*ADH2* and pUC19-*RNR3* plasmids incubated with extract made from either a wildtype strain (BY4741) grown logarithmically at 30°C or from an *spt6-1004* strain grown at the non-permissive temperature (39°C) overnight. **(B)** as **(A)** but for the pUC19-*PHO8*-short plasmid and with the indicated shorter incubation times at 39°C. **(A-B)** Ramps and markers as in Figure 10.

Initially, we did not see any specific involvement of a remodeling enzyme (see 3.6.1). Maybe this was due to redundancy in remodeling activities. Alternatively, ATP-dependency and/or nucleosome sliding activity in our assay could be provided by a "non-canonical" nucleosome remodeling enzyme. The little described Yil091c protein was prominently identified by LC-MS/MS. This essential protein is a member of the DEAD-box RNA helicase family, which is related to the Snf2-type ATPases (Fig. 3). While Yil091c was previously linked to rRNA processing [218], we speculated that Yil091c might also act as nucleosome sliding machine and therefore be part of the "positioning activity". As no conditional mutants were available, we tested Yil091c *in vitro* by immunodepletion in an approach similar to the depletion of myc-Sth1 (Fig. 28). Extracts from a strain carrying TAP tagged Yil091c were efficiently immunodepleted for Yil091c-TAP (Fig. 38A). However, this depleted extract could still reconstitute proper positioning at *PHO8* suggesting that Yil091c did not contribute essentially to the "positioning activity" (Fig. 38B).

In addition to these promising candidates, we also tested many more non-essential factors, which were present in our final fraction, by analysis of the respective deletion mutants. This included the RNA Pol II subunit Rpb4, two subunits of the Paf1 complex and the Taf14 protein, a subunit of several chromatin associated complexes. None of the tested strains showed any alterations in the chromatin structure at the *PHO8* promoter (Table S1 and Fig. S1).

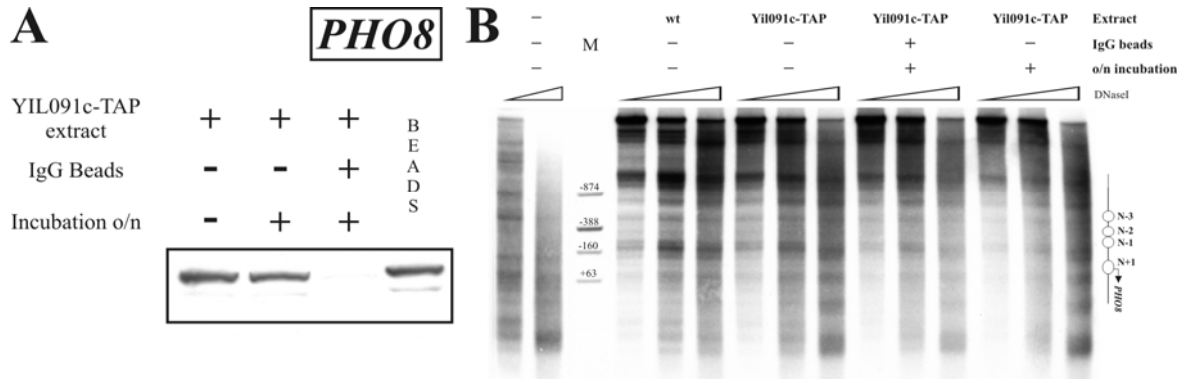

Figure 38. The putative RNA helicase Yil091c was not required to reconstitute nucleosome positioning at the *PHO8* promoter.
(A) Western blot analysis (PAP antibody) of immunodepletion of extracts from a strain expressing Yil091c-TAP. For comparison, boiled IgG Sepharose beads were also loaded ("BEADS"). **(B)** DNaseI indirect endlabelling analysis of pre-assembled pUC19-*PHO8*-short plasmids incubated with the extracts described in **(A)**. Schematics, ramps and marker as in Figure 8B.

2.6.4. Fractions positive for nucleosome positioning at *PHO8* contained an activity that specifically bound to the *PHO8* NDR1

The two major features of *PHO8* promoter chromatin that are properly reconstituted by the WCE and ATP are NDR1 and NDR3 (Fig. 6 and 31C). Sequence specific DNA binding factors were implicated in setting up such NDRs [131, 138, 139, 213]. Thus, we speculated that the nucleosome positioning activity in the WCE and in positive fractions may contain a sequence specific DNA binding protein (or proteins) that binds NDR1 and/or NDR3. This was tested by band shift assays. PCR fragments corresponding to NDR1 (= fragment #1) or NDR3 (= fragment #2) were terminally labelled with P^{32} (Fig. 39A) and incubated with WCE or positive fractions under the identical conditions as in the positioning assay. Some binding reactions also contained a 50-fold molar excess of poly(dI:dC) as unspecific competitor DNA to identify which interactions were sequence specific. Something in the final 350 mM DEAE fraction (Fig. 31A) bound both to fragment #1 and #2 in a concentration-dependent manner (Fig. 39B), but only the interaction with fragment #1 was specific (Fig. 39B, compare lanes 5 and 10 and Fig. 39C, compare lanes 5 and 13). Furthermore, there was binding to labelled fragment #1 even in the presence of 50 or 250-fold molar excess of unlabelled fragment #2 (Fig. 39C lane 6, and Fig. 39D lanes 6-7). As expected, a 50-fold molar excess of unlabelled fragment #1 was able to compete away the binding activity to labelled fragment #1 (Fig. 39D lane 8).

Removal of ATP increased the amount of shifted fragments (Fig. 39D lane 5) indicating that the binding of the unknown factor is stronger/more stable in the absence of ATP. We checked to what extent this binding activity correlated with our positioning activity. It was not present in the positioning negative (but comparatively still protein rich) 80 mM Heparin fraction (Fig. 31A and B)

(Fig. 39C lanes 7-8). The full WCE gave even two specifically shifted bands (Fig. 39D lane 13). The upper band corresponded to the band shift seen with the 350 mM DEAE fraction (Fig. 39D lanes 2-7), while the lower band shift ended up in the "SN" fraction of the first fractionation step (Fig. 31A), which contained the vast majority of the total protein amount from the WCE (Fig. 31B) (Fig. 39D lane 11). So the binding activity specific for fragment #1, i.e. binding to *PHO8* NDR1, co-fractionated with the nucleosome positioning activity and might thus be part of the positioning information. However, addition of a 20- or 100-fold molar excess of fragment #1 to a reconstitution reaction could not titrate the positioning activity away from the chromatin template as there was no noticeable effect on the reconstitution success (Fig. 40). So the specific binding activity for *PHO8* NDR1 was either present in even greater molar excess, or has a higher affinity for the fragment #1 sequence in the context of the entire chromatinised promoter, or is not part of the positioning activity after all.

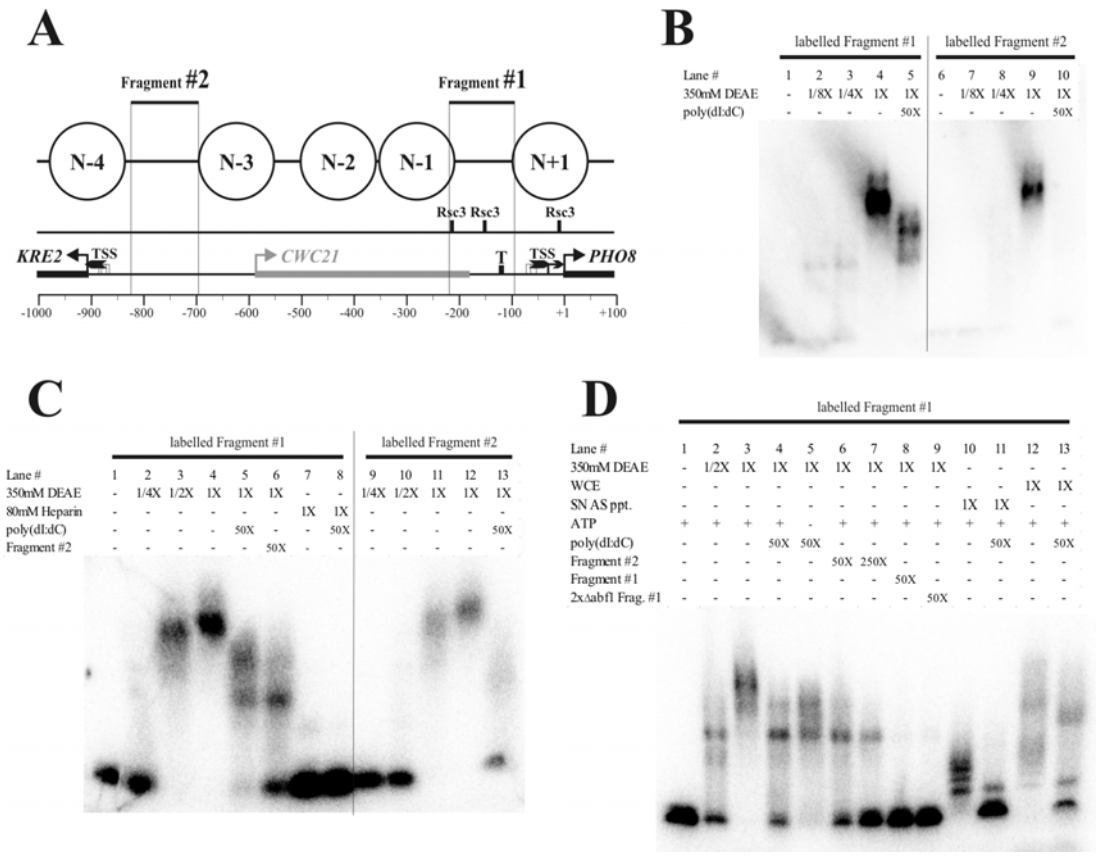

Figure 39. WCE as well as the "350 mM DEAE" fraction contained an unknown DNA binding activity specific for the *PHO8* NDR1.

(A) Schematics of the *PHO8* promoter (Fig. 7) showing the location of the two fragments used for band shifts in **(B-C)**. Figure is drawn to scale. **(B)** Band shift with labelled fragments #1 and #2. Labelled DNA fragments were incubated for 45 minutes at 30°C with increasing amounts of the "350 mM DEAE" fraction (Fig. 31) with or without poly(dI:dC) competitor in 50X fold molar excess as indicated. All samples contained 1.5 mM ATP. Samples were electrophoresed on a native 0.5X TBE 1.1 % agarose gel. **(C-D)** Same as **(B)** except for the indicated additional components "80 mM Heparin" and "SN AS ppt." fraction as in Fig. 31. poly(dI:dC), unlabelled fragment #2, unlabelled fragment #1 and unlabelled fragment #1 with two mutated putative Abf1 binding sites were added as competitors at the indicated molar excesses. All samples contained 1.5 mM ATP except for lane 5 .

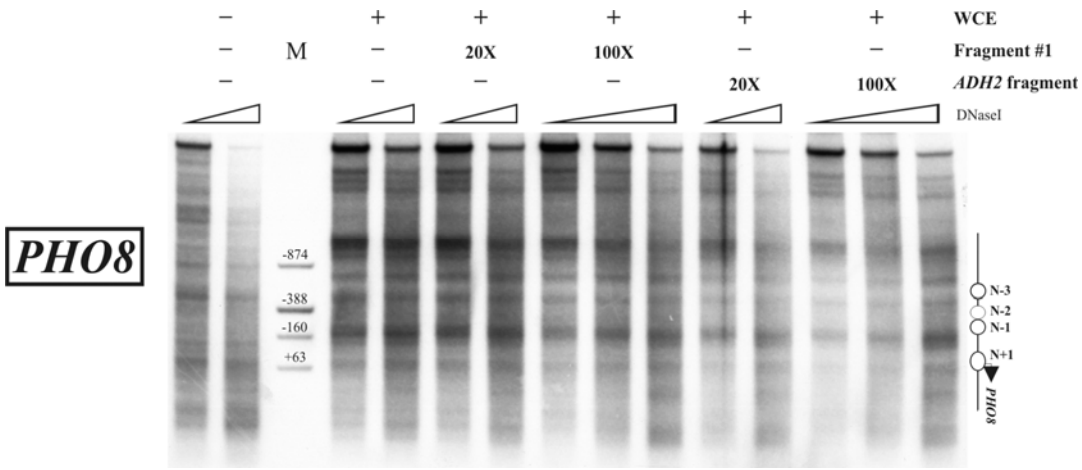

Figure 40. Competition with fragment #1 did not inhibit *in vitro* reconstitution of nucleosome positioning at the *PHO8* promoter.

DNaseI indirect endlabelling analysis of pre-assembled pUC19-*PHO8*-short plasmids incubated with WCE and ATP in the presence or absence of either fragment #1 (Figure 39A) or a 354 bp fragment that corresponds to region +381bp to +735bp of the *ADH2* ORF at the indicated molar excess. Ramps, schematics and marker as in Figure 8B.

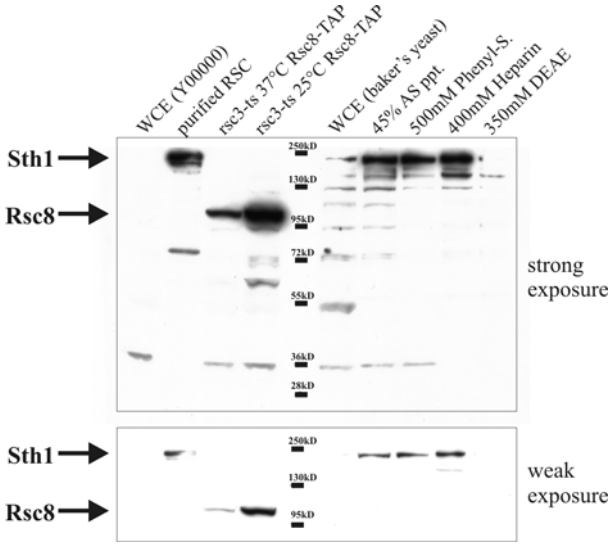

Figure 41. Sth1 is enriched in all fractions that carry the "*PHO8* positioning activity".

anti-Sth1 Western blot of various extracts and fractions. Extracts of the *rsc3-ts* Rsc8-TAP strain featured a strong band that corresponds to Rsc8-TAP. The TAP tag contains a protein A component and cross-reacts with the anti-Sth1 antibody. The missing/low Sth1 signal for WCEs is likely due to inefficient transfer of the large Sth1 subunit in the context of a WCE. The relative amounts loaded correspond to the amounts added to the reconstitution reactions in Figures 31 and 42-56 (1:5 ratio). Arrows indicate the bands that correspond to Sth1 and Rsc8. Molecular weight markers (in kDa) as indicated.

2.6.5. The RSC remodeling complex was required for proper nucleosome positioning at the *PHO8* promoter

The LC-MS/MS analysis identified 10 out of 17 subunits of the RSC remodeling complex in the final 350 mM DEAE fraction, and the ATPase subunit Sth1 was present in all positioning positive fractions (Fig. 41, see right half of the blot). However, results from us (Fig. 28) and others [140] suggested that RSC does not play a role in nucleosome positioning at the *PHO8* promoter. We therefore considered that RSC and some other remodeler could be redundantly involved. Arp9 was one of the proteins identified in the LC-MS/MS analysis with the highest MASCOT score [186]. This essential protein is one of three subunits (besides Arp7 and Rtt102) shared between the RSC and SWI/SNF remodeling complexes. Both complexes are members of the same remodeler subfamily, contain several more homologous subunits [219, 220] and display similar properties *in vitro* [221]. In an attempt to affect both remodeling complexes at the same time, we analyzed nucleosome positioning in a strain

carrying a temperature sensitive allele of *ARP9* (*arp9-ts*) [222] grown at the non-permissive temperature. Indeed, the *arp9-ts* strain displayed considerable alterations in the chromatin structure of the *PHO8* promoter. The DNaseI band corresponding to the *PHO8* NDR1 was diminished indicating increased nucleosome occupancy in this region (Fig. 42). Furthermore, the region normally protected by nucleosome N-3 became accessible to DNaseI cleavage, which resulted in a long hypersensitive region reaching from NDR2 to NDR3 and indicated a loss of this nucleosome (Fig. 42).

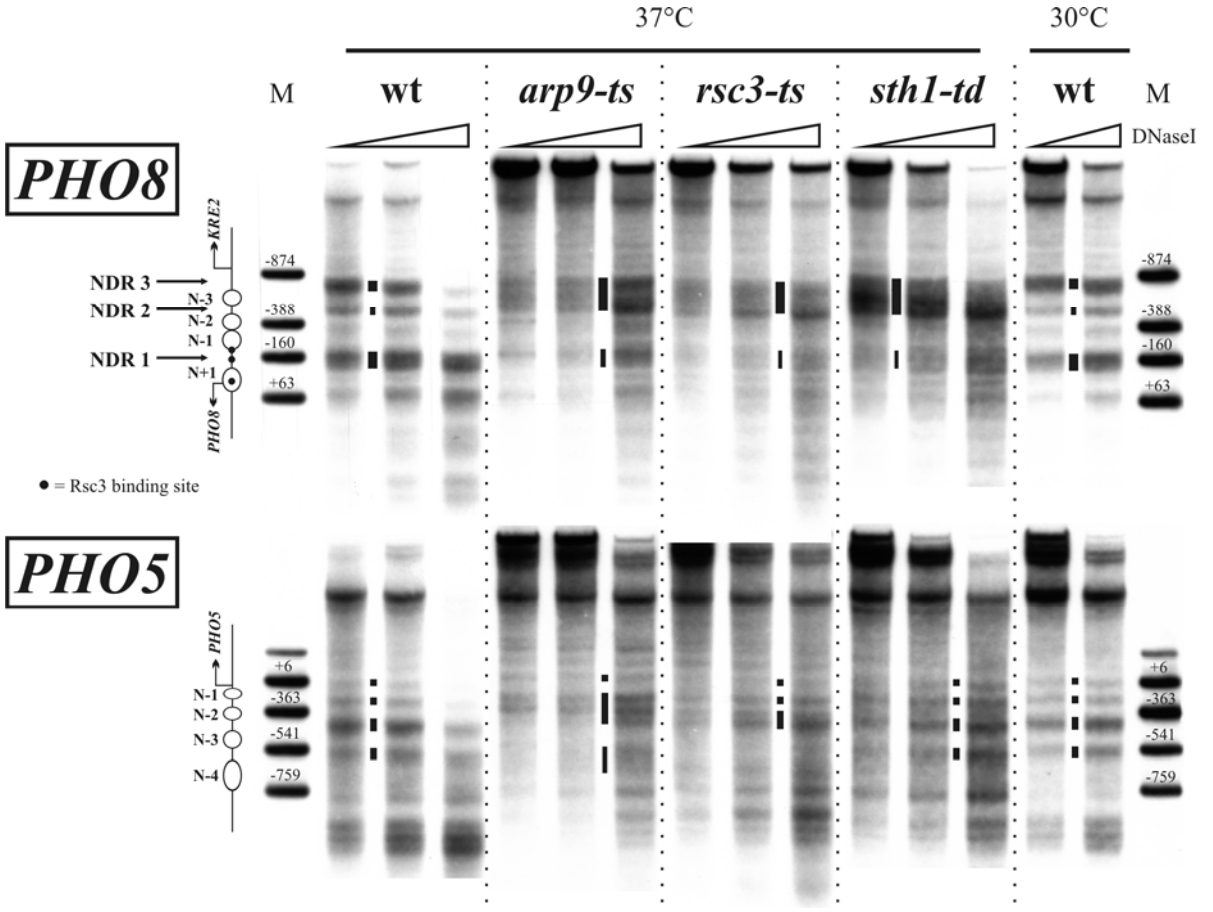

Figure 42. Ablation of RSC subunits altered chromatin structure at the promoters of *PHO8* and *PHO5* .

DNaseI indirect endlabelling analysis of the *PHO8* and *PHO5* promoter regions in a wildtype strain (wt; BY4741) and strains carrying a temperature sensitive (ts) or temperature sensitive degron (td) allele of the indicated RSC subunits. Strains were grown logarithmically at 25°C and then shifted to the non-permissive temperature (37°C) overnight. Wt nuclei also for logarithmic growth at 30°C. Bars in-between lanes mark the intensity and extent of DNaseI hypersensitive sites. Samples separated by stippled lines were not electrophoresed alongside on the same gel. Schematics, ramps and markers as in Figure 8B.

In the meantime, Badis *et al.* published genome-wide nucleosome occupancy changes upon ablation of Rsc3 (*rsc3-ts*) another essential RSC subunit [138]. At *PHO8*, they noticed a very similar increase in nucleosome occupancy over NDR1 and some less clear effects in the region of N-3 (Fig. S4A). We analysed positioning in this *rsc3-ts* strain by DNaseI indirect endlabeling and found very similar alterations at the *PHO8* promoter as in the *arp9-ts* strain (Fig. 42). The reduced accessibility in the region of NDR1 was even more pronounced. We confirmed these results via restriction enzyme accessibility at sites within NDR1 (HindIII), nucleosome N-3 (HpaI), and NDR2 (NheI). Accessibility of NDR2 was unaffected in the *arp9-ts* and *rsc3-ts* strains as expected from the unchanged DNaseI pattern here (Fig. 43A). Also in keeping with the DNaseI patterns HpaI accessibility increased in the *arp9-ts* and *rsc3-ts* strains (49% and 47%, respectively, compared to 27% for wildtype), indicating an at least partial loss of this nucleosome, and the high accessibility (75%) of HindIII was slightly diminished in the *arp9-ts* (64%) and strongly reduced in the *rsc3-ts* (43%), as expected for the diminished hypersensitivity here (Fig. 42).

In light of these strong effects on *PHO8* promoter chromatin structure upon compromising two essential subunits of the RSC complex we decided to analyse positioning in the degron-sth1 (*sth1-td*) strain used by Parnell *et al.* [140]. Indeed, and in contrast to the results by Parnell *et al.*, the DNaseI pattern seen for this strain closely resembled that of the *arp9-ts* and *rsc3-ts* strains (Fig. 42). As Rsc3 and Sth1 are subunits unique for the RSC complex we concluded that the effects seen with the *arp9-ts* strain were likely independent of the SWI/SNF complex.

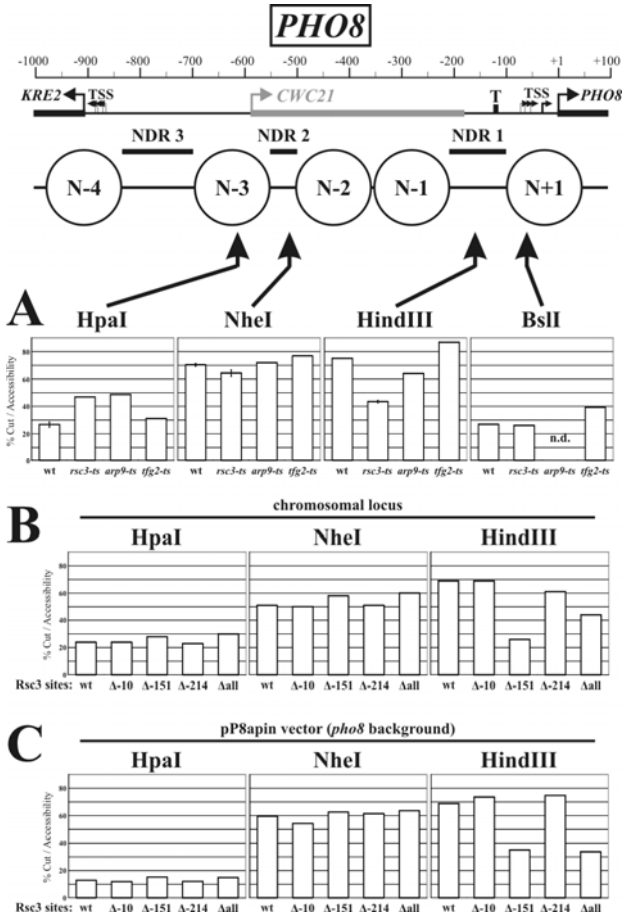

Figure 43. Ablation of RSC subunits or the TFIIF subunit Tfg2 and mutation of the Rsc3 binding site at -151 led to changes in restriction enzyme accessibilities at the *PHO8* promoter.

(A) Nuclei isolated from a wildtype strain (wt; BY4741) and strains carrying a temperature sensitive (ts) allele of *RSC3*, *ARP9* and *TFG2* grown at 37°C overnight were digested with the indicated restriction enzymes. Schematics of the *PHO8* promoter as in Figure 7. Arrows indicate the position of the corresponding restriction site. Error bars correspond to the variation of two biological replicates. n.d., "not determined". **(B)** Same as **(A)** but nuclei from strains grown logarithmically at 30°C and carrying mutations in none (wt), one (Δ-10, Δ-151 or Δ-214) or all (Δall) of the three predicted Rsc3 binding sites at chromosomal location of the *PHO8* promoter.
(C) Same as **(B)** but nuclei were isolated from a *PHO8* strain carrying the pP8apin vector with the Rsc3 site mutations described in **(B)**.

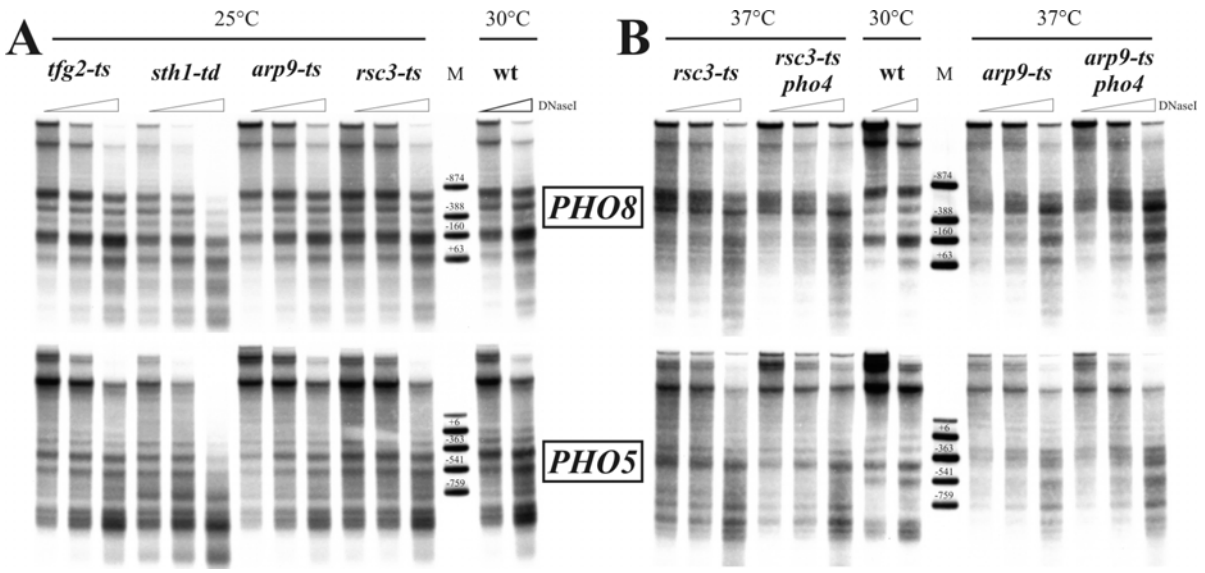

Figure 44. The chromatin effects seen with the RSC *ts* strains were Pho4-independent and were only seen at the non-permissive temperature.

(A) DNaseI indirect endlabelling analysis of the *PHO8* and *PHO5* promoter regions in strains carrying a temperature sensitive (*ts*) allele of the indicated RSC subunits or Tfg2 grown logarithmically at 25°C. All labels as in Figure 39. **(B)** Same as **(A)** except for strains carrying a temperature sensitive (*ts*) allele of the indicated RSC subunits either alone or in combination with a deletion mutant allele of Pho4. Strains were grown logarithmically at 25°C and then shifted to the non-permissive temperature (37°C) overnight. Wt nuclei also for logarithmic growth at 30°C.

Strains carrying the respective deletions of the non-essential RSC subunits Rsc30 and Rtt102 displayed wildtype positioning at the *PHO8* promoter (Fig. 59, S1 and S3). Importantly, the *rsc3-ts*, *arp9-ts* and *sth1-td* mutants appeared like wildtype at the permissive temperature of 25°C (Fig. 44A).

The DNaseI pattern after removal of either of the three essential RSC subunits resembled to some extent the pattern of the induced *PHO8* promoter, which is essentially dependent on the transactivator Pho4 [183, 212]. Nonetheless, *arp9-ts* and *rsc3-ts* strains that carried the *pho4* deletion allele still showed the same alterations to the *PHO8* promoter structure at the non-permissive temperature (Fig. 44B) speaking against a putative Pho4-mediated indirect effect due to ablation of essential RSC subunits. Moreover, nucleosome positioning at *PHO84*, which has a similar threshold of induction as *PHO8* [223], was unchanged in the *arp9-ts* and *rsc3-ts* mutants at the restrictive temperature (Fig. 46).

Badis *et al.* presented the *RIM9* locus as a prime example for the effects seen with their *rsc3-ts* strain, i.e. increased nucleosome occupancy over promoter NDRs [138] (Fig. S4B). We confirmed their results by our DNaseI indirect endlabelling approach not only for the *rsc3-ts* strain but also the *arp9-ts* and *sth1-td* strains (Fig. 45). All three strains, when grown at the restrictive temperature, showed a loss of DNaseI accessibility of the *RIM9* NDR region. This effect was very specific as the two neighbouring NDRs (*AEP1* NDR1 and ECM40 NDR3) were not affected.

The *CHA1* locus was the first for which a role of RSC in nucleosome positioning was reported [149]. We noticed no change in the *sth1-td* strain here, but the extent of the CHA1 NDR was visibly diminished in the *rsc3-ts* and *arp9-ts* strains (Fig. 45). The observed changes at the *CHA1* NDR in the *rsc3-ts* strain showed some variability and were sometimes less clear (Fig. S3).

As negative control, we analyzed nucleosome positioning at the *SNT1* locus for which no effects upon removal of either Rsc3 [138] or Sth1 [139] had previously been observed (Fig. S4C). We also noticed no changes in the *rsc3-ts* or the *arp9-ts* strain at *SNT1* (Fig. 45). Importantly, the unaltered DNaseI patterns at *SNT1*, *PHO84* and *ADH2* (Figs. 45 and 46) suggest that the changes at the *PHO8*, *RIM9*, and *CHA1* loci were not due to unspecific global effects caused by the removal of an essential protein and/or the growth conditions at elevated temperature as, for example, seen with the *spt6-1004* strain (Fig. 36).

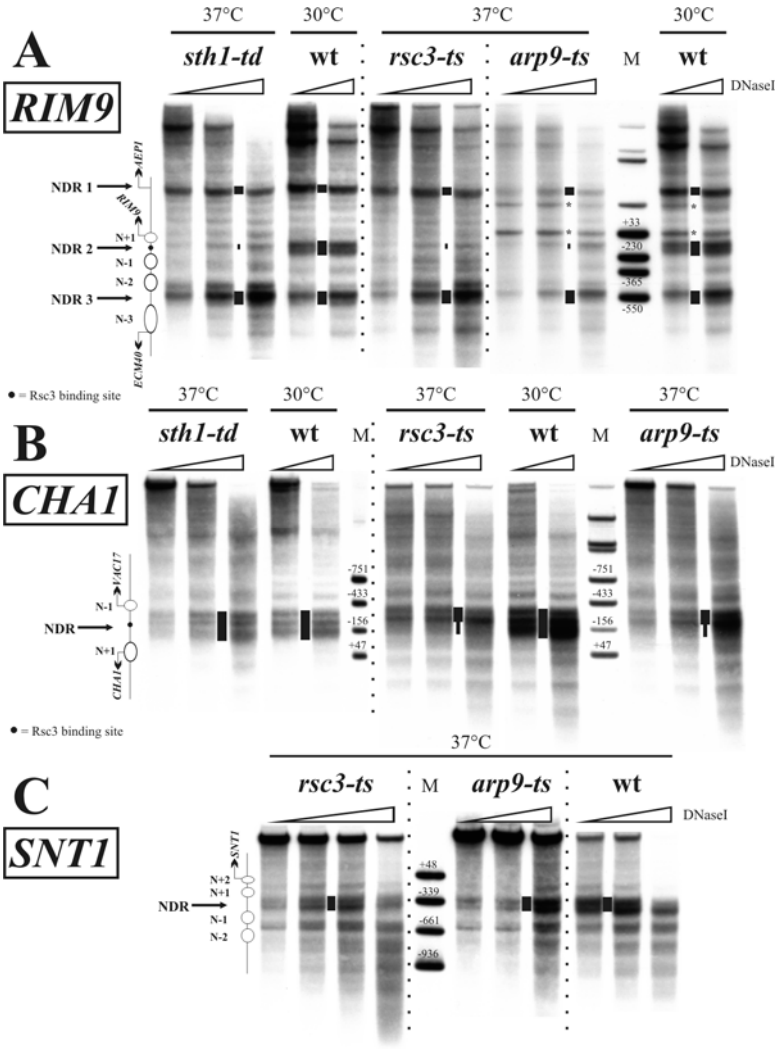

Figure 45. Loss of RSC subunits at elevated temperature altered chromatin structure at the promoters of *RIM9* and *CHA1* but not of *SNT1*.

DNaseI indirect endlabelling analysis of the **(A)** *RIM9*, **(B)** *CHA1* and **(C)** *SNT1* promoter regions in a wildtype strain (wt; BY4741) and strains carrying a temperature sensitive (*ts*) or temperature sensitive degron (*td*) allele of the indicated RSC subunits. Strains were grown logarithmically at 25°C and then shifted to the non-permissive temperature (37°C) overnight. Wt nuclei also for logarithmic growth at 30°C. Bars in-between lanes mark the intensity and extent of DNaseI hypersensitive sites. Samples separated by stippled lines were not electrophoresed alongside on the same gel. Schematics, ramps and markers as in Figures 10 and 42.

At each of the aforementioned loci the effects in the *rsc3-ts*, *arp9-ts* and *sth1-td* strains were mostly identical (Figs. 42 and 45). However, this was not the case for all loci we looked at. For example, analysis of the *arp9-ts* strain revealed a major disruption of the regular nucleosomal structure at the *PHO5* promoter, while the *rsc3-ts* mutation showed only minor effects, and the pattern of the *sth1-td* strain was nearly identical to the wildtype positioning (Figs. 42 and 44B). Similarly differential effects were also seen for the *RIO1*, *RNR3* and *GAL1-10* loci (Fig. 46). Importantly, the *sth1-td* strain was grown in the presence of galactose for degron induction, which likely explains the broad accessible region seen at the *GAL1-10* promoter in the *sth1-td* strain and may explain some of the differential effects seen at the other loci. Nevertheless, these differences suggest that not all components of the RSC complex might be required to the same extent for setting up or maintaining chromatin architecture at specific loci.

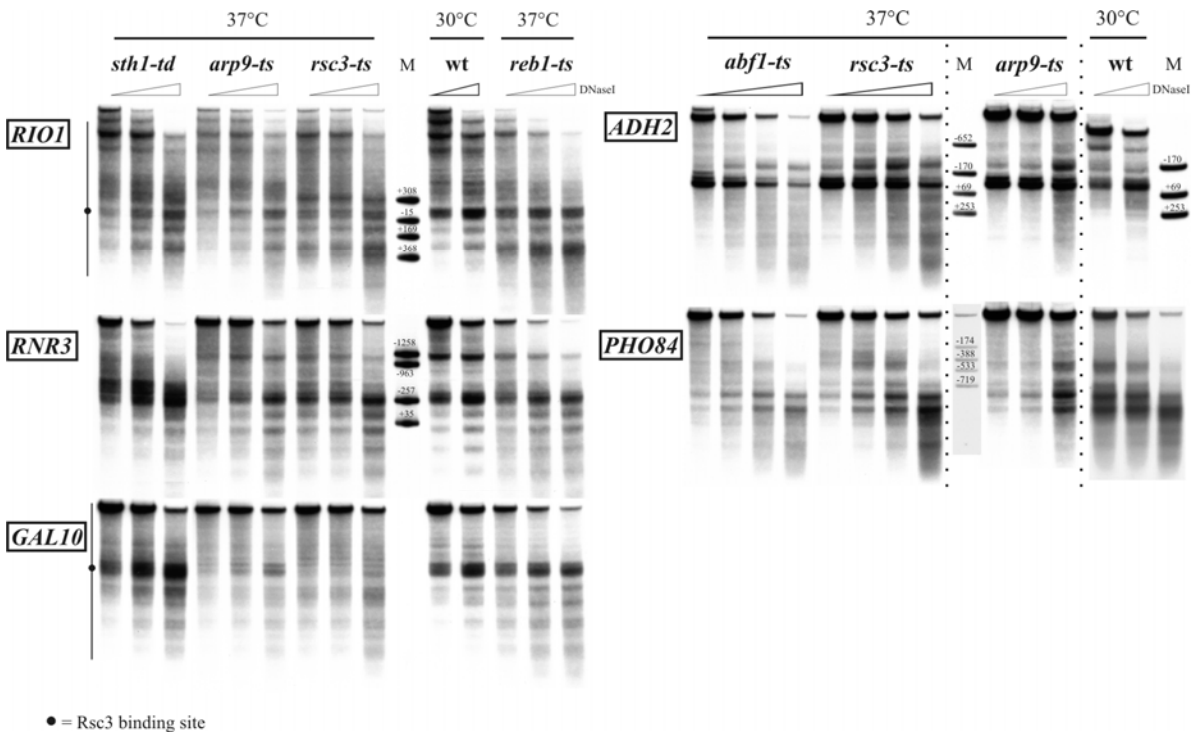

Figure 46. Loss of RSC subunits at elevated temperature altered chromatin structure at the promoters of *RIO1*, *RNR3 and GAL10* but not of *ADH2* and *PHO84*.

DNaseI indirect endlabelling analysis of the *RIO1*, *RNR3*, *GAL10*, *ADH2* and *PHO84* promoter regions in a wildtype strain (wt; BY4741) and strains carrying a temperature sensitive (ts) or temperature sensitive degron (td) allele of the indicated RSC subunits or of the sequence specific DNA binding proteins Reb1 or Abf1. Strains were grown logarithmically at 25°C and then shifted to the non-permissive temperature (37°C) overnight. Wt nuclei also for logarithmic growth at 30°. Bars in-between lanes mark the intensity and extent of DNaseI hypersensitive sites. Samples separated by stippled lines were not electrophoresed alongside on the same gel. Schematics, ramps and markers as in Figures 10 and 42.

Arp9 and Arp7 are essential proteins in the S288C strain background, while *arp9*, *arp7* and *arp7arp9* deletion mutants are just viable in the W303 background [222]. Due to the severe sickness of these strains, they pick up suppressor mutations with considerable frequency [222], which all map to a single locus (termed *mra1* (modify the requirement for actin-related proteins) [222]). We analysed positioning in strains lacking Arp7, Arp9 or both in combination with the *mra1* allele to see if we could reproduce the effects seen with the *arp9-ts* strain. These strains, whether grown either at the permissive temperature of 25°C or at the semi-permissive temperature of 30/33 °C, displayed only very subtle, if at all, alterations to the DNaseI pattern at the *PHO8* and *PHO5* locus (Figs. 47 and 48). Moreover, DNaseI accessibility at the *RIM9* NDR2 and the *GAL1-10* NDR was only very slightly reduced in contrast to the strong reduction seen in the *arp9-ts* strain (Fig. 47). Apparently, the *mra1* mutations not only suppresses the growth defect of the *arp7*/*arp9* strains but also restores most of the nucleosome positioning activity of a Arp7/9-devoid RSC complex.

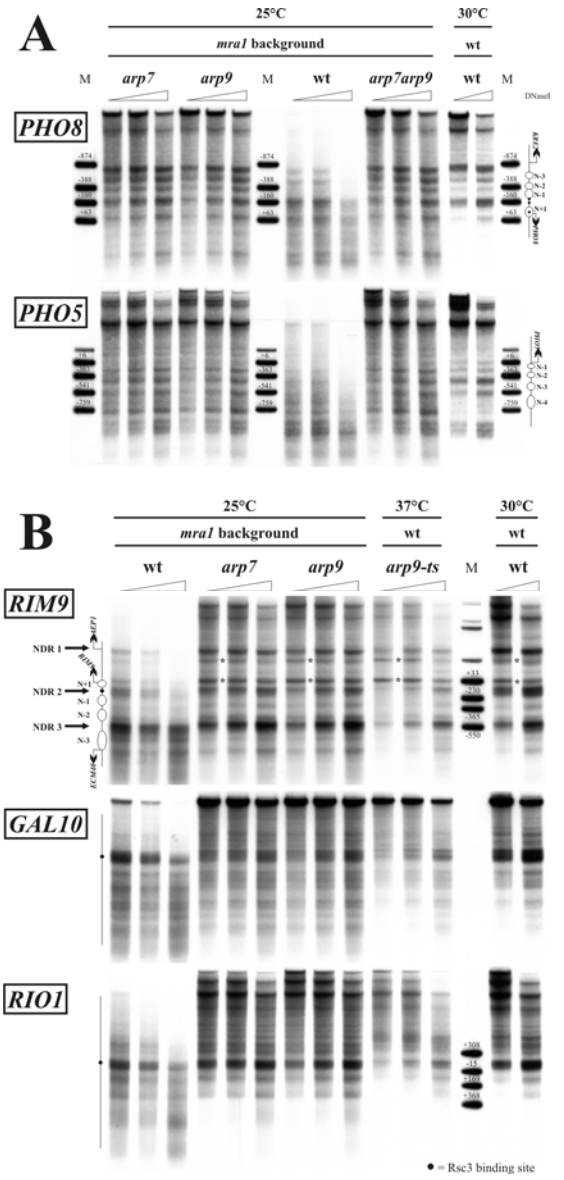

Figure 47. Strains that carry *arp7* or *arp9* deletion mutant alleles in combination with the *mra1* suppressor mutation did not show the positioning defects seen with the RSC *ts* strains.

DNaseI indirect endlabelling analysis of the **(A)** *PHO8*, *PHO5*, (**B**) *RIM9*, *GAL10* and *RIO1* promoter regions. Nuclei were prepared from *mra1* (BCY 430), *mra1arp7* (BCY 427), *mra1arp9* (BCY 426) or *mra1arp7arp9* (BCY 395) strains grown logarithmically at 25°C. Nuclei were also prepared from a wildtype strain (BY4741) grown logarithmically at 30°C and from an *arp9-ts* strain (YBC1536) grown at 37°C overnight. Schematics, ramps and markers as in Figure 42.

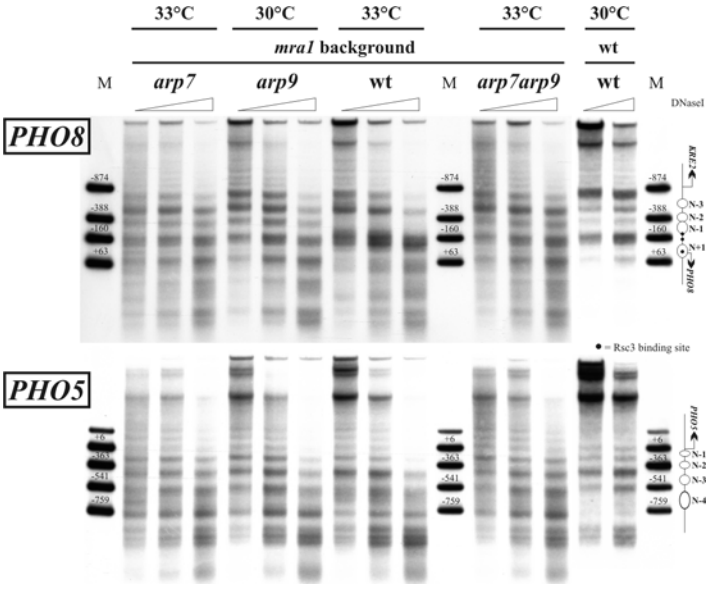

Figure 48. Strains that carry *arp7* or *arp9* deletion mutant alleles in combination with the *mra1* suppressor mutation showed little positioning defects even at semi-permissive temperatures.

DNaseI indirect endlabelling analysis of the *PHO8* and *PHO5* promoter regions in the strains described in Figure 43 but grown at the indicated semi-permissive temperatures. Schematics, ramps and markers as in Figure 42.

2.6.6. The evolutionarily conserved Rsc3 binding site at position -151 was required for maintenance of the *PHO8* NDR1, basal expression of *PHO8* but not for RSC recruitment

The RSC complex contains two subunits (Rsc3 and Rsc30) that can bind a specific DNA sequence motif *in vitro* [138]. Such putative binding sites commonly locate to within promoter NDRs and overlap with sites of increased nucleosome occupancy in a *rsc3-ts* strain [138]. This suggested that such RSC binding motifs could play a role in RSC's ability to position nucleosomes. We scanned the *PHO8* promoter for Rsc3 binding sites using the position weight matrix (PWM) obtained by Badis *et al.* [138] and identified three putative binding sites at positions -214, -151 and -10 relative to the *PHO8* ORF (Fig. 6 and 49A). The site at -10 lies within nucleosome N+1, the site at -151 centrally within the *PHO8* NDR2, and the site at -214 right at the NDR2/N-1 border.

A ***PHO8***

	Rsc3 site at -10	Rsc3 site at -151	Rsc3 site at -214
S.cerevisiae	C G C G C A T	T C G C G C G T	A G G C G C G
S.paradoxus	C G C G C A T	T C G C G C G T	A G G C G C G
S.mikatae	C G C G C A T	T C G C G C G T	A G G C G C G
S.bayanus	T A A G C A T	T C G C G C G T	A G G C G C G
S.kudriavzevii	C T A G C A T	T C G C G C G T	A G G C G C G
S.castelli	A G A G T A A	G T A C A C A G	C C A C T C G
S.cer. mutated	C C T A C A T	T C C T A C G T	A G T A C C G

B

	RIM9 Rsc3 site at -133	*CHA1* Rsc3 site at -239	*GAL10* Rsc3 site at -214	*RIO1* Rsc3 site at -134
S.cerevisiae	C G G C G C G C G C A A	C T G C G C G	C G G C G C G	T G G C G C G C G C A G
S.paradoxus	C G G C G C G C G C T A	T T T C G T G	C G G C G C G	T A G C G C G C G C A G
S.mikatae	C G G C G C G C C T A A	C T G C G C G	T G G T G C G	T A G C G C G C G C A A
S.bayanus	C G G C G C G C A A G A	C C G T G C G	C G G C G C G	C A T C G C G C G A C G
S.kudriavzevii	C G G C G C G C G C A A	C C G C G C G	- - - - - - -	T A G C G C C C G A C G
S.castelli	T G G C G C G T A T G T	A G C G G T G	C T T C A T C	A A G T C A G T A C A G
S.kluyveri	T C G C A T A A T T A A	G C T C T T T	- - - - - - -	- - - - - - - - - - - -

***SNT1, PHO5, ADH2, RNR3, PHO84, SUC2, HIS3, POT1, HO*: no Rsc3 binding sites found**

Figure 49. The *PHO8* promoter harbours three predicted and conserved Rsc3 binding sites.
(A) Sequence alignment of the predicted Rsc3 binding sites at the *PHO8* promoter in the indicated *Saccharomyces* species. The CGCGC motif that mostly defines the consensus sequence is highlighted in bold and cross-species conservation is indicated by black dots. "*S. cer.* mutated" gives the sequence after mutagenesis of the corresponding Rsc3 binding site. **(B)** Same as **(A)**, but for the indicated loci. Promoters for which no putative Rsc3 biding was identified are listed in the bottom box.

A sequence alignment of this region from closely related *Saccharomyces* species revealed strong conservation of the sites at -151 and -214 in all yeasts except for the more distantly related *S. castelli* (Fig. 49B). The site at -10, in contrast, was conserved only in the two closest *S. cerevisiae* relatives. We mutated all three sites individually (Δ-10, Δ-151 and Δ-214) as well as in combination (Δall), both in the chromosome locus as well as in plasmid pP8apain, and analysed positioning *in vivo* by DNaseI indirect endlabelling. The DNaseI pattern for the Δ-10 and the Δ-214 *PHO8* promoter mutants was as for the wildtype whereas the Δ-151 and the Δall mutants showed strongly reduced DNaseI accessibility at the *PHO8* NDR1 (Fig. 50A). The effect at NDR1 was similar to that seen with the *arp9-ts*, *rsc3-ts* and *sth1-td* strains, but there was no effect on nucleosome N-3 upon removal of the putative Rsc3 site at Δ-151. Again we confirmed these effects by restriction enzyme accessibility analysis (Fig. 43B). In keeping with the DNaseI pattern, all Rsc3-mutants displayed similar HpaI (cuts in N-3) and NheI (cuts in NDR2) accessibility. Accessibility of the HindIII site was strongly reduced in

the Δ-151 and Δall mutants (26% and 43%) compared to the wildtype (69%) or the Δ-10 and Δ-214 mutants. Almost identical results were obtained when mutating the respective Rsc3 binding sites on the pP8apin shuttle vector (Fig. 43C and S2) arguing that the effects were independent of the larger chromatin context. Collectively, the putative Rsc3 site at Δ-151 seemed to be required for excluding nucleosomes from the *PHO8* NDR1.

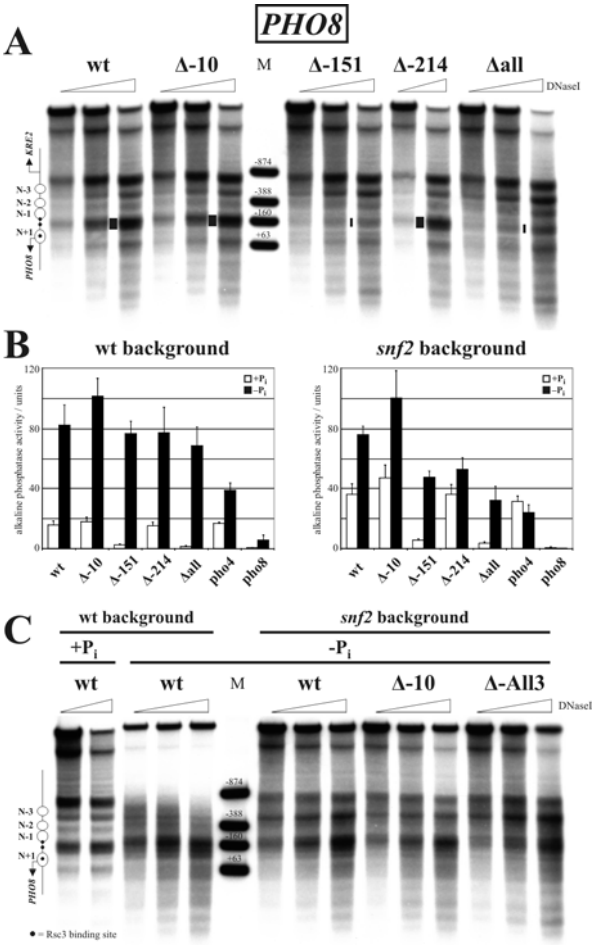

Figure 50. The Rsc3 binding site at position -151 was required for nucleosome depletion over the *PHO8* promoter NDR and basal expression of *PHO8*.

(A) DNaseI indirect endlabelling analysis of the *PHO8* promoter region in strains with mutations in none (wt, CY337 background), one (Δ-10, Δ-151 or Δ-214) or all (Δall) of the three predicted Rsc3 binding sites at the *PHO8* promoter. Bars in between lanes mark the position of the *PHO8* promoter NDR. Their thickness corresponds to the extent of DNaseI accessibility, i.e. thin bars highlight increased nucleosome occupancy. **(B)** Measurement of alkaline phosphatase activity of wt (CY337) and *snf2* (CY408) strains with mutations in none (wt), one (Δ-10, Δ-151 or Δ-214) or all (Δall) of the three predicted Rsc3 binding sites at the *PHO8* promoter or with *pho4* or *pho8* deletion. Cells were grown logarithmically in phosphate containing medium (+P_i, repressive conditions) or placed overnight in phosphate free medium (-P_i, inducing conditions). The mean and standard deviation of three to five independent biological replicates are shown. **(C)** DNaseI indirect endlabelling analysis of the *PHO8* promoter region in wt and *snf2* strains with mutations in none (wt), one (Δ-10) or all (Δall) of the three predicted Rsc3 binding sites as indicated. Except for the wildtype sample on the left (+P_i), all nuclei were prepared after overnight growth in phosphate free medium (-P_i). **(B-C)** Schematics, ramps and makers as in Figure 42.

Next, we checked whether mutation of any of the putative Rsc3 binding sites (and the resulting changes in occupancy over the *PHO8* NDR1) was reflected as changes in *PHO8* expression. The *PHO8* gene codes for an alkaline phosphatase that is the major contributor to the total cellular alkaline phosphatase activity (Fig. 50B - compare activity of *pho8* strain to the wildtype). We measured alkaline phosphatase activity both under repressing (+P_i) and inducing (-P_i) conditions to discriminate between a role of the putative binding sites in basal and activated transcription (Fig. 50B). Alkaline phosphatase activity under repressing conditions was greatly reduced in the Δ-151 mutant (2.5 units compared to 15.7 units for the wildtype promoter; $p<0.00016$; two-sided paired t-test). In contrast, the basal alkaline phosphatase activity for the Δ-10 promoter was slightly but significantly elevated ($p<0.001$; two-sided paired t-test). For the Δ-214 promoter however there was no significant difference to the wildtype. Mutation of all three putative binding sites resulted in a reduced phosphatase level under repressive conditions similar to the level seen for the Δ-151 promoter (Fig. 50B). In contrast, the induced level of alkaline phosphatase activity was not significantly affected in any Rsc3 binding site mutant ($p>0.05$; two-sided paired t-test). Hence, the putative Rsc3 binding site at -151 is required for basal transcription but not for maximal activity upon induction. Interestingly,

basal transcription did not depend on the transactivator Pho4, albeit induced activity levels were greatly reduced in the *pho4* mutant (Fig. 50B).

The Rsc30 subunit of the RSC complex recognises an almost identical motif as the Rsc3 subunit [138] and hence the effects seen upon removal of the "Rsc3 binding sites" could equally be attributed to loss of Rsc30 binding. However, a *rsc30* deletion mutant did not show any increased occupancy over the *PHO8* promoter and no reduction in alkaline phosphatase activity under repressing conditions (Fig. 59, S3 and data not shown). Together these results argue that the putative Rsc3 binding site at -151 is required for basal transcription because of its role in keeping NDR1 nucleosome depleted. We wondered if the strict Snf2-dependency of *PHO8* promoter remodeling [201] was due to some aspect of the chromatin structure as shaped by Rsc3-recruited RSC. However, inducing the Δall or the Δ-10 mutant promoter in the *snf2* background did not lead to any more remodeling as for a wild type promoter (Fig. 50C). We also checked alkaline phosphatase activity of the various Rsc3-site mutants in the *snf2* background. Under non-inducing (+P_i) conditions the relative levels of the mutant as compared to the wt-promoter were very similar to those seen in the wildtype (*SNF2*) background. However under inducing conditions (-P_i), alkaline phosphatase levels for the Δ-151 and the Δ-214 mutant were significantly lower (p=0.004 and 0.037 respectively; two-sided paired t-test) than for the wildtype promoter. Moreover, levels in the Δall mutant were even lower than for the Δ-151 and Δ-214 single mutants. Evidently, the two putative sites at Δ-151 and Δ-214 play a role in *PHO8* expression under inducing conditions in the absence of SWI/SNF but this influence appears to be independent of effects on nucleosome positions.

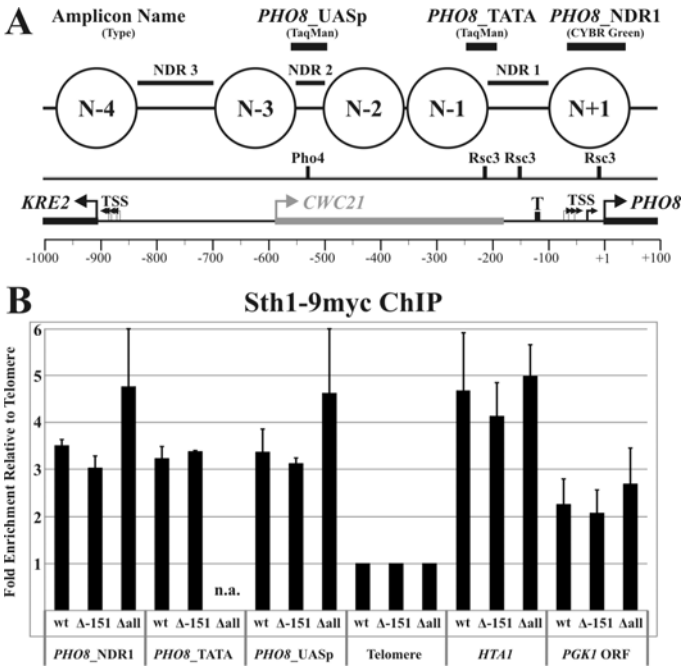

Figure 51. RSC is not recruited to the *PHO8* promoter via any of the putative Rsc3 binding sites.
(A) Schematics as in Figure 7. Location and type of the *PHO8* promoter amplicons used in **(B)** as indicated. **(B)** RSC occupancy was determined via ChIP using an anti-myc antibody (9E11) for strains carrying the *STH1-9MYC* allele (FT4 *STH1-9MYC::TRP*) in combination with either the wildtype *PHO8* promoter (wt) or mutations in one (Δ-151) or all (Δall) putative Rsc3 binding sites (see Fig. 49). Used amplicons are shown in **(A)** and for the *HTA1* promoter, the *PGK1* coding region and for the telomere region on the short arm of chromosome 6 as described in Methods (chapter 4.2.3.). Sth1-Myc occupancy was normalized against the telomere. Error bars correspond to the variation of two biological replicates.

Given the aforementioned effects observed in the Δ-151 mutant, we decided to test if the CGCGC motif at -151 acts through recruitment of RSC. We measured RSC occupancy by ChIP at three different sites along the *PHO8* promoter (Fig. 51A) in a wildtype strain and in the Δ-151 and Δ-all mutants. At all three sites along the wildtype *PHO8* promoter we observed an approximate three fold enrichment of Sth1 (the ATPase subunit of RSC) relative to telomere confirming the presence of RSC at the *PHO8* promoter (Fig. 51B). As there was no reduction in RSC occupancy neither in the Δ-151

nor the Δ-all strain we concluded that the putative Rsc3 binding sites play no role in the recruitment to or binding of RSC to the *PHO8* promoter region.

2.6.7. Purified RSC alone did not generally reconstitute proper positioning but was sufficient for a few individual positions

Prompted by the identification of RSC in our final fraction positive for the "nucleosome positioning activity" *in vitro* and by the strong effects on chromatin patterns upon ablation of essential RSC subunits *in vivo* (Fig. 42, 44, 45 an 46) we used our *in vitro* system to see if the RSC complex was the sole component of the "nucleosome positioning activity", i.e. if RSC was sufficient to reconstitute *in vivo*-like positioning on its own. We added purified RSC complex to reconstitution reactions where plasmids carrying the *PHO8*, *RIM9*, *CHA1* and *SNT1* loci were present in the same tube at equimolar amounts and were pre-assembled by salt gradient dialysis. Initially, we titrated the amount of RSC required to achieve any alterations to the DNaseI pattern and found an approximate molar ratio of one RSC complex per 20 nucleosomes to be a lower limit in our reconstitution system (data not shown).

The DNaseI pattern observed at all four loci for the reconstitution reactions containing only salt assembly chromatin, purified RSC and ATP differed from that achieved by salt gradient dialysis assembly alone and from that of free DNA (Fig. 52A-D, compare lanes 6 to 9 with lanes 10 to 13 and lanes 14 to 15, respectively). Note that both the addition of RSC alone or of WCE in the absence of ATP does not lead to any changes, i.e., the pattern is identical to the pattern of untreated salt gradient dialysis chromatin [175].

At the *PHO8* promoter, RSC alone was unable to reconstitute *in vivo*-like positioning (Fig. 52A, compare lanes 6 to 9 with lanes 1 to 2, respectively). The most significant change to the DNaseI pattern in the RSC +ATP samples (lanes 6 to 9) compared to the -ATP samples (lanes 10 to 13) was an increase in DNaseI accessibility over the region normally occupied by nucleosome N-3. Since this region is already somewhat protected after salt gradient dialysis assembly, RSC appears to counteract the intrinsic propensity of this region to become incorporated into a nucleosome. So with regard to increasing nuclease sensitivity in the region of nucleosome N-3, the addition of RSC *in vitro* led in the same direction as the removal of RSC components *in vivo* (Fig. 42).

For the *RIM9* locus, salt gradient dialysis assembly already seemed to reconstitute the *RIM9* and *ECM40* NDRs to some extent correctly (Fig. 52B; NDR2 and NDR3, respectively). Together with *PHO84* [169], this is another example for a rather *in vivo*-like reconstitution of nucleosome patterns just by salt gradient dialysis. Addition of RSC alone appeared to reduce the extent of the *RIM9* NDR2, while addition of WCE broadens it. At first glance it seemed that RSC alone could establish the NDR at the beginning of the *AEP1* ORF (Fig. 52B; NDR1). However as the resolution in this upper part of the gel is very low, we reanalyzed the samples using an alternative secondary cleavage site closer to the *AEP1* NDR1. This way it became clear that the DNaseI hypersensitive band generated by RSC did not correspond to the *AEP1* NDR1 (Fig. 53). All in all, the *RIM9* locus turned out to be a rare example for a locus where *in vivo*-like nucleosome positioning could not be reconstituted properly in our *in vitro* system even by the WCE.

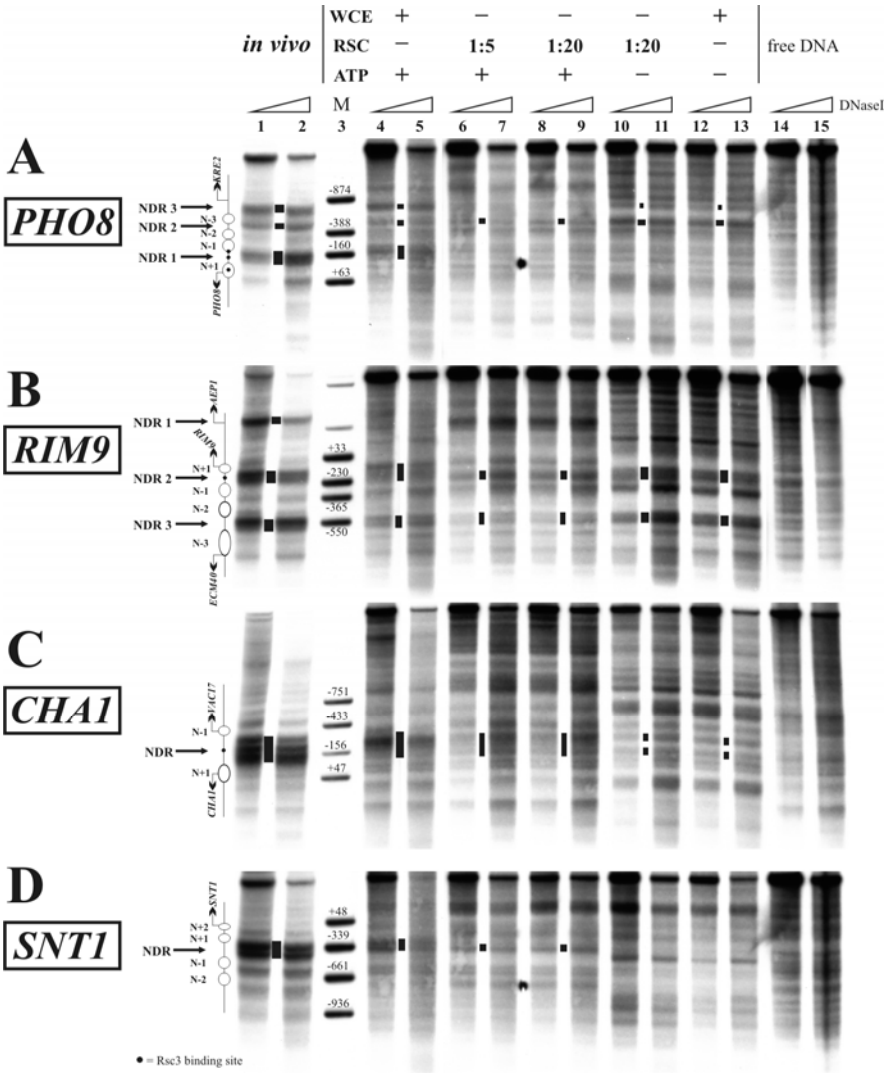

Figure 52. Purified RSC repositioned nucleosomes in salt gradient dialysis chromatin and was sufficient to determine *in vivo*-like positioning in a few instances.

DNaseI indirect endlabelling analysis *in vitro* on the preassembled plasmids **(A)** pUC19-*PHO8*-long, **(B)** pUC19-*RIM9*, **(C)** pUC19-*CHA1*, **(D)** pUC19-*SNT1* incubated with WCE or purified RSC complex in the presence or absence of ATP as indicated. Amount of RSC is given as the molar ratio of RSC to nucleosomes. In each panel, the left two lanes show the wt *in vivo* DNaseI pattern. Arrows on the left point to positions of numbered NDRs in the *in vivo* patterns. Bars in between lanes mark hypersensitive regions that correspond, at least to some degree, to NDRs of the *in vivo* patterns. Free DNA sample, schematics, ramps and markers as in Figures 10 and 42.

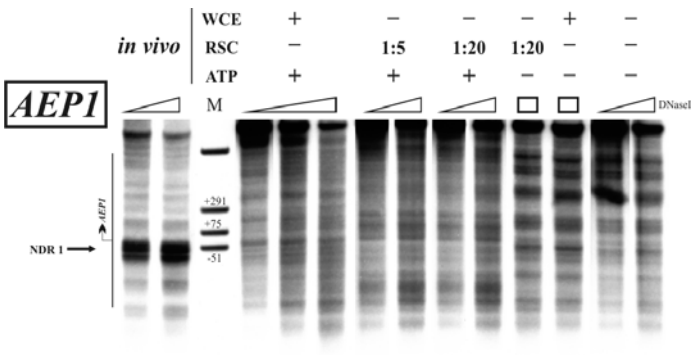

Figure 53. Neither RSC nor the WCE reconstituted the *AEP1* NDR1.

Shown are samples from Figures 52 and 53 that were analyzed for nucleosome positioning around the *AEP1* NDR1. All labels as in Figure 52.

The *CHA1-VAC17* promoter region features a particularly long NDR (Fig. 52C, [149]). Salt gradient dialysis did not recapitulate the nucleosome positioning seen *in vivo* as part of the region where the NDR should be was protected from DNaseI cleavage (Fig. 52C; compare the regions marked by vertical bars). Furthermore, there were strong bands in the pattern of salt gradient dialysis assembled chromatin that had no corresponding bands in the *in vivo* pattern. Addition of RSC, and, even more clearly, addition of WCE in the presence of ATP yielded a DNaseI pattern more similar to the *in vivo* pattern as the protection over the NDR region was abolished leading to a broad hypersensitive DNaseI band rather similar to the *in vivo* NDR in extent, albeit with lower intensity.

The DNaseI pattern of the *SNT1* promoter *in vivo* revealed a site of high DNaseI sensitivity corresponding to the *SNT1* NDR and regular nucleosomal arrays up- and downstream of the NDR (Fig. 52D; lanes 1 to 2). Salt gradient dialysis alone failed to generate any *in vivo*-like nucleosome positioning (Fig. 52D; compare lanes 10 to 13 with lanes 1 to 2). In contrast, the WCE could induce a DNaseI pattern that recapitulated at least the *in vivo* NDR and both its flanking nucleosomes on either side (Fig. 52D compare lanes 4 to 5 to lanes 1 to 2). Most strikingly, purified RSC alone was capable to position nucleosome N-1 rather well (Fig. 52D, compare lanes 6 to 9 with lanes 1 to 2 and 4 to 5). In particular, the prominent band in the salt gradient dialysis chromatin pattern (lanes 10 to 13), which overlapped with the *in vivo* position of nucleosome N-1 was abolished by the addition of RSC alone (or of the WCE) suggesting that RSC alone could move a nucleosome to a position strongly overlapping with, if not identical to, the *in vivo* position of N-1.

In summary, we take the generation of the NDR at the *CHA1* promoter and of the *in vivo*-like positioning of nucleosome N-1 at the *SNT1* promoter as proof of principle that the RSC complex alone can be sufficient to determine some *in vivo*-like nucleosome positions *in vitro*. This RSC activity was clearly dependent on ATP. Nonetheless, the similarity of *in vitro* reconstituted chromatin patterns by RSC alone (or by salt gradient dialysis) to the *in vivo* patterns was generally much lower than after incubation with the WCE. So we conclude that factors present in the WCE in addition to RSC or the intrinsic DNA sequence preferences are required to achieve more *in vivo*-like nucleosome positioning.

2.6.8. RSC had a direct and necessary role in generating *in vivo*-like nucleosome positions at *PHO8*, *RIM9*, *CHA1* and *SNT1 in vitro*

As RSC alone was usually not sufficient to generate *in vivo*-like nucleosome positioning *in vitro*, we wondered if it was even necessary. We prepared extracts from the *rsc3-ts* strain grown at the non-permissive temperature (overnight at 37°C) to see if this extract lost the ability to generate properly positioned nucleosomes. We tried to determine the relative Sth1 levels in the *rsc3-ts* extract made after growth at 37°C or 25°C, the standard wt extract and our purified RSC preparation by anti-Sth1 Western blot (Fig. 41), but failed to detect any Sth1 in the three whole cell extracts, although we could detect Sth1 in the WCE from the commercially available baker's yeast (that was used for the WCE fractionation). Since the Sth1 band even in the baker's yeast WCE was very weak, the lack of Sth1 signal was likely due to inefficient transfer from the gel to the membrane in the context of a whole cell extract. Nonetheless, the antibody also recognised the protein A component of the TAP-tagged Rsc8 present in the *rsc3-ts* strain, so we could see that growth of this mutant at the restrictive temperature reduced cellular Rsc8 levels (Fig. 41).

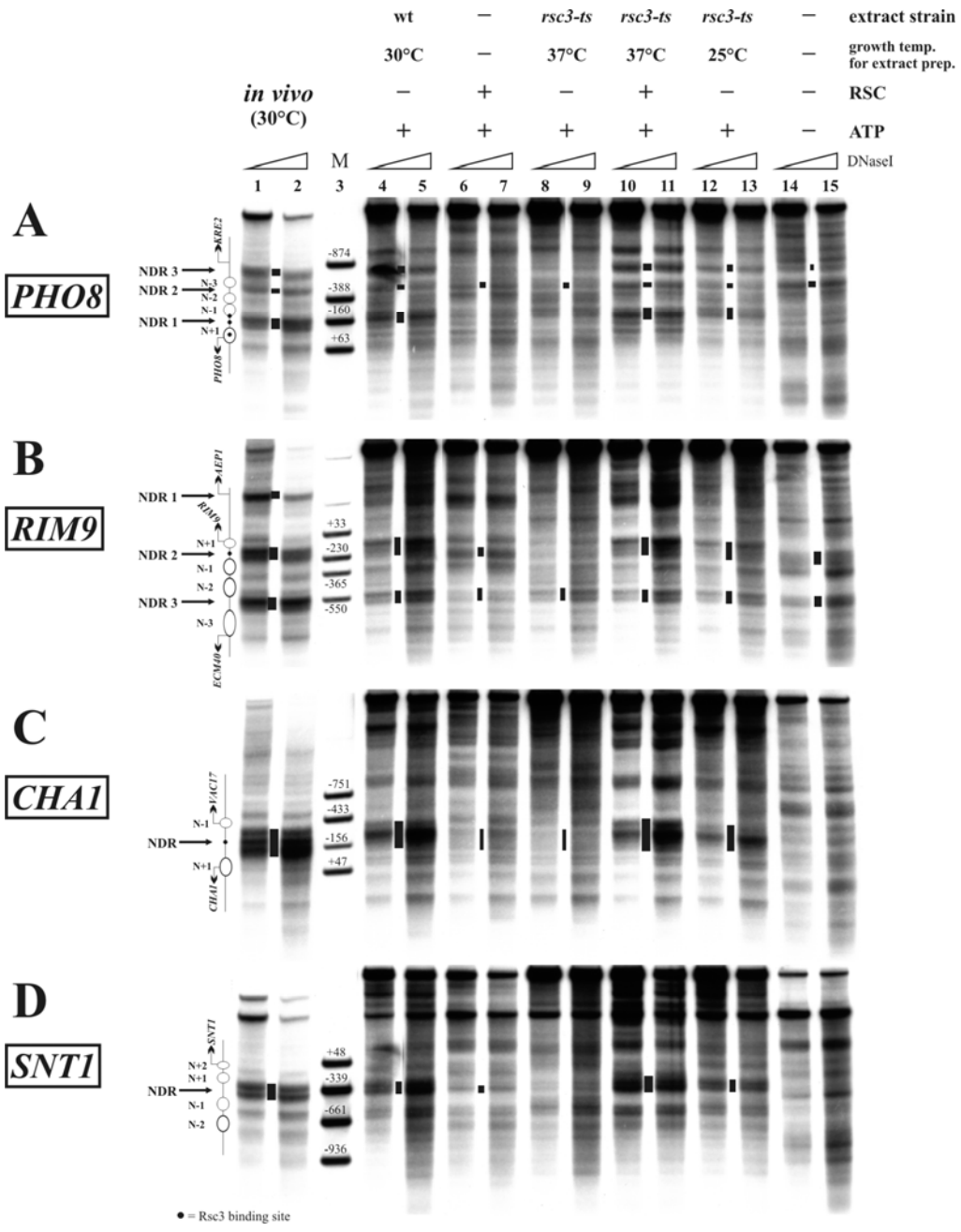

Figure 54. A direct and necessary role for RSC in generating *in vivo*-like nucleosome positions at *PHO8*, *RIM9*, *CHA1* and *SNT1 in vitro*.

DNaseI indirect endlabelling analysis *in vitro* on plasmids **(A)** pUC19-*PHO8*-long, **(B)** pUC19-*RIM9*, **(C)** pUC19-*CHA1*, **(D)** pUC19-*SNT1* preassembled into chromatin by salt gradient dialysis and incubated with one of three different WCEs or purified RSC complex or both in the presence or absence of ATP as indicated. Extracts were made from wildtype (BY4741) grown logarithmically at 30°C, or from the *rsc3-ts* strain grown logarithmically at 25°C with or without an overnight shift to 37°C. RSC was added to approximately one RSC molecule per 5 nucleosomes. Schematics, markers, bars, and ramps as in Figure 52.

The *rsc3-ts* 37°C extract (Figs. 54 and 55, "*rsc3-ts* 37°C" extract) was much less effective in positioning nucleosomes properly than the wildtype WCE. It failed to reconstitute NDR1 and NDR3 at the *PHO8* promoter (Fig. 54A), NDR2 at the *RIM9* promoter (Fig. 54B), the broad NDR at the *CHA1-VAC17* promoter (Fig. 54C), and the strong NDRs at the *SNT1, ADH2* and *RNR3* promoter (Figs. 54D and 55A and D). The effects at the *PHO8* and *RIM9* promoters closely resembled those seen with the *rsc3-ts* strain *in vivo* (compare the reduction of intensities of the respective NDRs in Figures 42 and 45). In

contrast, the strong hypersensitivity between NDR2 and NDR3 at the *PHO8* promoter (Fig. 42) was not recapitulated by the *rsc3-ts* 37°C extract *in vitro*, and there were effects at the *CHA1* and *SNT1* promoters, even though these promoters were little or unaffected *in vivo*, respectively. Nonetheless, the *rsc3-ts* 37°C extract was sufficiently impaired in its nucleosome positioning activity to show that RSC is necessary for proper nucleosome positioning and could serve as a background for rescue experiments using purified RSC complex.

Strikingly, the addition of purified RSC to the *rsc3-ts* 37°C extract completely rescued the positioning activity of the extract for all tested loci (Figs. 54 and 55, compare "*rsc3-ts* 37°C +RSC" with "wt 30°C"). The reconstitution seen for the "*rsc3-ts* 37°C +RSC" sample was even slightly better than for the wildtype WCE indicating that RSC might be a limiting factor for reconstitution in the wildtype WCE. The rescue of the *rsc3-ts* 37°C extract strongly suggests that the effects seen with the *rsc3-ts*/*arp9-ts*/*sth1-td* strains by us (Figs. 42 and 45) and others [138-140] are not caused by indirect effects. Moreover, the *rsc3-ts* 37°C extract despite being unable to reconstitute *in vivo*-like nucleosome positioning on its own, clearly contributed to the reconstitution in the presence of RSC. This further strengthened the notion that so far unknown factors in addition to RSC and intrinsic DNA sequence preferences are required for reconstitution of nucleosome positioning *in vitro*.

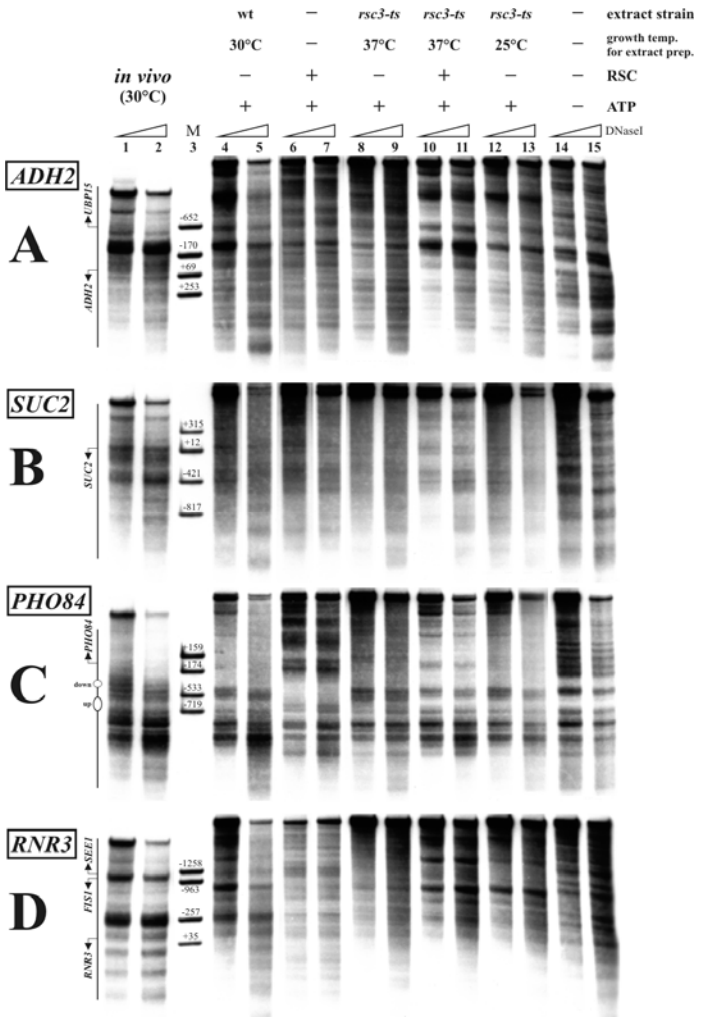

Figure 55. The DNA intrinsic *in vivo*-like positioning at the *PHO84* promoter was overwritten by RSC when present alone but not in the context of WCE.

As Figure 54 except for plasmids **(A)** pUC19-*ADH2*, **(B)** pUC19-*SUC2*, **(C)** pUC19-*PHO84* and **(D)** pUC19-*RNR3*.

Salt gradient dialysis alone reconstitutes rather *in vivo*-like nucleosome positioning at the *PHO84* promoter (Fig. 10). Nonetheless, addition of WCE still improved the similarity to the *in vivo* pattern (Fig. 10) [169]. Accordingly, rather similar and more or less equally *in vivo*-like nucleosome positioning was seen with the "*rsc3-ts* 37°C" extract, the WCE, the "*rsc3-ts* 37°C" extract plus purified RSC, or from salt gradient dialysis assembly alone (Fig. 55C, compare lanes 10-11 with lanes 4-5, 10-11 and 14-15, respectively). Surprisingly, purified RSC alone disrupted the *in vivo*-like pattern that was already set up by salt gradient dialysis assembly (Fig. 55C, compare lanes 6-7 with 14-15). Apparently, in this case, RSC on its own counteracts nucleosome positioning cues as encoded in the DNA sequence and as implemented by salt gradient dialysis and factors from the extract are necessary to maintain proper positioning

2.6.9. The role of the RSC complex in generating NDRs *in vitro* was specific and could not be substituted by the SWI/SNF or Isw2 remodelers

While the ability of RSC to rescue *in vivo*-like nucleosome positioning using the *rsc3-ts* 37°C extract speaks for a direct and necessary role of RSC in nucleosome positioning, we wondered if this role was specific to RSC or whether other remodeling complexes could achieve similar results. The *rsc3-ts* 37°C extract in principle should still contain all other remodelers. However, other remodelers might not be present in sufficient quantities to substitute for the loss of RSC function in this extract. Most other remodelers are less abundant in the cell to start with (~2000 copies of Sth1 per cell compared to ~220 copies for Snf2; [18]), and they may be less stable during extract preparation. In other words, we wondered if the RSC complex seemed to be the necessary remodeling activity for nucleosome positioning in our *in vitro* system simply because it was the most abundant activity.

We added purified SWI/SNF or Isw2 remodelers in the same molar amount as the RSC complex to the *rsc3-ts* 37°C extract to see if this also rescued the positioning activity. As mentioned above, SWI/SNF was a particularly good candidate as it is in the same subfamily and shares three subunits with RSC. For Isw2 an important role in nucleosome positioning at many genomic loci was previously demonstrated [95]. SWI/SNF and Isw2 on their own altered the nucleosome positioning of the salt gradient dialysis chromatin, which confirms that both remodelers were sufficiently active to remodel the chromatin templates *in vitro* (Fig. 56; compare lanes 8-9 and 10-11 to 13-14). However, neither of the remodeling complexes was able to generate the *in vivo*-like positioning alone or in combination with the *rsc3-ts* 37°C extract (Fig. 56; compare lanes 3-4 and 5-6 with 1-2).

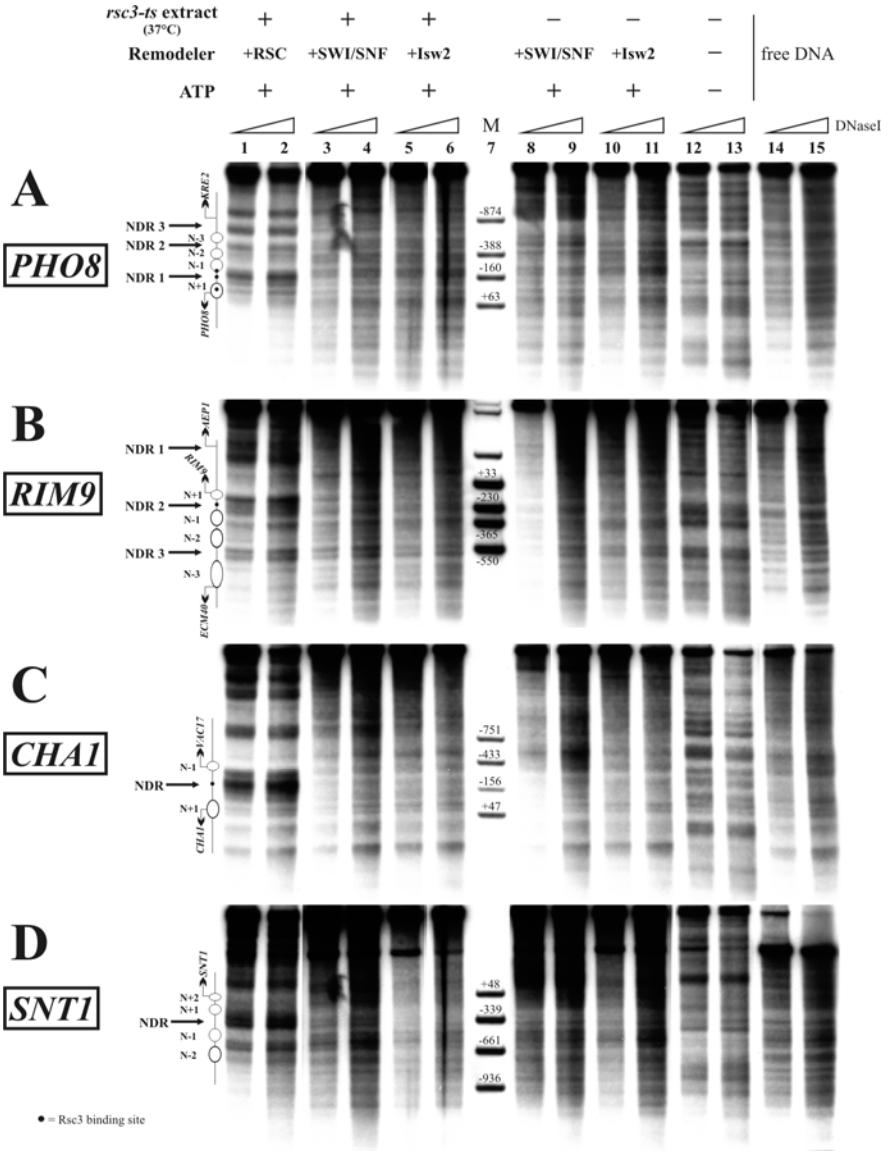

Figure 56. RSC was specifically required for nucleosome positioning *in vitro* as both SWI/SNF and Isw2 failed to rescue the *rsc3-ts* 37°C extract.

DNaseI indirect endlabelling analysis *in vitro* on plasmids **(A)** pUC19-*PHO8*-long, **(B)** pUC19-*RIM9*, **(C)** pUC19-*CHA1*, **(D)** pUC19-*SNT1* preassembled into chromatin by salt gradient dialysis and incubated with an extract made from a *rsc3-ts* strain grown overnight at 37°C and either one of purified RSC, SWI/SNF or Isw2 remodelers or with only SWI/SNF or Isw2. Free DNA DNaseI patterns are shown for comparison. All purified remodelling complexes were added at approximately one remodeler molecule per 5 nucleosomes. Schematics, markers, bars, and ramps as in Figure 52.

2.6.10. *In vitro* reconstitution of proper positioning at the *PHO8*, *RIM9* and *CHA1* promoters was largely unaffected by removal of putative Rsc3 sites

In vivo, removal of the Rsc3 binding site at *PHO8* lead to an increase in nucleosome occupancy over NDR1 that was similar to the one seen upon inactivation of essential RSC subunits (Figs. 42, 43 and 50A). Surprisingly, reconstitution of NDR1 *in vitro* was independent of the Rsc3 site at -151 or any of the other putative Rsc3 sites (Fig. 57). There was only a slight decrease in the relative intensity of the band that corresponded to the *PHO8* NDR1 upon removal of the site at -151 or of all three sites (Fig. 52, compare the three +WCE/+ATP samples). Correspondingly, HindIII accessibility at the Δ-151 and the Δall promoter (45% and 37% respectively) was only slightly decreased compared to the wt (52%) (Fig. 57). While the general trend of the DNaseI and HindIII data was in the direction expected from the *in vivo* results, it seemed overall that the Rsc3 sites at *PHO8* were generally not required *in vitro* for proper nucleosome positioning. Similarly, proper *in vitro* reconstitution of the *CHA1* and *RIM9* promoters was equally possible in the absence of the corresponding putative Rsc3 binding sites (data not shown).

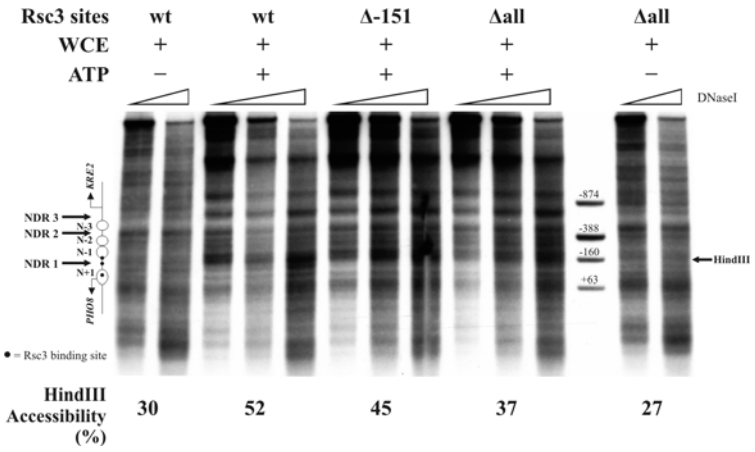

Figure 57. Proper *in vitro* reconstitution of nucleosome positioning at the *PHO8* promoter was not dependent on any of the putative Rsc3 binding sites.
DNaseI indirect endlabelling and HindIII accessibility analysis of the *PHO8* promoter region *in vitro* on pUC19-*PHO8*-long plasmids with mutations in none (wt), one (Δ-151) or all predicted Rsc3 binding sites (see Fig. 7A). Plasmids were preassembled into chromatin by salt gradient dialysis and incubated with WCE in the presence or absence of ATP as indicated. Schematics, ramps and markers as in Figures 6 and 42. The arrow on the right and the "-160" marker band indicate the HindIII site. HindIII-accessibility values below the lanes.

2.6.11. Ablation of general polymerase II transcription factors (GTFIIs) altered the chromatin architecture at the *PHO8* promoter

As RSC was necessary but mostly not sufficient, we wondered which other factors contributed to the "nucleosome positioning activity" of the WCE and re-evaluated the proteins identified by MS analysis of our final fraction. Some subunits of the general pol II transcription factors (GTFIIs) were detected, though with rather weak identification parameters (low MASCOT score; [186]). Nevertheless, GTFIIs were considered to be good candidates for contributing to nucleosome positioning as they are linked to TBP, which has DNA binding activity, and as they can recruit other chromatin associated factors and are enriched at a majority of yeast promoters [180, 224]. We obtained strains carrying temperature sensitive alleles of components of TFIID, TFIIE, TFIIF and TFIIH and analysed their *PHO8* and *PHO5* promoter chromatin structure *in vivo* by DNaseI indirect endlabelling under restrictive conditions.

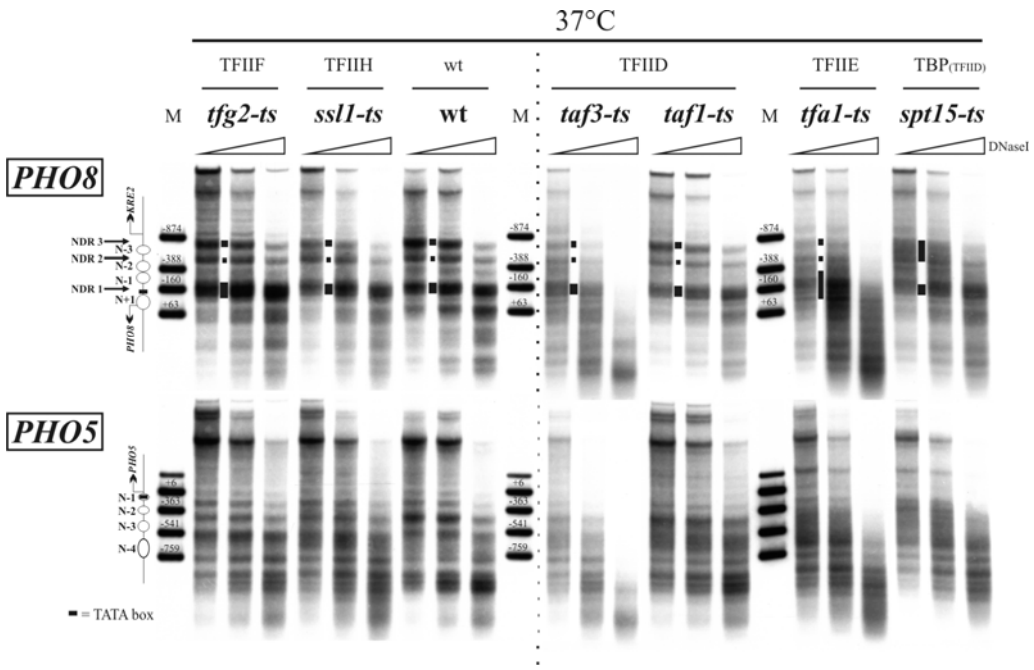

Figure 58. Loss of some general polymerase II transcription factors by elevated temperature altered the chromatin architecture at the *PHO8* and *PHO5* promoters.

DNaseI indirect endlabelling analysis of the *PHO8* and *PHO5* promoter region *in vivo* in a wildtype (wt) strain or in strains carrying a temperature sensitive (ts) allele of genes for subunits of the general transcription factors TFIIF (*tfg2-ts*), TFIIH (*ssl1-ts*), TFIID (*taf3-ts* (WCS203)), *taf1-ts* (YSW93), *spt15-ts* (=yeast TBP; YKS188-1)), and TFIIE (*tfa1-ts* (YSB331)). All strains were grown logarithmically at 25°C and then shifted to 37°C overnight. Samples were electrophoresed on two separate gels, demarcated by the stippled vertical line. Schematics, ramps and markers as in Figure 42.

At the *PHO8* promoter, the DNaseI patterns obtained for the *ssl1-ts* (TFIIH), *taf3-ts* and *taf1-ts* (TFIID) strains appeared very similar to the wildtype pattern (Fig. 58). However, the *tfa1-ts* (TFIIE) and s*pt15-ts* (=TBP; TFIID) strains revealed strong effects. In the *tfa1-ts* strain the *PHO8* NDR1 appeared extended as there was increased DNaseI sensitivity in the region normally occupied by the flanking nucleosomes N-1 and N+1 (Fig. 58), while in the *spt15-ts* mutant the region of nucleosome N-3 was strongly affected indicating a loss of this nucleosome. This latter effect seemed not to depend on direct binding of TBP to the TATA box as it was not recapitulated in a *PHO8* promoter TATA box point mutant (Fig. 59). The *tfg2-ts* strain displayed rather subtle effects at NDR1 as the DNaseI hypersensitivity was increased and extended further into the nucleosome N+1 region(Fig. 58). To confirm these subtle effects, we tested restriction enzyme accessibility for HpaI, NheI and HindIII as used above (Fig. 43) and included BslI that cuts within N+1 approximately 40bp downstream from the N+1/NDR1 border (Fig. 43A). There were no effects on HpaI and NheI accessibility, a bit increased HindIII accessibility (87% vs. 75% for wt), and significantly more cutting by BslI (39% vs. 27% for wt) (Fig. 43A). These increased accessibilities for HindIII and BslI confirmed the subtle effects at NDR1 seen with DNaseI indirect endlabelling. TFIIF is involved in transcriptional start site selection [225] and the subtle shift of nucleosome N+1 could be connected to an altered start site selection. An E346A substitution in the TFIIF subunit Tfg1 (*tfg1-E346A*) leads to an upstream shift of the transcriptional start site at a number of loci [225]. So we checked if this mutation would mimic the ablation of Tfg2 with regard to nucleosome positioning at the *PHO8* promoter, but found no effect (Fig. 59).

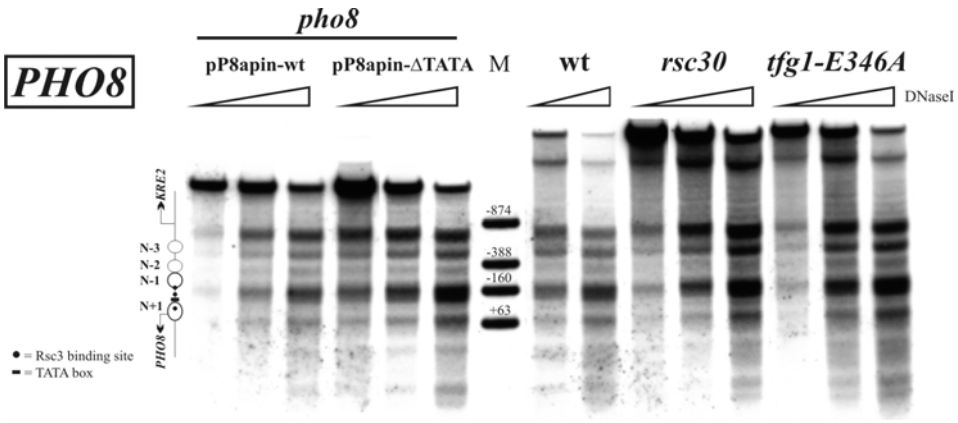

Figure 59. Nucleosome positioning at the *PHO8* promoter was unaltered in a *rsc30* strain, a *tfg1-E346A* strain and a strain where the *PHO8* TATA box was mutated.

DNaseI indirect endlabelling analysis of the *PHO8* promoter in two *pho8* strains carrying a pP8apin shuttle vector either with (pP8apin-wt) or without (pP8apin-ΔTATA) the *PHO8* TATA box, a wildtype strain (BY4741), a strain carrying a deletion mutant allele of a RSC subunit (*rsc30*) or in a strain carrying a allele of the TFIIF subunit Tfg1 with an E346A substitution (*tfg1-E346A*). Schematics, ramps and marker as in Figure 42.

We also analyzed the temperature sensitive strains that showed an effect on *PHO8* promoter chromatin for effects at other loci. There were strong effects on *PHO5* promoter chromatin in the *taf1-ts*, *tfa1-ts* and *spt15-ts* mutants (Fig. 58), subtle effects at *PHO84* in the *spt15-ts* mutant (Fig. 61) and no changes at all at the *RIM9*, *SNT1* (Fig. 60), *GAL10* and *RIO1* loci (Fig. 61). Such negative outcome at other loci confirmed that effects seen at the *PHO8* promoter were not caused indirectly by an unspecific loss of chromatin integrity under restrictive conditions of the respective temperature-sensitive strain, but were rather specific for the *PHO8* promoter. In the *taf3-ts*, *spt15-ts* and *tfa1-ts* strains, the NDR at the *CHA1-VAC17* promoter was reduced in the direction of the *CHA1* ORF roughly by slightly less than the size of one nucleosome. The DNaseI pattern for the *tfg2-ts* strain was largely unaltered except for a very subtle shift in the intensity distribution of the DNaseI bands that mark the *CHA1-VAC17* promoter NDR. In the wildtype the intensity of the DNaseI bands is strongest towards the *CHA1* ORF whereas the opposite was the case in the *tfg2-ts* strain (Fig. 60). In addition, at *SUC2* we noticed a strongly altered DNaseI pattern in the *taf3-ts* strain and changes in the *tfa1-ts* strain whereas the positioning appeared unaltered in the *spt15-ts* and *tfg2-ts* strains (Fig. 61).

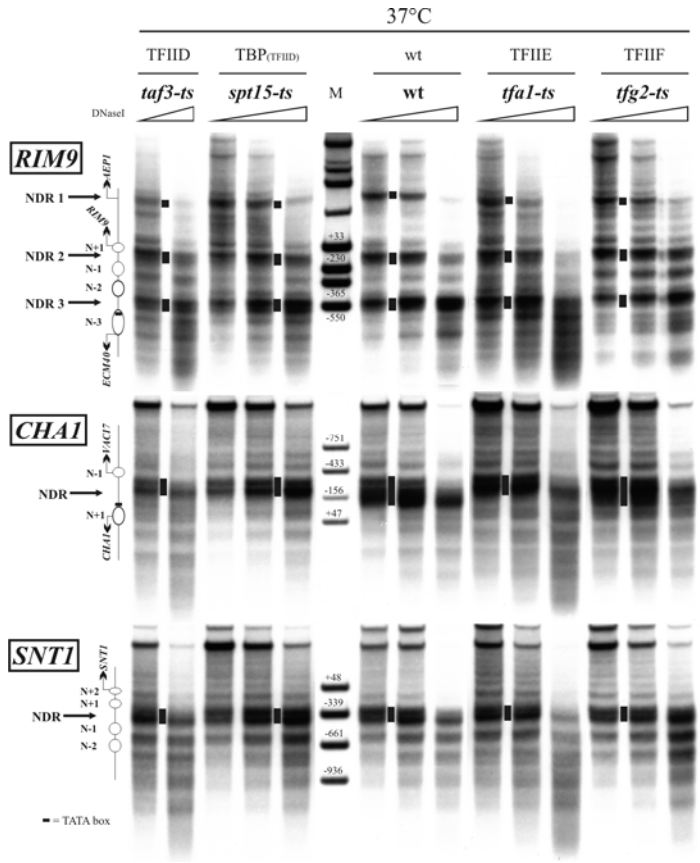

Figure 61. Loss of some general polymerase II transcription factors by elevated temperature altered the chromatin architecture at the *CHA1* promoter but not the *RIM9* and *SNT1* promoters.

Same as Figure 51 except for the *RIM9*, *CHA1* and *SNT1* promoters in the indicated strains.

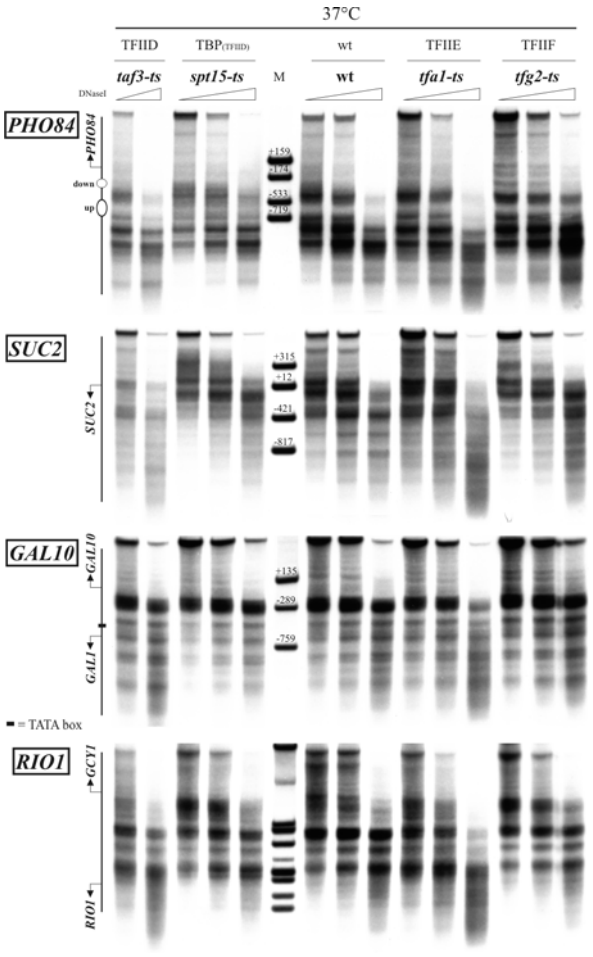

Figure 60. Loss of some general polymerase II transcription factors by elevated temperature altered the chromatin architecture at the *SUC2* promoter but not the *PHO84*, *GAL10* and *RIO1* promoters.

Same as Figure 51 except for the *SUC2*, *PHO84*, *GAL10* and *RIO1* promoters in the indicated strains.

2.6.12. A role for TBP in nucleosome positioning could not be confirmed *in vitro*

We aimed to confirm the involvement of the GTFIIs *in vitro* by the same approach as for RSC, i.e. rescue of a *ts*-extract with the corresponding purified GTFII. As TBP is the only GTFII with direct DNA binding activity and as the corresponding *ts* strain showed effects at *PHO8*, *PHO5* and *CHA1*, we first prepared an *spt15-ts* extract. Moreover, both the *PHO8* NDR1 and the *CHA1-VAC17* NDR contain a TATA box (*SNT1* and *RIM9* lack a TATA box [184]). Using our standard set of plasmids (*PHO8*/*RIM9*/*CHA1*/*SNT1*) in our *in vitro* reconstitution system, the *spt15-ts* extract indeed failed to properly reconstitute nucleosome positioning at the *CHA1*, *RIM9* and *SNT1* loci, whereas *PHO8* was reconstituted reasonably well though not as good as with a wildtype extract (Fig. 62). The DNaseI pattern at all four loci differed from that seen just after salt assembly showing that the *spt15-ts* extract contained nucleosome remodeling activities sufficient to remodel at least a majority of the templates. Addition of purified truncated TBP (Δ1-61) did not rescue the *spt15-ts* extract. In fact, the DNaseI patterns at all four loci where virtually identical with and without added TBP (Fig. 62). In another approach we incubated truncated TBP (Δ1-61) together with purified RSC (and ATP) to see if this minimal set of factors had some positioning activity.

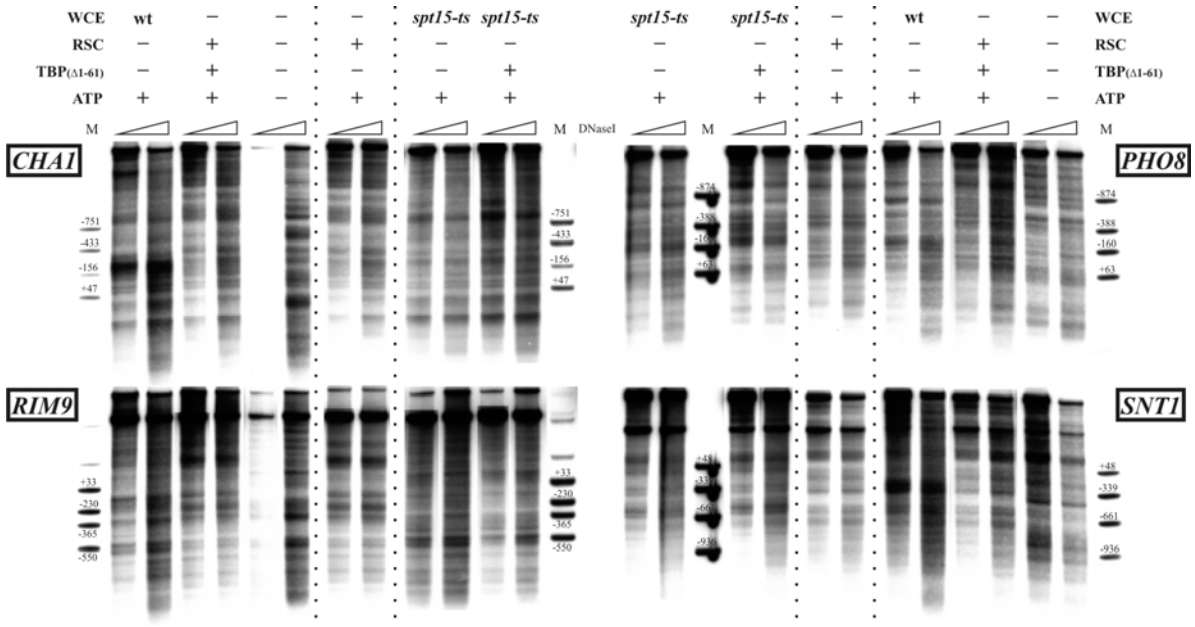

Figure 62. Purified TBP has no positioning activity *in vitro*.
DNaseI indirect endlabelling analysis of pre-assembled pUC19-*CHA1*, pUC19-*RIM9*, pUC19-*PHO8* and pUC19-*SNT1* plasmids. Chromatinised plasmids were incubated alone or with a combination of ATP, WCE (made either from a *spt15-ts* strain grown at 37°C overnight or a wildtype strain grown at 30°C), purified RSC (concentration approximately 15 nM, i.e. a RSC:nucleosome ratio of approximately 1:5) and purified truncated TBP (residues 61-240; concentration: 60 nM) in the presence of ATP. Stippled lines separate the samples electrophoresed on separate gels. The lanes of the +RSC and ATP sample were taken from Figure 54. Ramps and markers as in Figure 8B.

However, the DNaseI pattern observed upon incubation with RSC and TBP was identical to the pattern seen with RSC only. These results indicate that the positioning deficiencies of the *spt15-ts* extract (and the *spt15-ts* strain *in vivo*) could be due to indirect effects. Alternatively, TBP might be required in complex with other proteins (e.g. TFIID) and such a complex does not reform in the *spt15-ts* extract upon addition of just purified TBP. Similarly, as we did not have a positive control for TBP in our assay we could not exclude that the truncated form of TBP was insufficient and full-length TBP

required. The chosen TBP concentration (60 nM) was higher than those previously used for *in vitro* transcription assays [226, 227] and corresponded to a TBP:nucleosome ratio of almost 1. A previous study showed that the *in vitro* transcription ability of an *spt15-ts* extract can be rescued by purified TBP further implying that the failed rescue in Figure 62 is not due to insufficient TBP activity but because of indirect effects [228]. However, these previous experiments are not fully comparable with ours here as they used a different *ts*-allele, grew the strain at permissive conditions before extract prep and used full length TBP for the rescue. Overall, the *in vitro* experiments failed to provide any positive evidence for a direct role of TBP in nucleosome positioning, nevertheless it remains an open possibility that TBP might have positioning activity, which could be seen under optimised conditions. Full-length TBP or purified TFIID (or other GTFIIs) could be used to further investigate the direct role of GTFIIs in nucleosome positioning.

3. Discussion

This study features the first ever faithful reconstitution of nucleosome positioning across an entire genome. Our results argue very definitively against the "genomic code for nucleosome positioning" hypothesis as they highlight the predominant role of extrinsic factors for nucleosome positioning. Our results also argue against the widely referenced statistical positioning model and suggest a new, remodeling enzyme-based mechanism for generating the regular nucleosomal arrays that emanate from promoter NDRs. Furthermore, we initiated the biochemical dissection of the positioning mechanisms at work and demonstrate the direct role of the RSC complex in nucleosome positioning. We show that the RSC complex is specifically required for establishing NDRs *in vitro* but that RSC, in most cases, requires other factors to do so. Overall, our results provide major insight into the general principles of nucleosome positioning and into the specific involvement of the RSC remodeling complex.

3.1. *Trans* factors are predominant determinants of nucleosome positioning

The results presented in this study demonstrate that the major determinants of nucleosome positioning are extrinsic factors and not intrinsic sequence cues as the *in vitro* reconstitution of proper nucleosome positioning was mostly dependent on specific *trans* factors. Assembly of chromatin from naked genomic DNA and purified histones by salt assembly alone generally failed to reconstitute proper nucleosome positioning genome-wide [119, 120] (Fig. 20B and 21). Although depletion over NDRs and positioning of some N+1 or N-1 nucleosomes could be properly reconstituted by this approach to some extent, other "factors" were clearly missing from the *in vitro* system to achieve proper positioning for all other nucleosomes. In principle, the missing "factor" in all these experiments could have been the inadequate choice of reconstitution/assembly conditions. However, addition of WCE in the presence of ATP to the system under otherwise identical conditions resulted in the proper reconstitution of nearly all aspects of positioning at almost all yeast loci. It was a remarkable result that WCE/ATP allowed for the reconstitution of both the promoter NDRs and the nucleosomal arrays that emanate from these NDRs (Fig. 10, 22A and B). This showed that the experimental conditions (source of DNA/histones, buffer conditions, concentrations of all

components) as such were sufficient to achieve proper positioning. Moreover, this reconstitution clearly was not just due to unspecific nucleosome remodeling activity in the WCE since incubation with the purified remodeling enzymes ACF (genome-wide: [119]), temperature induced sliding (7 loci: Fig. 12; genome-wide: Fig.23) and incubation with *Drosophila* or *S.pombe* extracts (2 loci; Fig. 13A) all failed to reconstitute the proper nucleosome positions. We even showed the specific and direct role of one of the involved *trans* factors: the RSC remodeling complex (see discussion further below), further underscoring our notion that extrinsic factors are the main determinants of nucleosome positioning.

Conversely, the prominently suggested "Genomic Code", i.e. the notion that nucleosome positioning is primarily determined by sequence intrinsic features, can be rejected on the ground of the work by us and others [119, 135, 229]. Previous studies have questioned this hypothesis based on the inability of reconstituting proper positioning by salt assembly alone [119] or by the failure of predicting positioning from sequence alone [115, 132]. While these negative results are of great importance, we now provide positive evidence for the major contribution of *trans* factors. Intrinsic DNA sequence features contribute to nucleosome depletion at yeast promoters and can position few isolated nucleosomes [120, 129, 169] (Fig. 63). However, reconstitution of even these feature was greatly improved in the presence of *trans* factors (WCE) (Fig. 22), showing that intrinsic DNA sequence feature have an insufficient and subordinate role in determining nucleosome positioning. Moreover, most of the reconstitution success by intrinsic DNA sequences was likely due to enrichment of homopolymorphic dA:dT stretches at *S. cerevisiae* promoter regions. Other species, such as *S. pombe* [5], lack such an enrichment suggesting that the role of intrinsic sequence features in nucleosome positioning, which seems already secondary in *S. cerevisiae*, might even be less important in other organisms.

3.2. Regular nucleosomal arrays are generated by an active and directional packing process

The regular nucleosomal arrays that emanate from 5'NDR into coding regions are one of the major features of the primary structure of chromatin in *S. cerevisiae* and other species. Intrinsically DNA-encoded sequence preferences alone, though they were proposed to be the major determinants of nucleosome positioning [113, 120, 134], evidently cannot generate these regular arrays as several independent experiments have failed to detect any such arrays in salt assembled chromatin under a range of different conditions [74, 119, 120, 203] (Fig. 20B and 21).

Transcription was equally suggested to be involved in the generation of the nucleosomal arrays [75, 98]. Our reconstitution of nucleosomal arrays occurred in the absence of the nucleoside triphosphates other than ATP as these were depleted from the extract during extract preparation and omitted from the reconstitution reaction. It is highly unlikely that they were regenerated by some salvage pathway and it is equally unlikely that transcription was efficiently reconstituted at the majority of templates and at all genes including the normally quiescent ones [75]. Therefore, transcription does not seem to be essentially required to establish the nucleosomal arrays, though it cannot be excluded that transcription would improve the reconstitution even further.

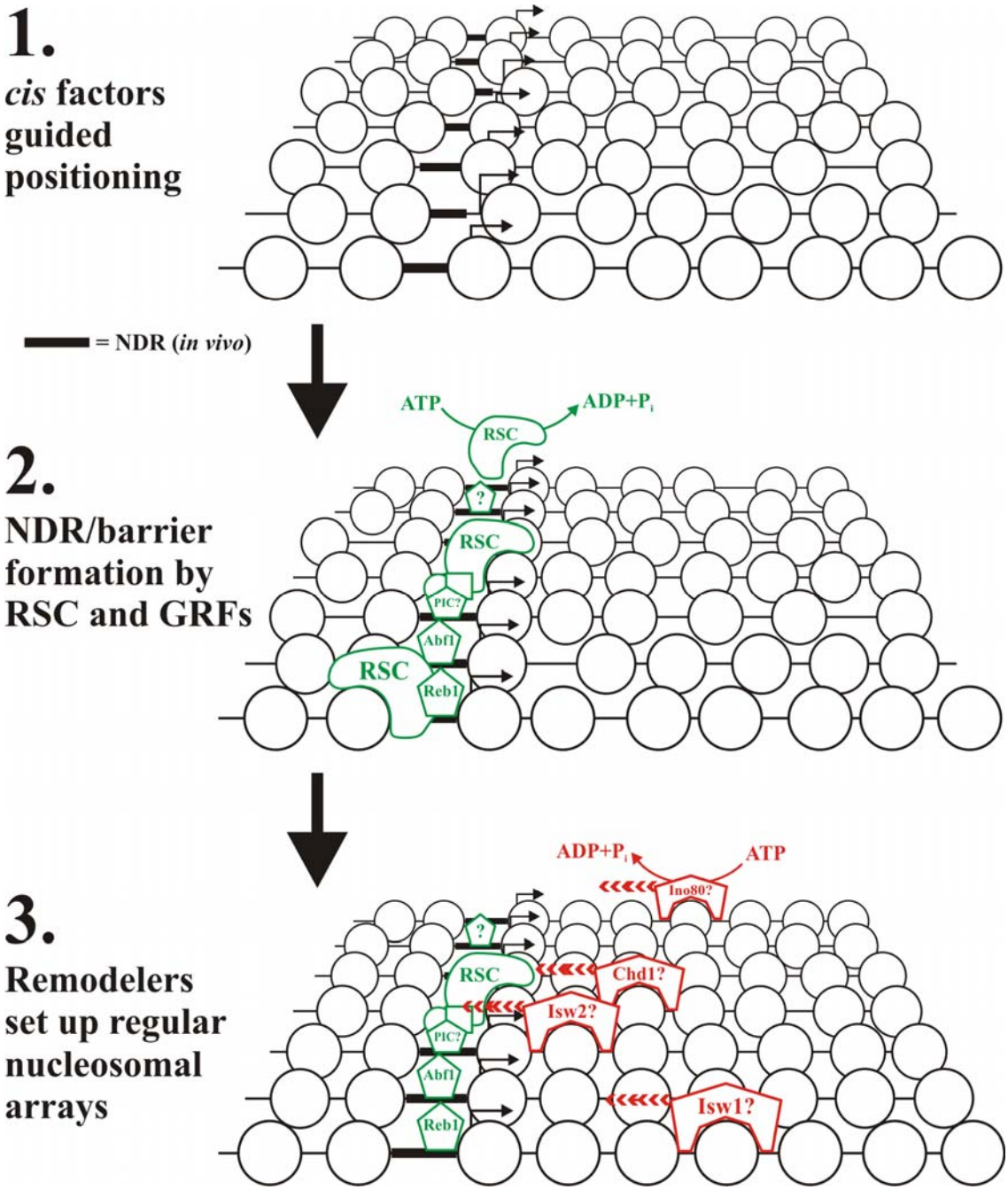

Figure 63. New model for nucleosome positioning in regular arrays.
The diagram shows the three major mechanistic contributors to nucleosome positioning at yeast promoters. **(1)** DNA intrinsic positioning is insufficient for proper positioning but contributes to NDR formation. **(2)** RSC in combination with GRFs (e.g. Reb1 and Abf1) and possibly other factors (e.g. PIC) (all in green) fully set up NDRs. **(3)** Nucleosome remodelers (top candidates in red) actively pack nucleosomes against the NDRs and establish regularly spaced arrays. Steps **(2)** and **(3)** may occur in parallel or independently of each other. This figure was inspired by Zhang *et al.* [74].

The most widely discussed positioning model, "Statistical Positioning" [75, 107], explains the regular nucleosomal arrays as the result of a fixed barrier (NDRs) against which nucleosomes stack statistically (see chapter 1.3.3.4.). As such, the model explains very well the observed nucleosomal arrays with decaying regularity. However, in this model the distance between the regularly spaced nucleosomes is a function of the nucleosome density, i.e. nucleosome arrays show wider spacing at lower nucleosome densities. In contrast, we reconstituted nucleosomal arrays on chromatin assembled at roughly half the physiological nucleosome density, yet the spacing within these arrays

was the same as in fully assembled templates or in *in vivo* chromatin (Fig. 24A and B). This suggests that the statistical positioning model, at least in its original form, is incorrect. Further, both the maintenance of physiological spacing and the shift of nucleosome density towards the 5'NDR in the 0.5:1 sample (Fig. 24D) speak for an active mechanism that sets up regular arrays and spacing within the array. The ATP dependency of the reconstitution system as well as the known ability of nucleosome remodeling enzymes to generate regular arrays suggest that such nucleosome remodeling enzymes are part of this "active packing mechanism" (Fig. 63). Also this model requires a barrier against which the remodelers actively pack the nucleosomes with spacing being determined by physical constraints, remodeler preferences and/or other factors (Fig. 63). Formation of the barrier itself likely involves the nucleosome excluding properties of poly(dA:dT) stretches, sequence specific binding factors (such as Abf1 or Reb1, or possibly even the pre-initiation complex) and, again, nucleosome remodeling enzymes (such as RSC - see below) (Fig. 63).

3.3. The RSC remodeling complex as a major regulator of nucleosome positioning

The RSC remodeling complex was previously implicated to participate in nucleosome positioning [149], especially in the establishment of promoter NDRs [138-140]. Furthermore, a specific DNA binding motif was identified for two RSC subunits and the location of these motifs was shown to overlap with sites of nucleosome occupancy change upon inactivation of one of these subunits [138]. In this study, we independently identified the RSC remodeling complex as a positioning factor for the *PHO8* and other promoters. Moreover, we showed for the first time that RSC is directly and specifically required for establishing promoter NDRs (Fig. 63). We show that mutation of a putative Rsc3 binding motif can affect nucleosome positioning although there is conflicting evidence on whether this putative Rsc3 binding motif is indeed recognised by RSC.

3.3.1. RSC is mostly not sufficient but directly and specifically required for nucleosome positioning.

Previous studies of the role of RSC in nucleosome positioning used temperature sensitive mutants of individual subunits [138-140]. Such experiments suffer from the inability to asses to what extent the observed changes were due to indirect effects, which are not unlikely as RSC is a major regulator of gene expression [62, 230] and essential for cell viability. Here we circumvented these problems by testing RSC in our *in vitro* reconstitution system. At most loci, purified RSC alone failed to reconstitute proper positioning indicating that RSC alone is generally not sufficient to set up promoter NDRs. Importantly, these results were not due to insufficient activity of our purified RSC since the employed amounts were sufficient to remodel all templates as indicated by a clear ATP-dependent change in the DNaseI pattern at all loci. Moreover, RSC alone did reconstitute some aspects of proper positioning at *SNT1* and *CHA1* showing that it can in principle be sufficient for proper positioning. Finally, the same amount of purified RSC fully rescued the positioning activity of the *rsc3-ts* 37°C extract. The inability of the *rsc3-ts* 37°C extract to reconstitute proper positioning *in vitro* could equally be due to indirect effects, however the ability to rescue the extract with purified RSC clearly shows that RSC is directly involved in setting up promoter NDRs. Formally, the direct role of RSC could be independent of its remodeling ability, and the ATP-dependency of *in vitro*

reconstitution could be due to some other factor. Testing the ability of catalytically dead RSC to rescue the *rsc3-ts* 37°C extract could help to settle this question.

Importantly, the inability of RSC to reconstitute proper positioning on its own demonstrates that in most instances RSC requires other factors for NDR generation. Identifying these factors and how they function in cooperation with RSC remains a future challenge. Astonishingly, neither SWI/SNF nor Isw2 were able to rescue the *rsc3-ts* 37°C extract. Given the high similarity of SWI/SNF to RSC in terms of remodeling mechanism [221, 231] and subunit composition [220] the specific requirement of the RSC remodeling complex for NDR formation remains to be explained. For one, this could be due to specific recruitment, orientation and or/activation of RSC by some other factor(s), which would also explain the dependency of RSC on other factors from the extract. Alternatively or in addition, RSC could have specific intrinsic properties not shared by SWI/SNF or Isw2. Since RSC, but neither SWI/SNF nor Isw2, could properly position nucleosome N-1 at *SNT1* in the absence of any other factors, specific intrinsic properties of RSC are in play at least at some loci.

3.3.2. A conserved Rsc3 site at *PHO8* is required for NDR maintenance and basal transcription *in vivo* but is dispensable for RSC recruitment *in vivo* and NDR formation *in vitro*

The DNA-binding domains of Rsc3 and Rsc30 specifically bind the motif CGCGC *in vitro* [138]. A role of this motif in nucleosome positioning was so far only inferred from the coincidence of such predicted Rsc3/Rsc30 sites with sites of changes in nucleosome occupancy in a *rsc3-ts* strain. Recently, Floer *et al.* studied the role of RSC in positioning at the *GAL1-10* locus [232]. They identified three putative Rsc3 sites at the *GAL1-10* promoter and the deletion of a 61 bp sequence encompassing all three sites led to some changes in nucleosome positioning/occupancy. However, the importance of the Rsc3 motif is difficult to infer from these experiments as deletion of such a large stretch could have caused effects independent of the putative Rsc3 sites, especially as the deleted segment contained a known Gal4 binding site.

We in contrast tested the three putative binding sites at the *PHO8* promoter by point mutations and showed that mutation of the evolutionary conserved binding site at -151 at the centre of the *PHO8* NDR1 leads to increased occupancy over this NDR similar to what was seen in the *rsc3-ts* mutant. This experiment alone suggests that formation of the *PHO8* NDR1 *in vivo* by RSC is dependent on the presence of a Rsc3 binding site either because RSC is recruited via this motif and/or because this motif orientates or activates RSC (i.e. the motif is involved mechanistically in the process of NDR generation). However, there is evidence against both explanations. The putative Rsc3 sites were mostly dispensable for NDR formation *in vitro*. This argues strongly against a critical mechanistic role of such sites. But as the specific recruitment of remodeling enzymes is notoriously difficult to reconstitute *in vitro* (Craig Peterson, personal communication; [233]), this *in vitro* result does not exclude that the putative Rsc3 sites are necessary for RSC recruitment *in vivo*. Still, the unaltered RSC occupancy in the absence of the Rsc3 sites *in vivo* argues that the Rsc3 sites are dispensable for recruitment of RSC.

Since both a mechanistic as well as a recruitment role seem unlikely, what is the basis of the observed effect upon mutation of the Rsc3 site at -151 *in vivo*? For one, some cellular process (e.g. transcription) might not be reconstituted *in vitro* and in the absence of such a process the Rsc3 sites

become dispensable *in vitro*. Alternatively, the CGCGC motif might be required to recruit some other (unknown) factor *in vivo*. In this context it is important to re-consider the specific but unknown "*PHO8* NDR1 binding activity" that co-purified with the "*PHO8* positioning activity" (Fig. 39). Determining whether or not this unknown binding activity is in fact RSC and whether or not this specific binding depends on the Rsc3 sites could help solve the enigmatic role of the putative Rsc3 sites at the *PHO8* promoter. It may also be re-considered how definitively the recruitment model is ruled out by the *in vivo* ChIP experiments, despite their positive and negative controls, especially as remodeling enzymes are notoriously difficult to detect this way (e.g. compare the variable results of the different ChIP studies: Table S2 and S3).

NDRs upstream of transcriptional start sites are thought to allow access to the transcription machinery [29, 127, 180]. In line with this notion, reduced accessibility of the NDR in the -151 mutant correlated with decreased basal ($+P_i$) *PHO8* expression. Similarly, a *rsc3-ts* strain grown at the restrictive temperature for 8h displayed a more than 3-fold decrease in *PHO8* mRNA levels [62]. Remarkably however, all Rsc3 sites were dispensable for fully induced expression under $-P_i$ conditions. Nonetheless, the Rsc3 site(s) may still be required for proper *PHO8* expression under intermediate and more physiological phosphate levels, and the Rsc3 site(s) could have an effect on the kinetics of induction.

Activation of *PHO8* is accompanied by promoter chromatin alterations , which critically depend on SWI/SNF [201] (Fig. 50C). Interestingly, a very similar loss of N-3 is observed both upon RSC inactivation and upon induced SWI/SNF recruitment. In line with the enrichment of RSC over N-3 (Fig. S4A) this suggests that RSC and SWI/SNF might have opposing functions with regard to N-3, i.e. RSC ensures proper placement under repressing conditions and SWI/SNF is recruited upon inactivation to counteract RSC and remove N-3. Such a competition mechanism between different remodeling enzymes could provide another explanation for the remodeler (or co-factor) dependency of certain nucleosomes, in addition to the intrinsic stability argument brought forward previously [169, 175].

3.3.3. Discrepancies between *in vivo* and *in vitro* - evidence for different mechanisms for formation versus maintenance of NDRs?

The *rsc3-ts* 37°C extract failed to reconstitute NDRs *in vitro* at a number of loci (namely *SNT1*, *ADH2* and *RNR3*) where neither we nor others had seen any or only very small effects in the RSC *ts* strains *in vivo* [138, 139] (Fig. S4C, F and H). Proper positioning was rescued upon addition of purified RSC suggesting a direct role of RSC in positioning also at these loci. Why was the *in vitro* reconstitution at these loci dependent on RSC but no changes were observed *in vivo* upon RSC inactivation? For one, it could be that *SNT1*, *ADH2* and *RNR3* require a particularly low concentration of RSC activity. *In vitro*, RSC activity might have been lower than upon ablation *in vivo,* for example due to inactivation during extract preparation, and the components in the reconstitution reactions are probably more diluted than *in vivo*.

Alternatively, the differences between *in vivo* and *in vitro* could point to different mechanisms for NDR formation and maintenance. The *in vivo* experiments address the loss of properly positioned nucleosomes upon RSC inactivation, whereas *in vitro* experiments monitor "*de novo*" generation of properly positioned nucleosomes in the absence of RSC. Hence for some loci other factors might

maintain proper positioning *in vivo* in the absence of RSC whereas such factors are unable to generate correctly positioned nucleosomes from scratch.

Such a maintenance mechanism appears particularly likely for the NDR at the *SNT1* promoter for which two other potential positioning factors were previously identified: Reb1 and Abf1. Reb1 is enriched at the *SNT1* NDR [180] (Fig. S4C) and the Reb1 binding site (together with an adjacent dA:dT tract) within the *SNT1* NDR was sufficient for NDR generation when placed at other ectopic sites e.g. within another ORF [42]. Furthermore, mutation of this putative binding site, as well as another putative Abf1 binding site at the other edge of the NDR, led to loss of H2A.Z enrichment in the nucleosomes flanking the NDR. So the *SNT1* NDR harbours functional/occupied binding sites for Abf1 and especially for Reb1, both of which were shown to play a role in NDR formation at many loci [138, 139]. Inactivation of neither Reb1 nor Abf1 alone lead to altered positioning at *SNT1* [139] (Fig. S4C). However, a strain carrying temperature sensitive degron alleles of both *REB1* and *ABF1* displayed increased nucleosome occupancy over the *SNT1* NDR showing that Reb1 and Abf1 are redundantly required for proper nucleosome depletion over the *SNT1* NDR *in vivo* [139] (Fig. S4C). Nevertheless, even in the *abf1-td reb1-td* strain the *SNT1* NDR was clearly present (despite the relative increase in nucleosome occupancy; Fig. S4C) indicating that further factors are involved in NDR formation. Our *in vitro* results suggest that this other factor is likely to be RSC. Moreover, the presence of both Reb1 and Abf1, two very potent nucleosome excluding factors [120, 138], as functional positioning factors at the *SNT1* NDR could readily explain why nucleosome depletion was maintained even in the absence of RSC.

Interestingly, the three promoters for which effects upon RSC inactivation were also seen *in vivo* (*PHO8*, *RIM9*, *CHA1*) all harbour a putative Rsc3 binding site and generally show high levels of RSC occupancy at such sites [140, 180, 234, 235] (Fig. S4A, B and D). In contrast, the three promoters (*SNT1*, *ADH2*, *RNR3*) for which RSC-dependency could only be shown for *in vitro de novo* NDR formation all lack putative Rsc3 sites and also show very low levels of RSC occupancy [138, 140, 180, 234, 235] (Fig. S4C, F and H). It is tempting to speculate that there could be two different classes of RSC target promoters. The first class requires RSC both for the establishment as well as for the maintenance of their NDRs. Putative Rsc3 binding sites appear common in this class. The second class also depends on RSC for the formation, but not for maintenance of NDRs.

3.3.4. Arp9 and Arp7 presumably are required for proper positioning as they are necessary for full RSC ATPase activity

Proper nucleosome positioning at *PHO8* was disrupted in the *arp9-ts* strain, but, somewhat surprisingly, only very slightly altered in the *arp7*/*arp9*/*mra1* strains. One would assume that the *arp9* deletion mutant should show the stronger phenotype than the *ts* mutant. This suggested that the additional *mra1* suppressor mutation in the *arp7/arp9* deletion mutants not only suppressed the growth deficit but also the diminished RSC activity. Szerlong *et al.* revealed that the various *mra* mutations all correspond to single amino acid changes in the post-HSA and protrusion 1 domains of the RSC ATPase subunit Sth1 (e.g. *mra1*: N384K)[222, 236].The Arp7/Arp9 dimer binds the RSC complex via the HSA domain and the post-HSA and protrusion 1 domain relay the bound state to the rest of the complex. The *mra* suppressor mutations apparently lead to structural alterations that signal the bound state even in the absence of Arp7/Arp9. More importantly, the complex lacking Arp7/Arp9 had only ~50% ATPase activity *in vitro* [236], which was increased to around 85% by the

N384K (= *mra1*) mutation [222]. Since this *mra1* mutation mostly suppressed the expected positioning deficit in the *arp7*/*arp9* null mutants at a number of loci (Fig. 47), we suggest that the role of Arp9 (and Arp7) in nucleosome positioning to a large extent is limited to stimulating full RSC activity. Thus Arp9 (and Arp7) possibly do not contribute much to the principle mechanism of RSC recruitment, NDR formation and stabilization. It is so far unknown if the *mra1* mutation alone (i.e. in the presence of Arp9/Arp7) increases RSC's ATPase activity beyond wildtype levels. The increased width of *PHO8* NDR1 in the *mra1 ARP7 ARP9* strain (Fig. 48) suggests that this could be the case and highlights the importance of fine-tuning RSC's ATPase levels to achieve proper positioning.

3.4. The *PHO84* promoter: even otherwise sufficient intrinsic DNA sequence features require *trans* factors for proper nucleosome positioning

Our combined *in silico*, *in vitro* and *in vivo* approaches identified differences in intrinsic stability to be (at least partially) responsible for the different remodeler dependencies of the upstream and the downstream nucleosomes of the *PHO84* promoter. At the *RNR3* locus, where gene activation is also Snf2-dependent, introduction of a poly dA:dT stretch facilitated activation [237]. Here, the introduction of (rather long) poly dA:dT stretches removed the underlying nucleosome leading to gene activation independent of induction conditions and Snf2 recruitment. In contrast, our 10A insertion at *PHO84* by itself had no effect on the occupancy of the upstream nucleosome under non-inducing conditions but allowed for partial removal of this nucleosome upon induction even in the absence of Snf2. Apparently, lowering the intrinsic stability of the upstream nucleosome made it a substrate for (an)other remodeling factor(s). As an extension to the previous correlations for the *PHO5* and *PHO8* promoters [175], our mutagenesis study directly argues for a causal relationship between intrinsic stability and remodeler requirement. DNA intrinsic sequence preferences have mainly been suggested to play a role in promoter regulation by determining/affecting nucleosome positioning or occupancy. Our results for the *PHO84* promoter suggest that intrinsic sequence cues might affect gene regulation also by determining what co-factors are required to remove or remodel certain nucleosomes. This would provide another level of fine-tuning gene regulation.

Contrary to all other loci studied, RSC activity was detrimental towards proper positioning at the *PHO84* promoter. *In vivo*-like positioning of the up- and downstream nucleosome was already achieved by salt assembly and this positioning remained unaltered when RSC was added in the context of the entire WCE. In contrast, purified RSC on its own disrupted both the upstream and downstream nucleosome. This disruption by RSC in the absence of other factors very likely explains why the two extract fractions positive for positioning at *PHO8* also altered the proper positioning at *PHO84* (Fig. 34). These fractions contained RSC but apparently lacked those factors that somehow prevent RSC from removing the upstream and downstream nucleosome.

The ability of RSC to readily remodel the upstream nucleosome *in vitro* raises the question as to why remodelling of this nucleosome critically depends on SWI/SNF (and under some conditions Ino80) *in vivo* [169]. For one, RSC might be excluded from the *PHO84* promoter under inducing conditions *in vivo*. There is some controversy on whether RSC is present at the *PHO84* promoter under repressing conditions as the high-resolution mapping by Venters *et al.* detected considerable amounts of RSC at *PHO84* [180](Fig. S4J) whereas the studies by Ng *et al.* and Damelin *et al.* did not [234, 235]

(Table S2). Alternatively, other factors might stabilise the up- and downstream nucleosome against the action of RSC.

The *PHO84* promoter harbours two putative Reb1 binding sites, one located upstream of the upstream nucleosome and one between the up- and downstream nucleosome. Venters *et al.* detected a strong enrichment of Reb1 over both binding sites. Another group, mapping DNaseI protected regions genome-wide at high resolution, found the latter putative Reb1 site protected from DNaseI [238]. A caveat for evaluating the Venters *et al.* factor enrichments at the *PHO84* promoter is that nearly all factors that were mapped at high resolution showed a strong enrichment at *PHO84*. The reason for this could be that the *PHO84* promoter is easily induced and loses its nucleosomes when grown in YPDA medium without additional phosphate. Presumably for this reason, the genome-wide nucleosome map of Whitehouse *et al.* detected the whole *PHO84* promoter as nucleosome free [142]. Such a long stretch (~1kb) of DNA devoid of nucleosomes could lead to "artificially" high ChIP binding levels. Nevertheless, if Reb1 were a factor stabilising positioning at *PHO84* against the action of RSC one might expect a disruption of the *PHO84* promoter architecture upon Reb1 inactivation. However, both we and Badis *et al.* identified only very subtle changes using two independently generated strains carrying a temperature sensitive allele of Reb1 [138] (Fig. 29). Again confusingly, Badis *et al.* found strong increases in nucleosome occupancy across almost the entire *PHO84* promoter upon inactivation of Tbf1, Mcm1, Rap1 and Cep3. Quite likely these changes are due to indirect effects possibly involving the partial induction of *PHO84* that sometimes occurs even in full medium as described above.

Collectively, it remains unclear why RSC does not remodel the upstream nucleosome *in vivo* but disrupts proper positioning at *PHO84 in vitro*. Nonetheless, the requirement of *trans* factors from the extract *in vitro* to maintain the proper positioning at the *PHO84* promoter in the presence of RSC, even though the positioning is largely determined by DNA intrinsic sequence cues, further questions the importance of DNA intrinsic sequence preferences in determining nucleosome positioning *in vivo*. Possibly even those few nucleosomes that are correctly positioned by the DNA sequence alone might nevertheless require extrinsic factors for protection/stabilization.

3.5. General transcription factors might contribute to nucleosome positioning

General transcription factors (GTFs) help to specify promoter identity and to assemble the transcription apparatus [29]. At least at some promoters, part of the PIC is constitutively present [180, 224]. So GTFs could contribute to NDR formation *in vivo*. Indeed, we found GTFs in our final extract fraction and wildtype nucleosome positioning at the *PHO8* promoter was disrupted in *tfa1-ts* (TFIIE subunit) and a *spt15-ts* (=TBP) strains under restrictive conditions. Further, the *PHO8* NDR is widened in a *tfg2-t*s (TFIIF) strain. Changes were also detected at the *SUC2*, *PHO5* and *CHA1* promoters in strains carrying temperature sensitive alleles of components of the TFIID as well as the TFIIE complex. These observations may be due to indirect effects as transcription of nearly all pol II genes were affected. However, there are some arguments for a direct role of GTFIIs in nucleosome positioning.

Firstly, the positioning at *SNT1*, *RIM9*, *PHO84* and *GAL1-10* was largely unaltered upon ablation of the GTFIIs ruling out global defects in chromatin architecture. Secondly, for *PHO8* and *CHA1* the affected

regions are located close to known transcriptional start sites [185]. Thirdly, the nucleosome organization at the *PHO5* [239] and at the *PHO8* promoter (Fig. 59) was unaltered in a TATA box deletion mutant. So the observed changes could not be mimicked by just downregulating basal transcription. Finally, the promoters that displayed changes show an enrichment of the corresponding GTFIIs [180].

In addition, the changes seen at the *CHA1* promoter due to inactivation of either TFIID or TFIIE subunits closely resemble those seen upon promoter inactivation by starvation for serine. Under these conditions an additional nucleosome covers the TATA box thereby reducing the extent of the *CHA1* promoter NDR [149]. Conversely, this nucleosome is removed not only upon promoter activation, i.e. in the presence of serine, but also by inactivation of RSC subunits, like Sth1 or Rsc8 [149]. So in the case of the *CHA1* promoter, RSC is required to maintain the closed chromatin structure. We saw a similar role for TFIID and TFIIE to maintain the open chromatin structure at the *CHA1* promoter as the extent of the *CHA1* NDR in the *tfa1-ts*, *spt15-t*s and *tfg2-ts* corresponded to the closed structure despite the presence of serine in the medium (Fig. 60).

Contrary to our *in vivo* results, we were unable to clearly confirm the role of the GTFIIs *in vitro*. While an *spt15-ts* extract was impaired in its positioning ability, this loss of activity was not rescued by addition of purified (truncated) TBP. However, due to the number of limitations of the *in vitro* approach (see chapter 2.6.12.), this does not exclude that TBP acts as a positioning factor. Further experiments are required to determine the extent to which GTFIIs act directly as nucleosome positioning factors. Nevertheless, we suggest that some GTFs (especially TBP) might occupy the NDR , thereby exclude nucleosomes, and function as a barrier maybe similar to sequence specific DNA binders such as Abf1 and Reb1 [139].

3.6. Are nucleosomes *in vivo* at their equilibrium positions?

The primary chromatin architecture and its associated factors are a complex and highly dynamic structure [38, 57]. An important conceptual consideration is if nucleosomes reside at equilibrium positions. If this were the case the observed nucleosome positioning would be the net result of the binding competition between histones and DNA binding factors, as recently suggested [240]. In such a system remodelers would allow free nucleosome movement to their equilibrium position, i.e. remodelers would act as mere kinetic lubricants. Changes in nucleosome positions, e.g. after a certain stress signal, would be caused by a change in the concentration of DNA binding factors (and maybe histone modifications and variants). Again, remodelers would merely allow the establishment of a new equilibrium. The specific requirement of RSC, which could not be substituted by SWI/SNF or Isw2 argues strongly against this view. Consequently, if an ATP-consuming molecular machine is specifically required to establish a certain organisation, this organisation can never be at equilibrium but only at steady state. Equilibrium, by definition, corresponds to a state without net fluxes and is incompatible with the continuous net consumption of ATP.

Nucleosome positions in regular arrays are not energetically preferred by intrinsic sequence preferences [74, 119, 120] (Fig. 20B). Such positioning under equilibrium conditions would require favourable interactions overriding the intrinsic sequence preferences, e.g. with specific factors binding to linker regions or bridging nucleosomes at fixed distances. Histone H1 is the best known plausible candidate. However, this variant is only present at substoichiometric amounts and spacing

was not affected in its absence [17, 19]. Alternatively, favourable interactions between the nucleosomes themselves, which may be strongest "at the right distance", could stabilise regular arrays under equilibrium conditions. However, such a mechanism would be at odds with the decaying regularity of the arrays. Again, the active and directional packing mechanism by which the arrays appear to be generated are difficult to reconcile with an equilibrium state.

In general it is important to realize that yeast cells, and living organisms in general, are complex non-equilibrium systems. Indeed, chromatinised DNA is the template for multiple non-equilibrium processes, such as transcription, replication, histone turnover, recombination and repair, all of which impact on the primary chromatin architecture. Importantly, these processes make use of various *trans* factors (e.g. remodeling enzymes) that also contribute to nucleosome positioning. As such it is not necessary at all to assume that primary chromatin architecture were an "island of equilibrium" within the non-equilibrium processes acting on it.

3.7. Nucleosome positioning - many mechanistic aspects are not yet fully understood.

The chromatin architecture at (yeast) promoters is comprised of two major features: the NDRs and the regular nucleosomal arrays that emanate from them. Several of the major *cis* and *trans* factors that contribute to the formation of both features were identified, yet many mechanistic aspects remain unclear. For one, it is known that a variable combination of nucleosome excluding sequences (poly dA:dT tracts [122]), GRFs (e.g. Abf1, Reb1 [138, 139]) and nucleosome remodeling enzymes (e.g. RSC [138, 139]) are required for NDR formation at most yeast promoters. However, how the nucleosome remodeling enzymes (RSC) contribute here is not quite clear.

It seems that the formation of a majority of NDRs requires RSC in combination with other *trans* factors such as GRFs (Abf1 and Reb1), but little is known about the interplay between the two types of *trans* factors. The GRFs might bind to their sites first (which could be accessible because of a nearby poly dA:dT tract, "background remodeling activities" or following DNA replication) and subsequently recruit RSC. RSC in turn might then expand the NDR width and/or position the +1 and -1 nucleosome. A different order of events, where RSC first "clears" the binding motif followed by GRF recruitment and further RSC actions, seems also plausible. We know from *in vitro* experiments that remodeling enzymes, such as RSC, can happily and readily remodel almost any nucleosome [141, 143, 186]. So how is RSC's nucleosome remodeling activity controlled / fine-tuned to set up the NDRs together with the precisely positioned flanking nucleosomes, i.e. what prevents RSC from disrupting also these structures? One of the primary roles of the "other" *trans* factors could indeed be to exactly regulate RSC activity. Factors such as Abf1 and Reb1 could properly orientate/activate RSC, help in its eviction after NDR formation is complete, or prevent RSC from remodeling the +1/-1 nucleosome after they are positioned correctly. But what about those promoters that lack GRF binding sites? Here individual/specialised DNA binding proteins such as transcription factors or the PIC might take over the role of the GRF. It would seem a bit surprising though if so many different types of proteins could set up nearly identical chromatin structures. This raises the question of whether there might be other unknown factor(s) or processes involved NDR formation.

Establishment of the second major feature, the regular nucleosomal arrays, appears to be primarily driven by remodeling enzymes. *In vitro*, array formation is ATP dependent [74], and *in vivo*,

mutations affecting remodeling enzymes cause (subtle) changes in the arrays [95, 151]. Moreover, our results suggest that remodeling enzymes actively pack nucleosomes against the 5'NDR / barrier. Several important aspects of this new model have to be elucidated. For example, the remodeling enzymes that actually participate in array formation have to be identified. However, the relatively small effects upon inactivating single remodeling enzymes *in vivo* suggest a likely redundant functionality of remodeling enzymes.

Even beyond the involved remodeling enzymes, several major questions remain. Most importantly, what determines the directionality of the overall remodeling reaction, i.e. why do remodeling enzymes pack nucleosomes against the 5'NDR? One possibility is the specific recruitment of remodeling enzymes at the 5'NDR. The chromatin template could be folded as to bring e.g. the +4 nucleosome in the vicinity of the 5'NDR. Another possibility would be the formation of a "remodeler array" on top of the nucleosomal array, i.e. a remodeler would be recruited at the barrier, positions the +1 nucleosome and recruits/orientates the next remodeler which then positions the +2 nucleosome and so on. In general, it is a major challenge to explain the observed directionality of array formation against the 5' NDR as there is only little if any evidence to date for directionality of remodeling activity.

It seems that the only possible "source" of directional is the 5'NDR/barrier. Consequently, NDR/barrier formation should precede array formation (Fig. 63) and array formation should be disturbed when the 5'NDR is affected. However, inactivation of RSC or any of several GRF, though leading to increased occupancy over 5'NDR, on average only had minor effects on the nucleosomal array. For example, effects on the array were reasonably strong for the *reb1-ts* strain, whereas the *abf1-ts* strain displayed hardly any effects [138]. This suggests that NDR and array formation are not necessarily tightly coupled. Alternatively, the barrier function (i.e. against which nucleosomes are packed and possibly where array-forming remodelers are recruited) might not arise from the nucleosome depleted region but rather from the (independently?) positioned +1 nucleosome. Or it could be that the arrays are unexpectedly stable such that (partial) loss of the NDRs does not lead to array collapse within the timeframe of the aforementioned experiments.

Another interesting question is by what mechanism RSC clears nucleosomes away from the promoter NDRs. If RSC was to remove nucleosomes in *cis* (i.e. slide) then RSC, unless it exclusively slides nucleosomes in the upstream direction, would push nucleosomes (or a nucleosome) in a direction opposite to the array-forming remodeling enzymes. Could it be such counter-acting activities of two different remodeling enzymes what positions the +1 nucleosomes so precisely?

Finally, it has to be resolved what exactly determines the spacing within the nucleosomal arrays. This information could be intrinsic to the physical or mechanistic properties of the remodelers involved or could also be (partially) determined by some other (unknown) factor.

3.8. Concluding remarks

The *S. cerevisiae* genome encodes "only" around 6000 proteins, a majority of which do not even localise to the nucleus. Furthermore, the *S. cerevisiae* nuclear and chromatin architecture lacks some of the additional complexities know from higher eukaryotes. Nevertheless, a true knowledge of the various nuclear structures and macro-molecular assemblies, how they interact and how their structure mediates function is still limited. The work presented here contributes to the understanding of one of the most basic aspect of nuclear organization: the primary chromatin architecture of nucleosome positioning.

4. Methods

4.1. Generation of *S.cerevisiae* strains

4.1.1. Plasmid bearing strains

To transfer plasmids into yeast strains, a 10 ml culture in either YPDA or YNB was grown logarithmically to an OD_{600} of 2-4. The cells were washed in sterile TE 7.5 buffer (10 mM Tris-HCl 7.5, 1 mM EDTA) and resuspended in the same buffer to a concentration of 50 OD/ml. An equal volume of sterile 0.2 M lithiumacetate solution was added and the mixture was incubated whilst shaking at 30°C for 1 hour. 1 µg of the plasmid to be transformed into the yeast strain were added to 100 µl of cell suspension and incubated at 30°C for 30 minutes without shaking. Next, an equal volume of pre-boiled 70% PEG solution was added and the mixture was thoroughly vortexed and then incubated for 1 hour at 30°C without shaking. The cell suspension was incubated at 42°C for 5 minutes, the cells subsequently washed with sterile H_2O and plated out on plates lacking the appropriate amino acid(s).

4.1.2. Mutagenesis of chromosomal Rsc3 sites at the *PHO8* promoter

The predicted Rsc3 binding sites at the *PHO8* promoter were mutated via two-step gene replacement using the *URA3*-containing derivatives of pUC19-*PHO8*-long with the respective point mutations (s. below). The mutagenesis plasmids were linearized via the unique BglII site within the *PHO8* ORF. Positive clones that were auxotrophic for uracil and grew on 5-fluoroorotic acid containing medium were tested by yeast colony PCR on with the primers 5'-TTGAAGTACAAGTTAGCGAGC-3' and 5'-ACCAATACAGACCACAGTGG-3' to generate a PCR product that spans the region from -370 upstream to +129 downstream of the *PHO8* ATG. Presence of the Rsc3 binding site mutations in the isolated PCR products was confirmed by dideoxy sequencing (data not shown).

4.1.3. Disruption of *PHO4* in *arp9-ts* and *rsc3-ts* strains

PHO4 ORF in the *rsc3-ts* and *arp9-ts* strains was disrupted by transformation with a linear DNA fragment of the *PHO4* locus with a *URA3* marker gene cassette inserted into the *PHO4* open reading frame. Fragment was generated by digestion of plasmid pDPHO4::Ura with HindIII/XbaI and transformed into the strains in a manner identical to transformation with plasmids except that 10 µg of DNA were used. Cells were selected on plates lacking uracil and successful transformants were confirmed by preparation of genomic DNA, digestion with HindIII/StuI and subsequent probing with the HindIII/BamHI fragment of pP4-12 [241]. Transformants were further controlled by confirming the expected decrease in basal *PHO5* acid phosphatase activity.

4.2. *In vivo* methods

4.2.1. Growth of *S.cerevisiae* strains carrying a temperature sensitive allele

Typically, strains were grown in 400 ml YPD supplemented with 0.1 g/l adenine and 1 g/l KH_2PO_4 in medium at 25°C to an OD_{600} of 1.2-1.5. An equal volume of medium pre-warmed to 49°C was added and the cultures were placed at 37°C over night followed by nuclei isolation. The *spt6-ts* strain was grown accordingly, except that the strain was placed at 39°C for the indicated length of time. The *sth1-td* strain was grown in YP medium supplemented with 2% w/v Raffinose, 2% w/v Glucose and 0.1 g/l adenine.

4.2.2. Alkaline phosphatase assay

Cells were grown to an OD_{600} of 1-2. Either ~3.5 $mlOD_{600}$ (+P_i conditions, wt background), ~2.5 ml $mlOD_{600}$ (+P_i conditions, *snf2* background), ~1.8 $mlOD_{600}$ (-P_i conditions, wt background) or ~1.4 $mlOD_{600}$ (-P_i conditions, *snf2* background) were washed with alkaline phosphatase buffer (5 mM $MgSO_4$, 50 mM Tris-HCl pH 8.8) and resuspended ad 1 ml with alkaline phosphatase buffer. 200 µl were used to measure the OD_{600} of the cell suspension. Then, 50 µl 0.1% SDS and 20 µl chloroform were added to the remaining 800 µl, vortexed and incubated at 30°C for 5 minutes whilst shaking. Next 200 µl phosphatase buffer containing an additional 100 mM o-nitro-phenylphosphate were added. After incubation for 5 minutes at 30°C without shaking, 500 µl 1 M NaOH were added to stop the reaction. Reaction was briefly centrifuged and the extinction of the supernatant was measured at 410 nm. Alkaline phosphatase activity units were calculated according to the formula (1000 * E_{410}) / (OD_{600}/ml * 0.8 ml * 5 min).

4.2.3. Chromatin immunoprecipitation

Chromatin immunoprecipitation (ChIP) was done as described previously [169, 242]. RSC occupancy at several loci (see table below) was determined in strains carrying *STH1* allele with 9-fold C-terminal myc tag (*STH1-9MYC* - see chapters 4.1.2. and 4.3.3.) and mutation(s) in putative Rsc3 binding sites (Fig. 51). Sth1-9myc was immunoprecipitated with the anti-myc antibody (9E11). DNA amounts were quantified by Real-time PCR using the TaqMan® or SYBR® green system and the primers listed in the table below.

Locus / Probe Name	Primer / Amplicon sequences	Type
PHO8_NDR	TGCCAGCAAGTGGCTACATA CGTGTCTGTTCGCTTGGTAA	SYBR green®
PHO8_UASp2	TGCGCCTATTGTTGCTAGCA AGTCGGCAAAAGGGTCATCTAC ATCGCTGCACGTGGCCCGA	TaqMan®
PHO8_TATA	CAGCGGATGTCCTCTTTGTACA TGCTGCTATTCATGTCGATGCT CCCTCGTAAGGCGCGTCTAACGGA	TaqMan®
HTA1_promoter	CGACATTGAGCGTCTAACCATAGT GAGCTCGGCGAGTTCAAATT AACGACCCAACCGCGTTTTCTTCA	TaqMan®
PGK1_ORF	GGACCGACACAGTCGTTCAAG TTGGCTCCAGTTGCTAAGGAA AGGTGACATCCTTACCCAACAATGATTGCA	TaqMan®
Telomere	TCCGAACGCTATTCCAGAAAGT CCATAATGCCTCCTATATTTAGCCTTT TCCAGCCGCTTGTTAACTCTCCGACA	TaqMan®

4.3. Preparations from *in vivo* material

4.3.1. Isolation of yeast nuclei

Yeast nuclei were typically prepared from 0.8-2 L of culture grown to an OD_{600} of 2-4. Cells were harvested by centrifugation and washed with 200 ml ice-cold H_2O per litre of culture. The weight of the cell pellet was subsequently determined. The cells were then resuspended in 5 ml of pre-incubation solution (0.7 M β-mercaptoethanol, 2.8 mM EDTA) per gram of cell pellet and incubated at either 30°C or the growth temperature of the original culture for 30 minutes while shaking. Cells were then washed with ice-cold 1 M Sorbitol solution and resuspended in 2 ml of 1 M Sorbitol, 5 mM β-mercaptoethanol per gram of cell pellet. OD_{600} was determined by diluting 20 µl of cell suspension into 2 ml of H_2O. Next, 100 µl of a 20 mg/ml Zymolyase 100 T solution was added per gram of cell

pellet and incubated at the same temperature as with the pre-incubation solution for 30 minutes (standard logarithmic culture) or 1 hour (strains carrying a temperature sensitive allele of an essential gene) with shaking. Efficiency of the lysis was checked by measuring the OD_{600} as before. Cells were then washed again in ice-cold 1 M Sorbitol and resuspended in 7 ml Ficoll Solution (180 mg/ml Ficoll, 20 mM KH_2PO_4, 1 mM $MgCl_2$, 0.25 mM EGTA, 0.25 mM EDTA, pH of the solution adjusted to 6.8 with KOH) per gram of cell pellet. The cell suspension was split into aliquots corresponding to 0.5 to 1.2 grams of original cell pellet. Aliquots were then centrifuged at 4°C for 30 minutes at 15000 rpm in a Sorvall SM-24 rotor. Supernatant was discarded and the pellets were frozen in ethanol pre-cooled to -90°C by the addition of dry ice. Frozen pellets were stored at -80 °C until further use.

4.3.2. Yeast whole cell extract preparation

Extracts were made from the corresponding strains grown at 30°C to an OD_{600} of 3.5-4, except were for strains carrying a temperature sensitive mutant allele, which were grown as described in chapter 4.2.1. The extract used for fractionation was made from a commercially available baker's yeast concentrate. The cell pellets were washed with ice-cold H_2O and then with 50 ml extraction buffer (200 mM HEPES-KOH pH 7.5, 10 mM $MgSO_4$, 10% glycerol, 1 mM EDTA, 390 mM $(NH_4)_2SO_4$, 1 mM DTT). Cells were resuspended in 20 ml extraction buffer containing 1X Complete protease inhibitor without EDTA and flash frozen in liquid nitrogen. The stated amounts of extraction buffer were used with up to 10 grams of cell mass. Corresponding amounts were used for extract preparations from larger starting amounts of cell mass. The frozen cells were grinded in an electric mortar pre-cooled with liquid nitrogen with an initial pestle setting of 1 until a fine powder was generated. Subsequently pestle setting was increased to 5-6 for another 5-10 minutes, during which about 2 ml extraction buffer (with 1X complete inhibitor) was added per 5 g of cells mass. The grinded cells were thawed rapidly and centrifuged in a SW 56 Ti rotor for 2h at 4°C with 28000 rpm. The supernatant was removed leaving behind the cloudy layer right on top of the pellet and the lipid rich top at the meniscus. 337 mg of solid $(NH_4)_2SO_4$ was added per 1 ml of withdrawn supernatant. The $(NH_4)_2SO_4$ was grinded to a fine powder prior to addition. The $(NH_4)_2SO_4$ was dissolved completely on a rotating wheel at 4°C. Next, the solution was centrifuged for 20 minutes in a TLA 55 rotor at 4°C with 26000 rpm. The pellets were resuspended in with approximately 0.5-1 ml dialysis buffer (20 mM HEPES-KOH pH 7.5, 10% glycerol, 80 mM KCl, 1 mM EGTA, 5 mM DTT, 0.1 mM PMSF and 1 mM sodium metabisulfite) per gram of starting cell mass and dialysed twice against 40-50 fold excess of the same buffer used for resuspension for 1.5 hours each. The extracts were portioned into 60-1000 µl aliquots, flash frozen in liquid nitrogen and stored at -80 °C.

4.3.3. Purification of *Drosophila* embryo histones

Purification of *Drosophila* embryo histones was carried out as described previously [243]. 100 gram *Drosophila* embryos were resuspended in 100-150 ml of lysis buffer (15 mM HEPES-KOH pH 7.5, 10 mM KCl, 5 mM $MgCl_2$, 0.05 mM EDTA, 0.25 mM EGTA, 10 % glycerol, 1 mM DTT, 0.2 mM PMSF) and homogenized in a Yamamoto homogenisator by passing the suspension through 6 times at 1000 rpm in the cold room. The homogenized mixture was then centrifuged at 8000 rpm, 4°C, 10 minutes in an HB-4 or HB-6 rotor. The top liquid supernatant was removed and the soft light brown jelly middle phase containing the desired nuclei transferred to new tubes. The nuclei were washed with 50 ml Suc buffer (15 mM HEPES-KOH pH 7.5, 10 mM KCl, 5 mM $MgCl_2$, 0.05 mM EDTA, 0.25 mM EGTA, 1.2 % sucrose, 1 mM DTT, 0.2 mM PMSF) and then resuspended in 30 ml Suc buffer. Next, 90 µl of 1 M $CaCl_2$ were added, the mixture pre-warmed to 26°C in a waterbath, and 125 µl of 50 U/µl MNase were added. Following a 10 minute incubation at 26°C in the waterbath, the reaction was stopped by the addition of 600 µl of 0.5 M EDTA. The mixture was then centrifuged as before and the pellet resuspended in 6 ml buffer (10 mM Tris-HCl 7.6, 1 mM EDTA, 1 mM DTT, 0.2 mM PMSF, 1X Roche Complete EDTA-free protease inhibitors). The sample was rotated for 45 minutes at 4°C and centrifuged at 12000 rpm for 30 minutes, 4°C in an HB-4 or HB-6 rotor. The supernatant was kept and transferred to fresh tube. The KCl concentration of the supernatant was adjusted to 0.63 M by

addition of 2 M KCl, 0.1 M potassium phosphate pH 7.2. The supernatant was then loaded onto a 30 ml hydroxylapatite column equilibrated with 0.63 M KCl, 0.1 M potassium phosphate pH 7.2. Histones were eluted with 2 M KCl, 0.1 M potassium phosphate pH 7.2 and aliquots of each fraction run on an 18% SDS-PAGE gel to identify the histone containing fractions. Those fractions were pooled and concentrated with Amicon-Ultra 10 kDa cut-off. Finally, an equal volume of 87% glycerol was added, Roche Complete protease inhibitor was added to a concentration of 1X and histones were stored at -20°C.

4.4. Plasmids

4.4.1. Plasmids for *in vitro* reconstitution of nucleosome positioning

DNA fragments for insertion were generated by PCR using primers shown in the table below and genomic DNA as template. PCR products were gel purified and subsequently inserted into the multiple cloning site of the pUC19 vector via the two restriction sites shown in the table below. Exception was the plasmid pUC19-*PHO8*-short for which the insert was generated by amplification with the primers listed below and pP8apin [175] as template. Sequences of the entire inserts were confirmed by dideoxy sequencing.

Plasmid	Primers	REs
pUC19-*PHO8*-long	5'-CCATGTGCATAGGATCCGGACGTTTGCCATAGTGTTG-3' 5'-CAGTCAGACGCTGCAGGGGAGAGTTAGATAGGATCAGT-3'	BamHI PstI
pUC19-*PHO8*-short	5'-GGCCTGCAGAGTTAGATAGGATCAG-3' 5'-CCGGATCCTCTTTCTCAGTAAGAG-3'	PstI BamHI
pUC19-*PHO5*	5'-CCATGTGCTACGAATTCTCCTGTCCTTGTATTCGTCC-3' 5'-CAGTCAGACGAAGCTTACTACAGGGATTGAAACATCC-3'	EcoRI HindIII
pUC19-*PHO84*	5'-CCGGAATTCTCGAGTCATGATTTGGAACAGCTCC-3' 5'-CGCGGATCCGCAGAGAGATGTGAGGAAAT-3'	EcoRI BamHI
pUC19-*ADH2*	5'-CCATGTGCATTGGTACCCGCTGTTATGTTCAAGGTCC-3' 5'-CAGTCAGACGCTGCAGATCCTCAATCCAAGGCGAAC-3'	KpnI PstI
pUC19-*CHA1*	5'-CCATGTGCATTGGTACCTCTCAAACTGATTCGACCAC-3' 5'-CAGTCAGTAATCTAGACAAGGGCAAATTGATGCTTC-3'	KpnI XbaI
pUC19-*GCY1*	5'-CAGTCGGATGGAGCTCACTTCTATTGGCTTAGGAGC-3' 5'-CACTGTGCATTTCTAGAACGACGAAGACGAGGATTAG-3'	SacI XbaI
pUC19-*HIS3*	5'-CCATGTGCAATGAGCTCGAATTACGTGTTCAACGTCG-3' 5'-CAGTCAGTTATCTAGACCCATATCCAACATTCTATC-3'	SacI XbaI
pUC19-*HO*	5'-CACTGACTAGAGAGCTCATAATTCAAGCAAGTTGCGG-3' 5'-CAGTCGTACATCTAGACAAATCAGTGCCGGTAACGC-3'	SacI XbaI
pUC19-*POT1*	5'-CCATGTGCATTGGTACCTTCTGTGACCGCTCTTCTAG-3' 5'-CAGTCAGACGGGATCCTTGGTTAAGGAGGACTGGAG-3'	KpnI BamHI
pUC19-*RIM9*	5'-CATGTCGATTGAGCTCGCATCTTCTGCAACGCCTTG-3' 5'-CAGTCAGTAAGGATCCCAGTGGATAGATTTCCGGAG-3'	SacI BamHI
pUC19-*RNR3*	5'-CACTGTGCATTTCTAGACATCCAACTGGTCAAGGGGT-3' 5'-CGTTCGTCTGGTCGACTCTTCCTGTTACATGCGTCC-3'	XbaI SalI
pUC19-*SNT1*	5'-CAGTCAAGCGTCTAGAAATGAGCGCAGAGCTATCAC-3' 5'-CTCTGTGCATTCTGCAGGAGTGTTTGCGGATTGGATC-3'	XbaI PstI
pUC19-*SUC2*	5'-CCATGTGCATTGAGCTCCAACAGAGCATAAGTCAGAC-3' 5'-CAGTCACGTCCTGCAGGCTAAAGCCCTTTAGAATGG-3'	SacI PstI

4.4.2. Site directed mutagenesis

Derivatives with minor sequence alterations were generated via directed mutagenesis using the QuickChange kit. The generated plasmids and the corresponding primers were as follows. Mutations of the Rsc3 binding sites at the *PHO8* promoter on plasmids pUC19-*PHO8*-long and pP8apin were generated with these primers:
Rsc3 site at -10: 5'-GGGACATTATTTGAACCTACATTAGCAGC-3' and 5'-GCTGCTAATGTAGGTTCAAATAATGTCCC-3';
Rsc3 site at -151: 5'- CTTTTCCTCTACGTAGGAAGCTTATCGC-3' and 5'-GCGATAAGCTTCCTACGTAGAGGAAAAG-3';
Rsc3 site at -214: 5'- CTTCCGTTAGACGGTACTTACGAGGGGTG-3' and 5'-CACCCCTCGTAAGTACCGTCTAACGGAAG-3'.
The putative Rsc3 sites at the *RIM9*, *CHA1* and *RIO1*/*GCY1* promoters on the corresponding pUC19-based plasmids were mutated with the following primers.
RIM9: 5'-GCTATAGTTTGATTTTCACCAGCGGTAAGCGCAAGTATAAGCTAAGAAACAAT-3' and 5'-ATTGTTTCTTAGCTTATACTTGCGCTTACCGCTGGTGAAAATCAAACTATAGC-3';
CHA1: 5'-CGGAAACTAATGAGTCCTCTGTAAGGAGACATGATTCCGCATGGG-3' and 5'-CCCATGCGGAATCATGTCTCCTTACAGAGGACTCATTAGTTTCCG-3';
RIO1/*GCY1*: 5'-AAAATTTTTCACTCTTTCTGCGTTAGCCAATGTCCCCGCAACTACTC-3' and 5'-GAGTAGTTGCGGGGACATTGGCTAACGCAGAAAGAGTGAAAAATTTT-3'.
Two putative Abf1 binding sites on pUC19-*PHO8*-long were mutated with the primers 5'-GAATAGCAGCATTGTACATAGCGATAAGC-3' and 5'-GCTTATCGCTATGTACAATGCTGCTATTC-3' (Abf1 site ~170bp upstream of *PHO8* ORF) as well as 5'-GGCAAGGAAGAACTTAGTAAGACCTCAAG-3' and 5'-CTTGAGGTCTTACTAAGTTCTTCCTTGCC-3' (site ~700bp upstream). The *PHO8* TATA box on the plasmid pP8apin was mutated with the primers 5'-GGGATTTTAGTCGACAAAGAAAGAAGTGTATC-3' and 5'-GATACACTTCTTTCTTTGTCGACTAAAATCCC-3'.
Plasmid pCB84a-10A was generated from pCB84a with the primers 5'-GTATAGGGCGCCTATAACAGCACCAACGTGCGTAAAAAAAAAAGCTGTCATTTCTTGGCATGTTTTCT-3' and 5'-AGAAAACATGCCAAGAAATGACAGCTTTTTTTTTTACGCACGTTGGTGCTGTTATAGGCGCCCTATAC-3'.
Plasmid pCB84a-19A was generated from pCB84a-10A with the primers 5'-TGCTGCACGTATAGG GCGCCTATAACAGCACCAAAAAAAAAAAAAAAAAAAGCTGTCATTTCTTGGCATGTTTTC-3' and 5'-GAAAAC ATGCCAAGAAATGACAGCTTTTTTTTTTTTTTTTTTGGTGCTGTTATAGGCGCCCTATACGTGCAGCA-3'.

4.4.3. Plasmids for two-step gene replacement

Plasmids for mutagenesis of the chromosomal Rsc3 sites at the *PHO8* promoter in wt (CY337), *snf2* (CY407) and *STH1-9MYC* (FT4 *STH1-9MYC*::*TRP* [234]) strains were generated as follows. The *URA3* marker gene was amplified by PCR with the primers 5'-CCTTTGTCCAGCATGCCTGAGAGTGCACCATACC AC-3' and 5'-CAGTCAGAGCATCGATTGTGCGGTATTTCACACCGC-3' and pRS406 as template. PCR product was gel purified and ligated with the large SphI/ClaI fragment obtained from pUC19-*PHO8*-long vectors carrying mutations of the various Rsc3 binding sites.

4.5. *In vitro* assays

4.5.1. Salt gradient dialysis assembly

Chromatin for *in vitro* reconstitution of nucleosome positioning was assembled by salt gradient dialysis. Assembly reactions contained 10 µg of plasmid DNA, 20 g bovine serum albumin, and variable amounts of purified *Drosophila melanogaster* embryo histone octamers in 100 µl high-salt buffer (10 mM Tris-HCl, pH 7.6, 2 M NaCl, 1 mM EDTA, 1 mM β-mercaptoethanol and 0.05% Igepal CA630). Unless otherwise stated, plasmids were assembled with a histone:DNA mass ratio of 1:1. Dialysis was carried out at room temperature for 15 hours during which 300 ml of high salt buffer

were diluted with 3 litres of low-salt buffer (same as high salt buffer except that it contained 50 mM NaCl) using a peristaltic pump. A final dialysis step for 1 hour against 1 litre of low salt buffer ensured dialysis to completion. The volume of the assembly reactions typically increased to 120-130 µl during the dialysis. Assembly reactions were stored at 4°C up to several months before further use.

4.5.2. Reconstitution assay

Reconstitution reactions were set up in a total volume of 100 µl containing 20 mM HEPES-KOH pH 7.5, 12% glycerol, 80 mM KCl, 0.5 mM EGTA and 2.5 mM DTT. Typically, between one and four different salt assembled plasmids were included in the reconstitution reaction. The total amount of salt assembled plasmid DNA added varied from 0.5 µg (single plasmid) to 1 µg (two or more different plasmids). Depending on the experiment, reconstitution reactions in addition contained 200-250 µg of WCE with or without a regenerative energy system (3 mM ATP/$MgCl_2$, 30 mM creatine phosphate, and 50 ng/µl creatine kinase).

4.5.3. Fractionation of WCE

Ten 1 ml aliquots of WCE were supplemented each with 176,5 mg of ammonium sulphate , and rotated in a wheel at 4°C until all ammonium sulphate was dissolved (corresponding to 30% saturation, ~ 1.21 M ammonium sulphate). The supernatants after centrifugation for 30 min at 4°C at 26000 rpm (max RCF of 41500) in a Beckmann TLA55 rotor were transferred to fresh tubes and another 92,4 mg each of ammonium sulphate were added to achieve to 45% saturation (~1.82 M). After centrifugation as before, the supernatants (“SN fraction”) were pooled in a fresh tube. The pellets from the first centrifugation step (“30 % fraction”) were resuspended in 5 ml of Basic Buffer (80 mM KCl, 20 mM Hepes-KOH pH 7.5, 10 % glycerol, 5 mM DTT, 0.1 mM PMSF and 1 mM sodium metabisulfite). The pellets from the second centrifugation step (“45 % fraction”) were resuspended in 5 ml Basic Buffer plus 1 M ammonium sulphate. The “30 % fraction” and the “SN fraction” as well as 500 µl of the “45 % fraction” were dialysed against Basic Buffer until completion.
A 5 ml HP Phenyl Sepharose FF low-sub column was equilibrated with Basic Buffer plus 1 M ammonium sulphate and loaded with the remaining 4.5 ml of the “45 % fraction”. The flow-through was collected and the column was step-eluted with Basic Buffer containing 500 or 200 or no ammonium sulphate All fractions were dialysed against Basic Buffer until completion.
Three 1 ml Heparin HP columns were connected in series, equilibrated with Basic Buffer, and loaded with the 500 mM ammonium sulphate fraction from the Phenyl Sepharose column. The flow-through was collected, and further fractions obtained by step-elution with Basic Buffer plus 200 mM, 400 mM and 1000 mM KCl, respectively. All fractions except for the flow-through were dialysed against Basic Buffer until completion.
A 1 ml DEAE FF column was equilibrated with Basic Buffer and loaded with the 400 mM KCl fraction from the Heparin column. was loaded and the flow-through collected. The column was eluted step-wise with Basic Buffer plus 150 mM, 350 mM and 500 mM KCl, respectively. All fractions except for the flow-through were dialysed against Basic Buffer until completion.

4.5.4. Band shifts

Fragment #1 and fragment #2 were prepared by PCR (Primers for fragment #1: 5'-TAAGGCGCGTCTAACGGAAG-3' and 5'-TAAACGTTTAGATACACTTCTTTC-3' / fragment# 2: 5'-CAAATTATCTCCTTTTCAGACTG-3' and 5'- GAGGTCTTACTTGATTCTTCC-3') and gel purified. The purified fragments were end-labelled with T4 polynucleotide kinase (T4 PNK). For this 50 µl reactions containing 20 pmol of the fragment #1 or #2, 2 µl (20U) T4 PNK, 10 µl 10X T4 Buffer and 50 pmol γ-P^{32}-ATP (3000 Ci/mmol) were incubated for 30 minutes at 37°C. 1 µl of the labelling reaction was removed and diluted into 19 µl H_2O. The labelled fragments were purified from the remainder with the Qiagen Nucleotide Removal kit and eluted in 100 µl H_2O. The efficiency of labelling was determined by comparing counts per minute (cpm) obtained from the 1 µl removed before purification to 2 µl of the purified fragment solution. The amount of labelled fragments used for each band shift corresponded to a total of 50000 cpm, i.e. 0.033 µl of purified fragment #1 and 0.081 µl of

purified fragment #2. The total volume of the reaction for each land of the band shift gel was 10 µl. In addition to the amounts of labelled fragment stated above, the band shift reactions contained varying amounts of WCE or fractions from the WCE fractionation. Some reactions also contained poly(dI:dC) or unlabelled fragments as competitor. The final buffer conditions for every reaction was adjusted to 20 mM HEPES-KOH pH 7.5, 12% glycerol, 80 mM KCl, 0.5 mM EGTA, 2.5 mM DTT, 1.5 mM $MgCl_2$, 1.5 mM ATP, 15 mM creatine phosphate unless otherwise stated. The reactions were incubated at 30°C for 45-50 minutes and then electrophoresed on a 0.5X TBE, 1.1% agarose gel (90 V / 30 mAmp). The gel was then dried and placed on a Fuji FLA3000 phosphoimager screen.

4.5.5. Topology assay

Samples for Figure 9A were set up in a total reaction volume of 150 µl containing 20 mM HEPES-KOH pH 7.5, 12% glycerol, 75 mM NaCl, 0.5 mM EGTA, 1 mM $MgCl_2$, 2.5 mM DTT, whereas samples for Figure 25 were set up in the standard reconstitution reactions, except for the "-ATP" samples that contained an additional 1 mM $MgCl_2$. Each assay contained 1.5 µg of pUC19-*PHO8*-long DNA, either in its naked form or preassembled by salt gradient dialysis. Where applicable, 2 µl (Fig. 9A) or 4 µl (Fig. 25) of topoisomerase I (5 U/µl) were included in the reaction. Samples were incubated at 30°C (Fig. 9A) or 37°C for 2 hours (Fig. 25). The topoisomerase I reaction was stopped by the addition of 2 µl 50 mM EDTA. Samples where deproteination by addition of 2.5 µl 20% SDS, 3 µl Proteinase K (20 mg/ml) and 1 µl glycogen (20 mg/ml) and incubation at 37°C for 2h (Fig. 9A), or by incubated overnight at 55°C with 3 µl 20% SDS, 10 µl Proteinase K (20 mg/ml) and 1.5 µl glycogen (20 mg/ml) (Fig. 25). Linearized plasmid DNA was generated by digestion of 1.5 µg of pUC19-*PHO8*-long with PstI. Half of the DNA from each sample was then electrophoresed on a 1X Tris-Glycine buffered (28.8 g glycine, 6 g Tris ad 1L H_2O) 1.3% agarose gel by applying a voltage of 40V for approximately 24h (or 60 V for 48 h, depending on gel apparatus). When applicable, chloroquine was added to a concentration of 3 or 3.3 mM to the gel and the running buffer and the electrophoresis was carried out in the dark. After electrophoresis, gels were washed for 20-30 minutes in 1X Tris-Glycine Buffer containing 1 µg/ml EtBr and for another 15-20 minutes in just 1X Tris-Glycine buffer to remove unbound EtBr and reduce the background. Pictures were subsequently taken with a standard gel documentation system. For Figure 25, the DNA from the gel was Southern blotted and analysed by hybridization of the *PHO8* indirect endlabelling probe.

4.5.6. WCE Immunodepletion

For immunodepletion of the Yil091c extract, 50 µl of IgG agarose beads suspension were transferred to a fresh tube and washed twice with 1X "SM-ATP" buffer (20 mM HEPES-KOH pH 7.5, 12% glycerol, 80 mM KCl, 0.5 mM EGTA and 2.5 mM DTT). 40 µl of Yil091c-TAP extract were diluted 1:5 by addition of 160 µl of 1X "SM-ATP" and then added to the pre-washed IgG beads pellet. The extract-beads mixture was then placed in a rotating wheel for 3-6 h at 4°C. For "mock" depletions the beads were omitted. Next, the reactions were centrifuged briefly in a table top centrifuge to bring the beads to the bottom of the tube. The supernatants were transferred to a fresh tube and flash frozen in liquid nitrogen and stored at -80°C until further use. To check if any of the target protein bound to the beads, the beads were washed twice again in 1X "SM-ATP" buffer and subsequently resuspended ad 50-60 µl 1X "SM-ATP" and also flash frozen in liquid nitrogen. To determine if the immunodepleted extract samples could still reconstitute nucleosome positioning, 50 µl of immunodepleted and mock-depleted were included in a standard reconstitution assay and analysed accordingly. The extent of removal of the target protein from the extract was determined by Western analysis. 2 µl of input extract was run next to 10 µl of immunodepleted and "mock"-depleted extract, and 10 µl of beads suspension. TAP-tagged protein was identified with the help of Peroxidase-Anti-Peroxidase Soluble Complex (PAP), which acts both as the primary and secondary antibody. PAP was used at a dilution of ~1:5000 . Immunodepletion of the Sth1-9myc extract was carried out by the same approach except that agarose beads coupled Rabbit anti c-myc antibodies were used for the immunodepletion and anti-myc antibodies (9E11) for the Western blot analysis.

4.5.7. Native gel analysis of *in vitro* chromatin

For native gel analysis of salt assembled chromatin, 1 µl of salt assembled chromatin (containing the plasmids pUC19-*PHO8*-long, pUC19-*PHO84*, pUC19-*ADH2* and pUC19-*RNR3*) was mixed with 15 µl of Low salt buffer (10 mM Tris-HCl pH 7.6, 75 mM NaCl, 1 mM EDTA, 1 mM β-mercaptoethanol and 0.05% Igepal CA630 and 4 µl of 6X Loading Buffer. Unassembled plasmids were analysed by including a corresponding amount of plasmids DNA instead of the salt assembled chromatin in the corresponding lane. The samples were run on a 0.35X TBE, 0.9% agarose, EtBr-free gel at 100V. To judge the required running time, one extra lane contained ~2 µg of pUC19-*POT1* together with 5 µl 1:10 EtBr solution. The gel was run approximately until the red pUC19-*POT1*/EtBr band reach the middle of the gel. The DNA was then transferred onto a Nylon membrane by Southern transfer. The location of the plasmid DNA was then analysed by hybridization with probes specific for the individual plasmids.

4.5.8. Whole genome reconstitution of nucleosome positioning

The genomic library constructed by Rose *et al.* [202] was used as a template for whole genome reconstitution of nucleosome positioning. This library consist of 10-30 kb genomic fragments inserted into the ~8 kb YCp50 vector. The library was assembled into chromatin using the standard salt assembly method. Standard reconstitution reactions were set up using the assembled library and WCE made from the Y00000 (=BY4741) strain. Initially, samples preparation included crosslinking with formaldehyde (2.78 µl of a 3.7% Formaldehyde solution added, incubated for 15 minutes at 30°C and quenched with 5.4 µl of 2.5 M glycine) followed by incubation with 1 µl of 1:10 diluted apyrase (50 U/ml; diluted in 10mM HEPES-KOH 7.5, 0.1 mg/ml BSA) at 30°C for 5 minutes. Then 2.2 µl of 75 mM $CaCl_2$ were added and samples digested with 50 U/µl MNase for 5 minutes at 30°C. The amount of MNase added to the different samples was titrated beforehand to achieve a near maximal amount of mononucleosomal DNA. Typical MNase amounts were 0.45 µl (no WCE / no ATP), 6 µl (+WCE / no ATP) and 10 µl (+WCE / +ATP). For each replicate and each condition, three 100 µl reconstitution reactions were set up that were pooled after the MNase digestion step. Mononucleosomal DNA was immunoprecipitated in the lab of Frank Pugh and used to generate a library for high throughput sequencing (for further details see [74]). For the samples in Fig. 23 and 24, crosslinking and immunopurification was omitted. Instead samples were treated with 4 µl of apyrase (instead of 0.1 µl) and deproteinated after the MNase digest by incubation overnight at 55°C with 3 µl 20% SDS, 10 µl proteinase K (20 mg/ml) and 1.5 µl glycogen (20 mg/ml) and subsequent phenol-chloroform extraction. Samples were resuspended in 100 µl TE buffer plus 1 µl RNase A (20 mg/ml) and incubated at 37°C for 3 hours. The DNA was purified by isopropanol precipitation and the air dried DNA was shipped to the Pugh lab for library generation.

4.6. DNaseI and RE analysis of *in vivo* and *in vitro* samples

4.6.1. DNaseI indirect endlabelling and restriction enzyme accessibility assay for *in vitro*-reconstituted chromatin

25 µl aliquots of a reconstitution reaction were mixed with 25 µl of 20 mM HEPES-KOH pH 7.5, 12% glycerol, 5.5 mM $MgCl_2$, 5.5 mM $CaCl_2$, 2.5 mM DTT, 80 mM NaCl, 0.1 mg/ml bovine serum albumin containing DNaseI at a concentration in the range of 0.005 to 0.02 U/ml (free DNA), 0.02 to 0.1 U/ml (salt gradient dialysis chromatin), or 2 to 10 U/ml (salt gradient dialysis chromatin with extract). Reactions were incubated at room temperature for 5 minutes and stopped by the addition of 10 µl Stop buffer (10 mM EDTA, 4% SDS). Samples were deproteinated by addition of 3 µl proteinase K (20 mg/ml) and 1 µl of glycogen solution (20 mg/ml) and incubation at 37°C overnight. Samples were ethanol precipitation, secondary cleavage with the restriction enzyme(s) shown in chapter 4.7.1. and ethanol precipitated again. Pellets were resuspended in 10 (4 different plasmids in the reconstitution reaction) or 20 (<4 different plasmids) µl TE buffer. 5 µl 6X DNA Loading Buffer (40% (w/v) sucrose,

10 mM Tris-HCl pH 8.0, 0.25% bromophenol blue) and 0.5 µl sheared salmon sperm DNA (20 mg/ml) were added per 10 µl of TE buffer. For samples containing DNA from 4 different plasmids all of the sample was loaded onto the gel whereas for the other samples only half of the total was loaded.
For restriction enzyme accessibility assays reconstitution reactions were initially incubated with 0.1 U apyrase (50 U/ml) for 30 minutes at 30°C to remove ATP from the reaction mixture and inhibit ATP dependent chromatin remodeling. One or two microliter aliquots of the reaction mixture were then added to 30 µl of RE buffer (20 mM HEPES-KOH pH 7.5, 4.5 mM $MgCl_2$, 2.5 mM DTT, 80 mM NaCl, 0.5 mM EGTA). Samples were digested with two different amounts of each restriction enzyme as follows: HindIII (100 U/ µl): 2.5 µl / 7.5 µl; NheI (50 U/µl): 3 µl / 10 µl; HpaI (5 U/µl): 15 µl / 30 µl; TaqI (100 U/µl): 0.87 µl / 3.5 µl; MfeI (10 U/µl): 0.87 µl / 3.5 µl; BsrBI (10 U/µl): 0.87 µl / 3.5 µl; PacI (10 U/µl): 1.25 µl / 5 µl. Samples were incubated with the corresponding RE at 37°C for 2 hours. Digests were stopped by addition of 7.5 µl Stop buffer (same as for DNaseI digest), and deproteinated by incubation with 2.5 µl proteinase K + 1 µl glycogen overnight. Following an ethanol precipitation, samples were secondary cleaved with the restriction enzymes in chapter 4.7.1. and ethanol precipitated again. Pellets were resuspended in 15 µl TE Buffer and loaded together with 4 µl 6X Loading Buffer and 0.5 µl sheared salmon sperm DNA (20 mg/ml).

4.6.2. Nuclei digest with DNaseI

A nuclei aliquot (usually) corresponding to 1 gram of cell pellet was washed with ice-cold DNaseI buffer (15 mM Tris-HCl pH 7.5, 75 mM NaCl, 3 mM $MgCl_2$, 0.05 mM $CaCl_2$, 1 mM β-mercaptoethanol) and resuspended ad 900 µl of DNaseI buffer. 300 µl aliquots of the nuclei suspension were digested with varying amounts of DNaseI in the range of 1.5 to 6.5 U/ml. Samples were incubated at 37°C for 20 minutes and the digestion stopped by the addition of 30 µl of "Nuclei Stop" buffer (5.25% SDS, 42 mM EDTA, 525 mM Tris-HCl pH 8.8). Next, 30 µl proteinase K was added and samples incubated at 37°C for 1 hour. Next, 70 µl of 5 M $NaClO_4$ were added and samples followed by 400 µl of phenol and thorough vortexing (~1 minute). Then, 400 µl of IAC (chloroform:isoamylacohol ratio of 24:1) were added an the samples centrifuged for 5 minutes in a table top centrifuge. The top aqueous was then transferred into a fresh tube followed by the addition of IAC and centrifugation as before. Again, the aqueous layer was transferred to a fresh tube and the DNA was ethanol precipitated. Samples were resuspended in 100 µl of TE buffer containing 1 mg/ml of RNase A, incubated at 37°C for 1 hour and ethanol precipitated again. The final pellet was resuspended in 100 µl TE buffer.

4.6.3. Nuclei digest with restriction enzymes

A nuclei aliquot corresponding to 0.5 gram of original cell pellet was washed with ice-cold SSTEEM buffer (50 mM NaCl, 0.15 mM Spermine, 0.5 mM Spermidine, 10 mM Tris-HCl pH 7.4, 0.2 mM EDTA, 0.2 mM EGTA, 10 mM $MgCl_2$, 5 mM NaCl, 5 mM β-mercaptoethanol, pH adjusted to 7.4 with HCl) and resuspended ad 1.4-2 ml of SSTEEM buffer. 200 µl aliquots were digested with two different concentrations of the desired restriction enzyme (typically 50 and 200 units) by incubation at 37°C for 30 minutes. The samples were subsequently deproteinated and RNase A digested as for the DNaseI digested nuclei (see above).

4.7. Analysis of DNaseI and RE digested samples

4.7.1. Secondary cleavage of DNaseI and RE digested samples

The table below lists the various restriction enzymes used for secondary cleavage of in vivo and in vitro DNaseI or RE digested samples. Reactions were incubated at 37°C for 2 hours except for ApaI were samples were incubated at 30°C for 2 hours (followed by another 2 h at 37°C if another RE was also added).

Locus	DNaseI	RE
PHO8	BglII (or BglI)	BglII/EcoRV
PHO5	ApaI	
PHO84	SspI or HindIII	HindIII or HindIII/SalI (pCB84- based plasmids); For TaqI digests: AvaII/ClaI or BamHI/SalI (pCB84- based plasmids)
ADH2	HindIII	
AEP1	ApaLI	
BRE4	EcoRV	
CHA1	BamHI	
FEN2	EcoRI	
GAL1-10	HpaI	
GCY1 / RIO1	BamHI, EcoRV or HpaI	
HIS3	ApaI	
HO	ClaI	
MEH1	HpaI	
MRPL49	EcoRV	
MUB1	NheI	
POT1	EcoRI	
RIM9	HpaI	
RNR3	PstI	
SNT1	SspI	
SUC2	SspI	
TVP38	HpaI	

4.7.2. Markers

Marker fragments for DNaseI indirect endlabelling gels were generated by digestion of pUC19 plasmids carrying the corresponding locus with the following combinations of restriction enzymes: *PHO8*: BglII/SacI, BglII/HindIII, BglII/EcoRV; *PHO5*: DraI/ApaI, ClaI/ApaI, BamHI/ApaI, FokI/ApaI BglII/NdeI; *PHO84*: ClaI/SspI, AgeI/SspI, ApaI/SspI, BsrBI/SspI; *ADH2*: EcoRV/HindIII, SphI/HindIII, DpnI/HindIII, SacI/HindIII; *AEP1*: SspI/ApaLI, KpnI/ApaLI, SpeI/ApaLI; *CHA1*: NciI/BamHI, HindIII/BamHI, EcoRV/BamHI, HaeII/BamHI; *GCY1*/*RIO1*: FokI/BamHI, NciI/BamHI, DraI/BamHI, HhaI/BamHI; *HIS3*: DraI/ApaI, AccI/ApaI, MspI/ApaI; *HO*: HindIII/ClaI, XmnI/ClaI, BglII/ClaI; *POT1*: NcoI/EcoRI, MluI/EcoRI, HindIII/EcoRI; *RIM9*: NheI/HpaI, SphI/HpaI, BglII/DraI, XbaI/NsiI; ; *RNR3*: BanII/PstI, AvaII/PstI, ApaI/PstI, ClaI/PstI; *SNT1*: KpnI/SspI, MspI/SspI, SacI/SspI, SpeI/SspI; *SUC2*: AvaI/SspI, MluI/SspI, HindIII/SspI, NcoI/SspI; Exceptions are the following loci for which the marker bands where generated by digestion of genomic DNA: *BRE4*: DraI/EcoRV, NcoI/EcoRV; *FEN2*: HindIII/EcoRI, BglII/EcoRI; *GAL1-10*: AgeI/HpaI, AvaI/HpaI; *MEH1*: XbaI/HpaI, NheI/XbaI; *MRPL49*: EcoRI/EcoRV, SpeI/EcoRV; *MUB1*: ClaI/NheI, StuI/NheI; *TVP38*: NcoI/HpaI, XhoI/HpaI.

4.7.3. Southern blotting and hybridisation

Samples were separated on a 1.5% (DNaseI) or 1.2% (RE) agarose gel in 1X Loehning Buffer (DNaseI) or 1X TAE buffer (RE). DNA was transferred onto nylon membranes by Southern Blotting (capillary transfer) [244] using 2XSSC (900 mM NaCl, 90 mM Na-Citrate) as transfer buffer. After blotting overnight, membranes were baked at 80°C for 2 hours and prewashed at 68°C for 30minutes in 2XSSC and subsequently for 2 hours in 2X SCC 1XDenhardt's (0.5 % SDS, 1 mM EDTA, 0.02 % BSA, 0.02 % PVP-40, 0.02 % Ficoll). Before hybridization membranes were incubated for 1 hour at 68°C in pre-incubation solution (2XSSC, 1XDenhardt's an denatured salmon sperm carrier DNA). Membranes were subsequently incubated overnight at 68°C in a rotating cylinder with 5 ml pre-incubation solution containing a radioactively labelled probe (see below). Membranes were washed three times with 3XSSC 1XDenhardt's for 30 minutes at 68°C and then analyzed by exposure to X-ray films (DNaseI samples) (Fuji Super RX) at −80 °C using intensifier screens (DuPont, Lightening Plus) or by exposure to Fuji FLA3000 phosphoimager screens.

4.7.4. Probes

Probes were labelled with the Prime-It (II) labelling kit according to the manufacturer's instructions. Input DNA for the labelling reactions was generated by PCR using certain primers (see list below) and either genomic or plasmid DNA as template. PCR products were gel-purified.

Locus	Primers	Use
PHO8	5'-GACGGATCTCGAAGAGATCA-3' 5'-CCTGCCATCTGTAATCAACA-3'	DNaseI and RE
PHO5	5'-GTCTTCAGCGTCAACTTTAG-3' 5'-GCCAATGTGCAGTAGTAACT-3'	DNaseI
PHO84	5'-CCTTGAGAACTTCAGTTGAC-3' 5'-GAGTGAAGGCCATCAAAATC-3'	DNaseI and all RE (except TaqI)
ADH2	5'-AGAATACGCTACCGCTGACG-3' 5'-ATTGATGATACCGTGGGCAC-3'	DNaseI
AEP1	5'-ACAGTACAGATGTCGACTCC-3' 5'-ATAGCATGAACGTTGGCAGC-3'	DNaseI
BRE4	5'-TAGTCCTTCACCTTATGTACG-3' 5'-TGTCAAAGTGAACGTGCCAG-3'	DNaseI
CHA1	5'-CATGTCAAAGACTGTCTCTAC-3' 5'-CCATACCTTTCCAAACCTTG-3'	DNaseI
FEN2	5'-AGTATCGCTTCGCAACCAAG-3' 5'-TCTTGGCCCTCAGCATCTTC-3'	DNaseI
GAL1-10	5'-TCTGCAACGACCGTAATACG-3' 5'-GGAAGTTCGATTTGCCGTTG-3'	DNaseI
GCY1 / RIO1	5'-CTAAACTCATTGGATGTTCA-3' 5'-GTCTTAGATCCGAGAACTAT-3'	DNaseI
HIS3	5'-GACACCACAGGCGTCAAAGG-3' 5'-GACATGGACACCAGTTCAGC-3'	DNaseI
HO	5'-TGTCAGACGCTTGATGGTAG-3' 5'-CTCTTAAACTCTCCATTAGC-3'	DNaseI
MEH1	5'-ACATATATGTTTGGTGACGCG-3' 5'-CCAGGGATAAGATTACGTCTG-3'	DNaseI
MRPL49	5'-TGGGATGAAGAAGAACAGGC-3' 5'-TTGGATGCTCTTGATGGACC-3'	DNaseI
MUB1	5'-TGTCTGGGGTCTTATCTGTG-3' 5'-AAACCGGCCCCATATATCAC-3'	DNaseI
POT1	5'-TGAGTTCATCGGGAGGTTTC-3' 5'-CAGCGAACTCGTCTTGATCC-3'	DNaseI
RIM9	5'-GTGACCGAGTTAGCACAACC-3' 5'-CATTGCTTCAACGCTCGAAG-3'	DNaseI
RNR3	5'-TGCTCCTATGATTTCGGACG-3' 5'-GATAGAGTCATCCTTCATGGC-3'	DNaseI
SNT1	5'-TGAAAAGAACAGGTCCGTCG-3' 5'-CGAAATTAATCATGTCCCAG-3'	DNaseI
SUC2	: 5'- TCCAAGACAAAGATGCGTTG-3' 5'-TTGAAGGAACCGCCAGCAGG-3'	DNaseI
TVP38	5'-AGAACTACAAAACCGCGACC-3' 5'-CTGGTCCCTTTTCCAAATCC-3'	DNaseI

4.8. *In silico* methods

4.8.1. Binding site prediction

The Find Individual Motif Occurrences (FIMO) program (Version 4.1.0; available at http://meme.sdsc.edu/meme4_1/cgi-bin/fimo.cgi) was used to predict possible binding sites for Rsc3, Reb1, Abf1, Mcm1, Tbf1, Cep3 and Rap1 at the *PHO8*, *PHO5* and *PHO84* promoters and Rsc3 binding sites at all other promoters described in this thesis. The position weight matrices were taken from supplementary Table S6 [138] and from The Promoter Database of Saccharomyces Cerevisiae (SCPD; http://rulai.cshl.edu/SCPD/). The sequences of the various promoters from position -1000 to +320 relative to their start codon were obtained from the Saccharomyces Genome Database (http://www.yeastgenome.org/).

4.8.2. Sequence alignments

The orthologous sequences for *PHO8*, *RIM9*, *CHA1*, *GAL10* and *RIO1* from *S.paradoxus*, *S.mikatae*, *S.bayanus*, *S.kudriavzevii*, *S.castelli* and *S.kluyveri* were taken from [245] and [246]. The ORF sequence plus 1000 bp of upstream sequence from each yeast species were aligned with the ClustalW2 program (http://www.ebi.ac.uk/Tools/ clustalw2/index.html) using the default settings.

4.8.3. Preparation of figures

Hybridized Southern blots were exposed to X-ray films (Fuji Super RX) at −80 °C using intensifier screens (DuPont, Lightening Plus). Blots were exposed for varying times to obtain an even exposure for all lanes. Films were scanned in grey-scale modus (MikroTek ScanMaker i900) and different exposure times combined into one image with Adobe Photoshop CS2. All plots and images were imported in CorelDraw X3 for final figure layout.

4.9. Materials

Unless stated otherwise, all common chemicals were obtained from Merck (analytical grade).

4.9.1. Chemicals

α-^{32}P-dCTP	Hartmann Analytics
Agarose	SeaKem® ME Biozym
Amino acids	Sigma and Merck
Ampicillin	Roth
ATP	Sigma
Bacto Peptone	Becton Dickinson
Bacto Yeast extract	Becton Dickinson, Difco
Bacto Yeast nitrogen base	Becton Dickinson, Difco
Bromophenol blue	Merck
BSA	Sigma
β-Mercaptoethanol	Sigma
Chloroform	Merck
Complete protease inhibitors, EDTA-free	Roche
Colloidal coomassie	Invitrogen
Creatine phosphate	Sigma
dNTP mix	NEB
DTT	Roth
EDTA	Sigma
EGTA	Sigma

EtBr	Roth
Ficoll	Sigma
Formaldehyde	Sigma
γ-P^{32}-ATP	Perkin Elmer
Glycogen	Roche
Hepes	Roth
Hydroxylapatite	BioRad
Isoamylalcohol	Merck
Igepal CA-630	Sigma
o-nitro-phenylphosphate	Fluka
Orange G	Sigma
Phenol	Sigma
PEG 4000	Roth
PMSF	Sigma
SDS	Serva
Spermidine	Fluka
Spermine	Fluka
Tris	Invitrogen
Triton X-100	Sigma
Tween 20	Sigma
Zymolyase 100 T	MP Biomedicals

4.9.2. Enzymes

Apyrase	NEB
DNaseI	Roche
Creatine kinase	Roche
MNase	Sigma
Pfu turbo polymerase	Stratagene, Agilent
Phusion polymerase	Finnzymes, NEB
Proteinase K	Roche
Restriction endonucleases	NEB and Roche
RNase A	Roche
RNase H	NEB
RNase III	NEB
T4 DNA Ligase	NEB
T4 polynucleotide kinase	NEB
Taq DNA Polymerase	NEB
Topoisomerase I	NEB

4.9.3. Other

2-Log DNA Ladder (0.1–10.0 kb)	NEB
100 bp DNA Ladder	NEB
Amicon-Ultra 10 kDa	Milipore
anti c-myc agarose	Sigma
Baker's yeast concentrate	Deutsche Hefewerke GmbH
DEAE FF column	GE Healthcare
Dialysis membrane Spectra/Por, 3.5 kDa	Roth
Enliten Luciferase reagent	Promega
Fuji medical X-ray film	Fuji
Gel Extraction Kit	Qiagen
Heparin HP columns	GE Healthcare
Microsep Centrifugal Concentrators	Pall Corporation

Miracloth	Merck
Nucleotide Removal kit	Qiagen
Nylon Transfer membrane, Biodyne B 0.45 µm	Pall Corporation
Peroxidase-Anti-Peroxidase Soluble Complex	Sigma
Phenyl Sepharose FF low-sub column	GE Healthcare
Plasmid Maxi, Midi, Mini Kit	Qiagen
Prime-It II Random Primer Labeling Kit	Stratagene
Rabbit IgG agarose	Sigma
QiaQuick purification kit	Qiagen
QuickChange kit	Stratagene
Quick spin columns (Sephadex G-50)	Roche
Siliconised reaction tubes, 1.5 ml	Biozym
Whatman 3MM Blotting Paper	Whatman

5. Supplementary Material

5.1. Supplementary Tables

Complex	Identified Subunits	Function of the complex / protein	Approach taken to test candidate	Results for *PHO8*
Nucleosome Remodeling				
RSC	**Rsc3** **Rsc6** **Rsc8** **Rsc9** **Rsc58** **Sth1** **Rsc4** **Npl6** **Arp9** **Rtt102**	Transcriptional regulation. Nucleosome positioning / maintenance of nucleosome depleted regions	*in vivo:* i) *rsc3-ts*, *sth1-td*, *arp9-ts* *in vitro*: ii) *rsc3-ts* extract iii) purified RSC	i) positioning altered ii) fails to reconstitute positioning iii) alone not sufficient but rescues *rsc3-ts* extract
SWI/SNF	**Arp9** **Rtt102** **Taf14**	Transcription regulation and DNA repair	i) *snf2 in vivo* ii) *snf2* extract *in vitro*	i) no effect ii) no effect
INO80	**Taf14**	Transcription regulation and DNA repair	*ino80 in vivo*	no effect
Isw2	**Isw2**	Nucleosome positioning at genic/intergenic interface	i) *isw2 in vivo* ii) *isw2* extract *in vitro*	i) no effect ii) no effect
Swr1	**Swc3**	H2A.Z exchange	*swr1 and swc3 in vivo*	no effect
General Transcription Factors				
TFIID	**Taf11** **Taf7** **Taf14**	Promoter recognition and transcription initiation	in vivo i) *taf1-ts*, *taf3-ts* ii) *spt15-ts*	i) no effect ii) positioning altered
TFIIE	**Tfa1** **Tfa2**	TFIIH recruitment and regulation. Promoter clearance	*tfa1-ts in vivo*	positioning altered
TFIIF	**Tfg1** **Taf14**	RNA pol II recruitment. Promotes elongation	*tfg2-ts in vivo*	stronger NDR
TFIIH	**Ssl2**	Promoter melting and clearance	*ssl1-ts in vivo*	no effect
Sequence Specific DNA Binders				
-	**Abf1**	Regulation of transcription and DNA replication. Nucleosome positioning around binding motif	abf1-ts in vivo	no effect
-	**Rap1**	Transcriptional regulation and silencing. Nucleosome positioning around binding motif	*rap1-ts* in vivo	no effect
-	**Cbf1**	Transcription factor. Nucleosome positioning around binding motif	i) *cbf1 in vivo* ii) binding site removal *in vivo* and *in vitro*	i) no effect ii) no effect
Hap2/3/4/5	**Hap5** **Hap3**	Transcriptional activator and global regulator of respiratory gene expression	*hap5 in vivo*	no effect
-	**Hsf1**	Heat shock transcription factor	not tested	
-	**Sef1**	Putative transcription factor	*sef1 in vivo*	no effect
Chromatin Modifiers				
Class II deacetylase	**Hda1** **Hda3**	H2B, H3 and H4 deacetylase	*hda1 in vivo*	no effect
NuA4 complex	**Eaf1** **Eaf3** **Tra1**	Histone H4 acetyltransferase	*eaf1 in vivo*	no effect
SAGA complex	**Sgf29** **Tra1**	Transcriptional coactivator	*sgf29 in vivo*	no effect
COMPASS	**Set1**	Histone H3 methyltransferase	*set1 in vivo*	no effect
SET3 complex	**Set3**	Histone deacetylase	not tested	

Transcription				
RNA pol II	**Rpb4**	Non-essential RNA pol II subunit	*rpb4 in vivo*	no effect
Paf1 complex	**Paf1**	Binds and modulates RNA pol I and II activity	*paf1* and *cdc73 in vivo*	no effect
	Ctr9			
	Cdc73			
	Rtf1			
	Leo1			
Spt6-Spn1	**Spt6**	Transcription elongation factor. Maintenance of chromatin structure.	*in vivo*: i) *spt6-ts* (2h 39°C) ii) *spt6-ts* (o/n 39°C) *in vitro:* iii) *spt6-ts* extract (4h 39°C)	i) no effect ii) unspecific loss of positioning iii) no effect
	Spn1			
Rat1/Rai1/ Rtt103	**Rtt103**	Involved in RNA pol II transcriptional termination	*rtt103 in vivo*	no effect
mRNA Cap binding complex	**Sto1**	Nuclear mRNA cap binding complex	*sto1 in vivo*	no effect
	Cbc2			
Pol II mediator	**Rgr1**	Central RNA pol II coactivator	not tested	
-	**Rtr1**	S5-P CTD phosphatase	not tested	

Supplementary Table S1.

Proteins identified (selection of 47 out of 212, for a complete list see Supplementary Table S2 in [169]) by LC-MS/MS analysis of the final fraction positive for the nucleosome positioning activity. Many of these candidate proteins were tested for their effect on nucleosome positioning at the *PHO8* promoter, as indicated.

#

Locus	Ng *et al.* (2002) RSC (Rsc1/2/8 and Sth1) occupancy (p-val)	Damelin *et al.*(2002) Rsc9 Occupancy (Median Percentile)	Floer *et al.* (2010) RSC/Nucleosome peaks (Location relative to ATG)
PHO8	**6.33E-08**	48.7	**-520** / **-269 /** +362 / +1438
RIM9	**4.34E-05**	**93.0**	none
CHA1	5.88E-01	**96.4**	none
SNT1	7.18E-01	71.6	none
GAL10	3.18E-01	**94.5**	**-275** / +1002
RIO1	**1.27E-06**	**95.5**	+1251
ADH2	7.87E-01	**80.2**	+144 / +522 / +814
RNR3	1.03E-01	**86.4**	-652 / +191 / +488
PHO5	3.55E-01	37.1	+612
PHO84	5.99E-01	40.5	none

Supplementary Table S2.

RSC binding scores obtained by Ng *et al.* [234] (combined p-value for the Rsc1, Rsc2, Rsc3, Rsc8 and Sth1 ChIPs; significant values in bold) and Damelin *et al.* [235] (promoters above the 71st / 72nd median percentile were classified as bound by RSC; significant values in bold) as well as the location of RSC-bound nucleosomes reported by Floer *et al.* [232] (locations within promoter regions in bold).

	Subunit(s) tested	*PHO8*	*RIM9*	*CHA1*	*SNT1*	*GAL10*	*RIO1*	*ADH2*	*RNR3*	*PHO5*	*PHO84*
		Changes in nucleosome occupancy/positioning upon inactivation of RSC subunits									
Wippo *et al.* [186]	**Sth1/Rsc3/Arp9**	+ + +	+ + +	- (+) (-)	- - -	- + (-)	(-) + (+)	n.d. - -	+ - -	- (+) +	n.d. - -
Badis *et al.* [138]	**Rsc3**	+	+	+	-	+	+	(+)	-	(+)	-
Parnell *et al.* [140]	**Sth1**	-	n.d.	+	n.d.	+	(-)	n.d.	n.d.	n.d.	n.d.
Hartley and Madhani [139]	**Sth1**	n.d.	n.d.	(+)	-	n.d.	n.d.	n.d.	n.d.	n.d.	n.d.
		RSC-bound nucleosomes at the promoter									
Floer *et al.* [232]	**Rsc8**	+	-	-	-	+	-	-	-	-	-
		RSC occupancy									
Parnell *et al.* [140]	**Rsc3/Rsc8**	+	n.d.	-	n.d.	-	+	n.d.	n.d.	n.d.	n.d.
Venters *et al.* [180]	**Rsc9**	+	+	+	-	+	+	-	-	+	+
Ng *et al.* [234]	**Rsc1/2/8, Sth1**	+	+	-	-	-	+	-	-	-	-
Damelin *et al.* [235]	**Rsc9**	-	+	+	(-)	+	+	+	+	-	-

Supplementary Table S3.
Overview comparison of our data (Wippo *et al.* [186]) with data from the indicated sources for effects on nucleosome occupancy at the indicated loci upon ablation of the indicated RSC subunits and for binding of the indicated RSC subunit (also compare with Supplementary Figure S4 and Supplementary Table S2). Classification of the respective data: +, clear effect/binding; -, no effect/binding; (+), weak effect; (-), very weak effect/binding; n.d., not determined.

5.2. Supplementary Figures

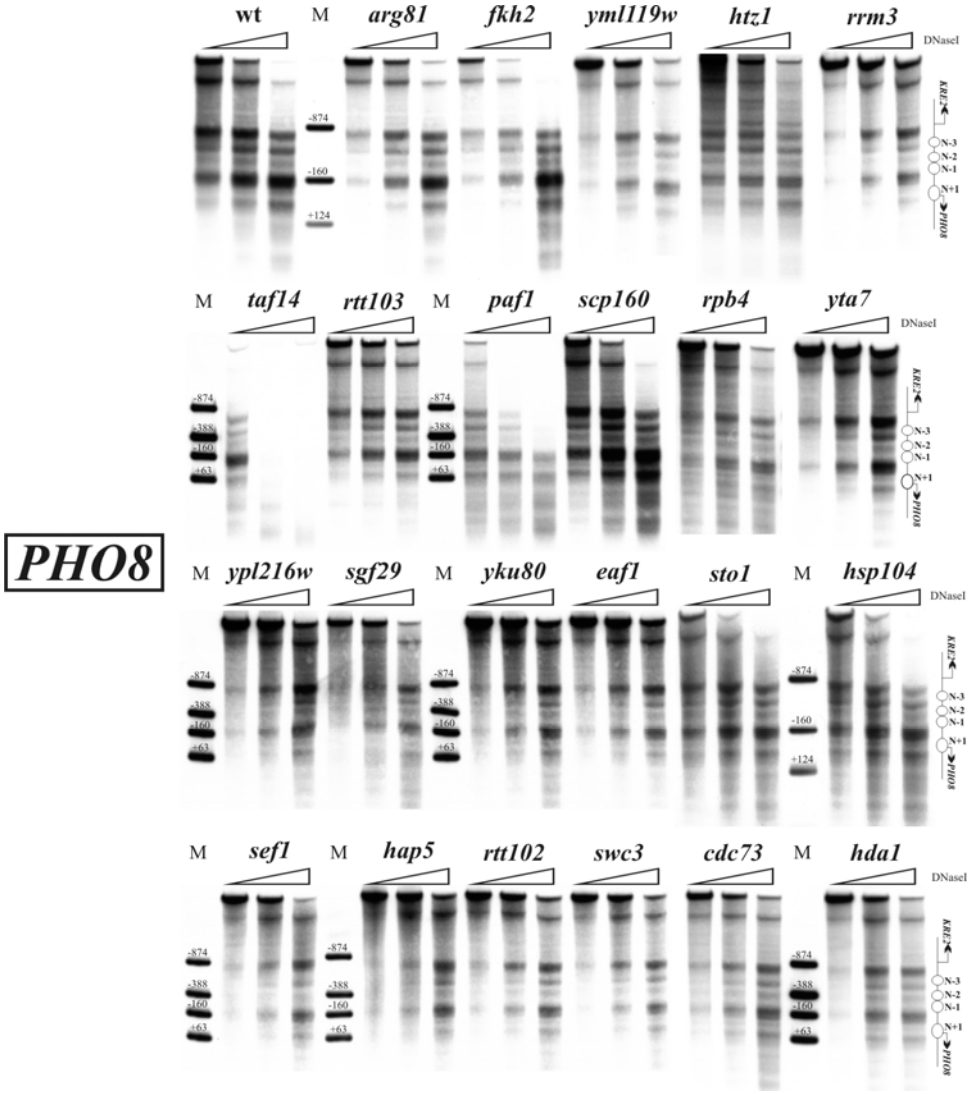

Figure S1. None of the non-essential candidate factors was required for proper nucleosome positioning at the *PHO8* promoter *in vivo*.

DNaseI indirect endlabelling analysis of the *PHO8* promoter in a wildtype strain (BY4741) and strains carrying a deletion mutant allele of the indicated genes after logarithmic growth at 30°C. Schematics, ramps and markers as in Figure 8B.

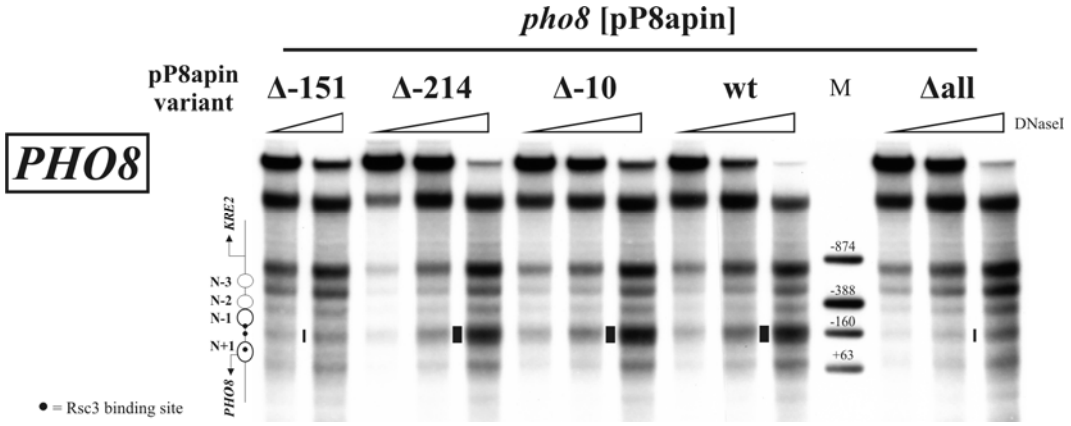

Figure S2. The Rsc3 binding site at position -151 was required for nucleosome depletion over the *PHO8* promoter NDR also on the pP8apin shuttle vector.

DNaseI indirect endlabelling analysis of the plasmid borne *PHO8* promoter in *pho8* strains (Y04315) carrying the indicated pP8apin plasmid variants. All labels as in Figure 46B.

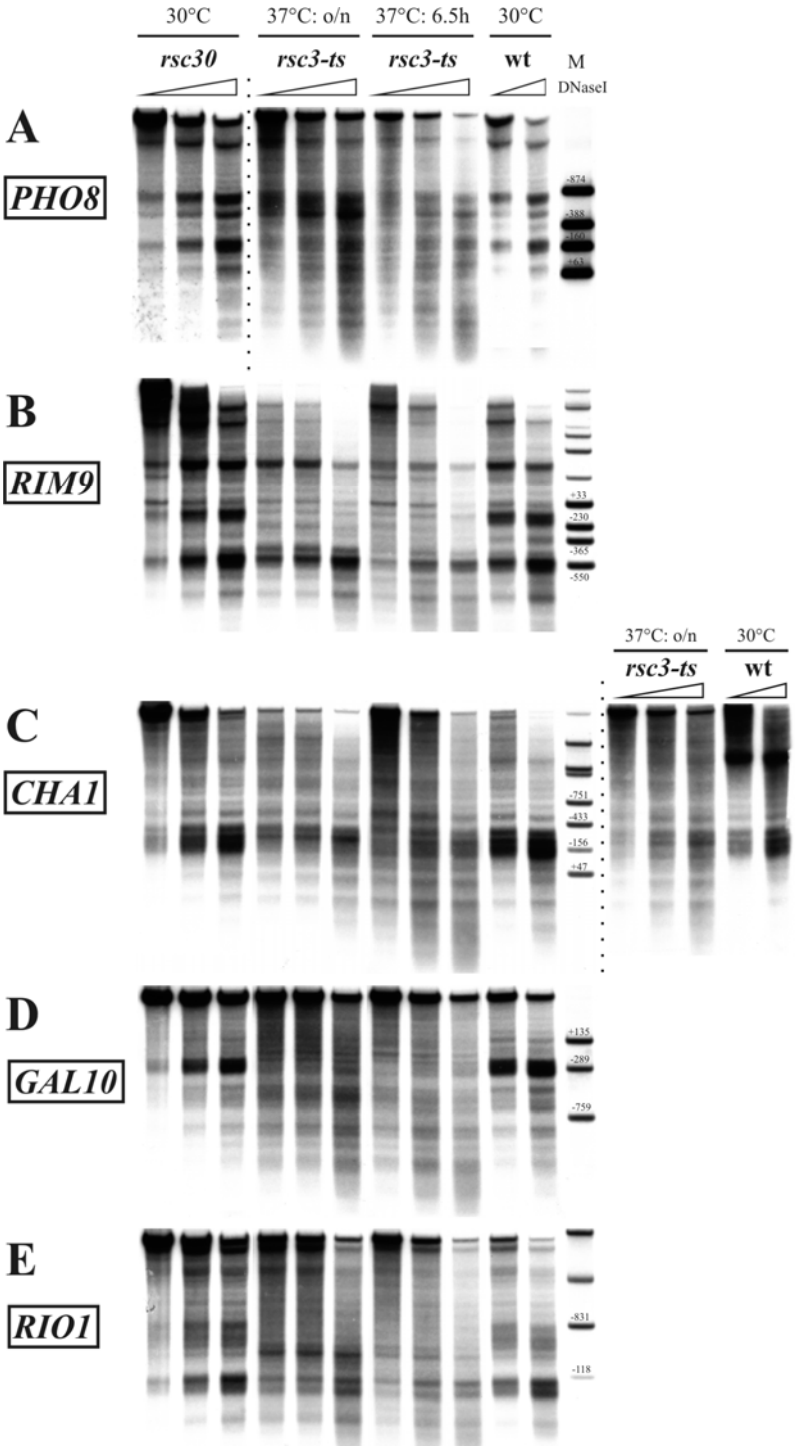

Figure S3. The altered chromatin structures at the *PHO8*, *RIM9* and *CHA1* promoters were already seen after shorter incubation at the restrictive temperature.

DNaseI indirect end labeling of the **(A)** *PHO8*, **(B)** *RIM9*, **(C)** *CHA1*, **(D)** *GAL10* and **(E)** *RIO1* promoter regions in a wildtype strain (wt; BY4741), a strain carrying a deletion mutant allele of Rsc30 and a strain carrying a temperature sensitive allele of Rsc3. *rsc3-ts* strain was grown logarithmically at 25 °C and then shifted to the non-permissive temperature (37 °C) overnight or for 6.5h [138]. Wt and *rsc30* nuclei after logarithmic growth at 30 °C. Stippled lines separate samples electrophoresed on separate gels. Ramps, markers and schematics as in Figure 39.

5.2.1. Supplementary Figure S4

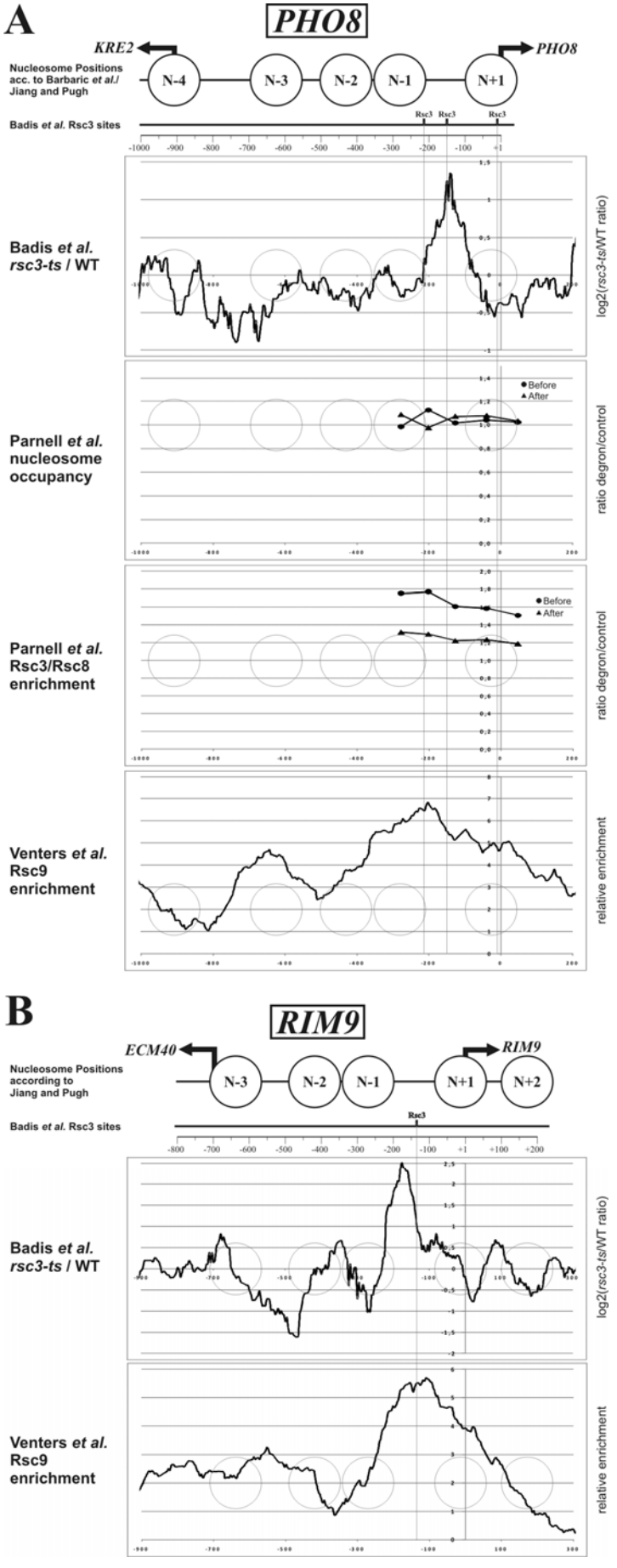

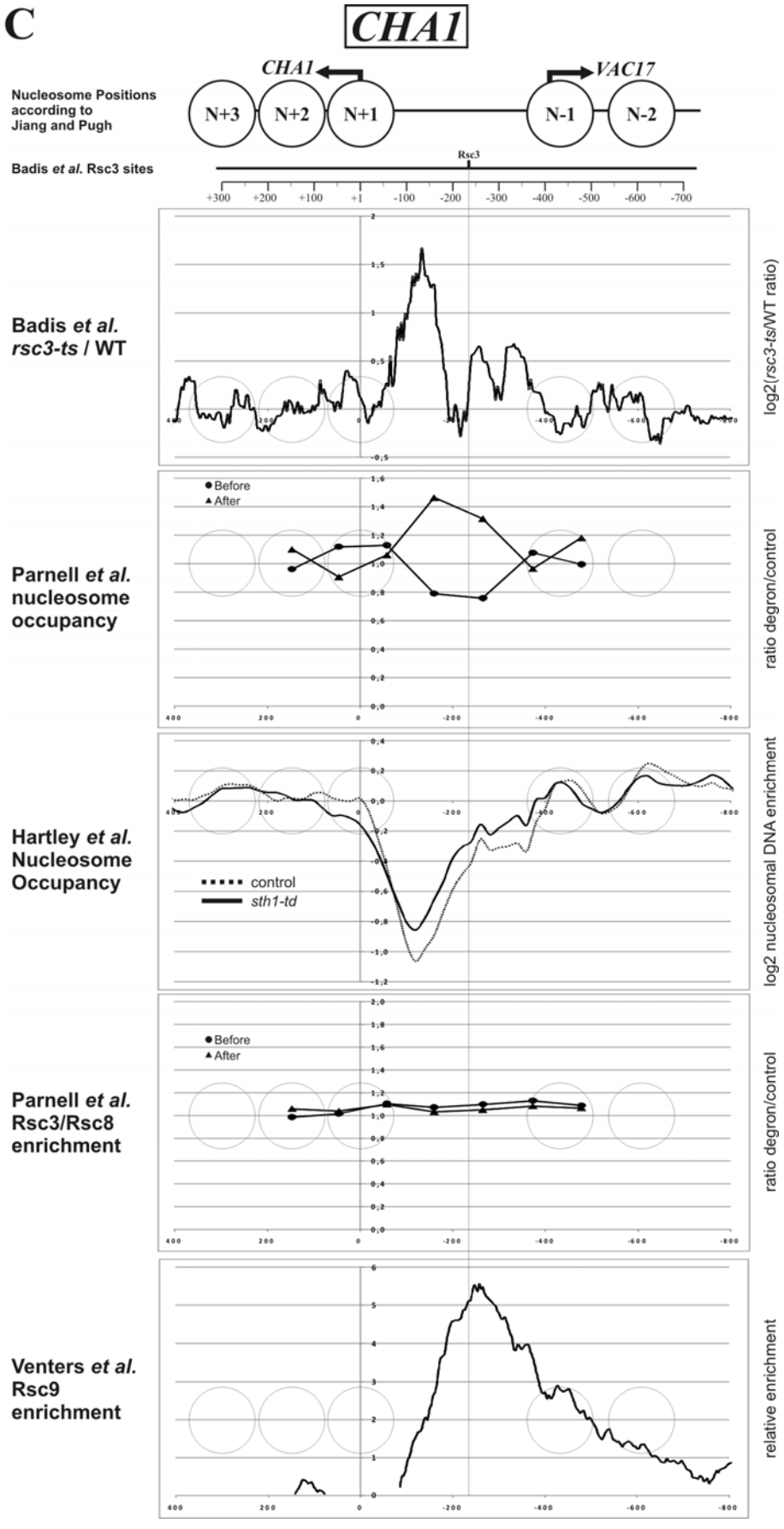
C
CHA1
CHA1
VAC17
Nucleosome Positions according to Jiang and Pugh
N+3
N+2
N+1
N-1
N-2
Badis et al. Rsc3 sites
Rsc3
+300 +200 +100 +1 -100 -200 -300 -400 -500 -600 -700
Badis et al. rsc3-ts / WT
log2(rsc3-ts/WT ratio)
Parnell et al. nucleosome occupancy
Before
After
ratio degron/control
Hartley et al. Nucleosome Occupancy
control
sth1-td
log2 nucleosomal DNA enrichment
Parnell et al. Rsc3/Rsc8 enrichment
Before
After
ratio degron/control
Venters et al. Rsc9 enrichment
relative enrichment

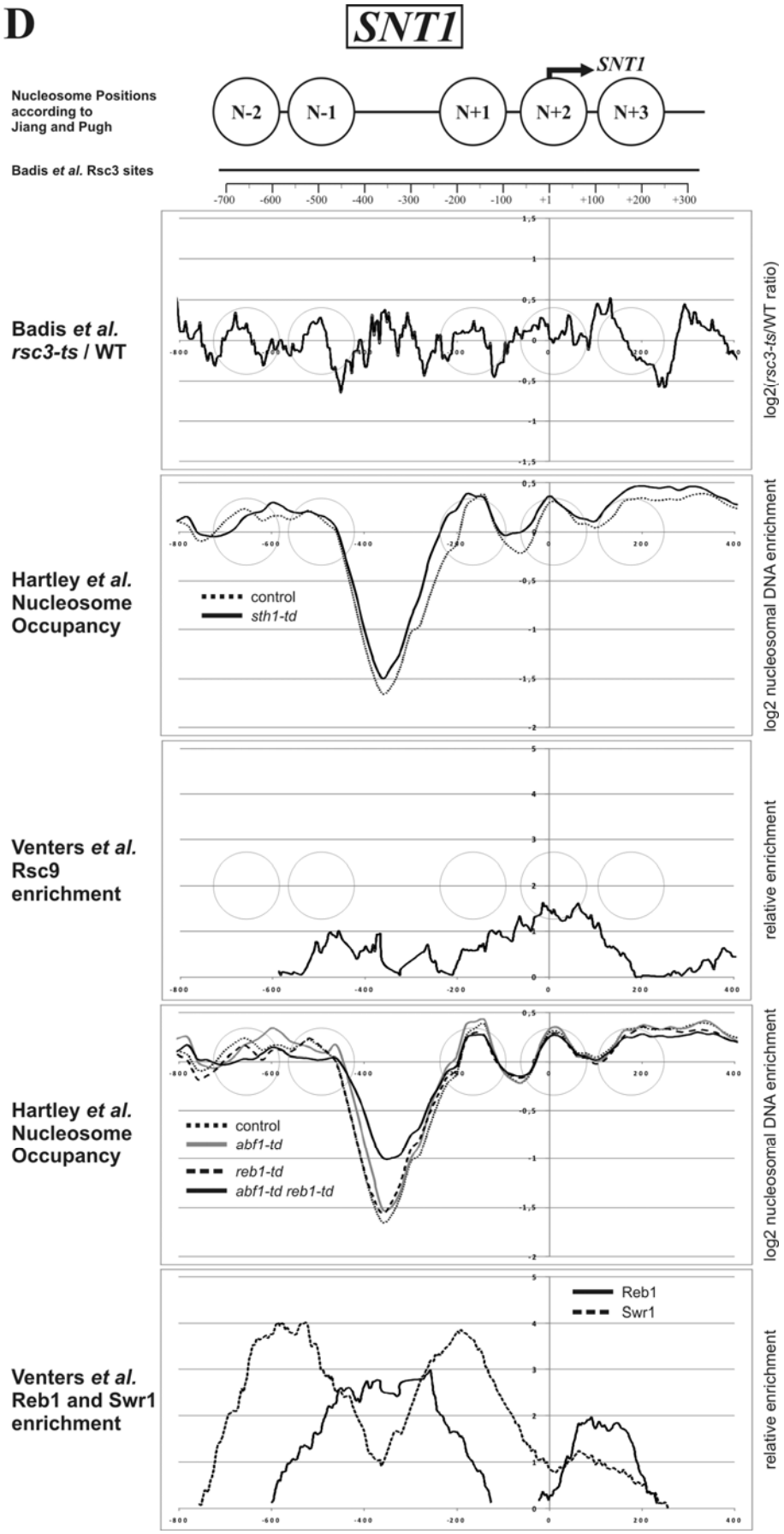
D
SNT1
SNT1
Nucleosome Positions according to Jiang and Pugh
N-2
N-1
N+1
N+2
N+3
Badis et al. Rsc3 sites
-700 -600 -500 -400 -300 -200 -100 +1 +100 +200 +300
Badis et al. rsc3-ts / WT
log2(rsc3-ts/WT ratio)
Hartley et al. Nucleosome Occupancy
control
sth1-td
log2 nucleosomal DNA enrichment
Venters et al. Rsc9 enrichment
relative enrichment
Hartley et al. Nucleosome Occupancy
control
abf1-td
reb1-td
abf1-td reb1-td
log2 nucleosomal DNA enrichment
Venters et al. Reb1 and Swr1 enrichment
Reb1
Swr1
relative enrichment

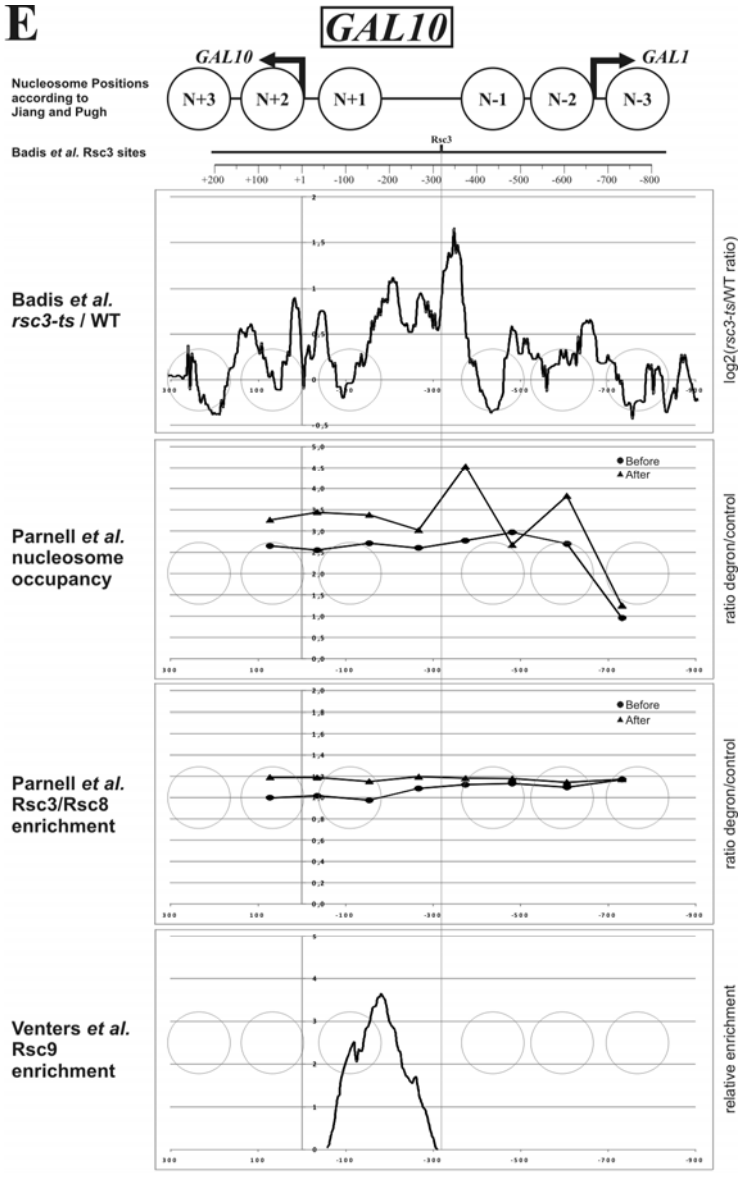
E
GAL10
GAL10
GAL1
Nucleosome Positions according to Jiang and Pugh
N+3
N+2
N+1
N-1
N-2
N-3
Badis et al. Rsc3 sites
Rsc3
+200 +100 +1 -100 -200 -300 -400 -500 -600 -700 -800
Badis et al. rsc3-ts / WT
log2(rsc3-ts/WT ratio)
Parnell et al. nucleosome occupancy
Before
After
ratio degron/control
Parnell et al. Rsc3/Rsc8 enrichment
Before
After
ratio degron/control
Venters et al. Rsc9 enrichment
relative enrichment
F
ADH2
ADH2
UBP15
Nucleosome Positions according to Jiang and Pugh
N+3
N+2
N+1
N-1
N-2
Badis et al. Rsc3 sites
+200 +100 +1 -100 -200 -300 -400 -500 -600 -700 -800
Badis et al. rsc3-ts / WT
log2(rsc3-ts/WT ratio)
Venters et al. Rsc9 enrichment
relative enrichment

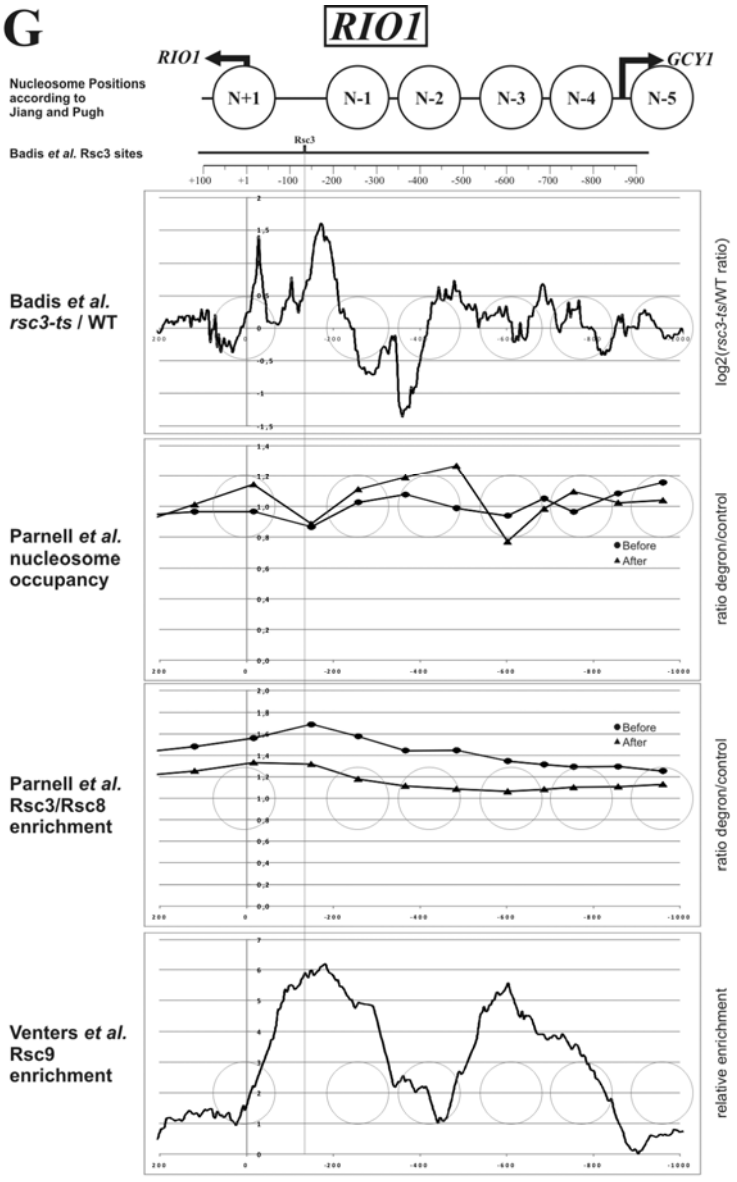
G
RIO1
RIO1
GCY1
Nucleosome Positions according to Jiang and Pugh
N+1
N-1
N-2
N-3
N-4
N-5
Badis et al. Rsc3 sites
Rsc3
Badis et al. rsc3-ts / WT
log2(rsc3-ts/WT ratio)
Parnell et al. nucleosome occupancy
Before
After
ratio degron/control
Parnell et al. Rsc3/Rsc8 enrichment
Before
After
ratio degron/control
Venters et al. Rsc9 enrichment
relative enrichment

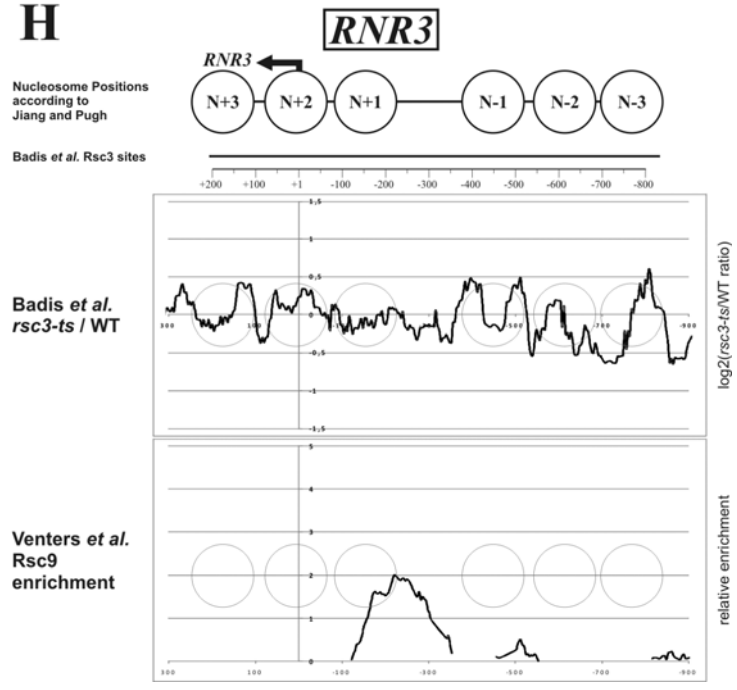
H
RNR3
RNR3
Nucleosome Positions according to Jiang and Pugh
N+3
N+2
N+1
N-1
N-2
N-3
Badis et al. Rsc3 sites
Badis et al. rsc3-ts / WT
log2(rsc3-ts/WT ratio)
Venters et al. Rsc9 enrichment
relative enrichment

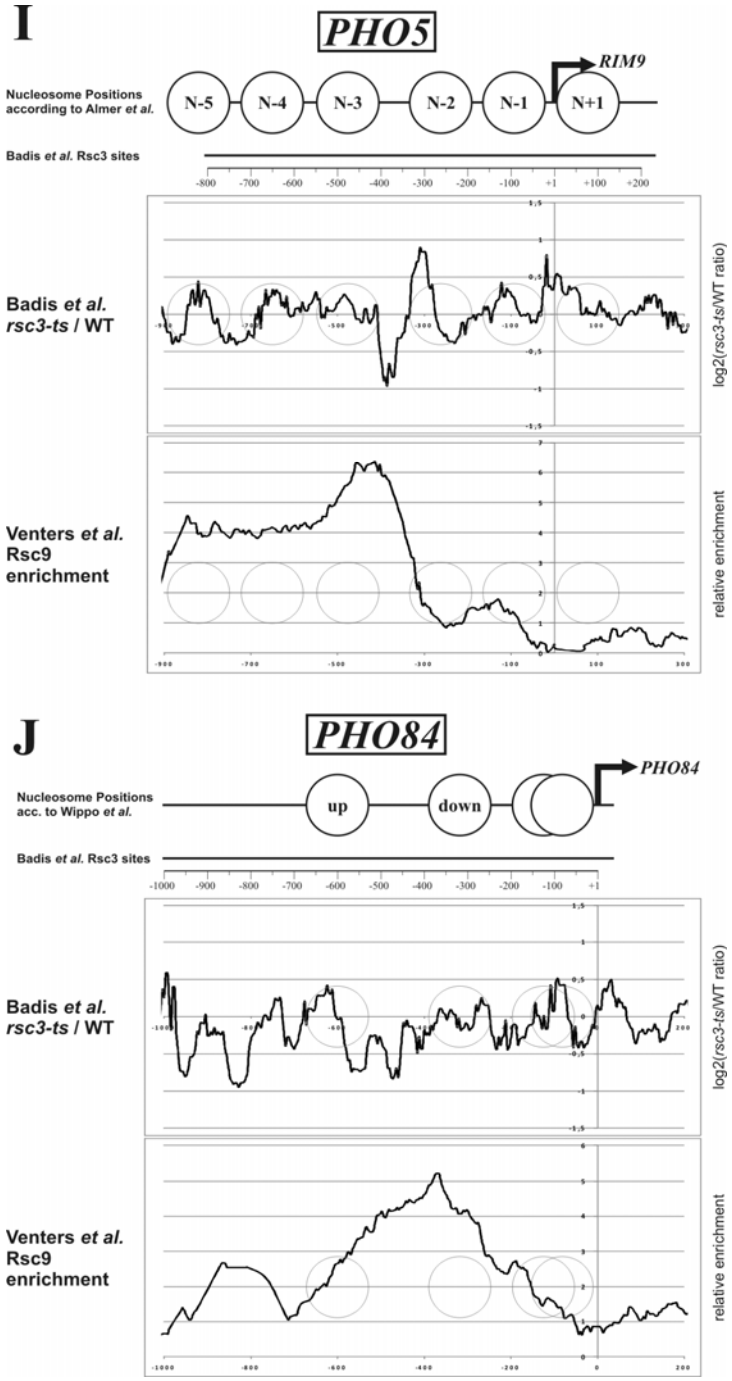

Figure S4. Comparison of the available datasets on RSC localization and effects on nucleosome occupancy upon ablation of RSC subunits.

(A-J) Schematics at the top indicate the position of the nucleosomes (according to Jiang and Pugh [7] unless otherwise stated) and the ORF starts. Putative Rsc3 binding sites were identified using the Badis *et al.* [138] PWM and are shown in the panel below. Graphs below the schematics show nucleosome occupancy changes in a *rsc3-ts* strain (Badis *et al.*) and *sth1-td* strains (Parnell *et al.* [140] and Hartley *et al.* [139]) as well as RSC occupancy profiles obtained by Parnell *et al.* and Venters *et al.* [180] as indicated. For some loci only limited amounts of data were available, since the microarray of Parnell *et al.* only included selected promoters and the microarray of Hartley *et al.* was limited to chromosome III. Gaps in the Venters *et al.* Rsc9 profile correspond to unavailable data for the corresponding regions.

5.3. Yeast strains

Strain	Genotype	Reference
Y00000	MATa *his3*Δ1 *leu2*Δ0 *met15*Δ0 *ura3*Δ0	EUROSCARF http://web.uni-frankfurt.de /fb15/mikro/euroscarf/
Y00397	MATa *his3*Δ1 *leu2*Δ0 *met15*Δ0 *ura3*Δ0 *scw3*::kanMX4	
Y00994	MATa *his3*Δ1 *leu2*Δ0 *met15*Δ0 *ura3*Δ0 *rrm3*::kanMX4	
Y01076	MATa *his3*Δ1 *leu2*Δ0 *met15*Δ0 *ura3*Δ0 *ypl216w*::kanMX4	
Y01285	MATa *his3*Δ1 *leu2*Δ0 *met15*Δ0 *ura3*Δ0 *rpb4*::kanMX4	
Y01343	MATa *his3*Δ1 *leu2*Δ0 *met15*Δ0 *ura3*Δ0 *scp160*::kanMX4	
Y01514	MATa *his3*Δ1 *leu2*Δ0 *met15*Δ0 *ura3*Δ0 *hsp104*::kanMX4	
Y01655	MATa *his3*Δ1 *leu2*Δ0 *met15*Δ0 *ura3*Δ0 *hap5*::kanMX4	
Y02123	MATa *his3*Δ1 *leu2*Δ0 *met15*Δ0 *ura3*Δ0 *taf14*::kanMX4	
Y03092	MATa *his3*Δ1 *leu2*Δ0 *met15*Δ0 *ura3*Δ0 *sef1*::kanMX4	
Y03418	MATa *his3*Δ1 *leu2*Δ0 *met15*Δ0 *ura3*Δ0 *sgf29*::kanMX4	
Y03648	MATa *his3*Δ1 *leu2*Δ0 *met15*Δ0 *ura3*Δ0 *rtt103*::kanMX4	
Y04196	MATa *his3*Δ1 *leu2*Δ0 *met15*Δ0 *ura3*Δ0 *eaf1*::kanMX4	
Y04315	MATa *his3*Δ1 *leu2*Δ0 *met15*Δ0 *ura3*Δ0 *pho8*::kanMX4	
Y05326	MATa *his3*Δ1 *leu2*Δ0 *met15*Δ0 *ura3*Δ0 *cdc73*::kanMX4	
Y05347	MATa *his3*Δ1 *leu2*Δ0 *met15*Δ0 *ura3*Δ0 *hda1*::kanMX4	
Y05727	MATa *his3*Δ1 *leu2*Δ0 *met15*Δ0 *ura3*Δ0 *paf1*::kanMX4	
Y05922	MATa *his3*Δ1 *leu2*Δ0 *met15*Δ0 *ura3*Δ0 *yta7*::kanMX4	
Y05927	MATa *his3*Δ1 *leu2*Δ0 *met15*Δ0 *ura3*Δ0 *rtt102*::kanMX4	
Y06520	MATa *his3*Δ1 *leu2*Δ0 *met15*Δ0 *ura3*Δ0 *yml199w*::kanMX4	
Y06546	MATa *his3*Δ1 *leu2*Δ0 *met15*Δ0 *ura3*Δ0 *yku80*::kanMX4	
Y06566	MATa *his3*Δ1 *leu2*Δ0 *met15*Δ0 *ura3*Δ0 *sto1*::kanMX4	
Y05852	MATa *his3*Δ1 *leu2*Δ0 *met15*Δ0 *ura3*Δ0 *irc5*::kanMX4	
Y00389	MATa *his3*Δ1 *leu2*Δ0 *met15*Δ0 *ura3*Δ0 *fun30*::kanMX4	
Y04530	MATa *his3*Δ1 *leu2*Δ0 *met15*Δ0 *ura3*Δ0 *rad54*::kanMX4	
Y03210	MATa *his3*Δ1 *leu2*Δ0 *met15*Δ0 *ura3*Δ0 *rdh54*::kanMX4	
Y06430	MATa *his3*Δ1 *leu2*Δ0 *met15*Δ0 *ura3*Δ0 *rad5*::kanMX4	
Y03253	MATa *his3*Δ1 *leu2*Δ0 *met15*Δ0 *ura3*Δ0 *rad16*::kanMX4	
Y02447	MATa *his3*Δ1 *leu2*Δ0 *met15*Δ0 *ura3*Δ0 *uls1*::kanMX4	
Y05156	MATa *his3*Δ1 *leu2*Δ0 *met15*Δ0 *ura3*Δ0 *irc20*::kanMX4	
Y06833	MATa *his3*Δ1 *leu2*Δ0 *met15*Δ0 *ura3*Δ0 *rad26*::kanMX4	
Y01601	MATa *his3*Δ1 *leu2*Δ0 *met15*Δ0 *ura3*Δ0 *isw2*::kanMX4	

SC1141	MATa *ade2 arg4 leu2-3 leu2-112 trp1-289 ura3-52 YIL091c*::TAP-K.I.*URA3*	
PKY813	(UKY403) MATa *ade2-101*$^{(och)}$ *arg4-1 his3-201 leu2-3,112 lys2-801*$^{(amb)}$ *trp1-901 ura3-52 thr*$^{-}$ *tyr*$^{-}$ *hhf1*::*HIS3 hhf2*::*LEU2* [pK626 *hhf2*(Δ4-28)]	Durrin *et al.* 1991 [247]
PKY899	(UKY403) MATa *ade2-101*$^{(och)}$ *arg4-1 his3-201 leu2-3,112 lys2-801*$^{(amb)}$ *trp1-901 ura3-52 thr*$^{-}$ *tyr*$^{-}$ *hhf1*::*HIS3 hhf2*::*LEU2* [pK626 *HHF2*]	
MY610	MATα(?) *ura3-52 trp-Δ1 leu2*::*PET56 gal2 gcn4-Δ1 his3*::*TRP1 mot1-1*	Collart 1996 [207]
FT4	MATa *ura3-52 trp1Δ63 his3Δ200 leu2*::*PET56*	Ng *et al.* 2002 [234]
FT4 STH1-9MYC	MATa *ura3-52 trp1-Δ63 his3-Δ200 leu2*::*PET56 sth1-9MYC*::*TRP*	
CJW105	MATa *ura3-52 trp1-Δ63 his3-Δ200 leu2*::*PET56 sth1-9MYC*::*TRP pho8*-Rsc3Δ-151	This work
CJW106	MATa *ura3-52 trp1-Δ63 his3-Δ200 leu2*::*PET56 sth1-9MYC*::*TRP pho8*-Rsc3Δ-10-151-214	This work
YBC1536	MATa *lys2-128δ leu2Δ1 ura3-52 trp1Δ63 his3Δ200 arp9Δ*::*LEU2* [p1014; *arp9* G337F G338L; CEN *TRP1*]	Szerlong *et al.* 2003 [222]
BCY 426	MATα *ade2-1 trp1-1 can1-100 leu2-3,112 his3-15 ura3-1 arp9*Δ::*LEU2 mra1*	
BCY 427	MATa *ade2-1 trp1-1 can1-100 leu2-3,112 his3-15 ura3-1 arp7*Δ::*TRP1 mra1*	
BCY 430	MATα *ade2-1 trp1-1 can1-100 leu2-3,112 his3-15 ura3-1 mra1*	
BCY 395	MATα *ade2-1 trp1-1 can1-100 leu2-3,112 his3-15 ura3-1 arp7*Δ::*TRP1 arp9*Δ::*LEU2 mra1*	
CJW001	MATa *ade2-1 ura3-1 his3-11,15 trp1-1 leu2-3,112 can1-100 ubr1*::*GAL-HA-UBR1*::*HIS3 reb1Δ*::pCUP1-*reb1*^{td}::*URA3*	This work
TH8242	MATa *his3Δ1 leu2Δ0 met15Δ0 ura3Δ0 abf1-101*::KanMX	Badis *et al.* 2008 [138]
TH8243	MATa *his3Δ1 leu2Δ0 met15Δ0 ura3Δ0 cep3-1*::KanMX	
TH8244	MATa *his3Δ1 leu2Δ0 met15Δ0 ura3Δ0* KanMX::*mcm1-URA3*	
TH8245	MATa *his3Δ1 leu2Δ0 met15Δ0 ura3Δ0 rap1-1*::KanMX	
TH8246	MATa *his3Δ1 leu2Δ0 met15Δ0 ura3Δ0* KanMX::*reb1-212-URA3*	
TH8247	MATa *his3Δ1 leu2Δ0 met15Δ0 ura3Δ0 rsc3-1*::KanMX	
TH8233	MATa *his3Δ1 leu2Δ0 met15Δ0 ura3Δ0* KanMX::*tbf1-URA3*	
TH8239	MATa *his3Δ1 leu2Δ0 met15Δ0 ura3Δ0 rsc3-1*::kanMX *rsc8*-TAP::*HIS3*MX6	
FY2810	MATa *leu2Δ1 his4-912δ lys2-128δ* FLAG-*spt16-1004*	F. Winston
YBC2191	MATa *ura3-52 trp1Δ63 his3Δ200 leu*::*PET56 ubr1*Δ::pGAL1-*UBR*::*HIS3* sth1Δ::pCUP1-sth1^{td}::URA3	Parnell *et al.* 2008 [140]
YBC602	MATa *ade2Δ*::*hisG his3Δ200 leu2Δ0 lys2Δ0 met15Δ0 trp1Δ63*	Angus-Hill *et al.* 2001 [62]
YBC693	MATa *ade2Δ*::*hisG his3Δ200 leu2Δ0 lys2Δ0 met15Δ0 trp1Δ63 ura3Δ0 rsc30Δ*::*LEU2*	
arp9-ts pho4	MATa *lys2-128δ leu2Δ1 ura3-52 trp1Δ63 his3Δ200 arp9Δ*::*LEU2 pho4*::*URA3* [p1014; *arp9* G337F G338L; CEN *TRP1*]	This work
rsc3-ts pho4	MATa *his3Δ1 leu2Δ0 met15Δ0 ura3Δ0 rsc3-1*::KanMX *pho4*::*URA3*	This work
tfg2-ts	MATa *ura3Δ0 leu2Δ0 his3Δ1 lys2Δ0 met15Δ0 can1Δ*::*LEU2*-MFA1pr::*HIS3 tfg2-ts*::*URA3*.	Ben-Aroya *et al.* 2008 [248]
ssl1-ts	MATa *ura3Δ0 leu2Δ0 his3Δ1 lys2Δ0 met15Δ0 can1Δ*::*LEU2*-MFA1pr::*HIS3 ssl1-ts*::*URA3*.	
FP297	MATα *ura3-52 trp1Δ63 tfg1Δ1* [p314; *tfg1*-E346A (*TRP1*)]	Ghazy *et al.* 2004 [249]
WCS203	MATa *ade2-101a his3Δ200 leu2-Δ1 lys2-801a trp1-Δ63 ura3-52 taf3*::*HIS3* [pRS414; *taf3-ts3* (CEN *TRP1*)]	Shen *et al.* 2003 [250]

YSW93	MATa *ade2-101 his3Δ200 leu2-Δ1 lys2-801 ura3Δ99 GAL2 GAL3 taf1*::*LEU2* [pSW104; *taf1-ts2* (CEN *HIS3*)]	
YSB331	MATa *ura3-52 leu2-3,112 his3Δ200 tfa1Δ1*::*HIS3* [pNK6; *tfa1*(C127F) *LEU2* (CEN/ARS f1+ ori AmpR)]	Kuldell and Boratowski 1997 [251]
YKS188-1	MATα *ade2-101*^{ochre} *his3-Δ200 leu2-Δ1 lys2-801*^{amber} *ura3-52 trp1-Δ1 Δspt15*::TRP1 [pDP13-2D188EI]	Poon *et al.* 1993 [226]
CY337	MATa *ura3-52 lys2-801 ade2-101 leu2-Δ1 his3-Δ200*	Richmond and Peterson 1996 [252]
CY407	MATa *ura3-52 lys2-801 ade2-101 leu2-Δ1 his3-Δ200 snf2*::*HIS3*	
CY338	MATa *ura3-52 lys2-801 ade2-101 leu2-Δ1 his3-Δ200 pho4*::*URA3*	Our group
CY408	MATa *ura3-52 lys2-801 ade2-101 leu2-Δ1 his3-Δ200 snf2*::*HIS3 pho4*::*URA3*	Our group
CY407pho8	MATa *ura3-52 lys2-801 ade2-101 leu2-Δ1 his3-Δ200 snf2*::*HIS3 pho8*::KanMX	This work
CJW101	MATa *ura3-52 lys2-801 ade2-101 leu2-Δ1 his3-Δ200 pho8*-Rsc3Δ-10	This work
CJW102	MATa *ura3-52 lys2-801 ade2-101 leu2-Δ1 his3-Δ200 pho8*-Rsc3Δ-151	This work
CJW103	MATa *ura3-52 lys2-801 ade2-101 leu2-Δ1 his3-Δ200 pho8*-Rsc3Δ-214	This work
CJW104	MATa *ura3-52 lys2-801 ade2-101 leu2-Δ1 his3-Δ200 pho8*-Rsc3Δ-10-151-214	This work
CJW201	MATa *ura3-52 lys2-801 ade2-101 leu2-Δ1 his3-Δ200 snf2*::*HIS3 pho8*-Rsc3Δ-10	This work
CJW202	MATa *ura3-52 lys2-801 ade2-101 leu2-Δ1 his3-Δ200 snf2*::*HIS3 pho8*-Rsc3Δ-151	This work
CJW203	MATa *ura3-52 lys2-801 ade2-101 leu2-Δ1 his3-Δ200 snf2*::*HIS3 pho8*-Rsc3Δ-214	This work
CJW204	MATa *ura3-52 lys2-801 ade2-101 leu2-Δ1 his3-Δ200 snf2*::*HIS3 pho8*-Rsc3Δ-10-151-214	This work

6. References

1. Thomas, J.O. and R.D. Kornberg, *An octamer of histones in chromatin and free in solution.* Proc Natl Acad Sci U S A, 1975. **72**(7): p. 2626-30.
2. Luger, K., et al., *Crystal structure of the nucleosome core particle at 2.8 A resolution.* Nature, 1997. **389**(6648): p. 251-60.
3. Ramakrishnan, V., *Histone structure and the organization of the nucleosome.* Annu Rev Biophys Biomol Struct, 1997. **26**: p. 83-112.
4. Oudet, P., M. Gross-Bellard, and P. Chambon, *Electron microscopic and biochemical evidence that chromatin structure is a repeating unit.* Cell, 1975. **4**(4): p. 281-300.
5. Lantermann, A.B., et al., *Schizosaccharomyces pombe genome-wide nucleosome mapping reveals positioning mechanisms distinct from those of Saccharomyces cerevisiae.* Nat Struct Mol Biol, 2010. **17**(2): p. 251-7.
6. Athey, B.D., et al., *The diameters of frozen-hydrated chromatin fibers increase with DNA linker length: evidence in support of variable diameter models for chromatin.* J Cell Biol, 1990. **111**(3): p. 795-806.
7. Jiang, C. and B.F. Pugh, *A compiled and systematic reference map of nucleosome positions across the Saccharomyces cerevisiae genome.* Genome Biol, 2009. **10**(10): p. R109.
8. Lee, W., et al., *A high-resolution atlas of nucleosome occupancy in yeast.* Nat Genet, 2007. **39**(10): p. 1235-44.
9. Dorigo, B., et al., *Nucleosome arrays reveal the two-start organization of the chromatin fiber.* Science, 2004. **306**(5701): p. 1571-3.
10. Widom, J. and A. Klug, *Structure of the 300A chromatin filament: X-ray diffraction from oriented samples.* Cell, 1985. **43**(1): p. 207-13.
11. Williams, S.P., et al., *Chromatin fibers are left-handed double helices with diameter and mass per unit length that depend on linker length.* Biophys J, 1986. **49**(1): p. 233-48.
12. Woodcock, C.L. and S. Dimitrov, *Higher-order structure of chromatin and chromosomes.* Curr Opin Genet Dev, 2001. **11**(2): p. 130-5.
13. Tremethick, D.J., *Higher-order structures of chromatin: the elusive 30 nm fiber.* Cell, 2007. **128**(4): p. 651-4.
14. Bassett, A., et al., *The folding and unfolding of eukaryotic chromatin.* Curr Opin Genet Dev, 2009. **19**(2): p. 159-65.
15. Maeshima, K., S. Hihara, and M. Eltsov, *Chromatin structure: does the 30-nm fibre exist in vivo?* Curr Opin Cell Biol, 2010. **22**(3): p. 291-7.
16. Bednar, J., et al., *Nucleosomes, linker DNA, and linker histone form a unique structural motif that directs the higher-order folding and compaction of chromatin.* Proc Natl Acad Sci U S A, 1998. **95**(24): p. 14173-8.
17. Freidkin, I. and D.J. Katcoff, *Specific distribution of the Saccharomyces cerevisiae linker histone homolog HHO1p in the chromatin.* Nucleic Acids Res, 2001. **29**(19): p. 4043-51.
18. Ghaemmaghami, S., et al., *Global analysis of protein expression in yeast.* Nature, 2003. **425**(6959): p. 737-41.
19. Patterton, H.G., et al., *The biochemical and phenotypic characterization of Hho1p, the putative linker histone H1 of Saccharomyces cerevisiae.* J Biol Chem, 1998. **273**(13): p. 7268-76.
20. Fan, Y., et al., *H1 linker histones are essential for mouse development and affect nucleosome spacing in vivo.* Mol Cell Biol, 2003. **23**(13): p. 4559-72.
21. Luger, K. and J.C. Hansen, *Nucleosome and chromatin fiber dynamics.* Curr Opin Struct Biol, 2005. **15**(2): p. 188-96.
22. Woodcock, C.L. and R.P. Ghosh, *Chromatin higher-order structure and dynamics.* Cold Spring Harb Perspect Biol, 2010. **2**(5): p. a000596.
23. Saez-Vasquez, J. and O. Gadal, *Genome organization and function: a view from yeast and Arabidopsis.* Mol Plant, 2010. **3**(4): p. 678-90.

24. Lander, E.S., et al., *Initial sequencing and analysis of the human genome.* Nature, 2001. **409**(6822): p. 860-921.
25. Werner, T., *Next generation sequencing allows deeper analysis and understanding of genomes and transcriptomes including aspects to fertility.* Reprod Fertil Dev, 2011. **23**(1): p. 75-80.
26. Buhler, M. and S.M. Gasser, *Silent chromatin at the middle and ends: lessons from yeasts.* EMBO J, 2009. **28**(15): p. 2149-61.
27. Felsenfeld, G., *Chromatin as an essential part of the transcriptional mechanism.* Nature, 1992. **355**(6357): p. 219-24.
28. Felsenfeld, G. and M. Groudine, *Controlling the double helix.* Nature, 2003. **421**(6921): p. 448-53.
29. Li, B., M. Carey, and J.L. Workman, *The role of chromatin during transcription.* Cell, 2007. **128**(4): p. 707-19.
30. Burgess, R.J. and Z. Zhang, *Histones, histone chaperones and nucleosome assembly.* Protein Cell, 2010. **1**(7): p. 607-12.
31. Groth, A., et al., *Chromatin challenges during DNA replication and repair.* Cell, 2007. **128**(4): p. 721-33.
32. Kouzarides, T., *Chromatin modifications and their function.* Cell, 2007. **128**(4): p. 693-705.
33. Bonisch, C., et al., *Chromatin proteomics and epigenetic regulatory circuits.* Expert Rev Proteomics, 2008. **5**(1): p. 105-19.
34. Strahl, B.D. and C.D. Allis, *The language of covalent histone modifications.* Nature, 2000. **403**(6765): p. 41-5.
35. Shogren-Knaak, M., et al., *Histone H4-K16 acetylation controls chromatin structure and protein interactions.* Science, 2006. **311**(5762): p. 844-7.
36. Strahl, B.D., et al., *Set2 is a nucleosomal histone H3-selective methyltransferase that mediates transcriptional repression.* Mol Cell Biol, 2002. **22**(5): p. 1298-306.
37. Zhang, Y. and D. Reinberg, *Transcription regulation by histone methylation: interplay between different covalent modifications of the core histone tails.* Genes Dev, 2001. **15**(18): p. 2343-60.
38. Dion, M.F., et al., *Dynamics of replication-independent histone turnover in budding yeast.* Science, 2007. **315**(5817): p. 1405-8.
39. Zlatanova, J. and A. Thakar, *H2A.Z: view from the top.* Structure, 2008. **16**(2): p. 166-79.
40. Meluh, P.B., et al., *Cse4p is a component of the core centromere of Saccharomyces cerevisiae.* Cell, 1998. **94**(5): p. 607-13.
41. Stoler, S., et al., *A mutation in CSE4, an essential gene encoding a novel chromatin-associated protein in yeast, causes chromosome nondisjunction and cell cycle arrest at mitosis.* Genes Dev, 1995. **9**(5): p. 573-86.
42. Raisner, R.M., et al., *Histone variant H2A.Z marks the 5' ends of both active and inactive genes in euchromatin.* Cell, 2005. **123**(2): p. 233-48.
43. Albert, I., et al., *Translational and rotational settings of H2A.Z nucleosomes across the Saccharomyces cerevisiae genome.* Nature, 2007. **446**(7135): p. 572-576.
44. Santisteban, M.S., T. Kalashnikova, and M.M. Smith, *Histone H2A.Z regulats transcription and is partially redundant with nucleosome remodeling complexes.* Cell, 2000. **103**(3): p. 411-22.
45. Meneghini, M.D., M. Wu, and H.D. Madhani, *Conserved histone variant H2A.Z protects euchromatin from the ectopic spread of silent heterochromatin.* Cell, 2003. **112**(5): p. 725-36.
46. Zhang, H., et al., *The Yaf9 component of the SWR1 and NuA4 complexes is required for proper gene expression, histone H4 acetylation, and Htz1 replacement near telomeres.* Mol Cell Biol, 2004. **24**(21): p. 9424-36.
47. Krogan, N.J., et al., *Regulation of chromosome stability by the histone H2A variant Htz1, the Swr1 chromatin remodeling complex, and the histone acetyltransferase NuA4.* Proc Natl Acad Sci U S A, 2004. **101**(37): p. 13513-8.
48. Jin, C. and G. Felsenfeld, *Nucleosome stability mediated by histone variants H3.3 and H2A.Z.* Genes Dev, 2007. **21**(12): p. 1519-29.

49. Jin, C., et al., *H3.3/H2A.Z double variant-containing nucleosomes mark 'nucleosome-free regions' of active promoters and other regulatory regions.* Nat Genet, 2009. **41**(8): p. 941-5.
50. Abbott, D.W., et al., *Characterization of the stability and folding of H2A.Z chromatin particles: implications for transcriptional activation.* J Biol Chem, 2001. **276**(45): p. 41945-9.
51. Park, Y.J., et al., *A new fluorescence resonance energy transfer approach demonstrates that the histone variant H2AZ stabilizes the histone octamer within the nucleosome.* J Biol Chem, 2004. **279**(23): p. 24274-82.
52. Thambirajah, A.A., et al., *H2A.Z stabilizes chromatin in a way that is dependent on core histone acetylation.* J Biol Chem, 2006. **281**(29): p. 20036-44.
53. Flaus, A., et al., *Sin mutations alter inherent nucleosome mobility.* Embo Journal, 2004. **23**(2): p. 343-353.
54. Li, B., et al., *Preferential occupancy of histone variant H2AZ at inactive promoters influences local histone modifications and chromatin remodeling.* Proc Natl Acad Sci U S A, 2005. **102**(51): p. 18385-90.
55. Becker, P.B. and W. Horz, *ATP-dependent nucleosome remodeling.* Annu Rev Biochem, 2002. **71**: p. 247-73.
56. Clapier, C.R. and B.R. Cairns, *The biology of chromatin remodeling complexes.* Annu Rev Biochem, 2009. **78**: p. 273-304.
57. Korber, P. and P.B. Becker, *Nucleosome dynamics and epigenetic stability.* Essays Biochem, 2010. **48**(1): p. 63-74.
58. Flaus, A., et al., *Identification of multiple distinct Snf2 subfamilies with conserved structural motifs.* Nucleic Acids Res, 2006. **34**(10): p. 2887-905.
59. Auble, D.T., et al., *Molecular analysis of the SNF2/SWI2 protein family member MOT1, an ATP-driven enzyme that dissociates TATA-binding protein from DNA.* Mol Cell Biol, 1997. **17**(8): p. 4842-51.
60. Sudarsanam, P., et al., *Whole-genome expression analysis of snf/swi mutants of Saccharomyces cerevisiae.* Proc Natl Acad Sci U S A, 2000. **97**(7): p. 3364-9.
61. Barbaric, S., et al., *Redundancy of chromatin remodeling pathways for the induction of the yeast PHO5 promoter in vivo.* Journal of Biological Chemistry, 2007. **282**(38): p. 27610-27621.
62. Angus-Hill, M.L., et al., *A Rsc3/Rsc30 zinc cluster dimer reveals novel roles for the chromatin remodeler RSC in gene expression and cell cycle control.* Mol Cell, 2001. **7**(4): p. 741-51.
63. Ebbert, R., A. Birkmann, and H.J. Schuller, *The product of the SNF2/SWI2 paralogue INO80 of Saccharomyces cerevisiae required for efficient expression of various yeast structural genes is part of a high-molecular-weight protein complex.* Mol Microbiol, 1999. **32**(4): p. 741-51.
64. Conaway, R.C. and J.W. Conaway, *The INO80 chromatin remodeling complex in transcription, replication and repair.* Trends Biochem Sci, 2009. **34**(2): p. 71-7.
65. Guzder, S.N., et al., *Yeast Rad7-Rad16 complex, specific for the nucleotide excision repair of the nontranscribed DNA strand, is an ATP-dependent DNA damage sensor.* J Biol Chem, 1997. **272**(35): p. 21665-8.
66. Shimada, K., et al., *Ino80 chromatin remodeling complex promotes recovery of stalled replication forks.* Curr Biol, 2008. **18**(8): p. 566-75.
67. Petukhova, G., et al., *Yeast Rad54 promotes Rad51-dependent homologous DNA pairing via ATP hydrolysis-driven change in DNA double helix conformation.* J Biol Chem, 1999. **274**(41): p. 29453-62.
68. Kawashima, S., et al., *The INO80 complex is required for damage-induced recombination.* Biochem Biophys Res Commun, 2007. **355**(3): p. 835-41.
69. Mizuguchi, G., et al., *ATP-driven exchange of histone H2AZ variant catalyzed by SWR1 chromatin remodeling complex.* Science, 2004. **303**(5656): p. 343-8.
70. Papamichos-Chronakis, M., et al., *Global regulation of H2A.Z localization by the INO80 chromatin-remodeling enzyme is essential for genome integrity.* Cell, 2011. **144**(2): p. 200-13.
71. Kaplan, N., et al., *Contribution of histone sequence preferences to nucleosome organization: proposed definitions and methodology.* Genome Biol, 2010. **11**(11): p. 140.

72. Poirier, M.G., et al., *Spontaneous access to DNA target sites in folded chromatin fibers.* Journal of Molecular Biology, 2008. **379**(4): p. 772-786.
73. Anderson, J.D., A. Thastrom, and J. Widom, *Spontaneous access of proteins to buried nucleosomal DNA target sites occurs via a mechanism that is distinct from nucleosome translocation.* Molecular and Cellular Biology, 2002. **22**(20): p. 7147-7157.
74. Zhang, Z., et al., *A packing mechanism for nucleosome organization reconstituted across a eukaryotic genome.* Science, 2011. **332**(6032): p. 977-80.
75. Mavrich, T.N., et al., *A barrier nucleosome model for statistical positioning of nucleosomes throughout the yeast genome.* Genome Research, 2008. **18**(7): p. 1073-1083.
76. Shivaswamy, S., et al., *Dynamic remodeling of individual nucleosomes across a eukaryotic genome in response to transcriptional perturbation.* PLoS Biol, 2008. **6**(3): p. e65.
77. Polisky, B. and B. McCarthy, *Location of histones on simian virus 40 DNA.* Proc Natl Acad Sci U S A, 1975. **72**(8): p. 2895-9.
78. Steinmetz, M., R.E. Streeck, and H.G. Zachau, *Nucleosome formation abolishes base-specific binding of histones.* Nature, 1975. **258**(5534): p. 447-50.
79. Ponder, B.A. and L.V. Crawford, *The arrangement of nucleosomes in nucleoprotein complexes from polyoma virus and SV40.* Cell, 1977. **11**(1): p. 35-49.
80. Scott, W.A. and D.J. Wigmore, *Sites in simian virus 40 chromatin which are preferentially cleaved by endonucleases.* Cell, 1978. **15**(4): p. 1511-8.
81. Waldeck, W., et al., *Origin of DNA replication in papovavirus chromatin is recognized by endogenous endonuclease.* Proc Natl Acad Sci U S A, 1978. **75**(12): p. 5964-8.
82. Brown, F.L., P.R. Musich, and J.J. Maio, *The repetitive sequence structure of component alpha DNA and its relationship to the nucleosomes of the African green monkey.* J Mol Biol, 1979. **131**(4): p. 777-99.
83. Horz, W., F. Fittler, and H.G. Zachau, *Sequence specific cleavage of African green monkey alpha-satellite DNA by micrococcal nuclease.* Nucleic Acids Res, 1983. **11**(13): p. 4275-85.
84. Musich, P.R., F.L. Brown, and J.J. Maio, *Nucleosome phasing and micrococcal nuclease cleavage of African green monkey component alpha DNA.* Proc Natl Acad Sci U S A, 1982. **79**(1): p. 118-22.
85. Gottesfeld, J.M. and L.S. Bloomer, *Nonrandom alignment of nucleosomes on 5S RNA genes of X. laevis.* Cell, 1980. **21**(3): p. 751-60.
86. Thoma, F., L.W. Bergman, and R.T. Simpson, *Nuclease digestion of circular TRP1ARS1 chromatin reveals positioned nucleosomes separated by nuclease-sensitive regions.* J Mol Biol, 1984. **177**(4): p. 715-33.
87. Wittig, B. and S. Wittig, *A phase relationship associates tRNA structural gene sequences with nucleosome cores.* Cell, 1979. **18**(4): p. 1173-83.
88. Almer, A. and W. Horz, *Nuclease hypersensitive regions with adjacent positioned nucleosomes mark the gene boundaries of the PHO5/PHO3 locus in yeast.* EMBO J, 1986. **5**(10): p. 2681-7.
89. Almer, A., et al., *Removal of positioned nucleosomes from the yeast PHO5 promoter upon PHO5 induction releases additional upstream activating DNA elements.* EMBO J, 1986. **5**(10): p. 2689-96.
90. Venter, U., et al., *A nucleosome precludes binding of the transcription factor Pho4 in vivo to a critical target site in the PHO5 promoter.* EMBO J, 1994. **13**(20): p. 4848-55.
91. Simpson, R.T., *Nucleosome Positioning - Occurrence, Mechanisms, and Functional Consequences.* Progress in Nucleic Acid Research and Molecular Biology, 1991. **40**: p. 143-184.
92. Lu, Q., L.L. Wallrath, and S.C. Elgin, *Nucleosome positioning and gene regulation.* J Cell Biochem, 1994. **55**(1): p. 83-92.
93. Yuan, G.C., et al., *Genome-scale identification of nucleosome positions in S-cerevisiae.* Science, 2005. **309**(5734): p. 626-630.
94. Field, Y., et al., *Distinct Modes of Regulation by Chromatin Encoded through Nucleosome Positioning Signals.* Plos Computational Biology, 2008. **4**(11): p. e1000216.

95. Whitehouse, I., et al., *Chromatin remodelling at promoters suppresses antisense transcription.* Nature, 2007. **450**(7172): p. 1031-U3.
96. Field, Y., et al., *Gene expression divergence in yeast is coupled to evolution of DNA-encoded nucleosome organization.* Nat Genet, 2009. **41**(4): p. 438-45.
97. Tsankov, A.M., et al., *The role of nucleosome positioning in the evolution of gene regulation.* PLoS Biol, 2010. **8**(7): p. e1000414.
98. Weiner, A., et al., *High-resolution nucleosome mapping reveals transcription-dependent promoter packaging.* Genome Res, 2010. **20**(1): p. 90-100.
99. Valouev, A., et al., *A high-resolution, nucleosome position map of C. elegans reveals a lack of universal sequence-dictated positioning.* Genome Research, 2008. **18**(7): p. 1051-1063.
100. Johnson, S.M., et al., *Flexibility and constraint in the nucleosome core landscape of Caenorhabditis elegans chromatin.* Genome Research, 2006. **16**(12): p. 1505-1516.
101. Mavrich, T.N., et al., *Nucleosome organization in the Drosophila genome.* Nature, 2008. **453**(7193): p. 358-62.
102. Schones, D.E., et al., *Dynamic regulation of nucleosome positioning in the human genome.* Cell, 2008. **132**(5): p. 887-898.
103. Ozsolak, F., et al., *High-throughput mapping of the chromatin structure of human promoters.* Nature Biotechnology, 2007. **25**(2): p. 244-248.
104. Tirosh, I. and N. Barkai, *Two strategies for gene regulation by promoter nucleosomes.* Genome Research, 2008. **18**(7): p. 1084-1091.
105. Cairns, B.R., *The logic of chromatin architecture and remodelling at promoters.* Nature, 2009. **461**(7261): p. 193-8.
106. Radman-Livaja, M. and O.J. Rando, *Nucleosome positioning: How is it established, and why does it matter?* Dev Biol, 2010. **339**(2): p. 258-66.
107. Kornberg, R.D. and L. Stryer, *Statistical distributions of nucleosomes: nonrandom locations by a stochastic mechanism.* Nucleic Acids Res, 1988. **16**(14A): p. 6677-90.
108. Arents, G., et al., *The nucleosomal core histone octamer at 3.1 A resolution: a tripartite protein assembly and a left-handed superhelix.* Proc Natl Acad Sci U S A, 1991. **88**(22): p. 10148-52.
109. Lowary, P.T. and J. Widom, *New DNA sequence rules for high affinity binding to histone octamer and sequence-directed nucleosome positioning.* Journal of Molecular Biology, 1998. **276**(1): p. 19-42.
110. Thastrom, A., P.T. Lowary, and J. Widom, *Measurement of histone-DNA interaction free energy in nucleosomes.* Methods, 2004. **33**(1): p. 33-44.
111. Thastrom, A., et al., *Sequence motifs and free energies of selected natural and non-natural nucleosome positioning DNA sequences.* Journal of Molecular Biology, 1999. **288**(2): p. 213-229.
112. Shrader, T.E. and D.M. Crothers, *Artificial Nucleosome Positioning Sequences.* Proceedings of the National Academy of Sciences of the United States of America, 1989. **86**(19): p. 7418-7422.
113. Segal, E., et al., *A genomic code for nucleosome positioning.* Nature, 2006. **442**(7104): p. 772-778.
114. Satchwell, S.C., H.R. Drew, and A.A. Travers, *Sequence periodicities in chicken nucleosome core DNA.* J Mol Biol, 1986. **191**(4): p. 659-75.
115. Ioshikhes, I.P., et al., *Nucleosome positions predicted through comparative genomics.* Nature Genetics, 2006. **38**(10): p. 1210-1215.
116. Ioshikhes, I., et al., *Nucleosome DNA sequence pattern revealed by multiple alignment of experimentally mapped sequences.* Journal of Molecular Biology, 1996. **262**(2): p. 129-139.
117. Widom, J., *Role of DNA sequence in nucleosome stability and dynamics.* Quarterly Reviews of Biophysics, 2001. **34**(3): p. 269-324.
118. Drew, H.R. and A.A. Travers, *DNA Bending and Its Relation to Nucleosome Positioning.* Journal of Molecular Biology, 1985. **186**(4): p. 773-790.

119. Zhang, Y., et al., *Intrinsic histone-DNA interactions are not the major determinant of nucleosome positions in vivo.* Nat Struct Mol Biol, 2009. **16**(8): p. 847-52.
120. Kaplan, N., et al., *The DNA-encoded nucleosome organization of a eukaryotic genome.* Nature, 2009. **458**(7236): p. 362-6.
121. Simpson, R.T. and P. Kunzler, *Cromatin and core particles formed from the inner histones and synthetic polydeoxyribonucleotides of defined sequence.* Nucleic Acids Res, 1979. **6**(4): p. 1387-415.
122. Segal, E. and J. Widom, *Poly(dA:dT) tracts: major determinants of nucleosome organization.* Curr Opin Struct Biol, 2009. **19**(1): p. 65-71.
123. Kunkel, G.R. and H.G. Martinson, *Nucleosomes will not form on double-stranded RNa or over poly(dA).poly(dT) tracts in recombinant DNA.* Nucleic Acids Res, 1981. **9**(24): p. 6869-88.
124. Prunell, A., *Nucleosome reconstitution on plasmid-inserted poly(dA) . poly(dT).* EMBO J, 1982. **1**(2): p. 173-9.
125. Anderson, J.D. and J. Widom, *Poly(dA-dT) promoter elements increase the equilibrium accessibility of nucleosomal DNA target sites.* Mol Cell Biol, 2001. **21**(11): p. 3830-9.
126. Bernstein, B.E., et al., *Global nucleosome occupancy in yeast.* Genome Biol, 2004. **5**(9): p. R62.
127. Iyer, V. and K. Struhl, *Poly(dA:dT), a ubiquitous promoter element that stimulates transcription via its intrinsic DNA structure.* EMBO J, 1995. **14**(11): p. 2570-9.
128. Peckham, H.E., et al., *Nucleosome positioning signals in genomic DNA.* Genome Research, 2007. **17**(8): p. 1170-1177.
129. Sekinger, E.A., Z. Moqtaderi, and K. Struhl, *Intrinsic histone-DNA interactions and low nucleosome density are important for preferential accessibility of promoter regions in yeast.* Mol Cell, 2005. **18**(6): p. 735-48.
130. Wong, B., et al., *Characterization of Z-DNA as a nucleosome-boundary element in yeast Saccharomyces cerevisiae.* Proceedings of the National Academy of Sciences of the United States of America, 2007. **104**(7): p. 2229-2234.
131. Lascaris, R.F., et al., *Different roles for abf1p and a T-rich promoter element in nucleosome organization of the yeast RPS28A gene.* Nucleic Acids Res, 2000. **28**(6): p. 1390-6.
132. Yuan, G.C. and J.S. Liu, *Genomic sequence is highly predictive of local nucleosome depletion.* Plos Computational Biology, 2008. **4**(1): p. -.
133. Stein, A., T.E. Takasuka, and C.K. Collings, *Are nucleosome positions in vivo primarily determined by histone-DNA sequence preferences?* Nucleic Acids Res, 2010. **38**(3): p. 709-19.
134. Kaplan, N., et al., *Nucleosome sequence preferences influence in vivo nucleosome organization.* Nat Struct Mol Biol, 2010. **17**(8): p. 918-20; author reply 920-2.
135. Zhang, Y., Moqtaderi, Z., Rattner, B.P., Euskirchen, G., Snyder, M., Kadonaga, J.T., Liu, X.S. & Struhl, K., *Evidence against a genomic code for nucleosome positioning. Reply to "Nucleosome sequence preferences influence in vivo nucleosome organization".* Nat Struct Mol Biol, 2010. **17**(8): p. 920-33.
136. Locke, G., et al., *High-throughput sequencing reveals a simple model of nucleosome energetics.* Proc Natl Acad Sci U S A, 2010. **107**(49): p. 20998-1003.
137. Fan, X., et al., *Nucleosome depletion at yeast terminators is not intrinsic and can occur by a transcriptional mechanism linked to 3'-end formation.* Proc Natl Acad Sci U S A, 2010. **107**(42): p. 17945-50.
138. Badis, G., et al., *A library of yeast transcription factor motifs reveals a widespread function for Rsc3 in targeting nucleosome exclusion at promoters.* Mol Cell, 2008. **32**(6): p. 878-87.
139. Hartley, P.D. and H.D. Madhani, *Mechanisms that Specify Promoter Nucleosome Location and Identity.* Cell, 2009. **137**(3): p. 445-458.
140. Parnell, T.J., J.T. Huff, and B.R. Cairns, *RSC regulates nucleosome positioning at Pol II genes and density at Pol III genes.* Embo Journal, 2008. **27**(1): p. 100-110.
141. Partensky, P.D. and G.J. Narlikar, *Chromatin Remodelers Act Globally, Sequence Positions Nucleosomes Locally.* Journal of Molecular Biology, 2009. **391**(1): p. 12-25.

142. Whitehouse, I. and T. Tsukiyama, *Antagonistic forces that position nucleosomes in vivo.* Nature Structural & Molecular Biology, 2006. **13**(7): p. 633-640.
143. Schnitzler, G.R., *Control of nucleosome positions by DNA sequence and remodeling machines.* Cell Biochemistry and Biophysics, 2008. **51**(2-3): p. 67-80.
144. Rippe, K., et al., *DNA sequence- and conformation-directed positioning of nucleosomes by chromatin-remodeling complexes.* Proceedings of the National Academy of Sciences of the United States of America, 2007. **104**(40): p. 15635-15640.
145. Flaus, A. and T. Owen-Hughes, *Dynamic properties of nucleosomes during thermal and ATP-driven mobilization.* Mol Cell Biol, 2003. **23**(21): p. 7767-79.
146. Sims, H.I., C.B. Baughman, and G.R. Schnitzler, *Human SWI/SNF directs sequence-specific chromatin changes on promoter polynucleosomes.* Nucleic Acids Research, 2008. **36**(19): p. 6118-6131.
147. Stockdale, C., et al., *Analysis of nucleosome repositioning by yeast ISWI and Chd1 chromatin remodeling complexes.* Journal of Biological Chemistry, 2006. **281**(24): p. 16279-16288.
148. Felle, M., et al., *DNA sequence encoded repression of rRNA gene transcription in chromatin.* Nucleic Acids Res, 2010. **38**(16): p. 5304-14.
149. Moreira, J.M.A. and S. Holmberg, *Transcriptional repression of the yeast CHA1 gene requires the chromatin-remodeling complex RSC.* Embo Journal, 1999. **18**(10): p. 2836-2844.
150. Zhang, Z. and J.C. Reese, *Ssn6-Tup1 requires the ISW2 complex to position nucleosomes in Saccharomyces cerevisiae.* Embo Journal, 2004. **23**(11): p. 2246-2257.
151. Tirosh, I., N. Sigal, and N. Barkai, *Widespread remodeling of mid-coding sequence nucleosomes by Isw1.* Genome Biol, 2010. **11**(5): p. R49.
152. Yang, J.G., et al., *The chromatin-remodeling enzyme ACF is an ATP-dependent DNA length sensor that regulates nucleosome spacing.* Nat Struct Mol Biol, 2006. **13**(12): p. 1078-83.
153. Racki, L.R., et al., *The chromatin remodeller ACF acts as a dimeric motor to space nucleosomes.* Nature, 2009. **462**(7276): p. 1016-21.
154. Varga-Weisz, P.D., et al., *Chromatin-remodelling factor CHRAC contains the ATPases ISWI and topoisomerase II.* Nature, 1997. **388**(6642): p. 598-602.
155. Ito, T., et al., *ACF, an ISWI-containing and ATP-utilizing chromatin assembly and remodeling factor.* Cell, 1997. **90**(1): p. 145-55.
156. Badenhorst, P., et al., *Biological functions of the ISWI chromatin remodeling complex NURF.* Genes Dev, 2002. **16**(24): p. 3186-98.
157. Deuring, R., et al., *The ISWI chromatin-remodeling protein is required for gene expression and the maintenance of higher order chromatin structure in vivo.* Mol Cell, 2000. **5**(2): p. 355-65.
158. Corona, D.F., et al., *ISWI regulates higher-order chromatin structure and histone H1 assembly in vivo.* PLoS Biol, 2007. **5**(9): p. e232.
159. Corona, D.F. and J.W. Tamkun, *Multiple roles for ISWI in transcription, chromosome organization and DNA replication.* Biochim Biophys Acta, 2004. **1677**(1-3): p. 113-9.
160. Udugama, M., A. Sabri, and B. Bartholomew, *The INO80 ATP-dependent chromatin remodeling complex is a nucleosome spacing factor.* Mol Cell Biol, 2011. **31**(4): p. 662-73.
161. Sugiyama, T., et al., *SHREC, an effector complex for heterochromatic transcriptional silencing.* Cell, 2007. **128**(3): p. 491-504.
162. Zaret, K.S. and K.R. Yamamoto, *Reversible and persistent changes in chromatin structure accompany activation of a glucocorticoid-dependent enhancer element.* Cell, 1984. **38**(1): p. 29-38.
163. Peterson, D.O., *Alterations in chromatin structure associated with glucocorticoid-induced expression of endogenous mouse mammary tumor virus genes.* Mol Cell Biol, 1985. **5**(5): p. 1104-10.
164. Zhu, Z. and D.J. Thiele, *A specialized nucleosome modulates transcription factor access to a C. glabrata metal responsive promoter.* Cell, 1996. **87**(3): p. 459-70.
165. Pina, B., U. Bruggemeier, and M. Beato, *Nucleosome Positioning Modulates Accessibility of Regulatory Proteins to the Mouse Mammary-Tumor Virus Promoter.* Cell, 1990. **60**(5): p. 719-731.

166. Workman, J.L. and R.G. Roeder, *Binding of transcription factor TFIID to the major late promoter during in vitro nucleosome assembly potentiates subsequent initiation by RNA polymerase II.* Cell, 1987. **51**(4): p. 613-22.
167. Barbaric, S., et al., *The homeodomain protein Pho2 and the basic-helix-loop-helix protein Pho4 bind DNA cooperatively at the yeast PHO5 promoter.* Nucleic Acids Res, 1996. **24**(22): p. 4479-86.
168. Fascher, K.D., J. Schmitz, and W. Horz, *Role of trans-activating proteins in the generation of active chromatin at the PHO5 promoter in S. cerevisiae.* EMBO J, 1990. **9**(8): p. 2523-8.
169. Wippo, C.J., et al., *Differential cofactor requirements for histone eviction from two nucleosomes at the yeast PHO84 promoter are determined by intrinsic nucleosome stability.* Mol Cell Biol, 2009. **29**(11): p. 2960-81.
170. Shore, D. and K. Nasmyth, *Purification and cloning of a DNA binding protein from yeast that binds to both silencer and activator elements.* Cell, 1987. **51**(5): p. 721-32.
171. Wiltshire, S., S. Raychaudhuri, and S. Eisenberg, *An Abf1p C-terminal region lacking transcriptional activation potential stimulates a yeast origin of replication.* Nucleic Acids Res, 1997. **25**(21): p. 4250-6.
172. Reed, S.H., et al., *Yeast autonomously replicating sequence binding factor is involved in nucleotide excision repair.* Genes Dev, 1999. **13**(23): p. 3052-8.
173. Miyake, T., et al., *Genome-wide analysis of ARS (autonomously replicating sequence) binding factor 1 (Abf1p)-mediated transcriptional regulation in Saccharomyces cerevisiae.* J Biol Chem, 2004. **279**(33): p. 34865-72.
174. Groth, A., *Replicating chromatin: a tale of histones.* Biochem Cell Biol, 2009. **87**(1): p. 51-63.
175. Hertel, C.B., et al., *Nucleosome stability at the yeast PHO5 and PHO8 promoters correlates with differential cofactor requirements for chromatin opening.* Molecular and Cellular Biology, 2005. **25**(24): p. 10755-10767.
176. Korber, P. and W. Horz, *In vitro assembly of the characteristic chromatin organization at the yeast PHO5 promoter by a replication-independent extract system.* Journal of Biological Chemistry, 2004. **279**(33): p. 35113-35120.
177. Papamichos-Chronakis, M. and C.L. Peterson, *The Ino80 chromatin-remodeling enzyme regulates replisome function and stability.* Nat Struct Mol Biol, 2008. **15**(4): p. 338-45.
178. Vincent, J.A., T.J. Kwong, and T. Tsukiyama, *ATP-dependent chromatin remodeling shapes the DNA replication landscape.* Nat Struct Mol Biol, 2008. **15**(5): p. 477-84.
179. Workman, J.L., *Nucleosome displacement in transcription.* Genes Dev, 2006. **20**(15): p. 2009-17.
180. Venters, B.J. and B.F. Pugh, *A canonical promoter organization of the transcription machinery and its regulators in the Saccharomyces genome.* Genome Res, 2009. **19**(3): p. 360-71.
181. Steinmetz, E.J., et al., *Genome-wide distribution of yeast RNA polymerase II and its control by Sen1 helicase.* Mol Cell, 2006. **24**(5): p. 735-46.
182. Mobius, W. and U. Gerland, *Quantitative test of the barrier nucleosome model for statistical positioning of nucleosomes up- and downstream of transcription start sites.* PLoS Comput Biol, 2010. **6**(8): p. e1000891.
183. Barbaric, S., K.D. Fascher, and W. Horz, *Activation of the Weakly Regulated PHO8 Promoter in Saccharomyces-Cerevisiae - Chromatin Transition and Binding-Sites for the Positive Regulatory Protein PHO4.* Nucleic Acids Research, 1992. **20**(5): p. 1031-1038.
184. Basehoar, A.D., S.J. Zanton, and B.F. Pugh, *Identification and distinct regulation of yeast TATA box-containing genes.* Cell, 2004. **116**(5): p. 699-709.
185. Miura, F., et al., *A large-scale full-length cDNA analysis to explore the budding yeast transcriptome.* Proc Natl Acad Sci U S A, 2006. **103**(47): p. 17846-51.
186. Wippo, C.J., et al., *The RSC chromatin remodelling enzyme has a unique role in directing the accurate positioning of nucleosomes.* EMBO J, 2011. **30**(7): p. 1277-88.
187. Vogel, K., W. Horz, and A. Hinnen, *The two positively acting regulatory proteins PHO2 and PHO4 physically interact with PHO5 upstream activation regions.* Mol Cell Biol, 1989. **9**(5): p. 2050-7.

188. MacIsaac, K.D., et al., *An improved map of conserved regulatory sites for Saccharomyces cerevisiae.* BMC Bioinformatics, 2006. **7**: p. 113.
189. Pondugula, S., et al., *Coupling phosphate homeostasis to cell cycle-specific transcription: mitotic activation of Saccharomyces cerevisiae PHO5 by Mcm1 and Forkhead proteins.* Mol Cell Biol, 2009. **29**(18): p. 4891-905.
190. Ogawa, N., et al., *Structure and distribution of specific cis-elements for transcriptional regulation of PHO84 in Saccharomyces cerevisiae.* Mol Gen Genet, 1995. **249**(4): p. 406-16.
191. Germond, J.E., et al., *Folding of the DNA double helix in chromatin-like structures from simian virus 40.* Proc Natl Acad Sci U S A, 1975. **72**(5): p. 1843-7.
192. Pfaffle, P. and V. Jackson, *Studies on rates of nucleosome formation with DNA under stress.* J Biol Chem, 1990. **265**(28): p. 16821-9.
193. Nightingale, K.P. and P.B. Becker, *Structural and functional analysis of chromatin assembled from defined histones.* Methods, 1998. **15**(4): p. 343-53.
194. Patterton, H.G. and C. von Holt, *Negative supercoiling and nucleosome cores. I. The effect of negative supercoiling on the efficiency of nucleosome core formation in vitro.* J Mol Biol, 1993. **229**(3): p. 623-36.
195. Horz, W. and W. Altenburger, *Sequence specific cleavage of DNA by micrococcal nuclease.* Nucleic Acids Res, 1981. **9**(12): p. 2643-58.
196. Dingwall, C., G.P. Lomonossoff, and R.A. Laskey, *High sequence specificity of micrococcal nuclease.* Nucleic Acids Res, 1981. **9**(12): p. 2659-73.
197. Luger, K., T.J. Rechsteiner, and T.J. Richmond, *Preparation of nucleosome core particle from recombinant histones.* Methods Enzymol, 1999. **304**: p. 3-19.
198. Ertel, F., et al., *In vitro reconstitution of PHO5 promoter chromatin remodeling points to a role for activator-nucleosome competition in vivo.* Mol Cell Biol, 2010. **30**(16): p. 4060-76.
199. Ertel, F., *The Role of Cofactors, Replication, and Intranucleosomal UASp Elements in Chromatin Remodeling at Yeast PHO Promoters.* PhD Thesis, Biological Faculty, University of Munich, 2010.
200. Baxevanis, A.D. and D. Landsman, *Histone Sequence Database: a compilation of highly-conserved nucleoprotein sequences.* Nucleic Acids Res, 1996. **24**(1): p. 245-7.
201. Gregory, P.D., et al., *Chromatin remodelling at the PHO8 promoter requires SWI-SNF and SAGA at a step subsequent to activator binding.* Embo Journal, 1999. **18**(22): p. 6407-6414.
202. Rose, M.D., et al., *A Saccharomyces cerevisiae genomic plasmid bank based on a centromere-containing shuttle vector.* Gene, 1987. **60**(2-3): p. 237-43.
203. Hughes, A. and O.J. Rando, *Chromatin 'programming' by sequence - is there more to the nucleosome code than %GC?* J Biol, 2009. **8**(11): p. 96.
204. Langst, G., et al., *Nucleosome movement by CHRAC and ISWI without disruption or trans-displacement of the histone octamer.* Cell, 1999. **97**(7): p. 843-852.
205. Kent, N.A., et al., *In vivo chromatin remodeling by yeast ISWI homologs Isw1p and Isw2p.* Genes & Development, 2001. **15**(5): p. 619-626.
206. Clapier, C.R., et al., *Critical role for the histone H4 N terminus in nucleosome remodeling by ISWI.* Mol Cell Biol, 2001. **21**(3): p. 875-83.
207. Collart, M.A., *The NOT, SPT3, and MOT1 genes functionally interact to regulate transcription at core promoters.* Mol Cell Biol, 1996. **16**(12): p. 6668-76.
208. Adkins, M.W. and J.K. Tyler, *Transcriptional activators are dispensable for transcription in the absence of Spt6-mediated chromatin reassembly of promoter regions.* Molecular Cell, 2006. **21**(3): p. 405-416.
209. Guillemette, B., et al., *Variant histone H2A.Z is globally localized to the promoters of inactive yeast genes and regulates nucleosome positioning.* Plos Biology, 2005. **3**(12): p. 2100-2110.
210. Fan, J.Y., et al., *The essential histone variant H2A.Z regulates the equilibrium between different chromatin conformational states.* Nat Struct Biol, 2002. **9**(3): p. 172-6.
211. Li, B., et al., *Preferential occupancy of histone variant H2AZ at inactive promoters influences local histone modifications and chromatin remodeling.* Proceedings of the National Academy of Sciences of the United States of America, 2005. **102**(51): p. 18385-18390.

212. Munsterkotter, M., S. Barbaric, and M. Horz, *Transcriptional regulation of the yeast PHO8 promoter in comparison to the coregulated PHO5 promoter.* Journal of Biological Chemistry, 2000. **275**(30): p. 22678-22685.
213. Angermayr, M. and W. Bandlow, *Permanent nucleosome exclusion from the Gal4p-inducible yeast GCY1 promoter.* J Biol Chem, 2003. **278**(13): p. 11026-31.
214. Moreau, J.L., et al., *Regulated displacement of TBP from the PHO8 promoter in vivo requires Cbf1 and the Isw1 chromatin remodeling complex.* Molecular Cell, 2003. **11**(6): p. 1609-1620.
215. Hertel, C.B., *In Vitro Studies of Nucleosome Positioning and Stability at the PHO5 and PHO8 Promoters in Saccharomyces cerevisiae.* PhD Thesis, Biological Faculty, University of Munich, 2006.
216. Huh, W.K., et al., *Global analysis of protein localization in budding yeast.* Nature, 2003. **425**(6959): p. 686-91.
217. Gavin, A.C., et al., *Functional organization of the yeast proteome by systematic analysis of protein complexes.* Nature, 2002. **415**(6868): p. 141-7.
218. Goldfeder, M.B. and C.C. Oliveira, *Utp25p, a nucleolar Saccharomyces cerevisiae protein, interacts with U3 snoRNP subunits and affects processing of the 35S pre-rRNA.* FEBS J, 2010. **277**(13): p. 2838-52.
219. Cairns, B.R., et al., *RSC, an essential, abundant chromatin-remodeling complex.* Cell, 1996. **87**(7): p. 1249-60.
220. Cairns, B.R., et al., *Two actin-related proteins are shared functional components of the chromatin-remodeling complexes RSC and SWI/SNF.* Mol Cell, 1998. **2**(5): p. 639-51.
221. Zhang, Y., et al., *DNA translocation and loop formation mechanism of chromatin remodeling by SWI/SNF and RSC.* Mol Cell, 2006. **24**(4): p. 559-68.
222. Szerlong, H., A. Saha, and B.R. Cairns, *The nuclear actin-related proteins Arp7 and Arp9: a dimeric module that cooperates with architectural proteins for chromatin remodeling.* EMBO J, 2003. **22**(12): p. 3175-87.
223. Lam, F.H., D.J. Steger, and E.K. O'Shea, *Chromatin decouples promoter threshold from dynamic range.* Nature, 2008. **453**(7192): p. 246-U16.
224. Venters, B.J., et al., *A comprehensive genomic binding map of gene and chromatin regulatory proteins in Saccharomyces.* Mol Cell, 2011. **41**(4): p. 480-92.
225. Khaperskyy, D.A., et al., *Functions of Saccharomyces cerevisiae TFIIF during transcription start site utilization.* Mol Cell Biol, 2008. **28**(11): p. 3757-66.
226. Poon, D., et al., *Genetic and biochemical analyses of yeast TATA-binding protein mutants.* J Biol Chem, 1993. **268**(7): p. 5005-13.
227. Parvin, J.D., H.T. Timmers, and P.A. Sharp, *Promoter specificity of basal transcription factors.* Cell, 1992. **68**(6): p. 1135-44.
228. Ranish, J.A., N. Yudkovsky, and S. Hahn, *Intermediates in formation and activity of the RNA polymerase II preinitiation complex: holoenzyme recruitment and a postrecruitment role for the TATA box and TFIIB.* Genes Dev, 1999. **13**(1): p. 49-63.
229. Stein, A., T.E. Takasuka, and C.K. Collings, *Are nucleosome positions in vivo primarily determined by histone-DNA sequence preferences?* Nucleic Acids Res, 2009.
230. Soutourina, J., et al., *Rsc4 connects the chromatin remodeler RSC to RNA polymerases.* Mol Cell Biol, 2006. **26**(13): p. 4920-33.
231. Logie, C., et al., *The core histone N-terminal domains are required for multiple rounds of catalytic chromatin remodeling by the SWI/SNF and RSC complexes.* Biochemistry, 1999. **38**(8): p. 2514-22.
232. Floer, M., et al., *A RSC/nucleosome complex determines chromatin architecture and facilitates activator binding.* Cell, 2010. **141**(3): p. 407-18.
233. Chandy, M., et al., *SWI/SNF displaces SAGA-acetylated nucleosomes.* Eukaryot Cell, 2006. **5**(10): p. 1738-47.
234. Ng, H.H., et al., *Genome-wide location and regulated recruitment of the RSC nucleosome-remodeling complex.* Genes Dev, 2002. **16**(7): p. 806-19.

235. Damelin, M., et al., *The genome-wide localization of Rsc9, a component of the RSC chromatin-remodeling complex, changes in response to stress.* Mol Cell, 2002. **9**(3): p. 563-73.
236. Szerlong, H., et al., *The HSA domain binds nuclear actin-related proteins to regulate chromatin-remodeling ATPases.* Nat Struct Mol Biol, 2008. **15**(5): p. 469-76.
237. Zhang, H.S. and J.C. Reese, *Exposing the core promoter is sufficient to activate transcription and alter coactivator requirement at RNR3.* Proceedings of the National Academy of Sciences of the United States of America, 2007. **104**(21): p. 8833-8838.
238. Hesselberth, J.R., et al., *Global mapping of protein-DNA interactions in vivo by digital genomic footprinting.* Nat Methods, 2009. **6**(4): p. 283-9.
239. Fascher, K.D., J. Schmitz, and W. Horz, *Structural and functional requirements for the chromatin transition at the PHO5 promoter in Saccharomyces cerevisiae upon PHO5 activation.* J Mol Biol, 1993. **231**(3): p. 658-67.
240. Segal, E. and J. Widom, *What controls nucleosome positions?* Trends Genet, 2009. **25**(8): p. 335-43.
241. Svaren, J., J. Schmitz, and W. Horz, *The transactivation domain of Pho4 is required for nucleosome disruption at the PHO5 promoter.* EMBO J, 1994. **13**(20): p. 4856-62.
242. Korber, P., et al., *Evidence for histone eviction in trans upon induction of the yeast PHO5 promoter.* Mol Cell Biol, 2004. **24**(24): p. 10965-74.
243. Simon, R.H. and G. Felsenfeld, *A new procedure for purifying histone pairs H2A + H2B and H3 + H4 from chromatin using hydroxylapatite.* Nucleic Acids Res, 1979. **6**(2): p. 689-96.
244. Southern, E.M., *Detection of specific sequences among DNA fragments separated by gel electrophoresis.* J Mol Biol, 1975. **98**(3): p. 503-17.
245. Kellis, M., et al., *Sequencing and comparison of yeast species to identify genes and regulatory elements.* Nature, 2003. **423**(6937): p. 241-54.
246. Cliften, P., et al., *Finding functional features in Saccharomyces genomes by phylogenetic footprinting.* Science, 2003. **301**(5629): p. 71-6.
247. Durrin, L.K., et al., *Yeast histone H4 N-terminal sequence is required for promoter activation in vivo.* Cell, 1991. **65**(6): p. 1023-31.
248. Ben-Aroya, S., et al., *Toward a comprehensive temperature-sensitive mutant repository of the essential genes of Saccharomyces cerevisiae.* Mol Cell, 2008. **30**(2): p. 248-58.
249. Ghazy, M.A., et al., *Amino acid substitutions in yeast TFIIF confer upstream shifts in transcription initiation and altered interaction with RNA polymerase II.* Mol Cell Biol, 2004. **24**(24): p. 10975-85.
250. Shen, W.C., et al., *Systematic analysis of essential yeast TAFs in genome-wide transcription and preinitiation complex assembly.* EMBO J, 2003. **22**(13): p. 3395-402.
251. Kuldell, N.H. and S. Buratowski, *Genetic analysis of the large subunit of yeast transcription factor IIE reveals two regions with distinct functions.* Mol Cell Biol, 1997. **17**(9): p. 5288-98.
252. Richmond, E. and C.L. Peterson, *Functional analysis of the DNA-stimulated ATPase domain of yeast SWI2/SNF2.* Nucleic Acids Res, 1996. **24**(19): p. 3685-92.

7. Abbreviations

Å	Armstrong
Abf1	ARS-Binding Factor 1
Ac	Acetylation
ACF	ATP-utilizing chromatin assembly and remodeling factor
AS	Ammonium sulphate
Asf1	Anti-Silencing Function 1
ATP	Adenosintriphosphate
ATPase	Adenosintriphosphatase
ARS	Autonomously replicating sequence
bp	Base pairs
BSA	Bovine serum albumin
C. elegans	*Caenorhabditis elegans*
CENP-A	Centromer protein A
Chd1	Chromodomain-helicase-DNA-binding
ChIP	Chromatin immunoprecipitation
Ci	Curie
cpm	counts per minute
D. hansenii	*Debaryomyces hansenii*
dCTP	Desoxycytosintriphosphate
DEAE	Diethylaminoethyl
DNA	Desoxyribonucleic acid
DNaseI	Bovine deoxyribonucleaseI
Drosophila	*Drosophila melanogaster*
DREX	*Drosophila* embryo extract
DTT	Dithiothreitrol
E. coli	*Escherichia coli*
EDTA	Ethylendiamintetraacetate
EGTA	Ethylenglycol-bis(2-aminoethyl)-N,N,N´,N`-tetraacetic acid
EtBr	Ethidiumbromide
Gcn5	General control non-derepressible 5
GRF	General regulator factor
GTFII	General transcription factor for RNA polymerase II
h	hour(s)
Hepes	(N-(2-Hydroxyethyl)piperazine-H´-(2-ethanesulfonic acid)
IgG	Immonglobulin G
Ino80	Inositol requiring 80
Isw1	Imitation switch 1 (*S. cerevisiae*)
Isw2	Imitation switch 2 (*S. cerevisiae*)
ISWI	Imitation switch (*Drosophila*)
kb	Kilobase
l	Liter
K. lactis	*Kluyveromyces lactis*
kDa	kilo Daltons
LC-MS/MS	Liquid chromatography-mass spectrometry/mass spectrometry
M	Molar
Mbp	Mega base pairs
MBT	Malignant Brain Tumor
Me	Methylation
min	Minute(s)
ml	Milliliter

mM	Milli molar
mmol	Milimole
MNase	Micrococcal nuclease
MW	Molecular weight
n.d.	not done
NDR	Nucleosome depleted region
NFR	Nucleosome free region
nm	Nanometre
nM	Nano molar
OD	Optical density
o/n	Overnight
ORF	Open reading frame
PAGE	Polyacrylamide gel electrophoresis
PCR	Polymerase chain reaction
PEG	Polyethylene glycol
PIC	Pre-initiation complex
pm	Picomole
PMSF	Phenylmethanesulfonyl fluoride
pol II	RNA polymerase II
PTM	Posttranslational modification
PVP-40	Polyvinylpyrrolidone 40
PWM	Position weight matrix
rDNA	Repetitive ribosomal DNA
RE	Restriction enzyme/endonuclease
Reb1	RNA polymerase I Enhancer Binding protein
RNA	Ribonucleic acid
RNase A/III/H	Ribonuclease A/III/H
rpm	Revolutions per minute
RSC	Remodels the structure of chromatin
S. cerevisiae	*Saccharomyces cerevisiae*
S. pombe	*Schizosaccharomyces pombe*
SDS	Sodium dodecyl sulfate
SGD	Saccharomyces genome database
SN	Supernatant
SV40	Simian vacuolating virus 40
SWI/SNF	Switch/sucrose non-fermenting
TAE	Tris acetate EDTA buffer
TBE	Tris borate EDTA buffer
TBP	TATA box binding protein
TAP	Tandem affinity purification
Topo I	Topoisomerase I
Tris	Tris(hydroxymethyl)aminomethane
ts	temperature sensitive
td	temperature sensitive degron
TF	Transcription factor
TSS	Transcriptional start site
TTS	Transcription termination site
YNB	Yeast nitrogen base
YPDA	Yeast peptone dextrose adenine
w/v	Weight per volume
WCE	Whole cell extract
wt	Wildtype
Xenopus	*Xenopus laevis*

8. Acknowledgements

First of all, I would like to thank Philipp Korber for providing me with the opportunity to work in such a wonderful group on such a great topic. I am especially thankful for his support and advice as well as the many stimulating discussions. Finally I would also like to express my appreciation of the granted freedom of how I approached my scientific goals.

I also want to express my gratitude to Prof. Dr. Peter Becker for his advice, for showing interest in my research and for his role as my official PhD supervisor. Many thanks also for providing such a scientifically stimulating and warm lab atmosphere.

I thank Prof. Dr. Stefan Jentsch for being my second PhD reviewer.

My most heartfelt thanks go to all the past and present colleagues in the Becker Department that I had the blessing to work with over the years. I especially would like to thank Dr. Christina Hertel for her help during the first few months of my PhD, Dorle for her experimental help and her unrivalledly humorous "Bauernweisheiten" as well as Franziska, Alexandra, Ramon, Nils, Julia, Sebastian and Gözde for the amazing time I had in the lab. Very special thanks also go to all members of the Hake group for the awesome North lab spirit. Furthermore, I would like to thank all those that I had regular pleasure of playing football with and/or that participated in the Kicker Manager game, and the members of the beer brewing team.

I am also very grateful to the members of the ENB network "Protein Dynamics in Health and Disease" and for all the wonderfully organized seminars, courses and retreats.

Dr. Andreas Hochheimer and Prof. Dr. Gernot Längst I would like to thank for their extremely valuable help and advice as members of my PhD committee.

I also wish to acknowledge all my collaborators for their excellent experimental contribution and scientific interest, especially Bojana Krstulovic, Dr. Franziska Ertel, Sanja Musladin, Dorothea Blaschke, Sabrina Stürzl, Prof. Dr. Guo-Cheng Yuan, Prof. Dr. Wolfram Hörz and Prof. Dr. Slobodan Barbaric for their work on the *PHO84* project, Dr. Lars Israel, Dr. Andreas Hochheimer, Prof. Dr. Axel Imhof, Dr. Shinya Watanabe and Prof. Dr. Craig Peterson for their contribution to the fractionation/RSC project as well as Dr. Zhenhai Zhang, Elissa Ward, Megha Wal and Prof. Dr. Frank Pugh for their work on the whole-genome reconstitution project.

I also want to thank all the people who shared data, strains or other material with us, especially Prof. Dr. Brad Cairns, Prof. Dr. Tom Owen-Hughes, Prof. Dr. Charlie Boone, Prof. Dr. Patrick Cramer, Prof. Dr. Hiten Madhani, Prof. Dr. Fred Winston, Prof. Dr. Tim Hughes, Prof. Dr. Steen Holmberg, Dr. Paul Hartley, Dr. Timothy Parnell and Dr. Harm van Bakel.

My special gratitude also goes to Prof. Dr. Louis Mahadevan for his support during my time in Oxford and for getting me interested in the field of "Epigenetics".

I very much want to thank our secretaries Edith Müller and Carolin Brieger for all the help they provided.

This work was supported by the German Research Community (Transregio 05) and the 6th Framework Program of the European Union (Network of Excellence The Epigenome).

Insbesondere danken möchte ich meinen Eltern, Beate und Wolfgang Wippo, sowie meinem Bruder Andreas für Ihre, nicht nur während der Doktorarbeit, dargebrachte Unterstützung und Vertrauen.

9. Curriculum vitae

Christian Johannes Wippo

Date of Birth: April 2nd 1984

Place of Birth: Oldenburg, Germany

Education

10/2005 - 9/2011	PhD thesis at the Ludwig-Maximilians-University of Munich, Adolf-Butenandt-Institut, Prof. Dr. Peter B. Becker; supervisor: Dr. Philipp Korber Project**:** *In vitro* reconstitution of the primary chromatin architecture of *Saccharomyces cerevisiae*
10/2001 - 06/2005	Studies of Molecular and Cellular Biochemistry (MBiochem), University of Oxford, Trinity College Master Thesis at the Weatherall Institute of Molecular Medicine, Oxford; supervisor: Dr. Richard J. Gibbons Project: Study of common polymorphisms in and around the alpha globin cluster of ATR-X patients
07/2003 - 08/2003	Research Internship, Institute of Molecular Pathology, Vienna, Prof. Dr. Thomas Jenuwein
1999 - 2001	A-levels, Chaterhouse, England
1995 - 1999	Domgymnasium Verden
1994 - 1995	Pestalozzischule Verden
1990 - 1994	Grundschule Luttum

Publications

Zhang Z*, **Wippo CJ***, Wal M, Ward E, Korber P, Pugh BF (2011). A packing mechanism for nucleosome organization reconstituted across a eukaryotic genome. Science, 2011. 332 (6032): p. 977-80.
* These authors contributed equally to the manuscript

Wippo CJ, Israel L, Watanabe S, Hochheimer A, Peterson CL, Korber P (2011). The RSC chromatin remodelling enzyme has a unique role in directing the accurate positioning of nucleosomes. EMBO Journal. 30(7): 1277-88

Wippo CJ and Korber P (2011). *In vitro* reconstitution of *in vivo*-like nucleosome positioning on yeast DNA. Methods in Molecular Biology [accepted for publication]

Wippo CJ, Krstulovic BS, Ertel F, Musladin S, Blaschke D, Stürzl S, Yuan GC, Hörz W, Korber P, Barbaric S (2009). Differential cofactor requirements for histone eviction from two nucleosomes at the yeast PHO84 promoter are determined by intrinsic nucleosome stability. Molecular and Cellular Biology. 29(11): 2960-81

10. Publications

Our findings suggest that PSA induces T_{regs} through TLR2 signaling to suppress T_H17 cell responses and promote mucosal colonization by *B. fragilis*. To test this model, we measured colonization levels of *B. fragilis* in *Rag1*$^{-/-}$ mice reconstituted with TLR2-deficient CD4$^+$ T cells. Tissue association by wild-type *B. fragilis* in the colon was reduced to the levels of *B. fragilis*ΔPSA in these mice (Fig. 3E and fig. S15). Moreover, Foxp3$^+$ T_{reg} ablation in *B. fragilis* mono-associated animals resulted in significantly reduced amounts of tissue-associated *B. fragilis* (Fig. 3F), without affecting bacterial numbers in the lumen of the gut (fig. S16). Finally, to functionally determine the role of IL-17 responses in mucosal association, we treated *B. fragilis*ΔPSA mono-associated animals with a neutralizing antibody to IL-17A. Whereas the amounts of *B. fragilis*ΔPSA in isotype control–treated animals remained low, neutralization of IL-17A resulted in a 1000-fold increase in tissue-associated bacteria (Fig. 3, G and H). These data indicate that IL-17 suppression by PSA is required by *B. fragilis* during association with its host. Therefore, unlike pathogens that trigger inflammatory responses through TLRs to clear infections, symbiotic colonization by *B. fragilis* is actually enhanced via the TLR pathway. We conclude that PSA evolved to engender host-bacterial mutualism by inducing mucosal tolerance through TLR2 activation of T_{reg} cells.

The gastrointestinal tract represents a primary portal for entry by numerous pathogens. Toll-like receptors recognize MAMPs (microbial-associated molecular patterns) expressed by bacteria and coordinate a cascade of innate and adaptive immune responses that control infections (*20*). Although TLRs have classically been studied on innate immune cells, recent reports have demonstrated their expression by T cells in both mice and humans (*4*, *21*–*23*). As bacteria contain universally conserved MAMPs, how do commensal microbes, unlike pathogens, avoid triggering TLR activation? It is historically believed that the microbiota is excluded from the mucosal surface (*24*). However, certain symbiotic bacteria tightly adhere to the intestinal mucosa (*9*–*11*), and thus immunologic ignorance may not explain why inflammation is averted by the microbiota. Our study provides new insight into the mechanisms by which the immune system distinguishes between pathogens and symbionts. The functional activity of PSA on T_{regs} contrasts with the role of TLR2 ligands of pathogens, which elicit inflammation, and thus reveals an unexpected function for TLR signaling during homeostatic intestinal colonization by the microbiota. Although engagement of TLR2 by previously identified ligands is known to stimulate microbial clearance of pathogens, TLR signaling by PSA paradoxically allows *B. fragilis* persistence on mucosal surfaces. These results identify PSA as the incipient member of a new class of TLR ligands termed "symbiont-associated molecular patterns (SAMPs)" that function to orchestrate immune responses to establish host-commensal symbiosis. On the basis of the importance of the microbiota to mammalian health (*25*), evolution appears to have created molecular interactions that engender host-bacterial mutualism. In conclusion, our findings suggest that animals are not "hard-wired" to intrinsically distinguish pathogens from symbionts, and that microbial-derived mechanisms have evolved to actively promote immunologic tolerance to symbiotic bacteria. This concept suggests a reconsideration of how we define self versus nonself.

References and Notes

1. R. E. Ley, D. A. Peterson, J. I. Gordon, *Cell* **124**, 837 (2006).
2. S. Manicassamy, B. Pulendran, *Semin. Immunol.* **21**, 185 (2009).
3. M. Fukata *et al.*, *J. Immunol.* **180**, 1886 (2008).
4. J. M. Reynolds *et al.*, *Immunity* **32**, 692 (2010).
5. I. Caramalho *et al.*, *J. Exp. Med.* **197**, 403 (2003).
6. P. B. Eckburg *et al.*, *Science* **308**, 1635 (2005).
7. I. I. Ivanov *et al.*, *Cell Host Microbe* **4**, 337 (2008).
8. K. Atarashi *et al.*, *Nature* **455**, 808 (2008).
9. V. Gaboriau-Routhiau *et al.*, *Immunity* **31**, 677 (2009).
10. I. I. Ivanov *et al.*, *Cell* **139**, 485 (2009).
11. K. Atarashi *et al.*, *Science* **331**, 337 (2011).
12. S. K. Mazmanian, J. L. Round, D. L. Kasper, *Nature* **453**, 620 (2008).
13. J. Ochoa-Repáraz *et al.*, *Mucosal Immunol.* **3**, 487 (2010).
14. J. L. Round, S. K. Mazmanian, *Proc. Natl. Acad. Sci. U.S.A.* **107**, 12204 (2010).
15. Materials and methods are available as supporting material on *Science* Online.
16. J. M. Kim, J. P. Rasmussen, A. Y. Rudensky, *Nat. Immunol.* **8**, 191 (2006).
17. S. K. Mazmanian, C. H. Liu, A. O. Tzianabos, D. L. Kasper, *Cell* **122**, 107 (2005).
18. Q. Wang *et al.*, *J. Exp. Med.* **203**, 2853 (2006).
19. C. A. Janeway Jr., R. Medzhitov, *Annu. Rev. Immunol.* **20**, 197 (2002).
20. R. Medzhitov, *Nature* **449**, 819 (2007).
21. H. Liu, M. Komai-Koma, D. Xu, F. Y. Liew, *Proc. Natl. Acad. Sci. U.S.A.* **103**, 7048 (2006).
22. R. P. Sutmuller *et al.*, *J. Clin. Invest.* **116**, 485 (2006).
23. S. Babu, C. P. Blauvelt, V. Kumaraswami, T. B. Nutman, *J. Immunol.* **176**, 3885 (2006).
24. L. V. Hooper, *Nat. Rev. Microbiol.* **7**, 367 (2009).
25. K. Smith, K. D. McCoy, A. J. Macpherson, *Semin. Immunol.* **19**, 59 (2007).
26. W. Lin *et al.*, *Nat. Immunol.* **8**, 359 (2007).

Acknowledgments: We thank S. W. McBride and Y. Shen (California Institute for Technology) for help with bacterial colonization and germ-free studies. We are grateful to A. Rudensky [Memorial Sloan-Kettering Cancer Center and Howard Hughes Medical Institute (HHMI)] for the gift of Foxp3-DTR mice and L. Hooper (University of Texas Southwestern and HHMI) for germ-free *Rag1*$^{-/-}$ mice. We thank members of the Mazmanian laboratory for their critical review of the manuscript. B.J. acknowledges support from the Crohn's and Colitis Foundation of America (CCFA) (award 2831) and T.A.C acknowledges support from the NIH (grant AI 080002). J.L.R. is a Merck Fellow of the Jane Coffin Childs Memorial Fund. S.K.M. is a Searle Scholar. This work was supported by funding from the NIH (grants DK 078938, DK 083633, AI 088626), the Damon Runyon Cancer Research Foundation, and the CCFA (award 2405) to S.K.M. J.L.R. and S.K.M. have a patent application (PCT/US2008/082928) on the use of PSA as a therapy for inflammatory bowel disease. The authors have no competing financial interests related to this publication.

Supporting Online Material

www.sciencemag.org/cgi/content/full/science.1206095/DC1
Materials and Methods
Figs. S1 to S16

15 February 2011; accepted 6 April 2011
Published online 21 April 2011;
10.1126/science.1206095

A Packing Mechanism for Nucleosome Organization Reconstituted Across a Eukaryotic Genome

Zhenhai Zhang,[1]* Christian J. Wippo,[2]* Megha Wal,[1] Elissa Ward,[1] Philipp Korber,[2]† B. Franklin Pugh[1]†

Near the 5′ end of most eukaryotic genes, nucleosomes form highly regular arrays that begin at canonical distances from the transcriptional start site. Determinants of this and other aspects of genomic nucleosome organization have been ascribed to statistical positioning, intrinsically DNA-encoded positioning, or some aspect of transcription initiation. Here, we provide evidence for a different explanation. Biochemical reconstitution of proper nucleosome positioning, spacing, and occupancy levels was achieved across the 5′ ends of most yeast genes by adenosine triphosphate–dependent trans-acting factors. These transcription-independent activities override DNA-intrinsic positioning and maintain uniform spacing at the 5′ ends of genes even at low nucleosome densities. Thus, an active, nonstatistical nucleosome packing mechanism creates chromatin organizing centers at the 5′ ends of genes where important regulatory elements reside.

Statistical positioning depends on the presence of a genomic barrier within a linear array of nucleosomes (*1*). Nucleosomes within the array will passively align at regular intervals from the barrier, independent of sequence or other external factors, rather than arrange randomly. Nucleosome organization in vivo displays patterns that are consistent with statistical

positioning (*2*–*4*). Yet studies have suggested that as much as half of all nucleosome positions are "encoded" in the DNA sequence (*5*, *6*), because nucleosome occupancy reconstituted in vitro with purified genomic DNA and histones is similar to that in vivo. However, occupancy and positioning are distinct metrics of nucleosome organization (fig. S1). Nucleosome positions around transcription start sites (TSS) in vivo are different from in vitro positions (*7*–*9*) (Fig. 1A), which has led to the suggestion that transcription promotes nucleosome organization in vivo (*7*, *10*).

To determine what is needed to reconstitute proper nucleosome positions across all genes, we added whole-cell extracts to nucleosomes reconstituted on genomic DNA (*11*). To facilitate visualization of nucleosome patterns, genes were clustered based on their in vivo nucleosome organization (Fig. 1B, left panel). We produced an equivalently ordered "native" nucleosome pattern (Fig. 1B, right panel), in which chromatin was first isolated from cells without prior cross-linking, then cross-linked in vitro, as a positive control for in vitro reconstitution. The native pattern was stable (fig. S4) and similar to the in vivo pattern (Fig. 1B).

We reevaluated the intrinsically DNA-encoded organization of nucleosomes in these five clusters in three ways: (i) existing datasets were re-examined (*6*, *7*), (ii) nucleosomes within native chromatin were allowed to redistribute to their thermodynamically favored DNA-guided positions by incubation in 600 mM NaCl, and (iii) purified *Drosophila* histones were deposited by salt gradient dialysis (SGD) onto recombinant plasmid libraries (1:1 histone/DNA ratio), containing 10- to 30-kb inserts of *Saccharomyces* genomic DNA.

These experiments recapitulated some of the more prominent features of the native patterns, including nucleosome-free promoter regions (NFRs) and nucleosome positions and occupancy at certain canonical locations, as evident by the similarity of some peaks and troughs between data sets (fig. S5). However, most positions were not predominantly sequence-intrinsic. Thus, sequence-intrinsic cues contribute to nucleosome exclusion at the 5′ ends of genes but are very limited in defining nucleosome occupancy and positioning in adjacent regions and are negligible for positioning further into the coding regions.

Poly(dA:dT) tracts are a major intrinsic determinant of low nucleosome levels in yeast promoters (*12*–*14*) but have not been linked to positioning of adjacent nucleosomes. We find a strong correlation between the consensus positions of poly(dA:dT) tracts and +1 nucleosomes

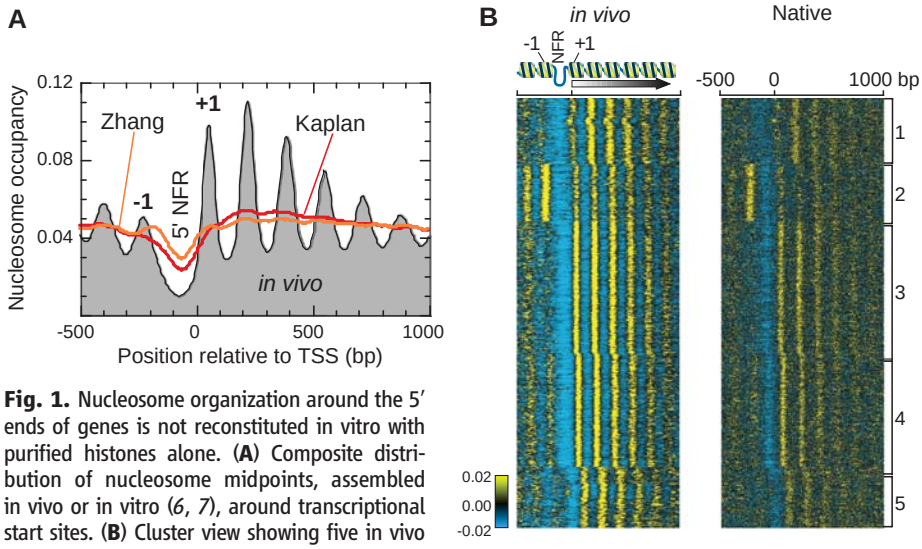

Fig. 1. Nucleosome organization around the 5′ ends of genes is not reconstituted in vitro with purified histones alone. (**A**) Composite distribution of nucleosome midpoints, assembled in vivo or in vitro (*6*, *7*), around transcriptional start sites. (**B**) Cluster view showing five in vivo patterns of nucleosome organization (left panel) and further characterized in fig. S3. All other cluster plots were ordered identically. A total of 4785 genes (rows) are aligned by their TSS. Yellow, black, and blue indicate a high, medium, and low occupancy level (tag counts), respectively.

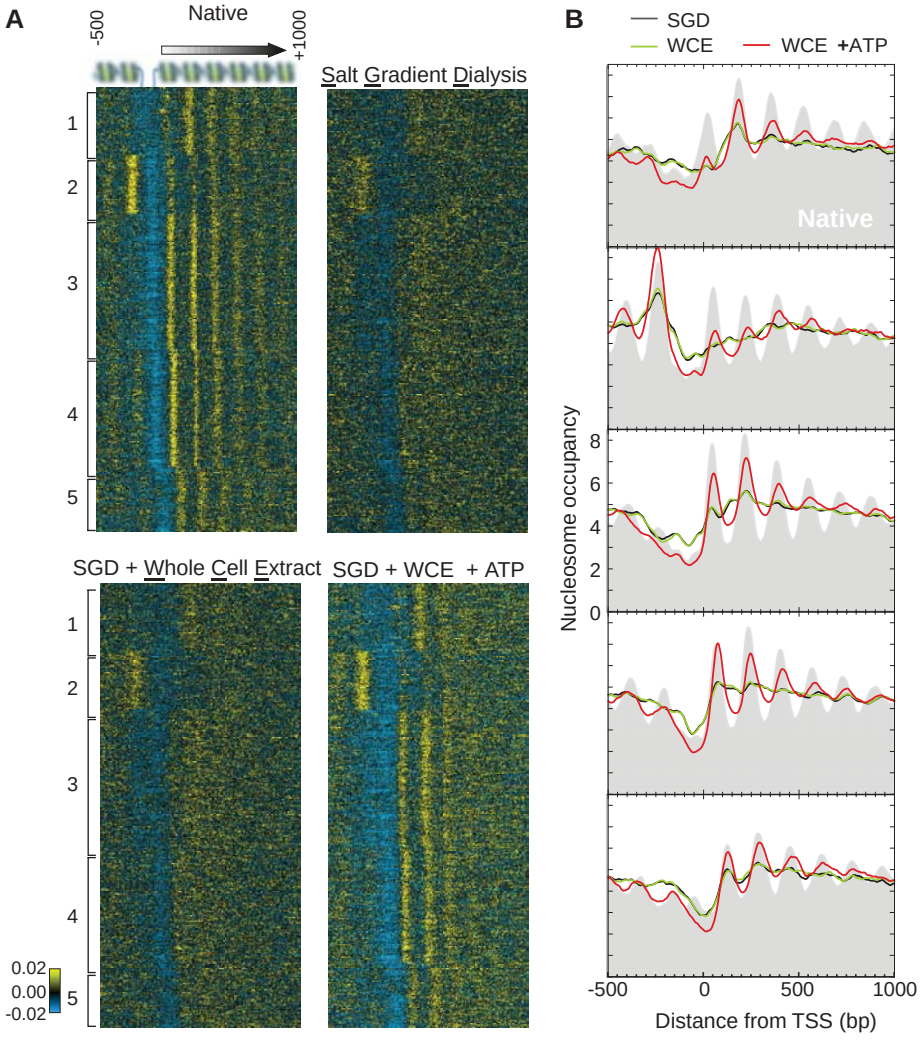

Fig. 2. Nucleosome organization around the 5′ ends of genes is reconstituted with whole-cell extracts and ATP. (**A**) Cluster plot and (**B**) corresponding composite plots of nucleosomes reconstituted by SGD. This reconstituted chromatin was either left untreated (SGD) or incubated with yeast whole-cell extracts in the absence (WCE) or presence (WCE+ATP) of ATP.

[1]Center for Eukaryotic Gene Regulation, Department of Biochemistry and Molecular Biology, The Pennsylvania State University, University Park, PA 16802, USA. [2]Adolf-Butenandt-Institut, Universität München, Munich, 80336, Germany.

*These authors contributed equally to this work.
†To whom correspondence should be addressed. E-mail: bfp2@psu.edu (B.F.P.); pkorber@lmu.de (P.K.)

(fig. S6). Thus, poly(dA:dT) tracts may contribute to positioning of the +1 nucleosome.

Statistical positioning requires fixed barriers as sole guides of nucleosome positioning and sufficiently high nucleosome density such that one nucleosome sterically restricts the position of a neighboring nucleosome (*1*). Three of the in vitro reconstitution experiments (SGD, 600 mM, and Zhang *et al.*) (fig. S5) seemingly met these criteria: (i) the NFRs, which may serve as barriers, were largely recapitulated, and (ii) the histone:DNA ratio was sufficiently high (1:1) to promote statistical positioning. Yet, in conflict with statistical positioning, no regular arrays aligned at the canonical +1 position were observed. Even thermal reequilibration of nucleosomes (*15*, *16*) did not allow statistical positioning to occur, because extended incubation of the SGD material at 55°C did not generate uniformly positioned arrays (fig. S7). The failure to achieve statistical positioning with only histones and DNA suggests that sequence-guided placement of each nucleosome predominates in vitro over statistical positioning.

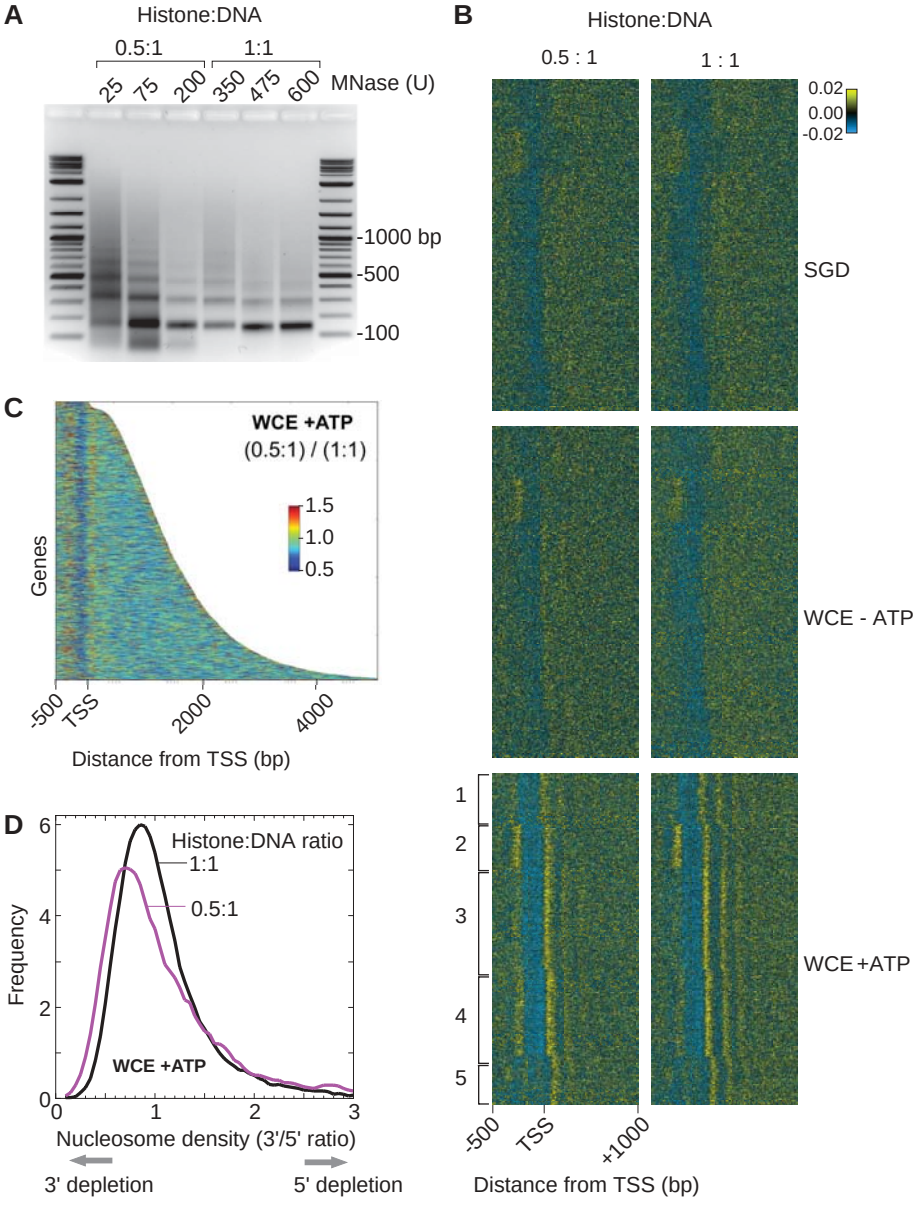

Fig. 3. Evidence that nucleosomes are actively packed against a barrier. (**A**) Ethidium bromide stained gel of SGD chromatin assembled at the indicated histone:DNA ratio (characterized in fig. S9), treated with whole-cell extracts and ATP, and then digested with micrococcal nuclease (MNase). (**B**) Cluster plots of nucleosomes reconstituted at 0.5:1 and 1:1 histone:DNA mass ratios. The bin-by-bin ratio of the bottom two panels to each other is shown in (**C**), but sorted by gene length. Data beyond the termination site is not shown. (**D**) Frequency distribution of 3′ histone density to 5′ histone density, on a per gene basis. The 3′ region is from +140 bp to the transcript termination site, whereas the 5′ region is from −20 to +140, relative to the TSS.

Given the central role adenosine triphosphate (ATP)–dependent chromatin remodeling complexes play in nucleosome organization (*17*), we considered that proper reconstitution of nucleosome positions might require ATP and trans-acting factors. The addition of whole-cell extracts plus ATP to the SGD material reconstituted nucleosome positions and occupancy levels around the 5′ ends of nearly all 4,785 tested yeast genes (Fig. 2). This was strictly ATP-dependent as incubation with extract in the absence of ATP had virtually no effect on nucleosome organization.

This reconstitution of in vivo–like nucleosome positioning did not require the other nucleoside triphosphates (*11*), indicating that transcription and DNA replication is not the predominant means by which nucleosomes become organized around genes, as originally demonstrated on *PHO5* (*18*). Moreover, the transcription initiation complex is not an obvious barrier against which nucleosomes are organized, because the TATA box position did not correlate with the position of the +1 nucleosome (fig. S8), and canonical nucleosome positioning is maintained in vivo at genes having little or no transcription (*3*). However, the binding site positions for Reb1, which is not part of the transcription machinery but functions similar to poly(dA:dT) tracts (*19*), did correlate with +1 positioning.

The data thus far argue against a DNA-intrinsic or transcription-based mechanism for organizing nucleosomes around the 5′ ends of genes but are entirely consistent with ATP-facilitated statistical positioning. For example, chromatin remodeling complexes could use ATP hydrolysis to override the DNA-intrinsic positioning landscape, thereby providing free bidirectional fluidity to nucleosomes that is only impeded by barriers. Although we favor the involvement of a remodeler adenosine triphosphatase (ATPase), we cannot formally exclude a kinase.

Statistical positioning predicts that internucleosomal spacing within arrays should be inversely related to nucleosome density (*1*), yet the cluster plots in Figs. 1 and 2 indicate that nucleosomal spacing is largely constant regardless of local nucleosome density (i.e., the periodicity of the yellow stripes is independent of the intensity of the yellow). As a direct test, we reconstituted ATP-dependent positioning on genomic DNA assembled at half the global histone:DNA density (0.5:1 instead of 1:1). Spacing remained largely unaltered [~165 base pairs (bp)], both globally (Fig. 3A) and in relation to a reference point like the TSS (Fig. 3B). Thus, a key test of statistical positioning failed.

Due to the bidirectional fluidity of nucleosomes inherent to the statistical positioning model, nucleosome density should remain relatively uniform, albeit periodic, outside of the barrier. This was not observed at the lower histone:DNA ratio. Instead, there was a decrease in nucleosome density in the NFR and internal to genes compared to the +1 nucleosome position. This was

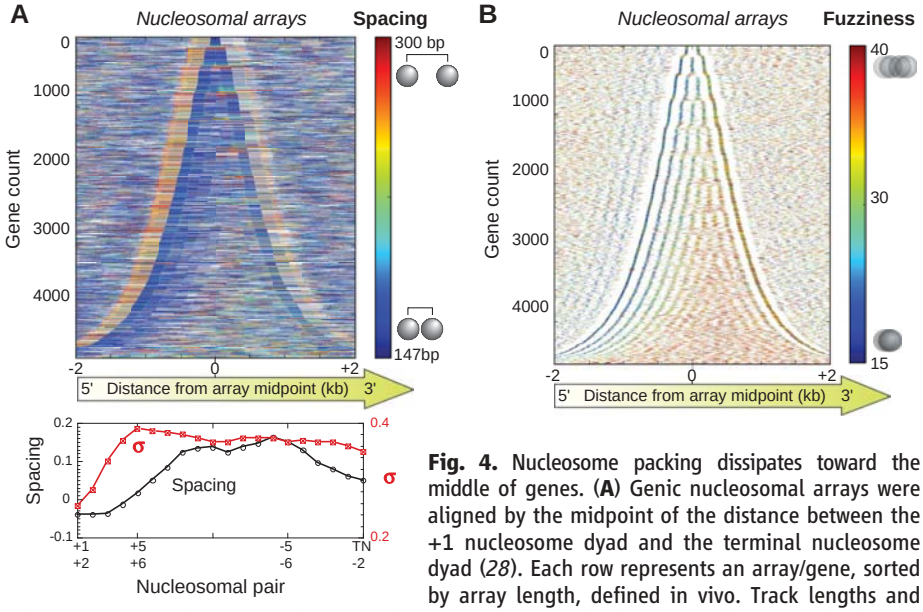

Fig. 4. Nucleosome packing dissipates toward the middle of genes. (**A**) Genic nucleosomal arrays were aligned by the midpoint of the distance between the +1 nucleosome dyad and the terminal nucleosome dyad (*28*). Each row represents an array/gene, sorted by array length, defined in vivo. Track lengths and coloring represent the spacing between adjacent nucleosome dyads measured in vivo. The bottom graph plots the median spacing (black) as well as its standard deviation, starting from the +1 nucleosome to the terminal nucleosome (TN). Median spacing is represented as the fractional change from the canonical 165 bp. (**B**) Same as (A), except that the track midpoints report the dyad position of each nucleosome measurement. Track lengths and heat map colors represent the standard deviation (fuzziness) of each cluster of tags measured in vivo.

evident on genes analyzed individually (Fig. 3C) or on aggregated data (Fig. 3D), suggesting that nucleosomes are actively packed against barriers at the 5′ ends of genes using ATP. This would occur at the expense of more distal nucleosomes under conditions of low nucleosome density. This model does not exclude bidirectional fluidity, but does implicate net directionality of nucleosome packing (fig. S10). This packing mechanism is consistent with previously proposed spacing mechanisms (*20*–*23*) but differs by the addition of a barrier and directionality. Together they provide constant spacing close to the barrier regardless of nucleosome density.

To analyze the packing mechanism further, we examined internucleosomal spacing in vivo along genic nucleosome arrays (Fig. 4A). The average spacing was relatively narrow and uniform from nucleosomes +1 through +4, and to a lesser extent also at the 3′ end. Spacing was, on average, wider but more variable toward the middle of longer genes, and thus less definable. This is not in conflict with the uniform spacing (peak-to-peak distances) in composite plots (e.g., Fig. 1A), because such measurements reflect modal internucleosomal distances (i.e., the most common spacing), rather than the average spacing. Modal internucleosomal distances are expected to remain constant along arrays until spacing activities and/or the influence of the barriers have fully dissipated. The wider and more variable spacing toward the middle of genes suggested that the active packing mechanism at 5′ barriers dissipates toward the middle of genes. The ATP-dependent packing activities may be constrained to position about four nucleosomes, because this was the extent to which ATP reconstituted proper positioning (Fig. 2).

More distally from barriers, nucleosome positioning may gradually transition to other mechanisms, for example through sequence-intrinsic preferences. If well-positioned nucleosomes resulted, then such positioning would be manifested as low fuzziness (standard deviation of sequencing tag positions) (*24*). However, nucleosome fuzziness increased toward the middle of genes, with some skewing toward the 3′ end (Fig. 4B). Thus, mechanisms outside the 5′ packing activity (and to a lesser extent at the 3′ end as well), whether active or passive, do not produce well-positioned nucleosomes.

Nucleosome positioning at the 5′ ends of most genes appears to be driven by ATP-dependent activities that directionally package nucleosomes against a 5′ barrier (and to a lesser extent 3′ barriers). Such nucleosome placement is not likely to be static and may involve dynamic exchange with free histones (*25*, *26*). Accordingly, the active nucleosome organization in vivo may be at steady state, under the continuous expense of energy, rather than at equilibrium (*27*). This barrier-packing combination may constitute an organizing center that operates for a limited distance to buffer nucleosome organization at the 5′ ends of genes from fluctuations in histone levels both globally and locally during DNA replication and transcription. If replication transiently decreases nucleosome density by half and if 5′ nucleosome packing operates faster than replication-dependent nucleosome assembly, old nucleosomes would be enriched toward the 5′ ends and new histones mainly would be deposited in the middle to 3′ ends of genes. A 5′ packing mechanism may also serve to regulate access to transcriptional start sites. Furthermore, the control of nucleosome positioning at each gene by a single organizing center would minimize evolutionary constraints on coding sequences that might otherwise occur if positioning was intrinsically encoded by the DNA sequence.

References and Notes

1. R. D. Kornberg, L. Stryer, *Nucleic Acids Res.* **16**, (14A), 6677 (1988).
2. G. C. Yuan *et al.*, *Science* **309**, 626 (2005).
3. T. N. Mavrich *et al.*, *Genome Res.* **18**, 1073 (2008).
4. W. Möbius, U. Gerland, *PLOS Comput. Biol.* **6**, e1000891 (2010).
5. E. Segal *et al.*, *Nature* **442**, 772 (2006).
6. N. Kaplan *et al.*, *Nature* **458**, 362 (2009).
7. Y. Zhang *et al.*, *Nat. Struct. Mol. Biol.* **16**, 847 (2009).
8. A. Stein, T. E. Takasuka, C. K. Collings, *Nucleic Acids Res.* **38**, 709 (2010).
9. A. Hughes, O. J. Rando, *J. Biol.* **8**, 96 (2009).
10. A. Weiner, A. Hughes, M. Yassour, O. J. Rando, N. Friedman, *Genome Res.* **20**, 90 (2010).
11. Materials and methods are available as supporting material on *Science* Online.
12. J. D. Anderson, J. Widom, *Mol. Cell. Biol.* **21**, 3830 (2001).
13. V. Iyer, K. Struhl, *EMBO J.* **14**, 2570 (1995).
14. R. M. Raisner *et al.*, *Cell* **123**, 233 (2005).
15. K. Luger, T. J. Rechsteiner, T. J. Richmond, *Methods Enzymol.* **304**, 3 (1999).
16. A. Flaus, T. Owen-Hughes, *Mol. Cell. Biol.* **23**, 7767 (2003).
17. G. R. Schnitzler, *Cell Biochem. Biophys.* **51**, 67 (2008).
18. P. Korber, W. Hörz, *J. Biol. Chem.* **279**, 35113 (2004).
19. P. D. Hartley, H. D. Madhani, *Cell* **137**, 445 (2009).
20. P. D. Varga-Weisz *et al.*, *Nature* **388**, 598 (1997).
21. G. LeRoy, G. Orphanides, W. S. Lane, D. Reinberg, *Science* **282**, 1900 (1998).
22. T. Ito, M. Bulger, M. J. Pazin, R. Kobayashi, J. T. Kadonaga, *Cell* **90**, 145 (1997).
23. T. Tsukiyama, J. Palmer, C. C. Landel, J. Shiloach, C. Wu, *Genes Dev.* **13**, 686 (1999).
24. I. Albert *et al.*, *Nature* **446**, 572 (2007).
25. A. Rufiange, P. E. Jacques, W. Bhat, F. Robert, A. Nourani, *Mol. Cell* **27**, 393 (2007).
26. M. F. Dion *et al.*, *Science* **315**, 1405 (2007).
27. E. Segal, J. Widom, *Trends Genet.* **25**, 335 (2009).
28. C. Vaillant *et al.*, *Genome Res.* **20**, 59 (2010).

29. We thank the members of the Penn State Center for Eukaryotic Gene Regulation and of the Molecular Biology Unit of the Adolf-Butenandt-Institut for valuable discussion and support. We are grateful to D. Blaschke for technical assistance and to S. Holmberg for the gift of the *S. cerevisiae* library. This work was supported by grant HG004160 from the National Institutes of Health to B.F.P.; and by the German Research Community (SFB/TR5) and the Epigenome Network of Excellence in the Sixth Framework Programme of the European Community (NET grant), both to P.K. Sequencing data are available at ArrayExpress under accession number: SRA030538.1.

Supporting Online Material

www.sciencemag.org/cgi/content/full/332/6032/977/DC1
Materials and Methods
Figs. S1 to S10
References

10.1126/science.1200508

The EMBO Journal (2011) 30, 1277–1288 | © 2011 European Molecular Biology Organization | All Rights Reserved 0261-4189/11
www.embojournal.org

THE
EMBO
JOURNAL

The RSC chromatin remodelling enzyme has a unique role in directing the accurate positioning of nucleosomes

Christian J Wippo[1], Lars Israel[2], Shinya Watanabe[3], Andreas Hochheimer[1,4], Craig L Peterson[3] and Philipp Korber[1,*]

[1]Adolf-Butenandt-Institut, University of Munich, Munich, Germany, [2]Protein Analysis Unit, Universität München, Munich, Germany and [3]Program in Molecular Medicine, University of Massachusetts Medical School, Worcester, MA, USA

Nucleosomes impede access to DNA. Therefore, nucleosome positioning is fundamental to genome regulation. Nevertheless, the molecular nucleosome positioning mechanisms are poorly understood. This is partly because *in vitro* reconstitution of *in vivo*-like nucleosome positions from purified components is mostly lacking, barring biochemical studies. Using a yeast extract *in vitro* reconstitution system that generates *in vivo*-like nucleosome patterns at *S. cerevisiae* loci, we find that the RSC chromatin remodelling enzyme is necessary for nucleosome positioning. This was previously suggested by genome-wide *in vivo* studies and is confirmed here *in vivo* for individual loci. Beyond the limitations of conditional mutants, we show biochemically that RSC functions directly, can be sufficient, but mostly relies on other factors to properly position nucleosomes. Strikingly, RSC could not be replaced by either the closely related SWI/SNF or the Isw2 remodelling enzyme. Thus, we pinpoint that nucleosome positioning specifically depends on the unique properties of the RSC complex.

The EMBO Journal (2011) **30,** 1277–1288. doi:10.1038/emboj.2011.43; Published online 22 February 2011
Subject Categories: chromatin & transcription
Keywords: *in vitro* reconstitution; nucleosome positioning; RSC chromatin remodelling complex; *S. cerevisiae* chromatin

Introduction

Eukaryotes package their nuclear DNA into a complex structure called chromatin. At the most basic level of chromatin, the DNA is wound around an octamer of histone proteins in ~1.7 turns (Luger *et al*, 1997) constituting a nucleosome core particle. Nucleosome core DNA is much less accessible to DNA-binding factors than DNA in linker regions between nucleosome cores or in nucleosome-depleted regions (NDRs). Therefore, the positioning of nucleosomes with respect to the DNA sequence is a powerful lever for the regulation of DNA-templated processes, such as transcription or replication (Simpson, 1990; Venter *et al*, 1994; Liu *et al*, 2006; Field *et al*, 2008; Lantermann *et al*, 2010). This global importance of nucleosome positioning was underscored by the high degree of defined positions in recent genome-wide nucleosome mappings in organisms from yeast to man (Yuan *et al*, 2005; Albert *et al*, 2007; Lee *et al*, 2007; Ozsolak *et al*, 2007; Whitehouse *et al*, 2007; Field *et al*, 2008, 2009; Schones *et al*, 2008; Shivaswamy *et al*, 2008; Valouev *et al*, 2008; Mavrich *et al*, 2008a, b; Lantermann *et al*, 2010). Nevertheless, the molecular mechanism for nucleosome positioning *in vivo* is by far not fully understood.

As nucleosomal DNA is tightly bent, it is an attractive hypothesis that intrinsic features of DNA sequences have a major role in nucleosome positioning. Some sequence features, like certain dinucleotide periodicities (Satchwell *et al*, 1986), intrinsically favour, and others, like poly(dA:dT) stretches (Simpson and Shindo, 1979), disfavour nucleosome formation (Travers *et al*, 2009). Indeed, there is a significant correlation of such features with nucleosome positioning *in vivo*. For example, poly(dA:dT) stretches are enriched in *S. cerevisiae* promoter NDRs (Iyer and Struhl, 1995; Bernstein *et al*, 2004; Yuan *et al*, 2005), and a 10 bp periodicity of AA/TT/AT dinucleotides is more prevalent in strongly positioned nucleosomes flanking NDRs (Ioshikhes *et al*, 2006; Segal *et al*, 2006; Mavrich *et al*, 2008a). However, such rules are not universal. *S. pombe* NDRs, for example, are not enriched for poly(dA:dT) stretches (Lantermann *et al*, 2010), and also other yeasts do not necessarily use such sequences to establish promoter NDRs (Tsankov *et al*, 2010).

Intrinsic DNA sequence rules of nucleosome formation may be probed by *in vitro* reconstitution via salt gradient dialysis, which involves only histones and DNA mixed at initially high salt concentration that is slowly diluted until nucleosomes form spontaneously (Widom, 2001). Recently, two groups reconstituted the whole *S. cerevisiae* genome by salt gradient dialysis and found some overall correlations of *in vitro* and *in vivo* nucleosome occupancy, particularly at the promoter NDRs (Kaplan *et al*, 2009; Zhang *et al*, 2009), but individual nucleosome positions were mostly not recapitulated (Zhang *et al*, 2009). Clearly, additional factors beyond just the DNA and histones determine nucleosome positions *in vivo*.

What are these nucleosome positioning factors? Besides a role of some abundant sequence-specific DNA-binding proteins, like budding yeast Reb1 and Abf1 (Raisner *et al*, 2005; Badis *et al*, 2008; Hartley and Madhani, 2009), ATP-dependent nucleosome remodelling enzymes are implicated in global nucleosome positioning. Such enzymes enable the assembly, disassembly or relocation of nucleosomes, and in some cases they can catalyse histone exchange events. They vary in the type of ATPase subunit and in the association with different subunits (Clapier and Cairns, 2009).

*Corresponding author. Adolf-Butenandt-Institut, University of Munich, Schillerstrasse 44, Munich 80336, Germany. Tel.: +498 921 807 5435; Fax: +498 921 807 5425; E-mail: pkorber@lmu.de
[4]Present address: B.R.A.I.N. AG, Zwingenberg, Germany

Received: 23 July 2010; accepted: 26 January 2011; published online: 22 February 2011

The *S. cerevisiae* Isw2 and Isw1 remodelling enzymes were shown to move nucleosomes over intrinsically unfavourable sequences at the 5′ and 3′ ends of genes (Isw2 (Whitehouse *et al*, 2007)) and at mid-coding regions (Isw1 (Tirosh *et al*, 2010)), which in both cases were associated with suppression of erroneous transcription. Conversely, in *S. pombe*, which does not encode a remodelling enzyme of the ISWI family, the remodelling enzyme Mit1 appears to be involved in generating regular nucleosomal arrays (Lantermann *et al*, 2010). Finally, the essential remodelling enzyme RSC appears to keep NDRs nucleosome-free in *S. cerevisiae* (Badis *et al*, 2008; Hartley and Madhani, 2009). Ablation of RSC in temperature-sensitive mutants increased nucleosome occupancy at ∼55% of NDRs (Hartley and Madhani, 2009). However, such effects in conditional mutants may be indirect or confounded by cell viability issues.

Therefore, complementary to the initial identification of nucleosome positioning factors *in vivo*, there is an urgent need for an *in vitro* reconstitution system that generates *in vivo*-like nucleosome positioning in order to elucidate the molecular mechanism. Previously, we reported the establishment of such an *in vitro* system using yeast extracts that was able to successfully generate *in vivo*-like patterns of nucleosome positions at several yeast promoters (Korber and Horz, 2004; Hertel *et al*, 2005; Wippo *et al*, 2009). In this study, we describe the enrichment of the nucleosome positioning activity by chromatography and by fractionation of the yeast extract. We identify the RSC nucleosome remodelling complex and show directly by *in vitro* reconstitution that it has a specific, necessary, and in some cases even sufficient, role in nucleosome positioning at yeast promoters.

Results

The nucleosome positioning activity for the PHO8 promoter could be enriched over four sequential fractionation steps

The *S. cerevisiae PHO8* promoter has promoter nucleosomes with stereotypical positioning (Yuan *et al*, 2005; Mavrich *et al*, 2008a; Jiang and Pugh, 2009), that is, an NDR of ∼120 bp that is flanked by two positioned nucleosomes with the downstream nucleosome N + 1 covering the TSS (Figure 1A). Upstream of *PHO8* is the divergently transcribed *KRE2* gene with a similarly stereotypical promoter. In short, in the following sections, we call this entire region the '*PHO8* promoter'.

We assembled plasmids carrying the *PHO8* promoter into chromatin by salt gradient dialysis using *Drosophila* embryo histone octamers. As shown before (Hertel *et al*, 2005), this assembly by itself was unable to reconstitute the *in vivo* nucleosome positions (Figure 1C, lane 4, note that the pattern of salt gradient dialysis chromatin does not change in the presence of extract if no ATP is added; Hertel *et al*, 2005). However, incubation of such chromatin templates with a yeast whole-cell extract (WCE) and ATP shifted the nucleosomes to their *in vivo* positions (Figure 1C, lane 5; Hertel *et al*, 2005). Importantly, we analyse *in vivo* and *in vitro* chromatin samples side-by-side by using the same methodology and in the same gels. This way the nucleosome positioning patterns of different samples can be directly compared. Using this assay, we traced the nucleosome positioning activity during extract fractionation over four sequential steps (Figure 1B and C). The protein complexity was greatly reduced (Supplementary Figure S1), with only a moderate loss of the nucleosome positioning activity. As our reconstitution system could also generate *in vivo*-like positioning at other loci (Korber and Horz, 2004; Hertel *et al*, 2005; Wippo *et al*, 2009; Figures 2 and 3, Supplementary Figure S2, and data not shown), we tested the 500-mM ammonium sulphate phenyl sepharose fraction and the final 350-mM KCl DEAE fraction on other promoters as well. While the former fraction was as positive as the WCE for almost all loci, the latter was mainly positive for *PHO8* (data not shown), indicating distinct nucleosome positioning activities for different loci.

LC-MS/MS analysis of the final 350-mM KCl DEAE fraction

LC-MS/MS analysis of the final 350-mM KCl DEAE fraction identified 212 proteins (Supplementary Table S2), of which 95 localized outside the nucleus and 117 localized at least partially to the nucleus or had no known localization (Huh *et al*, 2003). These 117 proteins were, in principle, the more promising candidates, but many of them were excluded from further analysis, as yeast strains harbouring deletion or temperature-sensitive alleles of the respective genes showed the wild-type DNaseI pattern at the *PHO8* promoter *in vivo* (Supplementary Table S2; data not shown).

Purified RSC repositioned nucleosomes in salt gradient dialysis chromatin, but only in few cases resulting in in vivo-like positions

Intriguingly, our final fraction contained 10 out of 17 subunits of the RSC complex (Supplementary Table S2), suggesting a role for this remodelling enzyme. To directly test whether the RSC complex was sufficient for proper nucleosome positioning, we chose a test set of four yeast loci in which a role of RSC in nucleosome organization had either previously been implicated (*RIM9* and *PHO8* (Badis *et al*, 2008), *CHA1* (Moreira and Holmberg, 1999; Badis *et al*, 2008; Parnell *et al*, 2008)) or not (*PHO8* (Parnell *et al*, 2008) and *SNT1* (Badis *et al*, 2008; Hartley and Madhani, 2009)). We assembled equimolar amounts of four plasmids, each carrying one of these loci, together in the same reaction by salt gradient dialysis with purified histones. This pool of pre-assembled plasmids was the common starting material for the following experiments.

Similar to the *PHO8* locus, the main NDRs and some of the positioned nucleosomes at both the *CHA1* and the *SNT1* locus were properly generated upon addition of WCE and ATP to salt gradient dialysis chromatin, whereas salt gradient dialysis by itself again did not recapitulate *in vivo*-like nucleosome positioning (Figure 2C and D, compare lanes 4–5 and 12–13 with lanes 1–2). The pattern of salt gradient dialysis chromatin and WCE without ATP was again the same as that for untreated salt gradient dialysis chromatin. So also at these loci as well, our yeast extract-based *in vitro* reconstitution system generated *in vivo*-like nucleosome organization from non-*in vivo*-like salt gradient dialysis chromatin. Nevertheless, salt gradient dialysis assembly alone could reconstitute the *RIM9* NDR2 and *ECM40* NDR3 to some extent correctly (Figure 2B, compare lanes 12–13 with lanes 1–2), while addition of WCE broadened *RIM9* NDR2. The *RIM9* locus turned out to be a rare example in which *in vivo*-like nucleosome positioning was less properly reconstituted in

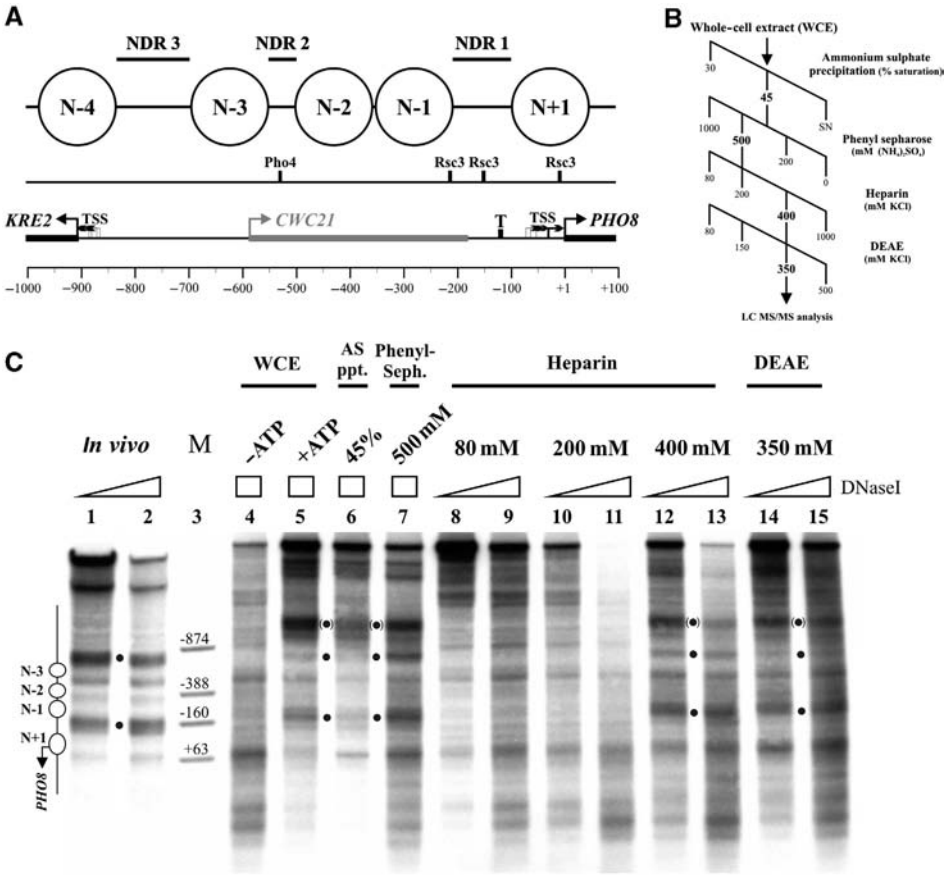

Figure 1 The nucleosome positioning activity for the *PHO8* promoter could be enriched from a yeast whole-cell extract (WCE) over four sequential fractionation steps. (**A**) Top panel: schematics of nucleosome positions at the *KRE2-CWC21-PHO8* locus, according to Barbaric *et al* (1992) and Jiang and Pugh (2009). Nucleosomes are numbered relative to NDR1. Middle panel: mapped Pho4 (Barbaric *et al*, 1992) or predicted Rsc3 (Badis *et al*, 2008) binding sites (Supplementary Figure S8A). Lower panel: *KRE2*, *CWC21* and *PHO8* open reading frames (rectangular bars with large broken arrows), TATA box (T; Basehoar *et al*, 2004) and transcriptional start sites (TSS, small broken arrows; Miura *et al*, 2006). Scale bar: distance in base pairs from *PHO8* ORF start. All panels drawn to scale. (**B**) Extract fractionation scheme. Fractions positive for the *PHO8* promoter nucleosome positioning activity are labelled in bold. SN, supernatant. (**C**) DNaseI indirect end labelling analysis of the *PHO8* promoter region *in vivo* or *in vitro* after salt gradient dialysis assembly and incubation with either WCE in the presence or absence of ATP, or with one of the indicated fractions (see **B**) in the presence of ATP. Black dots: diagnostic bands, which are characteristic for the *in vivo* pattern and seen *in vitro* only in the presence of ATP and the nucleosome positioning activity. Black dots in parentheses: hypersensitive site within the lacZ ORF of the pUC19 backbone specific for the *in vitro* pattern that always co-occurred with the *in vivo*-like *PHO8* promoter pattern. The yeast sequence terminates close to the top marker band. Schematics on the left analogous to (**A**). Position of marker bands is labelled relative to the *PHO8* ORF start. Ramps and boxes: relative DNaseI concentrations. All samples were electrophoresed alongside in the same gel, but the *in vivo* samples migrated slightly faster, probably because of different total DNA concentration.

our yeast extract-based *in vitro* system. Moreover, the NDR1 at *AEP1* was not met under any *in vitro* conditions. A strong band close to the position of NDR1 in the presence of RSC (Figure 2B, lanes 6–9) was not at the proper position as seen by indirect end labelling using a secondary cleavage with better resolution for this region (data not shown).

Strikingly, addition of purified RSC and ATP to salt gradient dialysis chromatin already generated the proper NDR at *CHA1* to some degree (Figure 2C, compare lanes 6–9 with lanes 1–2) and could clearly position nucleosome N-1 at the *SNT1* locus as *in vivo* (Figure 2D, compare lanes 6–9 with lanes 1–2). The prominent band in the salt gradient dialysis chromatin pattern (arrow between lanes 12 and 13) at the position of the *SNT1* nucleosome N-1 was removed by the addition of purified RSC (or of WCE) in the presence of ATP, suggesting that RSC alone could move a nucleosome to an *in vivo*-like position. This was true for both tested RSC concentrations (Figure 2C and D, compare lanes 6–7 with lanes 8–9).

In contrast, addition of purified RSC was unable to reconstitute *in vivo*-like positioning both at the *PHO8* (Figure 2A, compare lanes 6–9 with lanes 1–2) and at the *RIM9* locus (Figure 2B, compare lane 6–9 with lanes 1–2), although it did change the pattern of the salt gradient dialysis chromatin (Figure 2A–D, compare lanes 6–9 with lanes 12–13) arguing for sufficient remodelling activity in the assay. Importantly, and in accordance with our earlier findings (Korber and Horz, 2004; Hertel *et al*, 2005; Wippo *et al*, 2009), the nucleosome positioning activity of both purified RSC and of the WCE was strictly dependent on the presence of ATP (Figure 2A–D, compare lanes 10–13 with lanes 4–9).

A direct and necessary role for RSC in generating in vivo-like nucleosome positions at PHO8, RIM9, CHA1 and SNT1 in vitro

As purified RSC could generate only a minor fraction of the proper nucleosome positioning *in vitro*, we wondered

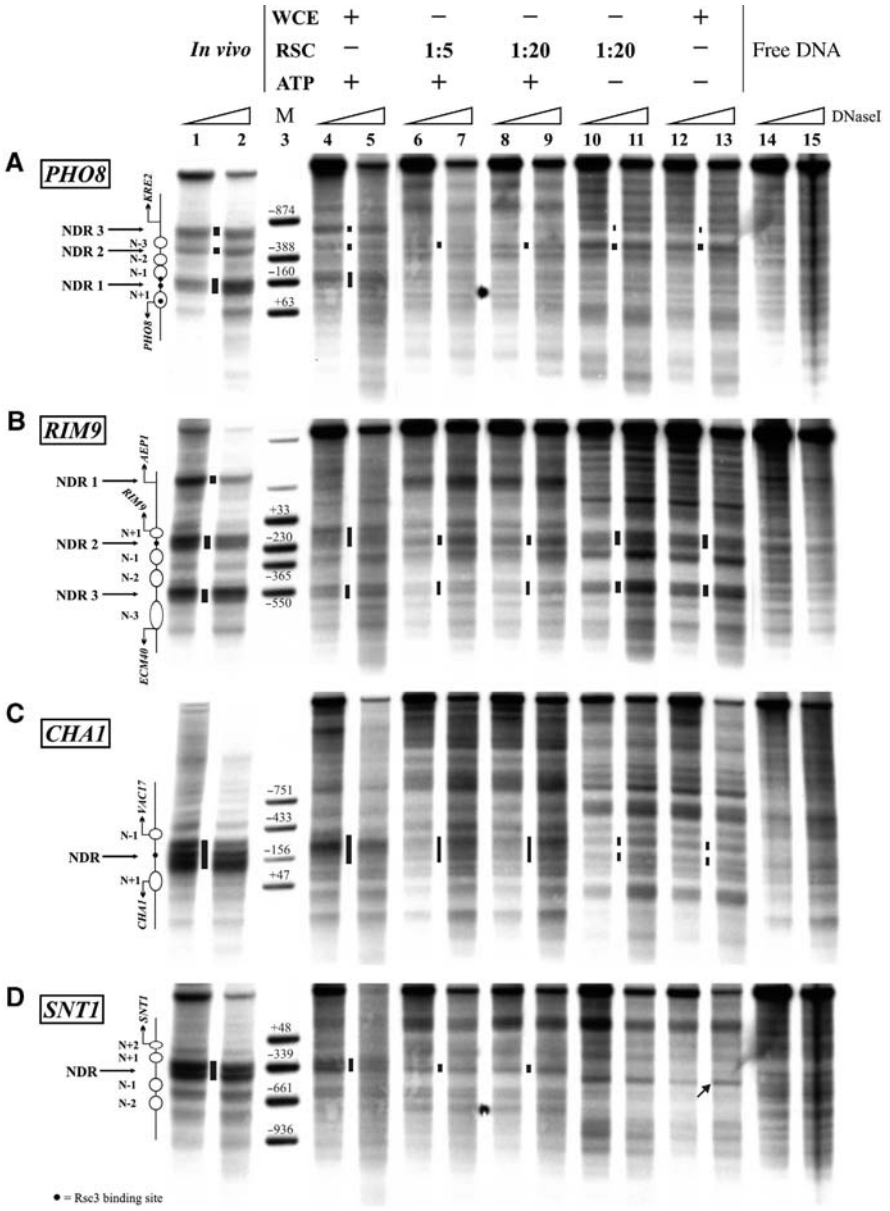

Figure 2 Purified RSC repositioned nucleosomes in salt gradient dialysis chromatin, but only in few cases, resulting in *in vivo*-like positions. DNaseI indirect end labelling analysis of the (**A**) *PHO8*, (**B**) *RIM9*, (**C**) *CHA1* and (**D**) *SNT1* promoter regions *in vitro* after assembly by salt gradient dialysis and incubation with WCE or purified RSC complex in the presence or the absence of ATP as indicated. The amount of RSC is given as the molar ratio of RSC to nucleosomes. In each panel, lanes 1 and 2 show the wt *in vivo* DNaseI pattern. Free DNA samples correspond to the respective non-assembled plasmids in the absence of WCE, RSC and ATP but under otherwise identical conditions. Bars in between lanes mark hypersensitive regions that correspond, at least to some degree, to NDRs of the *in vivo* patterns. The arrow between lanes 12 and 13 in **D** marks a nuclease-sensitive region that becomes inaccessible because of RSC activity. Ramps: increasing DNaseI concentrations. Position of marker bands is labelled relative to the ORF start of the respective locus. Schematics on the left are analogous to Figure 1A for the respective locus. Predicted Rsc3 binding sites (Supplementary Figure S8) are indicated by black dots.

whether it was even necessary. We prepared extracts from a strain carrying a temperature-sensitive allele of the gene coding for the essential Rsc3 subunit of the RSC complex (*rsc3-ts* mutant (Badis *et al*, 2008)) that was grown at the non-permissive temperature (37°C) overnight. Such an extract (Figure 3, '*rsc3-ts* 37°C' extract) was much less effective in positioning nucleosomes properly than the wild-type WCE (Figure 3A–D, compare lanes 8–9 with lanes 4–5), while an extract prepared from the *rsc3-ts* strain grown at 25°C functioned almost like the wild-type WCE (Figure 3A–D, compare lanes 12–13 with lanes 4–5). The *rsc3-ts* 37°C extract failed to reconstitute NDR1 and NDR3 at the *PHO8* promoter, NDR2 at the *RIM9* promoter, the broad NDR at the *CHA1* locus and the strong NDR at the *SNT1* promoter (Figure 3A–D, lanes 8–9). Nevertheless, it did change the pattern of the salt gradient dialysis chromatin starting material (Figure 3A–D, compare lanes 8–9 with 14–15), arguing for residual nucleosome remodelling activity also in this extract. In summary, the *rsc3-ts* 37°C extract was sufficiently impaired in its nucleosome positioning activity to confirm the necessary role of RSC and to serve as a background for rescue experiments using purified RSC complex.

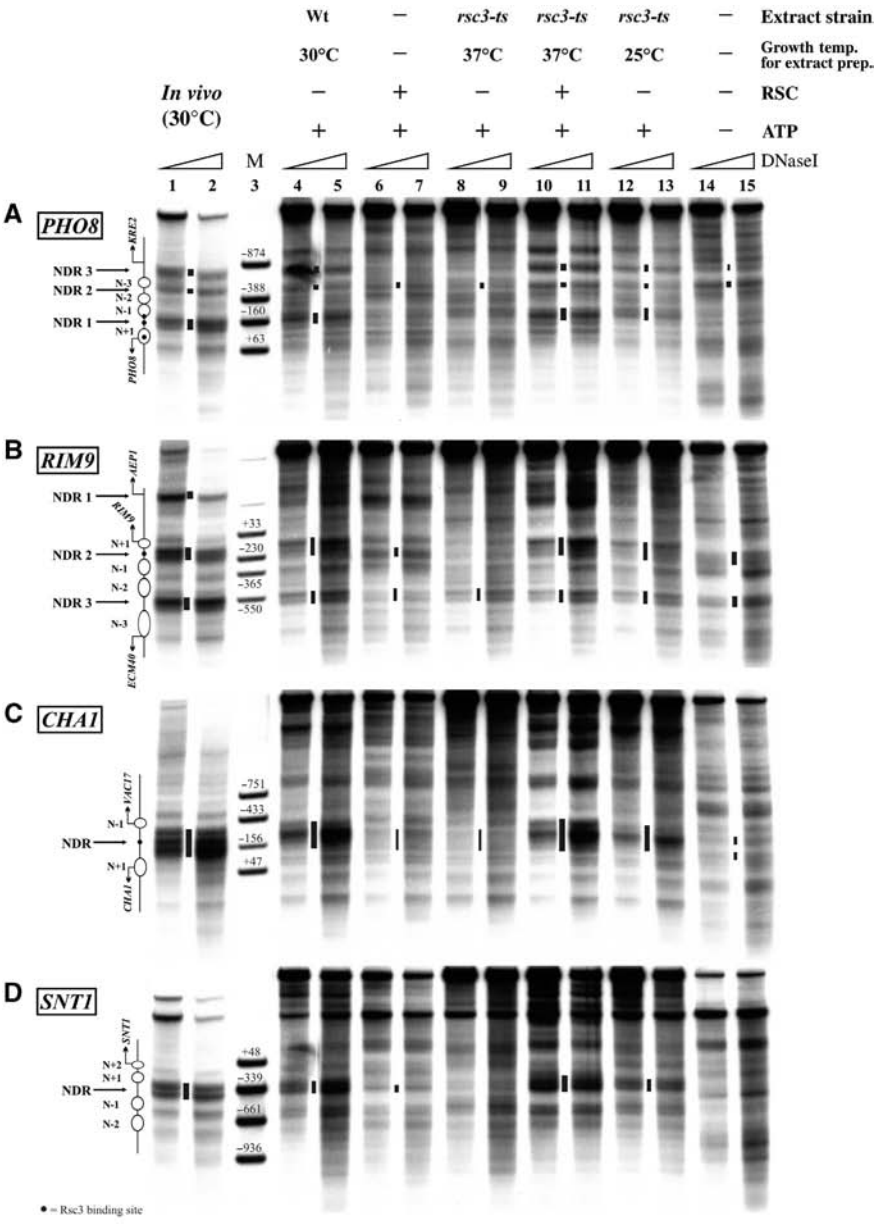

Figure 3 Purified RSC could rescue the nucleosome positioning activity of an extract generated from an *rsc3-ts* mutant grown under restrictive conditions. DNaseI indirect end labelling analysis of the (**A**) *PHO8*, (**B**) *RIM9*, (**C**) *CHA1*, and (**D**) *SNT1* promoter regions as in Figure 2, but with WCEs generated from wild-type (BY4741) grown logarithmically at 30°C, or from *rsc3-ts* strain (TH8239) grown logarithmically at 25°C with or without an overnight shift to 37°C. Addition of RSC corresponded to the 1:5 ratio in Figure 2.

Indeed, the addition of purified RSC to the *rsc3-ts* 37°C extract, completely rescued the nucleosome positioning activity for all four tested loci (Figure 3A–D, compare lanes 10–11 with lanes 4–5) and yielded patterns that were even slightly more *in vivo*-like than those generated by the wild-type WCE. This suggests that in the wild-type WCE, RSC may even be a limiting factor for proper nucleosome positioning. The rescue by purified RSC strongly suggests that the changes observed with the *rsc3-ts*, *arp9-ts* and *sth1-td* strains, by us (see below, Figure 5 and Supplementary Figure S3) and by others (Supplementary Figure S4, Supplementary Table S3) (Badis *et al*, 2008; Parnell *et al*, 2008; Hartley and Madhani, 2009), were not caused by indirect effects. Moreover, purified RSC could generate much less of the proper nucleosome positioning than in combination with the *rsc3-ts* 37°C extract (Figure 3A–D, compare lanes 6–7 with lanes 10–11). Therefore, both RSC and the *rsc3-ts* 37°C extract were unable to reconstitute *in vivo*-like nucleosome positioning on their own, but the combination of both reconstituted the full nucleosome positioning activity. Therefore, RSC is necessary but mostly not sufficient for proper nucleosome positioning.

Interestingly, we even found an example in which purified RSC counteracted the generation of *in vivo*-like nucleosome positioning. We published previously that almost *in vivo*-like nucleosome positioning was generated at the *PHO84* promoter by mere salt gradient dialysis reconstitution (Wippo *et al*, 2009). RSC alone disrupted this intrinsically encoded *in vivo*-like positioning, whereas the proper positioning was generated when RSC was added in the context of the *rsc3-ts* 37°C extract (Supplementary Figure S2, compare lanes 6–7 with

1–2, 4–5, 10–11 and 14–15). This further underscores the fact that additional factors from the extract are necessary to direct the role of RSC in nucleosome positioning.

The role of the RSC complex in nucleosome positioning in vitro is specific, as it could not be substituted by the SWI/SNF or Isw2 remodelling enzymes

We wondered whether the role of RSC was specific or whether other remodelling complexes could achieve similar results. The *rsc3-ts* 37°C extract likely still contained other remodelling enzymes. However, other remodelling enzymes might not be present in sufficient quantities to substitute for the loss of RSC function in our *in vitro* system. Most other remodelling enzymes are less abundant in the cell to start with (~2000 copies of Sth1 per cell compared to ~220 copies of Snf2; Ghaemmaghami *et al*, 2003), and they may be less stable during extract preparation or their concentration might have been affected indirectly because of the *rsc3-ts* conditions. Hence, the RSC complex might just have seemed necessary for nucleosome positioning in our *in vitro* system—and by extension also in previous *in vivo* studies—simply because it was the most abundant remodelling activity.

We added purified SWI/SNF or Isw2 remodelling enzymes in the same molar amount as previously carried out for the RSC complex to the *rsc3-ts* 37°C extract. These two remodelling complexes, whether alone or in combination with the *rsc3-ts* 37°C extract, were unable to generate *in vivo*-like positioning as achieved with RSC (Figure 4A–D, compare lanes 3–11 with lanes 1–2). Importantly, both remodelling enzymes individually (in the presence of ATP) altered the pattern of salt gradient dialysis chromatin (Figure 4A–D, compare lanes 8–9 and 10–11 with 12–13) to a certain extent, which confirmed sufficient activity to remodel the chromatin templates *in vitro*. Both remodelling enzymes did not change the pattern generated by the *rsc3-ts* 37°C extract (compare Figure 4A–D, lanes 3–6 with Figure 3A–D, lanes 8–9), possibly because both were already present in the *rsc3-ts* 37°C extract.

Loss of essential subunits of the RSC remodelling complex altered chromatin structure at the PHO8, RIM9 and other promoters in vivo

Our *in vitro* results strongly argue for a direct role of RSC in nucleosome positioning also *in vivo* as suggested previously (Badis *et al*, 2008; Parnell *et al*, 2008; Hartley and Madhani, 2009). Genome-scale microarray data on changes in nucleosome occupancy upon RSC ablation were already available for the temperature-sensitive *rsc3-ts* allele (Badis *et al*, 2008) and for *sth1-td* degron mutants (Parnell *et al*, 2008; Hartley and Madhani, 2009). However, a detailed comparison between different methods is often difficult and it is usually advisable to confirm genome-wide data with locus-specific techniques for regions of interest. Therefore, we monitored the *in vivo* effect of RSC on chromatin patterns at selected test loci, by the same method as used for the *in vitro* patterns, that is, by DNaseI indirect end labelling. We used the same temperature-sensitive strains as Badis *et al* and Parnell *et al* (*rsc3-ts* (Badis *et al*, 2008), *sth1-td* (Parnell *et al*, 2008)) and included an *arp9-ts* mutant (Cairns *et al*, 1998) as Arp9 came up very prominently in our LC-MS/MS analysis (Supplementary Table S2).

At the *PHO8* promoter, a broad DNaseI hypersensitive site replaced nucleosome N-3 between NDR3 and NDR2, and the short hypersensitive site at the migration position of the −160 marker band was slightly diminished, indicating increased nucleosome occupancy over NDR1. We confirmed the DNaseI indirect end labelling results by restriction enzyme accessibility. In both the *arp9-ts* and the *rsc3-ts* mutant, there was an increase in accessibility of the *Hpa*I site located within nucleosome N-3 and a decrease for the *Hin*dIII site located within NDR1 (Supplementary Figure S3). Consistently, Badis *et al* (2008) observed increased nucleosome occupancy at NDR1 and a broad region of decreased occupancy at the upstream edge of nucleosome N-3 in the *rsc3-ts* mutant under restrictive conditions (Supplementary Figure S4A). In contrast, Parnell *et al* (2008) did not see significant changes in the *sth1-td* strain, at least for which data are available for the *PHO8* promoter region (Supplementary Figure S4A), maybe because of a shorter incubation time (2 h) at the restrictive temperature (see below).

The altered *PHO8* promoter DNaseI pattern of the three temperature-sensitive mutants resembled the pattern of the *PHO8* promoter after induction by phosphate starvation (Barbaric *et al*, 1992). This induced promoter pattern essentially depends on binding of the transactivator Pho4 in NDR2 (Barbaric *et al*, 1992; Munsterkotter *et al*, 2000). To control for inadvertent induction of the *PHO* regulon or for other Pho4-mediated effects due to ablation of essential RSC subunits, we generated *pho4 rsc3-ts* and *pho4 arp9-ts* double mutants. Importantly, the same altered chromatin structure was observed at the *PHO8* promoter under restrictive conditions as in the ts single mutants (Supplementary Figure S5). Further, nucleosome positioning at the *PHO84* promoter, which has a similarly low threshold of *PHO* induction as *PHO8* (Lam *et al*, 2008), was largely unchanged in the *rsc3-ts* and *arp9-ts* mutants at the restrictive temperature, arguing also against inadvertent *PHO* regulon induction (Supplementary Figure S6).

The *RIM9* NDR2 was identified as a prominent example for increased nucleosome occupancy in the *rsc*3-*ts* mutant under restrictive conditions (Badis *et al*, 2008; Supplementary Figure S4B). We confirmed this by DNaseI indirect end labelling and found the same effect in the *arp9-ts* and *sth1-td* strains as well. All three strains displayed significantly reduced DNaseI hypersensitivity over the *RIM9* NDR2 (Figure 5B). Notably, this effect was locus specific as the nearby NDR1 at *AEP1* and NDR3 at *ECM40* were unaffected (Figure 5B).

At the *CHA1* locus, we did not see any effect in the *sth1-td* mutant, a weakly reduced NDR in the *rsc3-ts* mutant, although only in some experiments (Supplementary Figure S7C), and a very weak effect at the NDR in the *arp9-ts* mutant (Figure 5C). Hartley and Madhani (2009) also saw only small changes in a *sth1-td* mutant, whereas both Badis *et al* (2008) and Parnell *et al* (2008) reported clear effects (Supplementary Figure S4C and Supplementary Table S3). Therefore, in our experiment as well as in the literature, the *CHA1* locus was not a clear responder to *in vivo* ablation of RSC subunits. This ambiguity is mirrored by two studies reporting RSC binding at *CHA1* while two others did not (Supplementary Figure S4C, Supplementary Tables S3 and S4). Nevertheless, in the light of all available data we consider *CHA1* as RSC target *in vivo*.

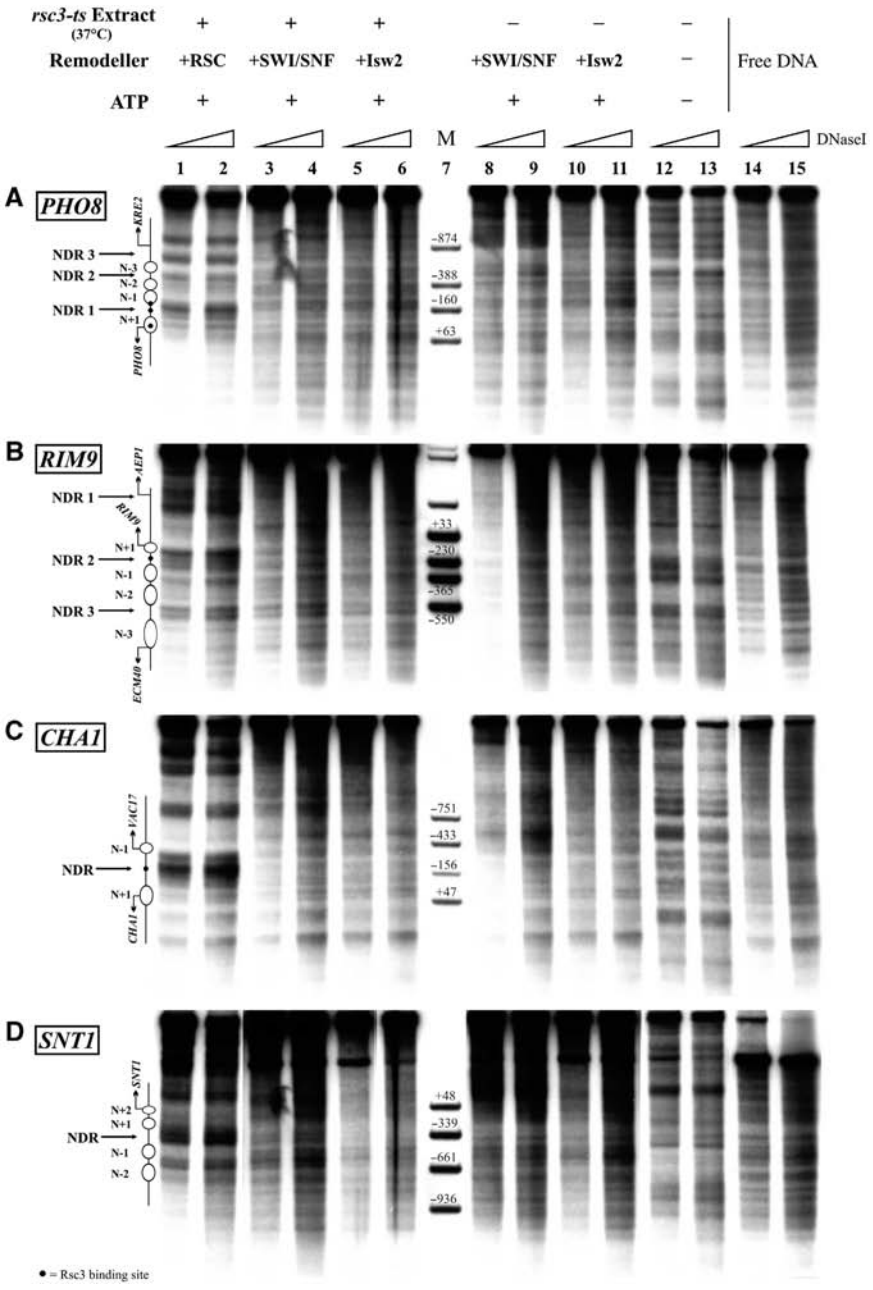

Figure 4 RSC was specifically required for nucleosome positioning *in vitro* as both SWI/SNF and Isw2 failed to rescue the *rsc3-ts* 37°C extract. DNaseI indirect end labelling analysis of the (**A**) *PHO8*, (**B**) *RIM9*, (**C**) *CHA1*, and (**D**) *SNT1* promoter regions as in Figures 2 and 3 but with addition of purified SWI/SNF or Isw2 remodelling enzymes as indicated. All remodelling enzymes were added at the same molar concentrations, corresponding to the 1:5 ratio in Figure 2.

Finally, we observed no effects at the *SNT1* locus (Figure 5D) consistent with other studies (Supplementary Figure S4D and Supplementary Table S3).

Besides the four loci that we used for our *in vitro* assays, we included six more loci in order to have a broader basis for the comparison of our data with published observations (Supplementary Figures S4 and S6, Supplementary Tables S3 and S4). To avoid missing any effects, we used rather harsh restrictive conditions (overnight incubation at 37°C), which compromised cell viability (47 ± 2% for *arp9-ts* and <5% for *rsc3-ts* and *sth1-td* mutants). Nevertheless, it is very unlikely that this led to exaggerated or artifactual effects as our results were in excellent agreement with published data or showed even a bit weaker effects, for example, at *ADH2* and *CHA1* (Supplementary Table S3 and Supplementary Figure S4). Further, we tested all loci in which we saw an effect in the *rsc3-ts* mutant after overnight incubation at 37°C also after 6.5 h, which are the same conditions as used by Badis *et al* (2008) for this same strain and raised the cell viability to 31 ± 3%. We observed the same effects as those after overnight incubation (Supplementary Figure S7). In addition, the unchanged patterns at the *SNT1*, *ADH2* and *PHO84* loci (Figure 5D and Supplementary Figure S6) argue against globally compromised chromatin structures even under the harsh overnight restrictive conditions. The only single case in which we observed more of an effect than

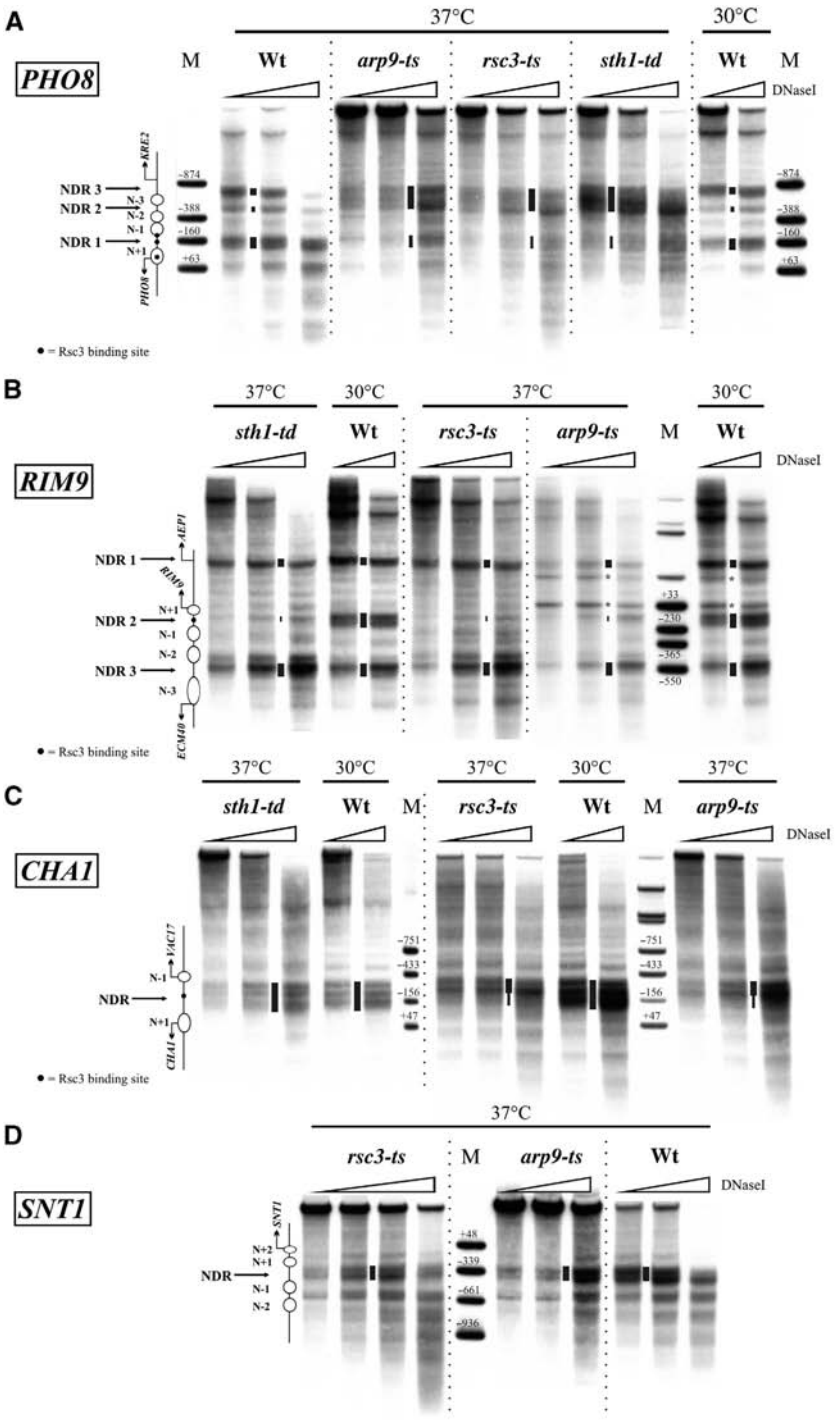

Figure 5 Loss of essential RSC subunits at elevated temperature altered chromatin structure at the *PHO8*, *RIM9* and *CHA1*, but not at the *SNT1* promoter. DNaseI indirect end labelling analysis of the (**A**) *PHO8*, (**B**) *RIM9*, (**C**) *CHA1* and (**D**) *SNT1* promoter regions *in vivo*. Nuclei were isolated from wild type (wt; BY4741) and strains carrying a temperature-sensitive (*rsc3-ts* (TH8247) and *arp9-ts* (YBC1536)) or temperature-sensitive degron (*sth1-td* (YBC2191)) allele of the indicated RSC subunits. Strains were grown logarithmically at 25°C and then shifted to the non-permissive temperature (37°C) overnight. Wt nuclei were also prepared from cells grown logarithmically at 30°C. Bars in-between lanes mark the intensity (bar width) and extent (bar length) of DNaseI hypersensitive sites. A stippled line separates samples that were not electrophoresed alongside on the same gel but combined in the figure. Asterisks indicate artefact bands. Ramps, markers and schematics as in Figure 2.

others was the altered *PHO8* promoter pattern in the *sth1-td* strain (see above). As this altered pattern was the same as that in the other two ts mutants (Figure 5A) and also that observed after shorter incubation times (Supplementary Figure S7A), it very likely reflects the true effect due to lack of RSC activity and could not be observed under the milder restrictive conditions used by Parnell *et al* (2008) (2 h at 37°C).

In summary, both our own as well as published *in vivo* data confirm that ablation of RSC activity *in vivo* interferes with nucleosome positioning. Interestingly, this was only true if essential RSC subunits were ablated as deletion of the genes

encoding the non-essential RSC subunits Rtt102 or Rsc30 showed unaltered chromatin patterns at selected loci (Supplementary Figure S7 and data not shown). This clear demonstration of a role for RSC in nucleosome positioning *in vivo* argues that the RSC-dependent mechanism observed *in vitro* is not just coincidental but reflects the *in vivo* mechanism.

Discussion

In this study, we show for the first time by *in vitro* reconstitution that the RSC nucleosome remodelling complex is directly and specifically required to generate *in vivo*-like nucleosome positioning, especially to set up yeast promoter NDRs. There are a few cases in which RSC alone can properly determine nucleosome positioning. Nevertheless, RSC mostly requires other protein factors. Our findings provide strong evidence for the hypothesis that the *in vivo* nucleosome positioning machinery relies upon specific remodelling enzymes to correctly interpret nucleosome positioning cues given by the combination of DNA sequence in *cis* and other factors in *trans*. In other words, remodelling enzymes can be part of the nucleosome positioning information.

RSC is directly and specifically required, and in few cases even sufficient, to set up nucleosome positioning in vitro

A role of RSC in maintaining the NDRs at a large fraction of yeast promoters was suggested by three recent *in vivo* studies (Badis *et al*, 2008; Parnell *et al*, 2008; Hartley and Madhani, 2009). We confirmed these genome-scale results at the level of several individual promoters by DNaseI indirect end labelling using temperature-sensitive alleles of three different genes encoding essential RSC subunits. Very recently, a non-canonical RSC/nucleosome complex was suggested to reside within the NDR at the *GAL1-10* promoter and to have a fine-tuning role for promoter induction (Floer *et al*, 2010). We confirmed that ablation of RSC activity affected this NDR, especially in the *rsc3-ts* mutant (Supplementary Figures S6 and S7D).

However, our own *in vivo* data as well as previous reports on roles for RSC in nucleosome positioning are based on conditional mutants that are compromised cells under restrictive conditions so that indirect effects may contribute to the changes at promoter NDRs. In addition, such experiments cannot distinguish whether RSC was just necessary or also sufficient for NDR formation. To answer these questions, we tested purified RSC in our *in vitro* reconstitution system starting from salt gradient dialysis-assembled chromatin.

In most cases, purified RSC in the presence of ATP was unable to achieve the same degree of *in vivo*-like nucleosome positioning as seen with the WCE. Importantly, this was not due to a lack of RSC activity in our preparation. This RSC preparation was sufficiently active to allow remodelling of the chromatin templates as the DNaseI pattern of the starting material was clearly changed by addition of RSC and ATP. Even more to the point, the successful positioning of nucleosome N-1 at the *SNT1* and part of the NDR at the *CHA1* locus by purified RSC in the presence of ATP is proof of principle that RSC alone can be sufficient to achieve even *in vivo*-like nucleosome positioning under the assay conditions. Finally, the same amount of purified RSC could completely rescue the proper nucleosome positioning activity of the *rsc3-ts* 37°C extract. Such an extract mimicked the *in vivo* phenotype in the sense that it was not able to generate the *in vivo*-like nucleosome positioning. As in the *in vivo* case, this could equally be caused by indirect effects of Rsc3 ablation on the activity of other factors. However, our rescue experiments strongly argue against indirect effects and show that RSC directly contributes to this nucleosome positioning activity. In addition, this experiment shows explicitly that additional factors from the extract are required in combination with RSC to generate the proper nucleosome positioning at most loci *in vitro*.

Intriguingly, both purified SWI/SNF and Isw2 remodelling enzymes failed to rescue the *rsc3-ts* 37°C extract, which argues that the RSC remodelling complex is specifically required for the nucleosome positioning activity and that only RSC can respond to the cues provided by the additional factors from the extract. Especially for the case of the SWI/SNF complex this specificity is somewhat surprising, as SWI/SNF and RSC are rather closely related remodelling enzymes with similar mechanistic properties in *in vitro* assays (Logie *et al*, 1999; Zhang *et al*, 2006), even sharing three subunits (Cairns *et al*, 1998). Nevertheless, both remodelling complexes may even have opposing roles; for example at the *PHO8* promoter. Activation of *PHO8* leads to a prominent chromatin transition at the *PHO8* promoter (Barbaric *et al*, 1992), which essentially depends on the remodelling enzyme SWI/SNF (Gregory *et al*, 1998). The enrichment of RSC over the region occupied by nucleosome N-3 (Venters and Pugh, 2009; and Supplementary Figure S4A) and the strikingly similar loss of nucleosome N-3, both upon RSC inactivation and upon promoter activation, suggests that RSC ensures the proper placement of N-3 under repressive conditions, whereas SWI/SNF overrides RSC and removes nucleosome N-3 under activating conditions.

The difference in remodelling enzyme specificity may reflect differences in recruitment specificity. The RSC complex contains two subunits, Rsc3 and Rsc30, which are able to recognize a specific DNA sequence (CGCGC). The location of this motif often overlaps with the sites of nucleosome occupancy change in the *rsc3-ts* mutant (Badis *et al*, 2008). Indeed, such Rsc3 sites are present and conserved at the *PHO8* promoter and other loci (Supplementary Figure 8A and B). However, recruitment of RSC through Rsc3/Rsc30 is unlikely the main or only reason for the specificity of RSC action. RSC was also necessary for proper formation of NDR3 at the *PHO8* promoter, both *in vivo* and *in vitro*, even though there is no Rsc3 site nearby. Further, *in vitro* nucleosome positioning at the *SNT1* locus, which does not contain an Rsc3 site, was strictly dependent on RSC.

Indeed, we were surprised that the *rsc3-ts* extract failed to reconstitute nucleosome positioning also at the *SNT1* locus, although along with others (Badis *et al*, 2008; Hartley and Madhani, 2009) we did not see significant changes here upon RSC ablation *in vivo*. Again, purified RSC was able to rescue *in vitro*. Why this discrepancy between the RSC requirement *in vivo* versus *in vitro* at *SNT1*? The *in vivo* experiment addresses the loss of properly positioned nucleosomes upon shift to the restrictive temperature, whereas *in vitro* reconstitution monitors the *de novo* generation of correct nucleosome positioning. Therefore, other factors may maintain

proper positioning *in vivo* even in the absence of RSC, while these factors are unable to set up proper positioning from scratch *in vitro*. Reb1 and Abf1 could be these factors at the *SNT1* locus, as they are redundantly involved in NDR formation. Only in an *abf1-td reb1-td* double mutant the *SNT1* NDR was compromised, but still not lost completely (Hartley and Madhani, 2009; Supplementary Figure S4D). It is also possible that nucleosome positioning at *SNT1* requires a particularly low concentration of RSC activity that is still present in the ts mutants even under restrictive conditions. *In vitro*, this low concentration may be even further reduced because of loss of activity during extract preparation or simply by unphysiological dilution. In any case, as a locus like *SNT1* was not scored in previous *in vivo* studies, the fraction of NDRs that depend on RSC *in vivo* may have been underestimated. Moreover, the presence of an Rsc3 site seems not to be a necessary indicator for a role of RSC.

Remodelling enzyme-intrinsic nucleosome positioning information

Our observation of the specific role for RSC in nucleosome positioning that could not be replaced by SWI/SNF or Isw2 agrees well with several *in vitro* studies showing that different remodelling enzymes have distinct sequence preferences for nucleosome positioning. These may differ significantly from the DNA-intrinsically favoured positions as determined by salt gradient dialysis (Brehm *et al*, 2000; Flaus and Owen-Hughes, 2003; Rippe *et al*, 2007; Schnitzler, 2008; Pham *et al*, 2009). We confirm this as purified RSC, SWI/SNF and Isw2 altered the salt gradient dialysis preassembled chromatin patterns at all tested loci (Figures 2 and 4). Others stressed that different remodelling enzymes moved nucleosomes with equal efficiency irrespective of the underlying DNA sequence (Partensky and Narlikar, 2009). We note that in many *in vitro* studies the patterns generated by different remodelling enzymes were mainly compared with each other and not to actual *in vivo* positions. In contrast, our system was always gauged relative to the gold standard of *in vivo* nucleosome patterns. In the light of the specificity of RSC in generating such proper patterns, we suggest that RSC not only provides the 'kinetic lubricant' for the equilibration of nucleosomes to stable positions determined by something else but also provides part of the positioning information in itself. This interpretation would also apply if the specificity of RSC function in nucleosome positioning was due to specificity of recruitment by some factor in the extract. In the case of nucleosome N-1 at the *SNT1* locus, the RSC-intrinsic information can be sufficient. Here, the combination of DNA, histones and RSC constitutes a self-organizing system yielding the exact nucleosome positioning, thus arguing against an exclusive recruitment mechanism.

Rippe *et al* (2007) suggested that remodelling enzyme-intrinsic preferences may be at the core of nucleosome positioning *in vivo* and accordingly proposed a 'remodeller code' for nucleosome positioning. Our *SNT1* data support this hypothesis to some extent. However, we showed that in most cases other factors in addition to RSC were required for proper positioning. Therefore, we think it unlikely that there is a pure 'remodeller code' for nucleosome positioning but a more diverse interplay of various factors.

A model of active non-equilibrium nucleosome positioning

Segal and Widom (2009) recently suggested an 'equilibrium model for dynamic nucleosome positioning', which assumes that nucleosomes equilibrate *in vivo* to their thermodynamically favoured positions as determined by the combined effects of intrinsic DNA features, neighbouring nucleosome exclusion, transcription factor binding, histone variants/modifications and DNA methylation. In this model, remodelling enzymes would act on nucleosome positioning only as 'kinetic lubricant', that is, as 'enzymes' (in addition to their enzymatic ATPase activity) that just help nucleosomes to overcome the activation energy barrier during the equilibration process without affecting the thermodynamics of nucleosome positions. We note that a living cell is not at equilibrium, but under steady-state conditions, so that there is no need to assume equilibrium nucleosome positioning. Accordingly, Segal and Widom (2009) explicitly remark that 'ATP-dependent chromatin remodelling complexes could actively subvert equilibrium'. As our data argue for remodelling enzyme-intrinsic nucleosome positioning in combination with other factors, we suggest that the input of energy from ATP-hydrolysis not only affects the kinetics of nucleosome positioning but also thermodynamically stabilizes positions even if they were energetically unfavourable otherwise (Korber and Becker, 2010). Indeed, we hypothesize that many if not most *in vivo* nucleosome architectures, as observed for example at promoter regions, are continuously and actively generated by ATP-dependent remodelling enzymes, and possibly other active processes, at the continuous expense of energy. The requirement for continuous energy input is incompatible with the assumption of equilibrium, but typical for the steady state of a living cell. It is to be noted that in our model as well, remodelling enzymes are necessary for nucleosome mobility on a physiologically relevant time scale. Therefore, once a nucleosome is positioned by a remodelling enzyme, it will stay there in a kinetically trapped state in the absence of remodelling activity. Hence, remodelling enzymes may determine nucleosome positions without remaining associated with the nucleosomes all the time.

Materials and methods

Strains and media

Yeast strains were as listed in Supplementary Table S1. Strains were grown in YPD with 0.1-g/l adenine and 1-g/l KH_2PO_4, except for the *sth1-td* strain that was grown in YP with 0.1-g/l adenine and 1-g/l KH_2PO_4 containing 2% raffinose and 2% galactose. Temperature-sensitive strains were grown in 400-ml medium at 25°C to an OD_{600} of 1.2–1.5 (spectrophotometer PMQ II, Zeiss, Germany). An equal volume of medium prewarmed to 49°C was added and the cultures were placed at 37°C for the indicated temperature overnight. Viability of temperature-sensitive mutants after overnight incubation under restrictive conditions was determined by comparing the number of single colonies after plating the same number of cells for mutant and wt (BY4741 for *rsc3-ts* and *arp9-ts* or YBC2192 for *sth1-td*) treated in parallel on YPDA plates at 25°C.

Yeast WCE preparation

The WCE were prepared as described (Wippo *et al*, 2009), with the following modifications. The extract used for the fractionation was made from commercially available baker's yeast concentrate (Deutsche Hefewerke GmbH, Nürnberg, Germany). The wild-type extract for all other experiments was made from strain BY4741-grown logarithmically at 30°C. For extract preparation of TH8239

(*rsc3-ts*) at permissive conditions, cells were grown at 25°C and overnight at 37°C for non-permissive conditions.

Chromatin assembly and reconstitution

Chromatin was assembled by salt gradient dialysis, treated with WCE and analysed as described (Wippo *et al*, 2009). A measure of 0.5 μg of plasmid pUC19-*PHO8*-short per salt gradient assembly reaction was used for experiments in Figure 1C, and a mix of 200 ng each of plasmids pUC19-*PHO8*-long, pUC19-*RIM9*, pUC19-*CHA1* and pUC19-*SNT1* per assembly reaction for experiments in Figures 2–4. For a detailed description of plasmids, see the Supplementary data.

Yeast nuclei preparation

Nuclei were prepared as described (Almer *et al*, 1986).

Yeast WCE fractionation

For a detailed description of the individual fractionation steps, see the Supplementary data.

Purification of remodelling enzymes

RSC2-TAP, SWI2-TAP and ISW2-FLAG were purified as described (Smith *et al*, 2003).

Binding site prediction

The Find Individual Motif Occurrences (FIMO) program (Version 4.1.0; available at http://meme.sdsc.edu/meme4_1/cgi-bin/fimo.cgi) was used to predict sites for Rsc3 at the *PHO8*, *RIM9*, *CHA1*, *SNT1*, *RIO1*, *RNR3*, *GAL10*, *PHO5*, *PHO84* and *ADH2* promoters. The position weight matrix was obtained from Supplementary Table S6 of Badis *et al* (2008). We note that a simple search for the Rsc3 motif CGCGC identifies the same sites as the FIMO program.

Rsc3 site alignment

The orthologous sequences for *PHO8*, *RIM9*, *CHA1*, *GAL10* and *RIO1* from *S. paradoxus*, *S. mikatae*, *S. bayanus*, *S. kudriavzevii*, *S. castelli* and *S. kluyveri* were taken from Kellis *et al* (2003) and Cliften *et al* (2003). The ORF sequence plus 1000 bp upstream from each yeast species were aligned with the ClustalW2 program (http://www.ebi.ac.uk/Tools/clustalw2/index.html) using the default settings.

Supplementary data

Supplementary data are available at *The EMBO Journal* Online (http://www.embojournal.org).

Acknowledgements

We thank Harm van Bakel, Tim Hughes, Charlie Boone (University of Toronto), Timothy Parnell and Brad Cairns (University of Utah) for sharing data and yeast strains. We also thank Paul Hartley and Hiten Madhani (UCSF) for sharing data, Christina Bech Hertel (University of Munich) for technical advice, Dorothea Blaschke (University of Munich) for technical assistance, Gözde Güçlüler (Izmir Technical Institute) for work on this project during her summer stay as an Amgen Scholar in the group of PK, Mark Ptashne (Sloan Kettering Institute) for sharing data before publication, Axel Imhof (University of Munich) for invaluable advice on mass spectrometry, Gernot Längst for technical and scientific advice and discussions and Peter Becker (University of Munich) for his continuous interest and support. This work was funded by the German Research Community (Deutsche Forschungsgemeinschaft (DFG), Transregio 05 to PK), by the European Community (NET grant within the Network of Excellence The Epigenome to PK) and by the Amgen Foundation (Amgen Scholarship to Gözde Güçlüler). CLP is supported by a grant from NIGMS (GM49650).

Author contributions: CJW designed and performed the vast majority of all experimental work. LI performed LC-MS/MS analysis. SW purified RSC, SWI/SNF and Isw2 complexes in the group of CLP. AH helped with the extract fractionation. PK conceived and supervised the entire study. CJW, CLP and PK wrote the manuscript. This paper is dedicated by CJW to his parents.

Conflict of interest

The authors declare that they have no conflict of interest.

References

Albert I, Mavrich TN, Tomsho LP, Qi J, Zanton SJ, Schuster SC, Pugh BF (2007) Translational and rotational settings of H2A.Z nucleosomes across the *Saccharomyces cerevisiae* genome. *Nature* **446:** 572–576

Almer A, Rudolph H, Hinnen A, Horz W (1986) Removal of positioned nucleosomes from the yeast PHO5 promoter upon PHO5 induction releases additional upstream activating DNA elements. *EMBO J* **5:** 2689–2696

Badis G, Chan ET, van Bakel H, Pena-Castillo L, Tillo D, Tsui K, Carlson CD, Gossett AJ, Hasinoff MJ, Warren CL, Gebbia M, Talukder S, Yang A, Mnaimneh S, Terterov D, Coburn D, Li Yeo A, Yeo ZX, Clarke ND, Lieb JD *et al* (2008) A library of yeast transcription factor motifs reveals a widespread function for Rsc3 in targeting nucleosome exclusion at promoters. *Mol Cell* **32:** 878–887

Barbaric S, Fascher KD, Horz W (1992) Activation of the weakly regulated Ph08 promoter in *Saccharomyces cerevisiae*—chromatin transition and binding-sites for the positive regulatory protein Ph04. *Nucleic Acids Res* **20:** 1031–1038

Basehoar AD, Zanton SJ, Pugh BF (2004) Identification and distinct regulation of yeast TATA box-containing genes. *Cell* **116:** 699–709

Bernstein BE, Liu CL, Humphrey EL, Perlstein EO, Schreiber SL (2004) Global nucleosome occupancy in yeast. *Genome Biol* **5:** R62

Brehm A, Langst G, Kehle J, Clapier CR, Imhof A, Eberharter A, Muller J, Becker PB (2000) dMi-2 and ISWI chromatin remodelling factors have distinct nucleosome binding and mobilization properties. *EMBO J* **19:** 4332–4341

Cairns BR, Erdjument-Bromage H, Tempst P, Winston F, Kornberg RD (1998) Two actin-related proteins are shared functional components of the chromatin-remodeling complexes RSC and SWI/SNF. *Mol Cell* **2:** 639–651

Clapier CR, Cairns BR (2009) The biology of chromatin remodeling complexes. *Annu Rev Biochem* **78:** 273–304

Cliften P, Sudarsanam P, Desikan A, Fulton L, Fulton B, Majors J, Waterston R, Cohen BA, Johnston M (2003) Finding functional features in Saccharomyces genomes by phylogenetic footprinting. *Science* **301:** 71–76

Field Y, Fondufe-Mittendorf Y, Moore IK, Mieczkowski P, Kaplan N, Lubling Y, Lieb JD, Widom J, Segal E (2009) Gene expression divergence in yeast is coupled to evolution of DNA-encoded nucleosome organization. *Nat Genet* **41:** 438–445

Field Y, Kaplan N, Fondufe-Mittendorf Y, Moore IK, Sharon E, Lubling Y, Widom J, Segal E (2008) Distinct modes of regulation by chromatin encoded through nucleosome positioning signals. *PLoS Comput Biol* **4:** e1000216

Flaus A, Owen-Hughes T (2003) Dynamic properties of nucleosomes during thermal and ATP-driven mobilization. *Mol Cell Biol* **23:** 7767–7779

Floer M, Wang X, Prabhu V, Berrozpe G, Narayan S, Spagna D, Alvarez D, Kendall J, Krasnitz A, Stepansky A, Hicks J, Bryant GO, Ptashne M (2010) A RSC/nucleosome complex determines chromatin architecture and facilitates activator binding. *Cell* **141:** 407–418

Ghaemmaghami S, Huh WK, Bower K, Howson RW, Belle A, Dephoure N, O'Shea EK, Weissman JS (2003) Global analysis of protein expression in yeast. *Nature* **425:** 737–741

Gregory PD, Barbaric S, Horz W (1998) Analyzing chromatin structure and transcription factor binding in yeast. *Methods* **15:** 295–302

Hartley PD, Madhani HD (2009) Mechanisms that specify promoter nucleosome location and identity. *Cell* **137:** 445–458

Hertel CB, Langst G, Horz W, Korber P (2005) Nucleosome stability at the yeast PHO5 and PHO8 promoters correlates with differential cofactor requirements for chromatin opening. *Mol Cell Biolo* **25:** 10755–10767

Huh WK, Falvo JV, Gerke LC, Carroll AS, Howson RW, Weissman JS, O'Shea EK (2003) Global analysis of protein localization in budding yeast. *Nature* **425:** 686–691

Ioshikhes IP, Albert I, Zanton SJ, Pugh BF (2006) Nucleosome positions predicted through comparative genomics. *Nature Genet* **38:** 1210–1215

Iyer V, Struhl K (1995) Poly(dA:dT), a ubiquitous promoter element that stimulates transcription via its intrinsic DNA structure. *EMBO J* **14:** 2570–2579

Jiang C, Pugh BF (2009) A compiled and systematic reference map of nucleosome positions across the *Saccharomyces cerevisiae* genome. *Genome Biol* **10:** R109

Kaplan N, Moore IK, Fondufe-Mittendorf Y, Gossett AJ, Tillo D, Field Y, LeProust EM, Hughes TR, Lieb JD, Widom J, Segal E (2009) The DNA-encoded nucleosome organization of a eukaryotic genome. *Nature* **458:** 362–366

Kellis M, Patterson N, Endrizzi M, Birren B, Lander ES (2003) Sequencing and comparison of yeast species to identify genes and regulatory elements. *Nature* **423:** 241–254

Korber P, Becker PB (2010) Nucleosome dynamics and epigenetic stability. *Essays Biochem* **48:** 63–74

Korber P, Horz W (2004) *In vitro* assembly of the characteristic chromatin organization at the yeast PHO5 promoter by a replication-independent extract system. *J Biol Chem* **279:** 35113–35120

Lam FH, Steger DJ, O'Shea EK (2008) Chromatin decouples promoter threshold from dynamic range. *Nature* **453:** 246 -U216

Lantermann AB, Straub T, Stralfors A, Yuan GC, Ekwall K, Korber P (2010) *Schizosaccharomyces pombe* genome-wide nucleosome mapping reveals positioning mechanisms distinct from those of *Saccharomyces cerevisiae*. *Nat Struct Mol Biol* **17:** 251–257

Lee W, Tillo D, Bray N, Morse RH, Davis RW, Hughes TR, Nislow C (2007) A high-resolution atlas of nucleosome occupancy in yeast. *Nat Genet* **39:** 1235–1244

Liu X, Lee CK, Granek JA, Clarke ND, Lieb JD (2006) Whole-genome comparison of Leu3 binding *in vitro* and *in vivo* reveals the importance of nucleosome occupancy in target site selection. *Genome Res* **16:** 1517–1528

Logie C, Tse C, Hansen JC, Peterson CL (1999) The core histone N-terminal domains are required for multiple rounds of catalytic chromatin remodeling by the SWI/SNF and RSC complexes. *Biochemistry* **38:** 2514–2522

Luger K, Mader AW, Richmond RK, Sargent DF, Richmond TJ (1997) Crystal structure of the nucleosome core particle at 2.8 A resolution. *Nature* **389:** 251–260

Mavrich TN, Ioshikhes IP, Venters BJ, Jiang C, Tomsho LP, Qi J, Schuster SC, Albert I, Pugh BF (2008a) A barrier nucleosome model for statistical positioning of nucleosomes throughout the yeast genome. *Genome Res* **18:** 1073–1083

Mavrich TN, Jiang C, Ioshikhes IP, Li X, Venters BJ, Zanton SJ, Tomsho LP, Qi J, Glaser RL, Schuster SC, Gilmour DS, Albert I, Pugh BF (2008b) Nucleosome organization in the Drosophila genome. *Nature* **453:** 358–362

Miura F, Kawaguchi N, Sese J, Toyoda A, Hattori M, Morishita S, Ito T (2006) A large-scale full-length cDNA analysis to explore the budding yeast transcriptome. *Proc Natl Acad Sci USA* **103:** 17846–17851

Moreira JMA, Holmberg S (1999) Transcriptional repression of the yeast CHA1 gene requires the chromatin-remodeling complex RSC. *EMBO J* **18:** 2836–2844

Munsterkotter M, Barbaric S, Horz M (2000) Transcriptional regulation of the yeast PHO8 promoter in comparison to the coregulated PHO5 promoter. *J Biol Chem* **275:** 22678–22685

Ozsolak F, Song JS, Liu XS, Fisher DE (2007) High-throughput mapping of the chromatin structure of human promoters. *Nat Biotechnol* **25:** 244–248

Parnell TJ, Huff JT, Cairns BR (2008) RSC regulates nucleosome positioning at Pol II genes and density at Pol III genes. *EMBO J* **27:** 100–110

Partensky PD, Narlikar GJ (2009) Chromatin remodelers act globally, sequence positions nucleosomes locally. *J Mol Biol* **391:** 12–25

Pham CD, He X, Schnitzler GR (2009) Divergent human remodeling complexes remove nucleosomes from strong positioning sequences. *Nucleic Acids Res* **38:** 400–413

Raisner RM, Hartley PD, Meneghini MD, Bao MZ, Liu CL, Schreiber SL, Rando OJ, Madhani HD (2005) Histone variant H2A.Z marks the 5′ ends of both active and inactive genes in euchromatin. *Cell* **123:** 233–248

Rippe K, Schrader A, Riede P, Strohner R, Lehmann E, Langst G (2007) DNA sequence- and conformation-directed positioning of nucleosomes by chromatin-remodeling complexes. *Proc Natl Acad Sci USA* **104:** 15635–15640

Satchwell SC, Drew HR, Travers AA (1986) Sequence periodicities in chicken nucleosome core DNA. *J Mol Biol* **191:** 659–675

Schnitzler GR (2008) Control of nucleosome positions by DNA sequence and remodeling machines. *Cell Biochem Biophys* **51:** 67–80

Schones DE, Cui KR, Cuddapah S, Roh TY, Barski A, Wang ZB, Wei G, Zhao KJ (2008) Dynamic regulation of nucleosome positioning in the human genome. *Cell* **132:** 887–898

Segal E, Fondufe-Mittendorf Y, Chen LY, Thastrom A, Field Y, Moore IK, Wang JPZ, Widom J (2006) A genomic code for nucleosome positioning. *Nature* **442:** 772–778

Segal E, Widom J (2009) What controls nucleosome positions? *Trends Genet* **25:** 335–343

Shivaswamy S, Bhinge A, Zhao Y, Jones S, Hirst M, Iyer VR (2008) Dynamic remodeling of individual nucleosomes across a eukaryotic genome in response to transcriptional perturbation. *PLoS Biol* **6:** e65

Simpson RT (1990) Nucleosome positioning can affect the function of a Cis-acting DNA element *invivo*. *Nature* **343:** 387–389

Simpson RT, Shindo H (1979) Conformation of DNA in chromatin core particles containing poly(dAdT)-poly(dAdT) studied by 31 P NMR spectroscopy. *Nucleic Acids Res* **7:** 481–492

Smith CL, Horowitz-Scherer R, Flanagan JF, Woodcock CL, Peterson CL (2003) Structural analysis of the yeast SWI/SNF chromatin remodeling complex. *Nat Struct Biol* **10:** 141–145

Tirosh I, Sigal N, Barkai N (2010) Widespread remodeling of mid-coding sequence nucleosomes by Isw1. *Genome Biol* **11:** R49

Travers A, Caserta M, Churcher M, Hiriart E, Di Mauro E (2009) Nucleosome positioning-what do we really know? *Mol Biosyst* **5:** 1582–1592

Tsankov AM, Thompson DA, Socha A, Regev A, Rando OJ (2010) The role of nucleosome positioning in the evolution of gene regulation. *PLoS Biol* **8:** e1000414

Valouev A, Ichikawa J, Tonthat T, Stuart J, Ranade S, Peckham H, Zeng K, Malek JA, Costa G, McKernan K, Sidow A, Fire A, Johnson SM (2008) A high-resolution, nucleosome position map of *C. elegans* reveals a lack of universal sequence-dictated positioning. *Genome Res* **18:** 1051–1063

Venter U, Svaren J, Schmitz J, Schmid A, Horz W (1994) A nucleosome precludes binding of the transcription factor Pho4 *in vivo* to a critical target site in the PHO5 promoter. *EMBO J* **13:** 4848–4855

Venters BJ, Pugh BF (2009) A canonical promoter organization of the transcription machinery and its regulators in the Saccharomyces genome. *Genome Res* **19:** 360–371

Whitehouse I, Rando OJ, Delrow J, Tsukiyama T (2007) Chromatin remodelling at promoters suppresses antisense transcription. *Nature* **450:** 1031–U1033

Widom J (2001) Role of DNA sequence in nucleosome stability and dynamics. *Q Rev Biophys* **34:** 269–324

Wippo CJ, Krstulovic BS, Ertel F, Musladin S, Blaschke D, Sturzl S, Yuan GC, Horz W, Korber P, Barbaric S (2009) Differential cofactor requirements for histone eviction from two nucleosomes at the yeast PHO84 promoter are determined by intrinsic nucleosome stability. *Mol Cell Biol* **29:** 2960–2981

Yuan GC, Liu YJ, Dion MF, Slack MD, Wu LF, Altschuler SJ, Rando OJ (2005) Genome-scale identification of nucleosome positions in *S.cerevisiae*. *Science* **309:** 626–630

Zhang Y, Moqtaderi Z, Rattner BP, Euskirchen G, Snyder M, Kadonaga JT, Liu XS, Struhl K (2009) Intrinsic histone-DNA interactions are not the major determinant of nucleosome positions *in vivo*. *Nat Struct Mol Biol* **16:** 847–852

Zhang Y, Smith CL, Saha A, Grill SW, Mihardja S, Smith SB, Cairns BR, Peterson CL, Bustamante C (2006) DNA translocation and loop formation mechanism of chromatin remodeling by SWI/SNF and RSC. *Mol Cell* **24:** 559–568

In vitro reconstitution of *in vivo*-like nucleosome positioning on yeast DNA

Christian J. Wippo and Philipp Korber*

Adolf-Butenandt-Institut, Molecular Biology Unit, University of Munich, Schillerstrasse 42, 80336 Munich, Germany

*corresponding author: +49-89-218075435 phone, +49-89-218075425 fax, pkorber@lmu.de

Summary/Abstract:
Genome-wide nucleosome mapping *in vivo* highlighted the extensive degree of well defined nucleosome positioning. Such positioned nucleosomes, especially in promoter regions, control access to DNA and constitute an important level of genome regulation. However, the molecular mechanisms that lead to nucleosome positioning are far from understood. In order to dissect this mechanism in detail with biochemical tools, an *in vitro* system is necessary that can generate proper nucleosome positioning *de novo*. We present a protocol that allows the assembly of nucleosomes with very much *in vivo*-like positioning on budding yeast DNA, either of single loci or of the whole-genome. Our method combines salt gradient dialysis and incubation with yeast extract in the presence of ATP. It provides an invaluable tool for the study of nucleosome positioning mechanisms, and can be used to assess the relative stability of properly positioned nucleosomes. It may also generate more physiological templates for *in vitro* studies of, e.g., nucleosome remodeling or transcription through chromatin.

Keywords:
nucleosome positioning, *in vitro* reconstitution, *S. cerevisiae*, yeast extract, salt gradient dialysis

1. Introduction

The majority of nucleosomes are non-randomly but rather well positioned *in vivo*, which regulates the access to functional DNA sites in eukaryotic genomes (*1-3*). This prominent level of genome regulation was recently underscored by genome-wide nucleosome maps for many organisms (*4-9*). However, we know rather little about the molecular determinants for this primary order of chromatin. In order to understand the molecular mechanisms of nucleosome positioning, a cell-free *in vitro* system is necessary that allows generating *in vivo*-like nucleosome positioning *de novo*.

Classically, nucleosomes are reconstituted *in vitro* via salt dialysis (*10-12*) where histones and DNA are initally mixed at high salt concentration, which is step-wise or gradually dialyzed away such that nucleosomes form on DNA. This technique has been used extensively to probe intrinsic DNA-sequence preferences for nucleosome formation (*13;14*), and the thus generated nucleosome occupancy (= probability of a given base pair to be in any nucleosome (*2*)) distribution may in some cases correlate reasonably well with *in vivo* distributions (*15;16*). However, *in vitro* reconstitution of sheared genomic yeast DNA by salt gradient dialysis could not recapitulate the majority of *in vivo* nucleosome positions (= defined position of a particular nucleosome relative to a given base pair) (*15-18*). Therefore it is common practice to resort to special "nucleosome positioning sequences", e.g. Sea Urchin 5S rDNA (*19*), satellite DNA (*20*), or the *in vitro* selected "601" sequence (*21*), as templates for salt gradient dialysis assembly if *in vitro* assays require well positioned nucleosomes.

Several chromatin assembly systems based on extracts or purified histone chaperones with or without ATP-dependent remodeling enzymes are available (*22*). In the presence of ATP they are especially powerful in generating extensive nucleosomal arrays with physiological spacing, but they usually do not achieve nucleosome positioning, apart from some cases where sequence specific DNA-binding factors were added (*23;24*).

Based on the pioneering work in the group of Michael Schultz who used yeast extracts for chromatin assembly *in vitro* (*25-27*), we established an *in vitro* chromatin reconstitution system that is able to generate *in vivo*-like nucleosome positioning on yeast DNA sequences (*28;29*). In a first step, nucleosomes are preassembled onto plasmid DNA by classical salt gradient dialysis. In a second step, these chromatin templates are incubated with a yeast whole cell extract in the presence of ATP to induce proper positioning (Figure 1). Very recently we showed that our method can be applied to yeast whole-genome plasmid libraries and combined with high-throughput sequencing (*30*). This allows to study genome-wide nucleosome positioning mechanisms *in vitro*.

If different nucleosome positions, either on the same template or on different templates present in the same reconstitution reaction, are compared between conditions of saturating and limiting histone concentrations, it is possible to assess the relative stability of these positioned nucleosomes (*28;29*). As defined by this assay, a nucleosome that remains properly positioned at sub-saturating histone concentrations is more stably positioned than a nucleosome that requires high assembly degrees for proper positioning.

Chromatin with *in vivo*-like nucleosome positioning as assembled by the here described method may be used as template for *in vitro* nucleosome remodeling (*31*) or transcription assays. However, if purified chromatin templates are required it is not trivial and remains to be established how the factors from the whole cell extract (WCE) can be removed without perturbation of nucleosome positioning. Nonetheless, WCEs prepared from mutants or that are immunodepleted may be used in order to assess the role of factors of interest in downstream assays.

2. Materials

2.1 Preparation of yeast whole cell extract

1. Yeast strain, e.g. BY4741, or any mutant of interest. For wt extracts we successfully used household baker's yeast from a convenience store. Huge amounts of extract can be prepared this way at very low cost.
2. Extraction buffer without protease inhibitor: 200 mM HEPES-KOH, pH 7.5, 10 mM $MgSO_4$, 10 % glycerol, 1 mM EDTA, 390 mM $(NH_4)_2SO_4$, 1 mM freshly added DTT
3. Extraction buffer with protease inhibitor:as above, with 1x Complete™ (Roche Applied Science) or equivalent protease inhibitors
4. Cold spatula
5. 5 or 10 ml plastic syringe with cut off nozzle
6. 100 and 600 ml plastic beaker
7. 250 and 50 ml conical tube
8. Liquid nitrogen
9. Porcelain mortar and pestle
10. Clear ultracentrifuge tubes (Beckman Ultra-Clear™ tubes or equivalent)
11. Cold mineral oil
12. Beckman Optima LE-80k ultracentrifuge, or equivalent
13. 5 ml plastic syringe with rubber seal plunger; syringe needle, e.g. 1.1 x 40 mm
14. Beckman Optima MAX-E ultracentrifuge with TLA55 rotor and Microfuge® Polyallomer tubes, or equivalent
15. Ammonium sulfate (solid)
16. Disposable inoculation loops
17. Rotating wheel in coldroom
18. Dialysis buffer: 20 mM HEPES-KOH, pH 7.5, 80 mM KCl, 10% glycerol, 1 mM EGTA and freshly added 5 mM DTT, 0.1 mM phenylmethylsulfonyl fluoride (PMSF) and 1 mM sodium metabisulfite
19. Dialysis tubing (MWCO 3.5 kDa)

2.2 Chromatin assembly by salt gradient dialysis
1. Template DNA. The DNA of your region of interest, usually in the context of a plasmid backbone. Several plasmids or even a whole-genome plasmid library may be used for a single reconstitution reaction. Prepare by using a Qiagen (or similar) plasmid preparation kit according to manufacturer's directions. Store DNA preparation in TE buffer (10 mM Tris-HCl, pH 8.0, 1 mM EDTA). We do not have much experience with linear templates, but it is usually more difficult to achieve high nucleosome assembly degrees on linear than on supercoiled templates (*32*).
2. Histones. *Drosophila* embryo histones (*33*) or recombinant *Drosophila*, *Xenopus* or yeast histones (*12*) (see Note 1). Histones are typically stored in 1 M NaCl, 50% glycerol, 5 mM DTT, 1x Complete™ (Roche Applied Science) or equivalent protease inhibitors at -20 °C.
3. ß-mercaptoethanol
4. Low Salt Buffer: 10 mM Tris-HCl, pH 7.6, 50 mM NaCl, 1 mM EDTA, 0.05% Igepal CA630, prepare as 20x stock
5. High Salt Buffer: 10 mM Tris-HCl, pH 7.6, 2 M NaCl, 1 mM EDTA, 0.05% Igepal CA630, prepare as 2x stock
6. Magnetic stirrer and large (e.g., 4 cm) stir bar
7. Peristaltic pump
8. Siliconized 1.5 ml tubes
9. Dialysis tubing (MWCO 3.5 kDa)
10. Two 3 l plastic beakers; small, e.g. 100 ml, beaker
11. Drawn out Pasteur pipets
12. Floater for 1.5 ml tubes
13. Bovine serum albumin (BSA) 5 mg/ml in water

2.3 Proper nucleosome positioning upon incubation with WCE and ATP
1. Block solution: 2 mg/ml BSA, 0.1% Igepal CA630, 20 mM HEPES-KOH, pH 7.5
2. Creatine kinase (CK): dissolve the lyophilized CK powder in 0.1 M imidazole-HCl, pH 6.6 at 20 mg/ml, and flash freeze in liquid nitrogen as 20 µl aliquots, store at -80 °C (see Note 2)
3. 0.1 M imidazole-HCl, pH 6.6
4. 0.25 M ammonium sulfate
5. 4x reconstitution mix: 80 mM HEPES-KOH, pH 7.5, 320 mM KCl, 12 mM $MgCl_2$, 2 mM EGTA, 10 mM DTT, 48 % glycerol, 12 mM ATP, 120 mM creatine phosphate, can be stored at -20°C, for conditions without energy, omit ATP, $MgCl_2$, and creatine phosphate (see Note 3).

2.4 Chromatin digestion with DNaseI, MNase or restriction enzymes
1. Proteinase K: 20 mg/ml in ddH_2O
2. Glycogen 20 mg/ml in ddH_2O
3. 50 U/ml apyrase (e.g. NEB M0393L) in ddH_2O
4. DNaseI (e.g. 04716728001; Roche Applied Science)
5. MNase: resuspend MNase (e.g. N5386; Sigma) in Ex50 buffer (10 mM HEPES-KOH pH 7.6, 50 mM NaCl, 1.5 mM $MgCl_2$, 0.5 mM EGTA, 10% (v/v) glycerol, 1 mM DTT and 0.2 mM PMSF) for example at 1 U/µl.
6. Appropriate restriction enzymes can be obtained from any manufacturer. It is usually advantageous to use the highest available concentrations.
7. DNaseI digestion buffer: 20 mM HEPES-KOH, pH 7.5, 80 mM NaCl, 12% glycerol, 5.5 mM $MgCl_2$, 5.5 mM $CaCl_2$, 2.5 mM DTT, 0.1 mg/ml BSA
8. DNaseI solutions: Dilute DNaseI with DNaseI digestion buffer to concentrations in the range of 0.005 to 0.02 U/ml (free DNA), 0.02 to 0.1 U/ml (salt gradient dialysis chromatin), or 2 to 10 U/ml (salt gradient dialysis chromatin with WCE). These DNaseI solutions are freshly prepared on ice and not stored.
9. Stop buffer: 10 mM EDTA, 4% sodium dodecyl sulfate
10. Restriction enzyme digestion buffer: 20 mM HEPES-KOH, pH 7.5, 4.5 mM $MgCl_2$, 2.5 mM DTT, 80 mM NaCl, 0.5 mM EGTA
11. Sheared salmon sperm DNA: salmon sperm DNA is dissolved in TE buffer (10 mM Tris-HCl, pH 8.0, 1 mM EDTA) at 25 mg/ml and sheared by sonication such that a mixture of DNA fragments in the range of 300 bp to several kb is generated. Store at -20 °C.
12. Orange G or Bromophenol blue loading dye: 40% (w/v) sucrose, 10 mM Tris-HCl, pH 8.0, 0.25% Orange G or bromopehnol blue, respectively.

3. Methods
3.1 Preparation of yeast whole cell extract
1. Grow 2-6 l of mid log phase yeast culture, harvest (30 min, 6000g, 4°C, 1 l centrifuge bottles), wash (use 50 ml of icecold water per 1 l of yeast culture to combine pellets in 250 ml conical bottom centrifuge tube), centrifuge again (15 min, 6000g, 4°C).

2. For buffer exchange, resuspend the washed cell pellet in 20 ml extraction buffer without protease inhibitor per 1 l of culture, collect cells (10 min, 6000g, 4°C), and resuspend in 10 ml extraction buffer with protease inhibitor per 1 l of culture, collect cells (4 min, 6000g, 4°C).
3. Determine wet cell weight (usually 1-2 g per 1 l of culture).
4. Scrape cell pellet with cold spatula into cold 5 or 10 ml syringe with cut off nozzle.
5. Cover a 600 ml plastic beaker with aluminum foil and poke a 50 ml conical tube through the foil such that it can stand upright in the beaker. Fill about 200 ml liquid nitrogen into the beaker and about 20 ml into the conical tube (see Note 4).
6. Extrude cell pellet with syringe into the liquid nitrogen in the conical tube, such that it looks like "frozen spaghetti". Carefully (see Note 4) pour off the liquid nitrogen without losing the cell pellet material, or let the nitrogen evaporate away. The frozen spaghetti may be stored at -80 °C.
7. Fill porcelain mortar (see Note 5) repeatedly with liquid nitrogen until the mortar is cooled down enough to keep the liquid nitrogen for a while. Have plenty of liquid nitrogen in a Dewar at hand for repletion during grinding.
8. Add the frozen spaghetti into the liquid nitrogen in the mortar and carefully start to crush them into small pieces with the pestle. Grind the frozen cell material carefully (avoid spills), but forcefully, as this is the only cell lysis step, for 45 minutes. Always replenish liquid nitrogen shortly after it is all evaporated. This is somewhat hard work, but can be interrupted at any moment by storing mortar with pestel and cell powder at – 80 °C. After about 20 min of grinding, add 0.4 ml extraction buffer with protease inhibitor per gram wet cell mass. The resultant ice particles are very crunchy and help with the lysis during the grinding. In the end this will generate a very fine powder.
9. Let all liquid nitrogen evaporate and scrape powder into 100 ml beaker. Let warm quickly at room temperature under continuous stirring with a metal spatula until the powder turns into a thick paste (see Note 6). Place on ice immediately to avoid warming beyond 0 °C.
10. Scrape paste into pre-cooled Ultra-Clear™ or equivalent tubes. If necessary, top off with cold mineral oil in order to fill the tube sufficiently and avoid tube collapse during ultracentrifugation.
11. Spin in SW56Ti rotor or equivalent for 2 h at 28000 rpm (80000 g average) and 4 °C with brake on.
12. Preform a hole into the ice of your ice bucket using an empty SW56 centrifuge tube and put there the sample tube after the ultracentrifugation. Be careful not to disturb the phase separation in the tube. There are four different phases now: i) the compact pellet of cell debris at the bottom, ii) a cloudy yellowish layer on top, which fades into a iii) clear supernatant, and finally a iv) whitish lipid rich top phase at the meniscus.
13. Using a precooled 5 ml syringe with needle (a rubber seal instead of all plastic plunger facilitates gentle suction) carefully remove the middle part of the clear supernatant (see above iii) by poking the needle through the lipid top layer. Avoid as much of the yellowish cloudy layer (ii) as possible, but usually it is not possible to avoid all of it (see Note 7). Transfer the withdrawn lysate into Microfuge® Polyallomer TLA55 or equivalent tubes on ice.
14. Determine the volume of the lysate with a pipet.
15. Grind ammonium sulfate into a fine powder and add in small portions 337 mg per ml of lysate; it may help to use a small funnel folded from a piece of paper. After each addition, mix with innoculation loop and place on rotating wheel at 4 °C. Avoid foam generation. After all the ammonium sulfate has dissolved (check if you still see tiny crystals sinking to the tube bottom when holding it against the light) rotate tubes for an additional 30 minutes.
16. Spin the solution in TLA55 rotor for 20 min at 25700 rpm (32000 g average) and 4 °C.
17. Carefully withdraw the supernatant with a cold 5 ml syringe and needle and discard it.
18. Redissolve the pellet in 0.5 to 1 ml of dialysis buffer per g wet cell mass, depending on how well it dissolves and how concentrated the final extract shall be. Again, twirling with an inoculation loop helps.
19. Transfer the solution into a dialysis tube and dialyse twice for 1.5 hours against 40 to 50 fold excess volume of dialysis buffer.
20. Remove dialyzed extract, flash freeze 50-1000 µl aliquots in liquid nitrogen, and store at -80 °C. The nucleosome positioning activity tolerates at least two freeze-thaw cycles. Such extracts usually retain their nucleosome positioning activity for at least 2 years (see Note 8).

3.2 Chromatin assembly by salt gradient dialysis

3.2.1. Pump and beakers:
1. Set up the salt dialysis apparatus in a hood as high concentrations of ß-mercaptoethanol are used.
2. Fill one 3 l beaker with 3 l of 1x Low Salt Buffer and another 3 l beaker with 300 ml 1x High Salt Buffer. Add 300 µl ß-mercaptoethanol to the beaker with Low Salt Buffer and mix well.
3. Place the beaker with High Salt Buffer on a magnetic stirrer and add a large stir bar.
4. Set up the peristaltic pump and place into each of the 3 l beakers one end of the tube. Fix the tube at each 3 l beaker with tape such that the tube cannot slide off. Make sure that the tube end in the beaker with the Low Salt Buffer is situated at the bottom of the beaker such that all buffer can be pumped out.

3.2.2. Dialysis mini chamber:
1. Cut off the end of a siliconised 1.5 ml tube, just above the 0.5 ml mark.
2. Using pointed scissors, puncture the thin center part of the tube lid that is circumscribed by the elevated edge that fits into the tube upon closing the lid, and scrape out the plastic up to the elevated edge. Basically, you generate a lid with a hole of about 0.8 cm diameter. Make sure not to generate sharp edges that could puncture or rip the dialysis membrane later on.
3. Cut off the thus perforated lid from the previously truncated tube.
4. Cut off about 1.5 to 2 cm of dialysis tubing and place in a small beaker filled with ddH_2O for about 10 minutes. Cut the tubing open at one side so that the dialysis membrane can be folded open as a single layer.
5. Place the perforated lid top down onto a sheet of cling film, which serves as a convenient and clean surface to prepare the dialysis mini chamber. Place the dialysis membrane centered on top of the lid. Press the truncated siliconised tube with its top over the dialysis membrane onto the lid such that the

membrane becomes wedged in between lid and tube like a drumhead (see Note 9). Cut away most of the excess membrane sticking outwards from the tube.
6. Use the floater to let the dialysis mini chamber float on top of the High Salt Buffer in the 3 l beaker with lid and membrane facing downwards and the truncated tube facing upwards. Airbubbles right underneath the membrane have to be removed. It is convenient to suck away the bubbles with a drawn out Pasteur pipet that has been bent twice into a U-shape over a Bunsen burner flame.

3.2.3. Samples:
Combine 10 µg plasmid DNA (see Note 10), 20 µg BSA and variable amounts of histones (see Note 11), 50 µl 2x High Salt Buffer and ddH_2O to make up 100 µl. Mix thoroughly by pipetting and avoid foam generation.
3.2.4. Salt gradient dialysis:
1. Pipet samples through the open end of the floating dialysis mini chamber onto the membrane. Be careful not to damage the membrane with the pipet tip!
2. Adjust magnetic stirrer underneath the High Salt Buffer beaker such that slow mixing is achieved without compromising easy floating of the dialysis mini chambers.
3. Add 300 µl ß-mercaptoethanol to the High Salt Buffer beaker and cover the beaker with cling film. Make sure, e.g. by using tape or placing a heavy glass plate on top, that the beaker is properly sealed (see Note 12).
4. Set speed of peristaltic pump such that all of the 3 l Low Salt Buffer will be pumped into the High Salt Buffer over the course of at least 15 hours. A trial run with water and without samples is advisable to determine the right pump speed.
5. After complete transfer of the Low Salt Buffer, transfer the floater with the dialysis mini chambers to a jug with 1 l fresh Low Salt Buffer plus 300 µl ß-mercaptoethanol. Remove again air bubbles from underneath the membranes.
6. Dialyse for 1 to 2 h with slow stirring to ensure complete buffer exchange.
7. Transfer the samples with a pipet from the dialysis mini chambers into fresh siliconized 1.5 ml tubes and determine the volume with the pipet. The volume usually increases to 120 to 130 µl. The salt gradient dialysed chromatin samples can be stored at 4 °C for several weeks up to a few months.

3.3 Proper nucleosome positioning upon incubation with WCE and ATP
1. Block siliconised 1.5 ml tubes by pipetting 1 ml block solution into and out of the tubes. The block solution can be reused many times. Collect remaining solution in the tubes by short centrifugation in table top centrifuge, remove the last droplet with yellow tip and let the tubes air dry. Such blocked tubes can be prepared in large quantities beforehand and stored indefinitely.
2. Prepare a fresh 1:20 dilution of CK by adding 380 µl 0.1 M imidazole buffer to a freshly thawed 20 µl CK aliquot (see Note 2). Mix by pipetting and keep on ice.
3. Spin down salt gradient dialysis chromatin and thawed WCE for 3 min at full speed in a cooled table top centrifuge to avoid carryover of aggregates. Especially the WCE usually shows a visible pellet. In this case avoid disturbance of the pellet when taking out aliquots.
4. Combine 25 µl 4x reconstitution mix, 4 µl 0.25 M ammonium sulfate, 2 µl CK 1:20 dilution, salt gradient dialysis chromatin corresponding to 0.5 to 1 µg of preassembled DNA, 10 µl of WCE (if the protein content is about 20 mg/ml, see Note 8) and ddH_2O to make up a volume of 100 µl (see Note 13). Start with water, 4x reconstitution mix, and ammonium sulfate, all three of which can be combined to a master mix if several reactions are done in parallel. If called for, any purified component, e.g. the transcription factor Pho4 or a remodeling enzyme (*31*), may be added.
5. Incubate for 2 h at 30°C. 1h can be sufficient (*28*) and the incubation can even be extended overnight.
6. Analyze chromatin by your favorite assay. As an example we describe briefly the digestion with DNaseI or restriction enzymes for indirect end-labeling analysis and the generation of MNase ladders.

3.4 Chromatin digestion with DNaseI, MNase,or restriction enzymes
(See also (*34*) for a detailed description of these methods.)
1. For DNaseI digestion, add 25 µl aliquots of a 100 µl reconstitution reaction to 25 µl of DNaseI solutions with appropriate DNaseI concentrations (see Note 14) , incubate for exactly 5 minutes at room temperature, and stop the digest with 10 µl Stop buffer.
2. For restriction enzyme digestion, ATP must be removed by the addition of 0.1 U apyrase per 100 µl reconstitution reaction and incubation for 30 min at 30 °C (see Note 3 and 14). One to two microliter aliquots of such an ATP-depleted reconstitution reaction are mixed with 30 µl of restriction enzyme digestion buffer and treated with various amounts of selected restriction enzymes (see Note 15) for 2 hours at 37 °C. Stop digest with 7.5 µl Stop buffer.
3. For both types of nuclease digestion, the DNA is deproteinized by addition of 0.06 µl proteinase K per µl digestion reaction together with 1 µl glycogen (as carrier for precipitation) and incubation at 37 °C over night, precipitated with ethanol, resuspended in TE buffer, digested with an restriction enzyme appropriate for secondary cleavage (see Note 16), again ethanol precipitated, and resuspended in TE buffer.
4. Southern blot and hybridization of the DNA is described elsewhere (*35*). For examples of plasmid-borne yeast loci reconstituted by the here described method see Figure 2.
5. For the generation of MNase ladders, MNase is used instead of DNaseI in the above protocol of Step 1. Higher degrees of digestion are chosen, and the secondary cleavage step is omitted. The resulting purified DNA samples are electrophoresed in 1.3% agarose gels with Orange G as loading dye (Bromphenol blue migrates close to the dinucleosomal band and may confound the pattern). As MNase may cut at several sites within the linker DNA, there will not be clearly defined fragment sizes but rather fuzzy bands. Include ethidium bromide in the gel for sharper appearance of the bands. Note that MNase will “trim” towards the nucleosome cores, i.e., the fragment sizes will get somewhat shorter with increasing MNase concentrations. Include a suitable size marker, e.g., the 123 bp ladder (Invitrogen) or the 100 bp ladder (NEB).

4. Notes

1. Histones are very sticky proteins. Use siliconized (and maybe even blocked, see 3.3.1) tubes. As many others, we noted that recombinant yeast histones are more difficult to work with, i.e., it is more difficult to achieve high assembly degrees and proper positioning of tricky loci like at the yeast *PHO5* promoter (*31*).

2. Prepare CK-dilution freshly before use and always use a fresh aliquot! Do not refreeze!

3. The concentration of ATP may be determined using a luciferase-based essay, e.g., Enliten, Promega, FF2021, in connection with a Berthold Lumat luminometer. Attention: This assay is very sensitive and therefore easily saturated. Measure serial tenfold dilutions (up to 10^{-6}) in water in order to find the actual working range of the assay. The high dilutions will also slow down ATPases from further depleting ATP if you are interested in the ATP concentration at a particular point in your procedure.

4. Careful with liquid nitrogen! Wear safety glasses and insulating gloves.

5. Alternatively, we use an electric mortar (Retsch RM100). Fill the electric mortar with liquid nitrogen and close lid with pestle. After most of the liquid nitrogen has evaporated, open the lid and refill the mortar with liquid nitrogen. Immediately add the "frozen spaghetti", close lid and start grinding at pestel setting of one ("1"). After all of the spaghetti fragments have been ground into a powder add the appropriate amount of extraction buffer. Subsequently, increase pestle setting to ~5.5. Keep grinding at this setting for ~8-10 minutes (assuming 10 g of wet weight material as input, shorter grinding for less material). Refill mortar with nitrogen through the small window at the top of the mortar each time shortly after its evaporation.

6. In our view it is a common misconception that sensitive biological samples should be flash frozen, but slowly thawed on ice. As thawing is the reversal of freezing it should also be fast, e.g., at room temperature, but “to point”, i.e., don’t let the sample get warmer than 0 °C.

7. It is possible to re-centrifuge after this step to allow better phase separation. But this is usually not necessary.

8. Our yeast extracts usually contain 10-30 mg/ml protein as assayed by Bradford assay with BSA as standard. Of these we usually take 5-15 µl per nucleosome positioning reaction. In contrast to the histone:DNA mass ratio (see Note 11), the amount of extract per nucleosome positioning reaction is much less critical, i.e. variation by a factor of 2 or 0.5 usually has hardly any effect. Nonetheless, too much extract will lead to chromatin aggregation. We routinely adjust our extracts with dialysis buffer to 50 mg protein per ml according to nanodrop reading at 280 nm and use 10 µl per nucleosome positioning reaction. This usually corresponds to a protein concentration of ~20 mg/ml as measured by Bradford assay. The nanodrop reading will be somewhat confounded by varying amounts of nucleic acids, especially RNA. Nonetheless, this procedure works just fine as a quick measure for how much extract to use per nucleosome positioning reaction.
Very recently, we showed that WCE fractions may be used as well in order to identify involved factors (*36*).

9. It is important that the membrane is tightly sealed between lid and tube and that the membrane surface is tense and smooth. Otherwise the dialysis mini chamber may be leaky. If several dialysis mini chambers are prepared at the same time, make sure that the membranes do not dry out at any point. You can make a small puddle of ddH_2O onto the cling film and store there the dialysis mini chambers lid-down, which will keep the membranes wet. Do not allow any water into the dialysis chamber as this will dilute your sample.

10. Mixtures of plasmids and even a whole-genome library (*30*) are also possible, but requires increasingly more material or more sensitive methods to analyse the chromatin structure at loci of interest. As formation of a nucleosome corresponds to about one negative supercoil (*37*), nucleosome reconstitution is more efficient on supercoiled plasmids (*38*).

11. The histone:DNA ratio is probably the most crucial parameter for the reconstitution of *in vivo*-like nucleosome positioning by this method as well as for other chromatin reconstitution protocols (*22;39*). Ideally, a physiological mass ratio of 1:1 should be achieved. In practice, one should aim at as high an assembly degree as possible without aggregation of the chromatin and without packing the nucleosomes too tightly such that they will be refractory to ATP-dependent remodeling. Aggregation can be tested by MNase ladders analysis as it will result in an increasing amount of undigestible material and less signal within the lane. The assembly degree can be estimated also via topology assay (*30*) if the template is a plasmid that is not too large for separation of topoisomers in agarose gels. Fully assembled chromatin usually has a similar degree of superhelicity as the plasmid prepared from *E. coli* (*39*). A more direct and functional read out with regard to nucleosome positioning is indirect end-labeling of a locus of interest. Both too low (*28*) and too high (Längst, G., Wippo, C.J., Ertel, F. and Korber, P., unpublished observation) degrees of assembly can interfere with the proper repositioning of nucleosomes upon incubation of salt gradient dialysis chromatin with WCE and ATP. In summary, the optimal assembly degree is difficult to be calculated from measured concentrations of DNA and histones, but usually found by careful and repeated titration using the mentioned assays as read out. The estimation of DNA and histone concentration, e.g., spectrophotometrically or by comparing band intensities on gels to standard samples, serves as an initial reference point to set up assembly reactions with histone:DNA mass ratios in the range of 0.5 to 2.0. We keep the DNA concentration constant and vary the histone concentration. Titrate in histones until you see overassembly by the assays mentioned above, then go back again to lower mass ratios and perform more assemblies with more and more finely varied mass ratios until the best ratio for the desired application is found. Importantly, this kind of titration has to be repeated for each new preparation of histones.

Prokaryotic DNA has an intrinsically lower propensity to be incorporated into nucleosomes (*16*). Therefore including prokaryotic DNA, either in *cis* as part of the vector backbone or in *trans*, may serve as buffer for excess histones regarding the eukaryotic DNA fraction. The assembly of prokaryotic competitor DNA as monitored in native agarose gel electrophoresis can be used as indicator for full assembly of eukaryotic or other high affinity target DNA as described elsewhere (*40*).

12. As this is in the hood and runs overnight, the sample volume decreases substantially due to evaporation if the beaker is not covered.

13. Addition of protease inhibitors is usually not necessary. We compared reconstitution reactions with and without inhibitors several times and never saw a difference in our assays. Nonetheless, depending on the application and readout adding protease inhibitors may become advisable.

14. Indirect end-labeling requires that each template has on average only one double strand cut in the region of interest. Typical DNaseI concentrations are given in the Materials section. One should always do several (typically three) different concentrations in parallel in order to catch a proper degree of digestion. Due to the single-cut limit digestion regime, DNaseI indirect end-labeling corresponds to a snap shot of the time and population average chromatin structure. This is why ATP - and concomittantly remodeling activty - need not be removed prior to digestion. In contrast, if remodeling enzymes are active during the exhaustive restriction enzyme digest, they will continuously generate windows of opportunity for DNA cleavage and the irreversibly cut DNA templates will accumulate over time resulting in apparent high accessibility, even though on time and population average the respective cutting site may be covered by a nucleosome (*41*).

15. The easiest way to ensure that the restriction enzyme digest was complete is to compare two different, e.g. fourfold, restriction enzyme concentrations, which should yield roughly the same accessibility value (*34*).

16. The gel will have to resolve the fragments resulting from the nuclease cuts in your region of interest in combination with the secondary cleavage (*34*). So the secondary cleavage site has to be chosen such that resulting fragments are within the resolution of the gel, and, of course, the restriction enzyme for secondary cleavage must not cut within the region of interest. Typically, for 1.5 % TAE agarose gels, the secondary cleavage site is about 0.7 to 1.2 kb up- or downstream of the region of interest.

Acknowledgements

Work in our laboratory is funded by the German Research Community (DFG, grant within the SFB/Transregio 5) and through the 6th Framework Programme of the European Community (NET grant within the Network of Excellence The Epigenome). We thank Nils Krietenstein for critical reading of the manuscript. This paper is dedicated to the memory of Eduard Buchner, who founded biochemistry by demonstrating the power of yeast extracts.

References

1. Radman-Livaja, M. and Rando, O. J. (2010) Nucleosome positioning: how is it established, and why does it matter? *Dev. Biol. 339*, 258-266.
2. Segal, E. and Widom, J. (2009) What controls nucleosome positions? *Trends Genet. 25*, 335-343.
3. Jiang, C. and Pugh, B. F. (2009) Nucleosome positioning and gene regulation: advances through genomics *Nat. Rev. Genet. 10*, 161-172.
4. Yuan, G. C., Liu, Y. J., Dion, M. F., Slack, M. D., Wu, L. F., Altschuler, S. J., and Rando, O. J. (2005) Genome-scale identification of nucleosome positions in S. cerevisiae *Science 309*, 626-630.
5. Mavrich, T. N., Jiang, C., Ioshikhes, I. P., Li, X., Venters, B. J., Zanton, S. J., Tomsho, L. P., Qi, J., Glaser, R. L., Schuster, S. C., Gilmour, D. S., Albert, I., and Pugh, B. F. (2008) Nucleosome organization in the Drosophila genome *Nature 453*, 358-362.
6. Valouev, A., Ichikawa, J., Tonthat, T., Stuart, J., Ranade, S., Peckham, H., Zeng, K., Malek, J. A., Costa, G., McKernan, K., Sidow, A., Fire, A., and Johnson, S. M. (2008) A high-resolution, nucleosome position map of C. elegans reveals a lack of universal sequence-dictated positioning *Genome Res. 18*, 1051-1063.
7. Schones, D. E., Cui, K., Cuddapah, S., Roh, T. Y., Barski, A., Wang, Z., Wei, G., and Zhao, K. (2008) Dynamic regulation of nucleosome positioning in the human genome *Cell 132*, 887-898.
8. Lee, W., Tillo, D., Bray, N., Morse, R. H., Davis, R. W., Hughes, T. R., and Nislow, C. (2007) A high-resolution atlas of nucleosome occupancy in yeast *Nat. Genet. 39*, 1235-1244.
9. Lantermann, A. B., Straub, T., Stralfors, A., Yuan, G. C., Ekwall, K., and Korber, P. (2010) Schizosaccharomyces pombe genome-wide nucleosome mapping reveals positioning mechanisms distinct from those of Saccharomyces cerevisiae *Nat. Struct. Mol. Biol. 17*, 251-257.
10. Stein, A. (1989) Reconstitution of chromatin from purified components *Methods Enzymol. 170*, 585- 603.
11. Rhodes, D. and Laskey, R. A. (1989) Assembly of nucleosomes and chromatin in vitro *Methods Enzymol. 170*, 575-585.
12. Luger, K., Rechsteiner, T. J., and Richmond, T. J. (1999) Expression and purification of recombinant histones and nucleosome reconstitution *Methods Mol. Biol. 119*, 1-16.
13. Widom, J. (2001) Role of DNA sequence in nucleosome stability and dynamics *Q. Rev. Biophys. 34*, 269-324.
14. Schnitzler, G. R. (2008) Control of nucleosome positions by DNA sequence and remodeling machines *Cell Biochem. Biophys. 51*, 67-80.
15. Kaplan, N., Moore, I. K., Fondufe-Mittendorf, Y., Gossett, A. J., Tillo, D., Field, Y., LeProust, E. M., Hughes, T. R., Lieb, J. D., Widom, J., and Segal, E. (2009) The DNA-encoded nucleosome organization of a eukaryotic genome *Nature 458*, 362-366.
16. Zhang, Y., Moqtaderi, Z., Rattner, B. P., Euskirchen, G., Snyder, M., Kadonaga, J. T., Liu, X. S., and Struhl, K. (2009) Intrinsic histone-DNA interactions are not the major determinant of nucleosome positions in vivo *Nat. Struct. Mol. Biol. 16*, 847-852.
17. Pugh, B. F. (2010) A preoccupied position on nucleosomes *Nat. Struct. Mol. Biol. 17*, 923.
18. Kaplan, N., Hughes, T. R., Lieb, J. D., Widom, J., and Segal, E. (2010) Contribution of histone sequence preferences to nucleosome organization: proposed definitions and methodology *Genome Biol. 11*, 140.
19. Simpson, R. T. and Stafford, D. W. (1983) Structural features of a phased nucleosome core particle *Proc. Natl. Acad. Sci. U. S. A. 80*, 51-55.
20. Neubauer, B., Linxweiler, W., and Hörz, W. (1986) DNA engineering shows that nucleosome phasing on the African green monkey alpha-satellite is the result of multiple additive histone-DNA interactions *J. Mol. Biol. 190*, 639-645.

21. Lowary, P. T. and Widom, J. (1998) New DNA sequence rules for high affinity binding to histone octamer and sequence-diected nucleosome positioning *J. Mol. Biol. 276*, 19-42.
22. Lusser, A. and Kadonaga, J. T. (2004) Strategies for the reconstitution of chromatin *Nat. Methods 1*, 19-26.
23. Pazin, M. J., Bhargava, P., Geiduschek, E. P., and Kadonaga, J. T. (1997) Nucleosome mobility and the maintenance of nucleosome positioning. *Science 276*, 809- 812.
24. Langst, G., Becker, P. B., and Grummt, I. (1998) TTF-I determines the chromatin architecture of the active rDNA promoter *EMBO J. 17*, 3135-3145.
25. Robinson, K. M. and Schultz, M. C. (2003) Replication-independent assembly of nucleosome arrays in a novel yeast chromatin reconstitution system involves antisilencing factor Asf1p and chromodomain protein Chd1p *Mol. Cell. Biol. 23*, 7937-7946.
26. Schultz, M. C. (1999) Chromatin assembly in yeast cell-free extracts *Methods 17*, 161-172.
27. Schultz, M. C., Hockman, D. J., Harkness, T. A., Garinther, W. I., and Altheim, B. A. (1997) Chromatin assembly in a yeast whole-cell extract *Proc. Natl. Acad. Sci. U. S. A 94*, 9034-9039.
28. Hertel, C. B., Längst, G., Hörz, W., and Korber, P. (2005) Nucleosome stability at the yeast PHO5 and PHO8 promoters correlates with differential cofactor requirements for chromatin opening *Mol. Cell. Biol. 25*, 10755-10767.
29. Wippo, C. J., Krstulovic, B. S., Ertel, F., Musladin, S., Blaschke, D., Sturzl, S., Yuan, G. C., Hörz, W., Korber, P., and Barbaric, S. (2009) Differential cofactor requirements for histone eviction from two nucleosomes at the yeast PHO84 promoter are determined by intrinsic nucleosome stability *Mol. Cell. Biol. 29*, 2960-2981.
30. Zhang, Z., Wippo, C. J., Wal, M., Ward, E., Korber, P., and Pugh, B. F. (2011) A packing mechanism for nucleosome organization reconstituted across a eukaryotic genome. *Science* 332, 977-80
31. Ertel, F., Dirac-Svejstrup, A. B., Hertel, C. B., Blaschke, D., Svejstrup, J. Q., and Korber, P. (2010) In vitro reconstitution of PHO5 promoter chromatin remodeling points to a role for activator-nucleosome competition in vivo *Mol. Cell. Biol. 30*, 4060-4076.
32. Patterton, H. G. and von Holt, C. (1993) Negative supercoiling and nucleosome cores. I. The effect of negative supercoiling on the efficiency of nucleosome core formation in vitro *J. Mol. Biol. 229*, 623-636.
33. Simon, R. H. and Felsenfeld, G. (1979) A new procedure for purifying histone pairs H2A + H2B and H3 + H4 from chromatin using hydroxylapatite *Nucleic Acids Res. 6*, 689-696.
34. Svaren, J., Venter, U., and Hörz, W. (1995) *In vivo* analysis of nucleosome structure and transcription factor binding in *Saccharomyces cerevisiae Methods in Mol. Genet. 6*, 153-167.
35. Sambrook, J., Fritsch, E. F., and Maniatis, T. (1989) *Molecular Cloning: A Laboratory Manual (2nd Edition)* Cold Spring Harbor Laboratory Press, Cold Spring Harbor, NY.
36. Wippo, C. J., Israel, L., Watanabe, S., Hochheimer, A., Peterson, C. L., and Korber, P. (2011) The RSC chromatin remodelling enzyme has a unique role in directing the accurate positioning of nucleosomes *EMBO J. 30*, 1277-1288.
37. Germond, J. E., Hirt, B., Oudet, P., Gross-Bellark, M., and Chambon, P. (1975) Folding of the DNA double helix in chromatin-like structures from simian virus 40 *Proc. Natl. Acad. Sci. U. S. A 72*, 1843-1847.
38. Pfaffle, P. and Jackson, V. (1990) Studies on rates of nucleosome formation with DNA under stress *J. Biol. Chem. 265*, 16821-16829.
39. Nightingale, K. P. and Becker, P. B. (1998) Structural and functional analysis of chromatin assembled from defined histones *Methods A Companion To Methods In Enzymology 15*, 343-353.
40. Huynh, V. A., Robinson, P. J., and Rhodes, D. (2005) A method for the in vitro reconstitution of a defined "30 nm" chromatin fibre containing stoichiometric amounts of the linker histone *J. Mol. Biol. 345*, 957-968.
41. Korber, P. and Hörz, W. (2004) In vitro assembly of the characteristic chromatin organization at the yeast PHO5 promoter by a replication-independent extract system *J. Biol. Chem. 279*, 35113-35120.

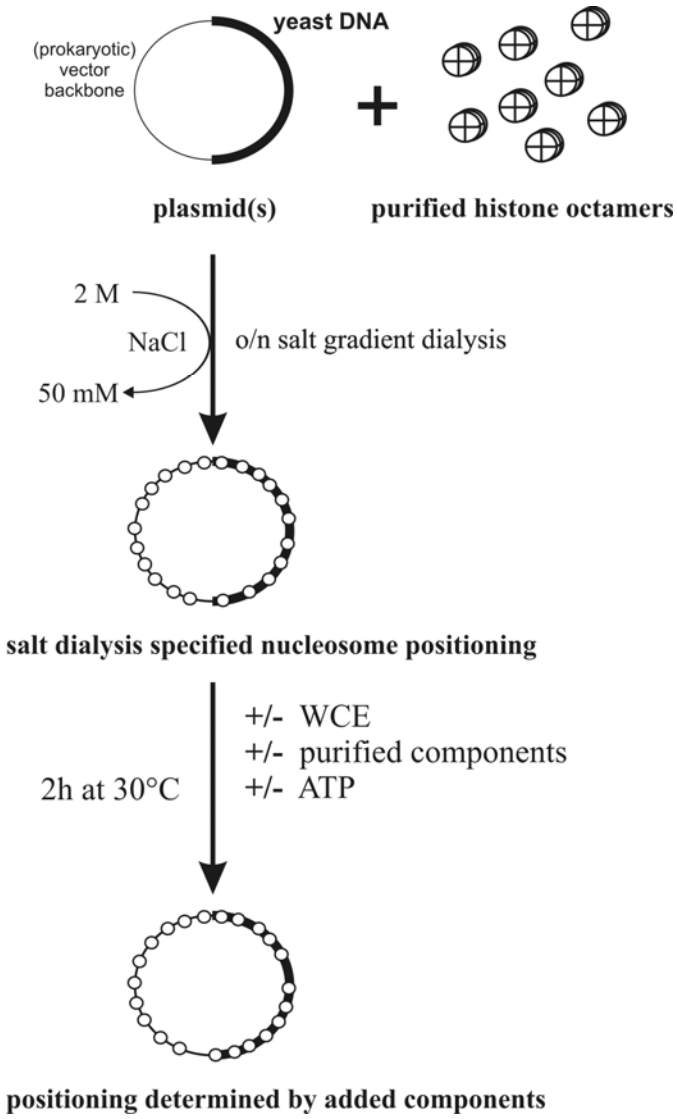

Figure 1. Schematic overview of the method.
Plasmid DNA and purified histones are preassembled into chromatin by salt gradient dialysis. This yields nucleosome positions that are specified by the intrinsic DNA preferences. Subsequent incubation with *S. cerevisiae* whole cell extract (WCE) and ATP will generate *in vivo*-like nucleosome positioning on *S. cerevisiae* DNA sequences. WCE fractions instead of WCE may be used (*36*) and additional components, like purified factors or acetyl CoA, can be added at any step.

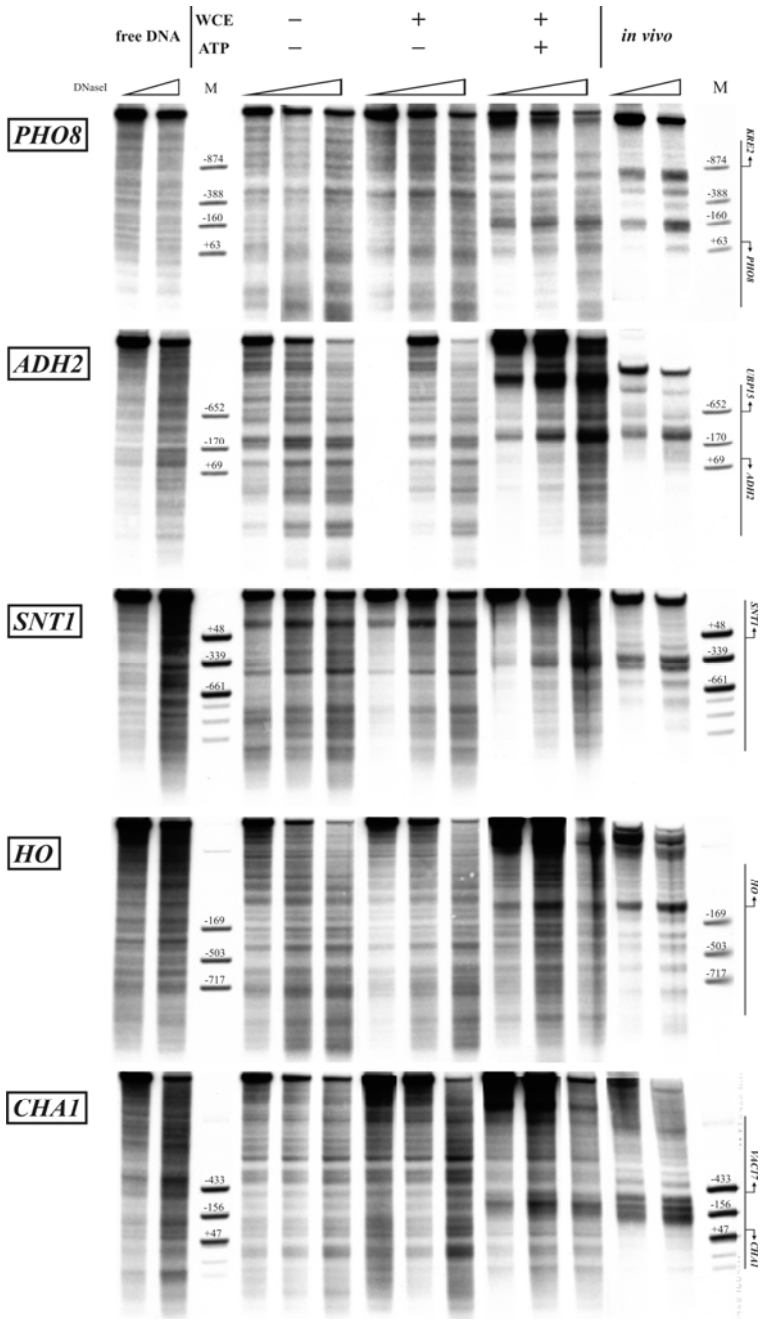

Figure 2. Examples of yeast loci with *in vitro* reconstituted *in vivo*-like nucleosome positioning.
In vitro reconstitution of nucleosome positioning at the *PHO8*, *ADH2*, *SNT1*, *HO*, and *CHA1* loci. pUC19 plasmids containing ~ 3.5 kb of the indicated locus were assembled into chromatin by salt gradient dialysis and incubated in the presence or absence of WCE and ATP. Lanes 4-6 show the pattern of chromatin reconstituted by salt gradient dialysis. Nucleosome positioning was analyzed by DNaseI indirect endlabeling. Free DNA samples were generated from non-assembled plasmids in the absence of WCE and ATP but under otherwise identical conditions. The *in vivo* samples were prepared from nuclei isolated from wildtype strain BY4741 grown logarithmically at 30 °C. Ramps indicate increasing DNaseI concentrations. The numbers above the marker bands refer to the position (in base pairs) relative to the start of the corresponding ORF. The approximate start of the indicated ORFs is indicated in the schematics on the right.

MOLECULAR AND CELLULAR BIOLOGY, June 2009, p. 2960–2981 Vol. 29, No. 11
0270-7306/09/$08.00+0 doi:10.1128/MCB.01054-08

Differential Cofactor Requirements for Histone Eviction from Two Nucleosomes at the Yeast *PHO84* Promoter Are Determined by Intrinsic Nucleosome Stability▽

Christian J. Wippo,[1] Bojana Silic Krstulovic,[2] Franziska Ertel,[1] Sanja Musladin,[2] Dorothea Blaschke,[1] Sabrina Stürzl,[1] Guo-Cheng Yuan,[3] Wolfram Hörz,[1]† Philipp Korber,[1]* and Slobodan Barbaric[2]

Adolf-Butenandt-Institut, Universität München, Munich, Germany[1]; Laboratory of Biochemistry, Faculty of Food Technology and Biotechnology, University of Zagreb, Zagreb, Croatia[2]; and Department of Biostatistics, Harvard School of Public Health, and Department of Biostatistics and Computational Biology, Dana-Farber Cancer Institute, Boston, Massachusetts[3]

Received 4 July 2008/Returned for modification 6 August 2008/Accepted 1 March 2009

We showed previously that the strong *PHO5* promoter is less dependent on chromatin cofactors than the weaker coregulated *PHO8* promoter. In this study we asked if chromatin remodeling at the even stronger *PHO84* promoter was correspondingly less cofactor dependent. The repressed *PHO84* promoter showed a short hypersensitive region that was flanked upstream and downstream by a positioned nucleosome and contained two transactivator Pho4 sites. Promoter induction generated an extensive hypersensitive and histone-depleted region, yielding two more Pho4 sites accessible. This remodeling was strictly Pho4 dependent, strongly dependent on the remodelers Snf2 and Ino80 and on the histone acetyltransferase Gcn5, and more weakly on the acetyltransferase Rtt109. Importantly, remodeling of each of the two positioned nucleosomes required Snf2 and Ino80 to different degrees. Only remodeling of the upstream nucleosome was strictly dependent on Snf2. Further, remodeling of the upstream nucleosome was more dependent on Ino80 than remodeling of the downstream nucleosome. Both nucleosomes differed in their intrinsic stabilities as predicted in silico and measured in vitro. The causal relationship between the different nucleosome stabilities and the different cofactor requirements was shown by introducing destabilizing mutations in vivo. Therefore, chromatin cofactor requirements were determined by intrinsic nucleosome stabilities rather than correlated to promoter strength.

Nuclear eukaryotic DNA is packaged into nucleosomes, where DNA is wrapped around a protein core consisting of eight histone proteins (48). The nucleosome forms the basic unit of a complex protein-nucleic acid structure termed chromatin. Chromatin structure has a strong influence on the regulation of gene transcription as the accessibility of DNA regions, for example, promoter elements and transactivator binding sites, is restricted and modulated by their incorporation into nucleosomes. Therefore, it has become an important field of research to understand the mechanisms by which transcription activators or repressors and the transcriptional machinery gain access to their binding sites and navigate the chromatin environment (51).

Many yeast nucleosomes are clearly positioned in relation to the DNA sequence (45, 49, 67, 82, 85), and nucleosomes are shown to occlude transactivator binding sites (47, 80). Nonetheless, it has become clear that nucleosomes, despite their intrinsic mostly repressive function, are highly dynamic. Especially in yeast promoter regions, there is a constant turnover of histones (20, 34, 62). The dynamics of chromatin are mediated by an intricate interplay of chromatin-related cofactors. For example, the so-called remodeling complexes, like the SWI/SNF, Ino80, or ISWI complexes, use the energy of ATP to either slide nucleosomes along the DNA, to alter the nucleosome structure to provide more accessible DNA, to exchange histones from the octamer core for variant histones, or even to completely disassemble nucleosomes and evict the histones from the previously nucleosomal region (10, 24, 46, 79). Remodeling complexes work in concert with a great variety of histone-modifying enzymes that add or remove chemical modifications like acetyl, methyl, or phosphate residues (11, 40). Further, free histones that are not part of a nucleosome are highly aggregation prone and are therefore bound by a diverse group of histone chaperones that assist nucleosome assembly and disassembly (56). At present it is not possible to predict which chromatin cofactors are required for chromatin remodeling in a particular case, as no comprehensive rules for cofactor requirements have been established.

The yeast *PHO5* promoter is a classical example for the role of chromatin in promoter regulation (74). Upon induction, an array of four positioned nucleosomes at the repressed promoter becomes mostly remodeled, leading to an extended nuclease-hypersensitive site that is largely depleted of histones (3, 14, 58). That way an additional binding site for the specific transactivator Pho4 becomes accessible, which is a critical prerequisite for gene induction (25, 26). The *PHO8* promoter is coregulated by the same transactivator as *PHO5* and also shows a pronounced chromatin transition upon induction (5) but has much lower promoter strength, i.e., the transcriptional activity in the fully induced state is much lower (52). In the past, we and others studied extensively the mechanisms that lead to promoter chromatin opening at these two promoters. At both promoters the SWI/SNF and Ino80 remodeling complexes, the histone acetyltransferase Gcn5, and the histone

* Corresponding author. Mailing address: Adolf-Butenandt-Institut, Universität München, Schillerstr. 44, 80336 Munich, Germany. Phone: 49-89-218075435. Fax: 49-89-218075425. E-mail: pkorber@lmu.de.
† Deceased, 13 November 2005.
▽ Published ahead of print on 23 March 2009.

chaperone Asf1 are involved in chromatin remodeling (6). However, the degree of cofactor requirement is markedly different. Whereas the *PHO8* promoter strictly depends on the ATPase subunit Snf2 of the SWI/SNF complex and on Gcn5 for promoter opening (28), there are redundant pathways for *PHO5* promoter chromatin remodeling, and no essential cofactor downstream of the transactivator Pho4 has been identified yet (6). Previously, we suggested that different intrinsic stabilities of promoter nucleosomes could be the reason for the differential cofactor requirement at these two promoters (31). Now, we wondered if it was a general trend that stronger promoters are packaged into less stable nucleosomes and show less dependency on chromatin cofactors.

In order to address this question without further complication by comparing different transactivation mechanisms, we turned to the *PHO84* promoter, which is coregulated with the *PHO5* and *PHO8* promoters but is even stronger than the *PHO5* promoter (54). The *PHO84* gene encodes a high-affinity phosphate transporter (15), and its mechanism of transcriptional regulation via regulation of Pho4 activity, as it is common to the phosphate-regulated genes, is mostly known (35, 37, 55). A comparative study of the transcriptional induction of the two coregulated *PHO5* and *PHO84* genes in response to phosphate starvation showed a lower threshold for *PHO84* induction. Cells grown in medium with intermediate phosphate concentrations activate transcription of *PHO84* but not of *PHO5* (71). Even growth in rich yeast extract-peptone-dextrose (YPD) medium, which is mostly repressive for *PHO5* induction, leads to significant levels of *PHO84* transcription (23, 53). Also, the induction of *PHO84* occurs more rapidly than induction of *PHO5*. However, this is not an intrinsic feature of the *PHO84* promoter but a consequence of the lower threshold of induction. Polyphosphate stores in the cell buffer the physiological signaling pathway of phosphate starvation, leading to a gradual increase in signal strength and an earlier response of the *PHO84* promoter than of the *PHO5* promoter. Mutants that are defective in polyphosphate storage induce *PHO5* and *PHO84* with similar kinetics (77).

The role of chromatin in the regulation of the *PHO84* promoter has not been explicitly studied yet. Nonetheless, there are several reports on effects of chromatin-related cofactors on the activity of *PHO84* under repressing or inducing conditions. This argues that also the *PHO84* promoter is regulated on the level of chromatin structure and makes it a promising model for the study of promoter chromatin remodeling mechanisms.

Genome-wide expression analyses in rich YPD medium revealed that *PHO84* is downregulated in the absence of Gcn5 or Snf2 (44). Shukla et al. (68, 69) demonstrated reduced acetylation of histone H3 and reduced recruitment of TATA binding protein and polymerase II at the *PHO84* promoter under such conditions in a *gcn5* mutant. The recruitment of Snf2 to the *PHO84* promoter in YPD medium has been directly shown, and this recruitment is dependent on Pho4 and vice versa (23). Also, both Snf2 and Ino80 are present at the induced *PHO84* promoter, and induced *PHO84* mRNA levels are reduced in the absence of these cofactors (36, 72). Further, basal transcription is increased in the absence of the histone methyltransferase Set1 (16). Very recently, during preparation of the manuscript, a comprehensive study of PHO regulon promoters explained very convincingly that the low threshold of *PHO84* induction and its high dynamic range are due to the affinities of the five Pho4 binding sites and their positions in relation to positioned nucleosomes at the *PHO84* promoter (41). That study also showed that *PHO84* promoter nucleosomes become remodeled upon induction, but the role of chromatin cofactors was not addressed.

We have now characterized the chromatin states at the *PHO84* promoter under repressing and inducing conditions and present findings of our comprehensive investigation of the role of Pho4 binding sites, i.e., UASp elements, and chromatin cofactors in *PHO84* promoter chromatin dynamics. The *PHO84* promoter in the repressed state exhibited a short hypersensitive region that was flanked by two positioned nucleosomes and harbored two high-affinity Pho4 binding sites. Upon induction, this chromatin structure was remodeled into an extensive hypersensitive region that was depleted of histones and allowed access to two additional UASp elements. This chromatin transition was strongly dependent on Snf2, Ino80, and Gcn5, weakly dependent on the histone acetyltransferase Rtt109, and even more weakly on the histone chaperone Asf1. Strikingly, remodeling of each of the two nucleosomes flanking the short hypersensitive region in the repressed state showed a markedly different degree of cofactor requirement. Remodeling of one was critically dependent on Snf2, whereas remodeling of the other one was not. In addition, remodeling of the latter was less dependent on Ino80 than remodeling of the former and was even remodeled in the simultaneous absence of both Snf2 and Ino80. Therefore, the strong *PHO84* promoter appeared to be a hybrid between the *PHO5* and *PHO8* promoters with regard to the presence of both a stable, strictly Snf2 dependent nucleosome and a less stable, redundantly remodeled nucleosome at the same promoter. We show that this differential cofactor requirement was caused by different intrinsic stabilities of the two nucleosomes, as manipulation of nucleosome stability resulted in corresponding changes in the degree of remodeling cofactor requirements. We suggest that cofactor requirements for remodeling of promoter nucleosomes are mainly determined by intrinsic stabilities of individual nucleosomes and that promoter strength is not stringently predictive for cofactor requirements.

MATERIALS AND METHODS

Strains and media. For a complete list of the *Saccharomyces cerevisiae* strains used in this study see Table 1. Strain CY338 is a derivative of CY337 where the *PHO4* locus was disrupted by transformation with a linear DNA fragment of the *PHO4* locus with a *URA3* marker gene cassette inserted into the *PHO4* open reading frame (ORF). CY339, CY409, and other *pho5* derivatives of strains were constructed by transformation with a linear fragment that inserted a *URA3* cassette instead of the BamHI-SalI fragment at the *PHO5* locus. Yeast strains were grown under repressive conditions (high phosphate [$+P_i$]) in YPD with 0.1 g/liter adenine plus 1 g/liter KH_2PO_4, in yeast nitrogen base selection medium supplemented with the required amino acids for plasmid-bearing strains, and in phosphate-free synthetic medium for induction (3, 6).

Plasmids. The plasmids pCB84a and pCB84b are derivatives of pCB/WT (26) in which a *LEU2* marker cassette is inserted into the HindIII site and where the *PHO5* promoter is exchanged for the *PHO84* promoter. In more detail, a PCR product, generated with the primers PHO84(do) (5′-AGATTTAAACATTTGGATTGTAT TCGTGG-3′) and either PHO84(up-885) (5′-CAGGATCCAAAGTGTCACGTG-3′) for pCB84a or PHO84(up-479) (5′-CAGGATCCCGTTCCTCTCACTG-3′) for pCB84b and genomic DNA as template, was ligated via BamHI and DraI into the *PHO5* promoter. As there are multiple DraI sites in the vector, the vector was opened via BamHI and SalI and the DraI-SalI fragment 5′ of the *PHO5* ORF was prepared separately and added to the ligation mixture, resulting in a triple ligation

TABLE 1. *Saccharomyces cerevisiae* strains used in this study

Strain	Genotype	Source	Reference
CY337	*MAT***a** *ura3-52 lys2-801 ade2-101 leu2-Δ1 his3-Δ200*	P. Hieter and C. L. Peterson	60
CY338	CY337 *pho4*::*URA3*	Our group	
CY339	CY337 *pho5*::*URA3*		
CY396	*MATα swi2Δ*::*HIS3 SWI2*-HA-6HIS::*URA3 HO-lacZ*	C. L. Peterson	60
CY397	*MATα swi2Δ*::*HIS3 swi2*(*K798A*)-HA-6HIS::*URA3 HO-lacZ*		
CY407	CY337 *snf2*::*HIS3*		
CY407 *ino80*	CY407 *ino80*::*URA3*	Our group	6
CY409	CY407 *pho5*::*URA3*		
CY53379 *pho5*	CY337 *gcn5*::*ura3* (URA3 function lost on 5-fluoroorotic acid) *pho5*::*URA3*		28
BY4741-0	wt	X. Shen	66
BY4741-1	BY4741-0 *ino80*::*HIS3*		
Y00000 (same as BY4741)	*MAT***a** *his3Δ1 leu2Δ0 met15Δ0 ura3Δ0*	EUROSCARF	http://web.uni-frankfurt.de/fb15/mikro/euroscarf/
Y01490	BY4741 *rtt109*::*kanMX4*		
Y01310	BY4741 *asf1*::*kanMX4*		
W303a	*MAT***a** *leu2-3,112 ura3-1 his3-11,15 trp1-1 ade2-1 can1-100*	A. Verreault	
W303a *asf1* (same as MAR 101)	W303a *asf1*::*kanMX*		
PKY4170	W303a *rtt109*::*kanMX bar1-1*	P. D. Kaufman	
PKY4182	W303a *rtt109*::*kanMX asf1*::*TRP1 URA3-VIIL*		
PKY4226	W303a *bar1-1 vps75*::*HIS3*		
W303a *asf1 pho5*	W303a *asf1 pho5*::*URA3*	This study	
PKY4170 *pho5*	PKY4170 *pho5*::*URA3*		
PKY4226 *pho5*	PKY4226 *pho5*::*URA3*		
FY1352	*MAT***a** *leu2Δ1 his3Δ200 ura3-52 lys2-173R2 snf2Δ*::*LEU2 gcn5Δ*::*HIS3*	F. Winston	61

of PCR product, BamHI-SalI-digested vector backbone, and the DraI-SalI fragment. Plasmid pCB84a was used as template for generating the UASp variants UASpCmut, -Dmut, and -Emut by the Megaprimer method (63) with the following primers that introduced the point mutations: PHO84-mutC, 5′-GCCAATTTAATAGTTCATCGATGATCAGTTATTTCCAGCACGTG-3′; PHO84-mutD, 5′-GGACGTGTTATTTCCACATCGATGGGCGGAAATTAGCGAC-3′; PHO84-mutE, 5′-GCTTATTAGCTAGATTAAAACTAGTCGTATTACTCATTAATTAAC-3′. The following primers were used as reverse primers for generating UASpCmut, -Dmut, and -Emut, respectively: PHO84-rev1, 5′-CCACAATAGTAAGTGG-3′; PHO84-rev2, 5′-CTGGTGATCTACGAG-3′. The point mutations introduced a ClaI site each instead of UASpC and UASpD and a SpeI site instead of UASpE. The combined mutations of UASpCEmut and UASpDEmut were generated by inserting the BsgI-MstII fragment from the UASpEmut plasmid into the UASpCmut and UASpDmut plasmids, respectively. The UASpBmut plasmid and plasmid pCB84a-10A were generated using pCB84a as template and the QuikChange kit (Stratagene) with the following mutagenesis primers: pho84-mut-Bfor, 5′-GAAATGACAGCAATCAGTATTACGGAATTCGGTGCTGTTATAGGCGCCCTATAC-3′, and pho84-mutBrev, 5′-GTATAGGGCGCCTATAACAGCACCGAATTCCGTAATACTGATTGCTGTCATTTC-3′ for pCB84a-Bmut and pho84-A10for, 5′-GTATAGGGCGCCTATAACAGCACCAACGTGCGTAAAAAAAAAAGCTGTCATTTCTTGGCATGTTTTCT-3′, and pho84-A10rev, 5′-AGAAAACATGCCAAGAAATGACAGCTTTTTTTTTTTACGCACGTTGGTGCTGTTATAGGCGCCCTATAC-3′, for pCB84a-10A, respectively. The point mutation in pCB84a-Bmut introduced an EcoRI site instead of UASpB. Plasmid pCB84a-19A was generated with the QuikChange kit and pCB84-10A as template and the primers pho84-A19for, 5′-TGCTGCACGTATAGGGCGCCTATAACAGCACCAAAAAAAAAAAAAAAAAAAAGCTGTCATTTCTTGGCATGTTTTC-3′, and pho84-A19rev, 5′-GAAAACATGCCAAGAAATGACAGCTTTTTTTTTTTTTTTTTTGGTGCTGTTATAGGCGCCCTATACGTGCAGCA-3′. Plasmid pUC19-PHO84 was prepared by ligating a 3.5-kb PCR product, generated with the primers 5′-CCGGAATTCTCGAGTCATGATTTGGAACAGCTCC-3′ and 5′-CGCGGATCCGCAGAGAGATGTGAGGAAAT-3′ and genomic DNA from strain BY4741 as template, via EcoRI and BamHI, into pUC19. Plasmids pUC19-PHO84-10A and -19A were generated from pUC19-PHO84 and from pUC19-PHO84-10A with the primers pho84-A10for/-rev and pho84-A19for/-rev, respectively, and the QuikChange kit. The DNA sequence of the *PHO84* promoter region in all plasmids constructed in this study was confirmed by dideoxy sequencing (data not shown). The Pho4 overexpression plasmid pP4-70L corresponds to YEpP4 (75) but carries the *LEU2* instead of the *URA3* marker.

Functional assays and chromatin analysis. Acid phosphatase assays were done as described previously (29). The preparation of yeast nuclei (3) and chromatin analysis of nuclei by restriction nucleases and DNase I digestion with indirect end labeling were as described previously (27, 76). Secondary cleavage for DNase I indirect end labeling was done with HindIII for both the chromosomal and the plasmid locus (at bp −1453 and −1239 from the ATG of the *PHO84* ORF for chromosomal and plasmid locus, respectively). For secondary cleavage after chromatin digestion with BsrBI, HhaI, MfeI, PacI, AgeI, SpeI, and FokI, we used HindIII for the chromosomal locus and HindIII/SalI for the plasmid locus. The probe for the chromosomal locus is a PCR product corresponding to bases −1428 to −1083 from the ATG of the *PHO84* ORF, and the probe for the plasmid locus corresponds to the HindIII-BamHI fragment of pBR322. Due to the presence of multiple HhaI sites in the plasmid probe region, i.e., the HindIII-BamHI fragment of pBR322, BamHI and EcoRV were used for secondary cleavage and a PCR product from −557 to −310 was used as probe in order to monitor HhaI accessibility at the plasmid locus. Due to the frequent occurrence of TaqI sites, AvaII/ClaI were used for the chromosomal and BamHI/SalI for the plasmid locus for secondary cleavage and a PCR product from −736 to −371 was used as a probe for monitoring TaqI accessibilities.

ChIP analysis. Yeast cultures with a density of 1×10^7 to 2×10^7 cells/ml were treated with 1% formaldehyde for 20 min at room temperature. Cross-linking was quenched by adding glycine to a final concentration of 125 mM. The cells were washed two times with ice-cold 0.9% NaCl, resuspended in HEG150 buffer (150 mM NaCl, 50 mM HEPES, pH 7.6, 10% glycerol, 1% Triton X-100, 1 mM EDTA, 1 mM dithiothreitol [DTT], 1 mM phenylmethylsulfonyl fluoride) and lysed with a French press (three times at 1,100 lb/in^2) or by sonication (Bioruptor; Diagenode; three times for 30 s with a 60-s pause, position high, ice water bath). In this last step, chromatin was sheared to an average size of 500-bp fragments. Chromatin immunoprecipitation (ChIP) was performed as described before (73). The anti-histone H3 C-terminal antibody was obtained from Abcam (ab1791-100). Immunoprecipitated DNA was quantitatively measured in triplicates with the ABI Prism 7000 sequence detection system using the following amplicons: TEL-1, 5′-TCCGAACGCTATTCCAGAAAGT-3′; TEL-B, 5′-CCATAATGCCTCCTATATTTAGCCTTT-3′; TEL-probe, 5′–6-carboxyfluorescein [FAM]–TCCAGCCGCTTGTTAACTCTCCGACA–6-carboxytetramethylrhodamine (TAM)–3′; ACT1-A, 5′-TGGATTCCGGTGATGGTGTT-3′; ACT1-B, 5′-TCAAAATGGCGTGAGGTAGAGA-3′; ACT1-probe, 5′-FAM-CTCACGTCGTTCCAATTTACGCTGGTTT-TAM-3′; PHO84 UASpC-A, 5′-GAAAAACACCCGTTCCTCTCACT-3′; PHO84 UASpC-B, 5′-CCCACGTG

CTGGAAATAACAC-3′; PHO84 probe, 5′-FAM-CCCGATGCCAATTTAATAGT TCCACGTG-TAM-3′.

Salt gradient dialysis chromatin assembly. Salt gradient dialysis was performed as described previously (42). A typical assembly reaction mixture contained 10 μg supercoiled plasmid DNA (Qiagen preparation), 20 μg bovine serum albumin (A-8022; Sigma), and variable amounts (for example, 6 or 10 μg) of *Drosophila melanogaster* embryo histone octamers (70) in 100 μl high-salt buffer (10 mM Tris-HCl, pH 7.6, 2 M NaCl, 1 mM EDTA, 1 mM β-mercaptoethanol, 0.05% Igepal CA630 [I-3063; Sigma]) and was dialyzed for 15 h at room temperature while slowly diluting 300 ml of high-salt buffer with 3 liters of low-salt buffer (same as the high-salt buffer, but with 50 mM NaCl) using a peristaltic pump. A final dialysis step versus low-salt buffer ensured a final NaCl concentration of 50 mM.

Yeast whole-cell extract preparation. Yeast whole-cell extract was prepared as previously described (31) with the following modifications. Commercially available baker's yeast concentrate (Deutsche Hefewerke GmbH, Nürnberg, Germany) was used as starting material for an upscaled version of the preparation. The extraction buffer was modified to 0.2 M HEPES-KOH, pH 7.5, 10 mM $MgSO_4$, 10% glycerol, 1 mM EDTA, 390 mM $(NH_4)_2SO_4$, 1 mM DTT, and 1× Complete protease inhibitor without EDTA (Roche Applied Science), and the buffer for resuspension after the ammonium sulfate precipitation was 20 mM HEPES-KOH, pH 7.5, 10% glycerol, 80 mM KCl, 1 mM EGTA, 5 mM DTT, and 1× Complete protease inhibitor without EDTA. For the final dialysis the same buffer as for resuspension but with 0.1 mM phenylmethylsulfonyl fluoride and 1 mM sodium metabisulfite instead of the Complete protease inhibitor was used and exchanged to completion.

In vitro chromatin reconstitution. A 100-μl reconstitution reaction mixture with 1 μg DNA preassembled by salt gradient dialysis was incubated with or without yeast extract (~250 μg protein, judged from Coomassie-stained gel lanes in comparison to standard protein) and with or without a regenerative energy system (3 mM ATP–$MgCl_2$, 30 mM creatine phosphate [Sigma], and 50 ng/μl creatine kinase [Roche Applied Science]) in assembly buffer (20 mM HEPES-KOH, pH 7.5, 10% glycerol, 80 mM KCl, 0.5 mM EGTA, 2.5 mM DTT) for 2 h at 30°C.

DNase I indirect end labeling and restriction enzyme accessibility assay for in vitro-reconstituted chromatin. Aliquots (25 μl) of a reconstitution reaction mixture were mixed with an equal volume of digestion buffer (20 mM HEPES-KOH, pH 7.5, 12% glycerol, 5.5 mM $MgCl_2$, 5.5 mM $CaCl_2$, 2.5 mM DTT, 80 mM NaCl, 0.1 mg/ml bovine serum albumin) containing DNase I (04716728001; Roche Applied Science) at a concentration in the range of 0.005 to 0.02 U/ml (free DNA), 0.02 to 0.1 U/ml (salt gradient dialysis chromatin), or 2 to 10 U/ml (salt gradient dialysis chromatin with extract) and incubated at room temperature for 5 min. The digestion reactions were stopped by adding 10 μl of Stop buffer (10 mM EDTA, 4% sodium dodecyl sulfate), deproteinated by proteinase K digestion overnight, and ethanol precipitated. SspI (bp −1440 from the ATG of the *PHO84* ORF) was used for secondary cleavage instead of HindIII. For direct comparison between in vitro-reconstituted chromatin and in vivo chromatin (see Fig. 7A, below), SspI was used for all loci.

Prior to restriction enzyme digestions, ATP was removed from the reconstitution reaction mixtures to inhibit ATP-dependent remodeling during the restriction digestion by adding 0.1 U of apyrase (M0393L; New England Biolabs) to the reaction mixtures and incubating for 30 min at 37°C. Two-microliter aliquots of an apyrase-treated reconstitution reaction mixture were combined with 30 μl of RE digestion buffer (20 mM HEPES-KOH, pH 7.5, 4.5 mM $MgCl_2$, 2.5 mM DTT, 80 mM NaCl, 0.5 mM EGTA) and treated with two different enzyme concentrations for each restriction enzyme, similar to the in vivo RE digests. The reactions were stopped by adding 7.5 μl Stop buffer, deproteinated by proteinase K digestion overnight, and ethanol precipitated. Secondary cleavage was performed as described above for the chromosome locus.

RESULTS

The chromatin structure at the *PHO84* promoter undergoes extensive remodeling upon induction. We characterized the *PHO84* promoter chromatin structure under repressing conditions, i.e., in rich or synthetic medium with additional phosphate to ensure full repression, and under inducing conditions, i.e., synthetic phosphate-free medium. By DNase I indirect end-labeling analysis of the repressed state ($+P_i$) we detected a short hypersensitive (sHS) region (about 150 bp), roughly between the MfeI and ApaI restriction sites, that was flanked by one positioned nucleosome upstream and one downstream (Fig. 1A and B, upstream nucleosome and downstream nucleosome). This sHS region contained two closely positioned high-affinity Pho4 binding sites, UASpC and UASpD, whereas the two low-affinity sites, UASpB and UASpE, were occluded by the positioned upstream and downstream nucleosomes, respectively (Fig. 1B) (54). In addition, we observed a broad hypersensitive region upstream of the BsrBI restriction site. Upon induction ($-P_i$), the upstream nucleosome and at least one nucleosome downstream of the sHS region were remodeled, leading to an extended hypersensitive (eHS) region of about 500 bp. Its upstream border was almost fused to the broad hypersensitive region and the downstream border faded into the core promoter region around the TATA box and the transcriptional start site (Fig. 1A and B; see also Fig. 4B, 5A, and 8A, below). This way UASpB and UASpE became accessible (Fig. 1B). Sometimes the eHS region appeared to contain a short region of lower DNase I accessibility between the MfeI and ApaI sites (see Fig. 4B and 8A), which may reflect Pho4 and recruited factors bound to UASpC and UASpD. In Fig. 1A the intensity of the broad hypersensitive region upstream of the BsrBI site appeared to change somewhat upon induction, which was probably attributable to an overall lower degree of digestion. However, in the majority of cases it did not undergo major changes upon induction (see Fig. 4B, 5A, and 8A, $-P_i$ panels, below; also, data not shown). Therefore we refer to it as a constitutive hypersensitive region (cHS).

The chromatin transition was fully dependent on the transactivator Pho4, as the *PHO84* promoter chromatin pattern under inducing conditions in a *pho4* deletion strain was virtually the same as the wild-type (wt) pattern of the repressed state (Fig. 1A). Interestingly, the unchanged nucleosome organization in a *pho4* mutant suggested that the nucleosome positioning at the repressed promoter did not depend on binding of Pho4, e.g., to its linker binding sites UASpC and UASpD.

In addition to DNase I indirect end labeling, we mapped the *PHO84* promoter chromatin structure of the repressed and the induced state more quantitatively by assaying the accessibility for several restriction enzymes along the promoter region that underwent the chromatin structure transition (Fig. 1C and D). Under $+P_i$ conditions, the accessibilities for the various restriction enzymes were rather different, as would be expected for an organization into nucleosomes and nucleosome-free linker regions. The accessibilities at the HhaI and TaqI sites were the lowest, speaking for their protection by the upstream and downstream nucleosome, respectively. The BsrBI site was fully accessible under both repressing and inducing conditions, which was in agreement with its localization at the downstream start of the cHS region (Fig. 1A). The MfeI site was substantially but not fully accessible in the repressed state, indicating a location at the very border between the downstream nucleosome and the sHS region (Fig. 1A). Interestingly, a region of about 100 bp between the downstream nucleosome and the TATA box was only semiprotected in the repressed state, as the accessibilities for PacI, AgeI, and FokI were in the range of 43% (FokI) to 57% (AgeI) (Fig. 1C and D). This argued against a clearly positioned but rather for a less-organized nucleosome or for a chromatin structure with increased plas-

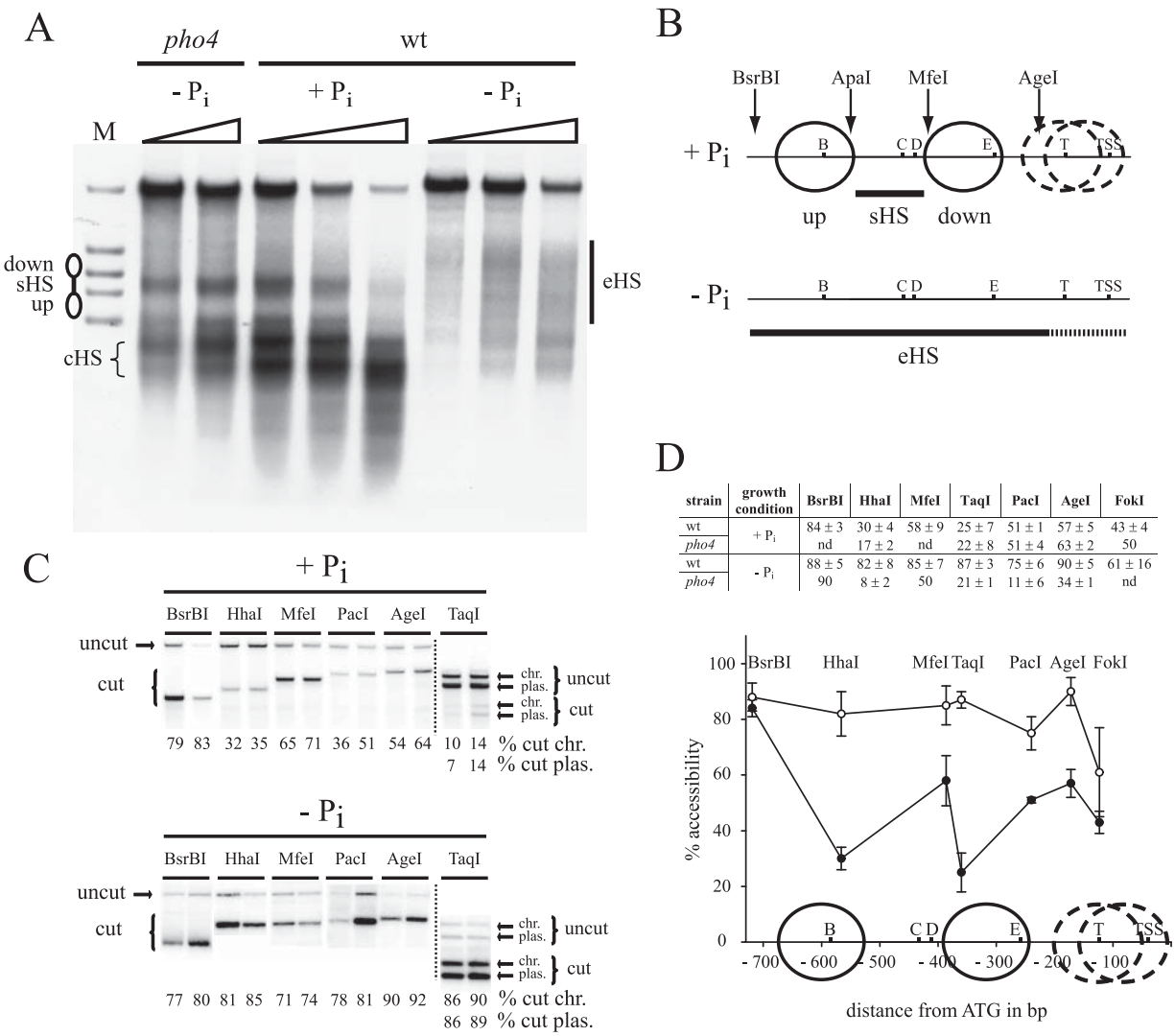

strain	growth condition	BsrBI	HhaI	MfeI	TaqI	PacI	AgeI	FokI
wt	+ Pi	84 ± 3	30 ± 4	58 ± 9	25 ± 7	51 ± 1	57 ± 5	43 ± 4
pho4		nd	17 ± 2	nd	22 ± 8	51 ± 4	63 ± 2	50
wt	- Pi	88 ± 5	82 ± 8	85 ± 7	87 ± 3	75 ± 6	90 ± 5	61 ± 16
pho4		90	8 ± 2	50	21 ± 1	11 ± 6	34 ± 1	nd

FIG. 1. The chromatin structure at the *PHO84* promoter undergoes extensive remodeling upon induction. (A) DNase I indirect end-labeling analysis of the chromatin structure at the chromosomal *PHO84* locus in wt (CY339 pCB84a) and *pho4* (CY338) strains grown in phosphate-containing medium ($+P_i$) or after overnight incubation in phosphate-free medium ($-P_i$). Ramps on top of the lanes designate increasing DNase I concentrations. The four marker fragments in the promoter region (lane M) were generated by double digests with HindIII and either AgeI, MfeI, ApaI, or BsrBI (from top to bottom in the lanes). The schematics on the left and right are analogous to the schematics of the $+P_i$ and $-P_i$ states in panel B, respectively. Down and up refer to positioned nucleosomes downstream and upstream of the sHS region, respectively. eHS denotes the extended hypersensitive region of the induced state, and cHS denotes the constitutive hypersensitive region. All samples were electrophoresed in the same gel, but for the $-P_i$ data a stronger exposure is shown. (B) Schematic of the nucleosomal organization of the *PHO84* promoter in the repressed ($+P_i$) and induced ($-P_i$) state. Large circles denote the positioned nucleosomes (up and down) flanking the sHS (short horizontal bar). Stippled circles stand for a less-organized nucleosome structure with ambiguous positioning. The positions of four Pho4 binding sites (B to E, taken from reference 54), the TATA box (T, taken from reference 9), the transcriptional start site (TSS, taken from reference 50), and the four restriction sites used for generating marker fragments (see panel A) are indicated. Upon induction ($-P_i$), there is an eHS region (long horizontal bar) ranging from near the BsrBI up to the AgeI site and fading into the core promoter region (stippled horizontal bar). (C) Nuclei isolated from wt (CY339 pCB84a) cells grown under repressive ($+P_i$) or inducing ($-P_i$) conditions were digested with two different concentrations each of the indicated restriction enzymes and analyzed by indirect end labeling with probing for the chromosomal locus. Due to the specific probe and secondary cleavage for the analysis of TaqI accessibility, both the chromosomal (chr.) and the plasmid (plas.) locus were seen at the same time. Quantification of the percentage of cleaved DNA (% cut) was done by PhosphorImager analysis. The samples of the $+P_i$ panel were electrophoresed on the same gel, but the samples of the $-P_i$ panel were on different gels; therefore, the relative migration positions cannot be compared directly. (D) Average accessibility values of two to seven biological replicates and their standard deviations are given for the indicated restriction endonucleases and for wt (CY background) and *pho4* (CY338) strains under repressive ($+P_i$) or inducing ($-P_i$) conditions. nd, not determined. The wt data of the table ($+P_i$, closed circles; $-P_i$, open circles) are plotted versus the positions of the restriction sites relative to the ATG start codon. As for panel B, the positions of four Pho4 binding sites (B to E), the TATA box (T), and the transcriptional start site (TSS) are indicated on the *x* axis of the plot as well as the inferred positions of clearly positioned (large circles) and less-organized (overlapping stippled circles) nucleosomes.

ticity. Alternatively, some other DNA-protecting entity, e.g., an assembly of general transcription factors, could be responsible for this semiprotection.

In the induced state, all restriction enzyme sites tested in the promoter region of more than 500 bp upstream of the TATA box were highly accessible (Fig. 1C and D), confirming the presence of an extended hypersensitive region as observed by DNase I indirect end labeling (Fig. 1A) and suggesting that the whole region was mostly nucleosome free. Restriction enzyme accessibility assays also confirmed that the transition to this open chromatin state was dependent on Pho4 (Fig. 1D). For unknown reasons, the accessibilities at the HhaI, PacI, and AgeI sites, but not at the TaqI site, were even decreased under inducing compared to noninducing conditions in the *pho4* strain.

In the wt strain, the accessibility of the FokI cleavage site, which overlaps with the TATA box sequence (15), also increased upon induction, but not to the same high level as for the other restriction enzyme sites. In addition, the accessibility of the FokI site in the induced state was quite variable. This altogether may be due to the poor performance of this restriction enzyme on chromatin templates or may indicate the presence of an unstable or partially remodeled nucleosome or of components of the general transcription machinery recruited to the TATA box under inducing conditions.

In summary, the restriction enzyme accessibility data in connection with the DNase I indirect end-labeling analysis led us to map the upstream and downstream nucleosome as shown in Fig. 1B and D. The main guidelines were the location of the ApaI and MfeI sites just at the borders of the nucleosomes toward the sHS region. For the reasons stated above, we have not assigned clear nucleosomal positions to the region between the downstream nucleosome and the TATA box region but suggest a less-organized DNA protective structure there.

This less-organized structure together with the somewhat elevated accessibilities at the HhaI and TaqI sites suggested to us that there may be a low level of Pho4 present at the promoter even under repressive conditions. Under $+P_i$ conditions Pho4 is mostly phosphorylated at multiple sites and mainly located in the cytosol (37), but some Pho4 may still be nuclear. For example, earlier we showed a Pho4 footprint at the repressed *PHO8* promoter (52) and *sin* mutations in histone H4 showed significantly derepressed *PHO5* activity in a UASp element-dependent, i.e., presumably Pho4-dependent, manner under otherwise-repressing conditions (81). Such nuclear Pho4 may bind especially to the accessible high-affinity sites UASpC and UASpD in the sHS region. This could lead to some basal recruitment of chromatin remodeling activities and a partially remodeled chromatin structure. We tested this by restriction enzyme analysis of the *PHO84* promoter region in a *pho4* deletion strain under high-phosphate conditions (Fig. 1D). However, only the accessibility of the HhaI site was decreased significantly, arguing that there was some basal Pho4-dependent remodeling only of the upstream nucleosome in the repressed state. This may also be noticeable based on the slightly more spread out sHS region in the presence of Pho4 (Fig. 1A, compare wt $+P_i$ and *pho4* $-P_i$). In contrast, the structure between the downstream nucleosome and the TATA box region was maintained semiopen also in the absence of Pho4.

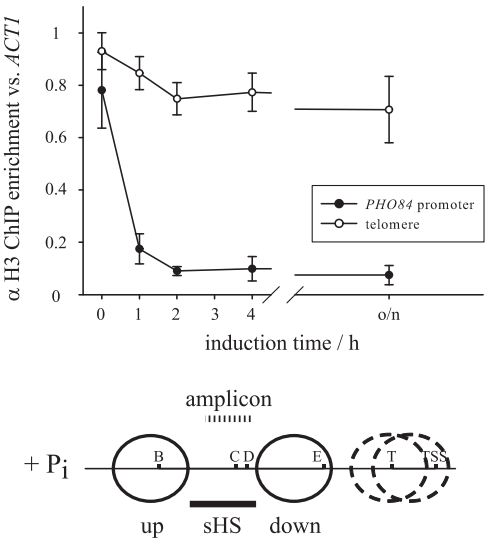

FIG. 2. Histones are depleted from the *PHO84* promoter region upon induction. The induction kinetics after transfer of a wt strain (CY337) to phosphate-free medium was followed by ChIP using a histone H3 C-terminal antibody and amplicons at the *PHO84* promoter, the telomere, and the *ACT1* open reading frame. ChIP data were normalized to input DNA and to the *ACT1* amplicon. Error bars show the standard deviations of three biological replicates. o/n, overnight induction. The scheme below the graph is analogous to Fig. 1B and shows the position of the *PHO84* promoter amplicon as a stippled bar.

Remodeling of *PHO84* promoter chromatin upon induction results in histone depletion from the promoter. The generation of an extended hypersensitive region at the induced *PHO84* promoter was reminiscent of our previous findings for the *PHO5* and *PHO8* promoters (3, 5). Such hypersensitivity was found by ourselves and others to reflect not just altered nucleosomal structures but also nucleosome disassembly leading to histone eviction from the promoter regions (1, 14, 38, 58). We checked if histones were lost also from the induced *PHO84* promoter. During *PHO84* induction kinetics, the histone H3 occupancy was monitored by ChIP using an antibody directed against the C terminus of histone H3. The histone H3 occupancy dropped after 2 hours of induction to about 10% of the level under repressing conditions (Fig. 2). At the same time there was no significant change of the histone H3 occupancy at a telomere control locus. Therefore, chromatin remodeling at the *PHO84* promoter eventually led to histone eviction.

The extent of chromatin remodeling critically depends on the intranucleosomal UASpE site. A special feature of the *PHO84* promoter is the presence of five Pho4 binding sites, UASpA to UASpE, which makes it one of the strongest PHO promoters (54). Ogawa et al. (54) showed previously by using a P_{PHO84}-*lacZ* reporter construct and deleting an extensive upstream region that UASpA and UASpB were not required for full *PHO84* activity. They further showed by site-directed mutagenesis that the low-affinity site UASpE in combination with either of the high-affinity sites UASpC or UASpD was necessary and sufficient for *PHO84* regulation. We wished to check if any of these effects on promoter activity actually reflected effects on chromatin remodeling.

We set up an analogous reporter system by constructing plas-

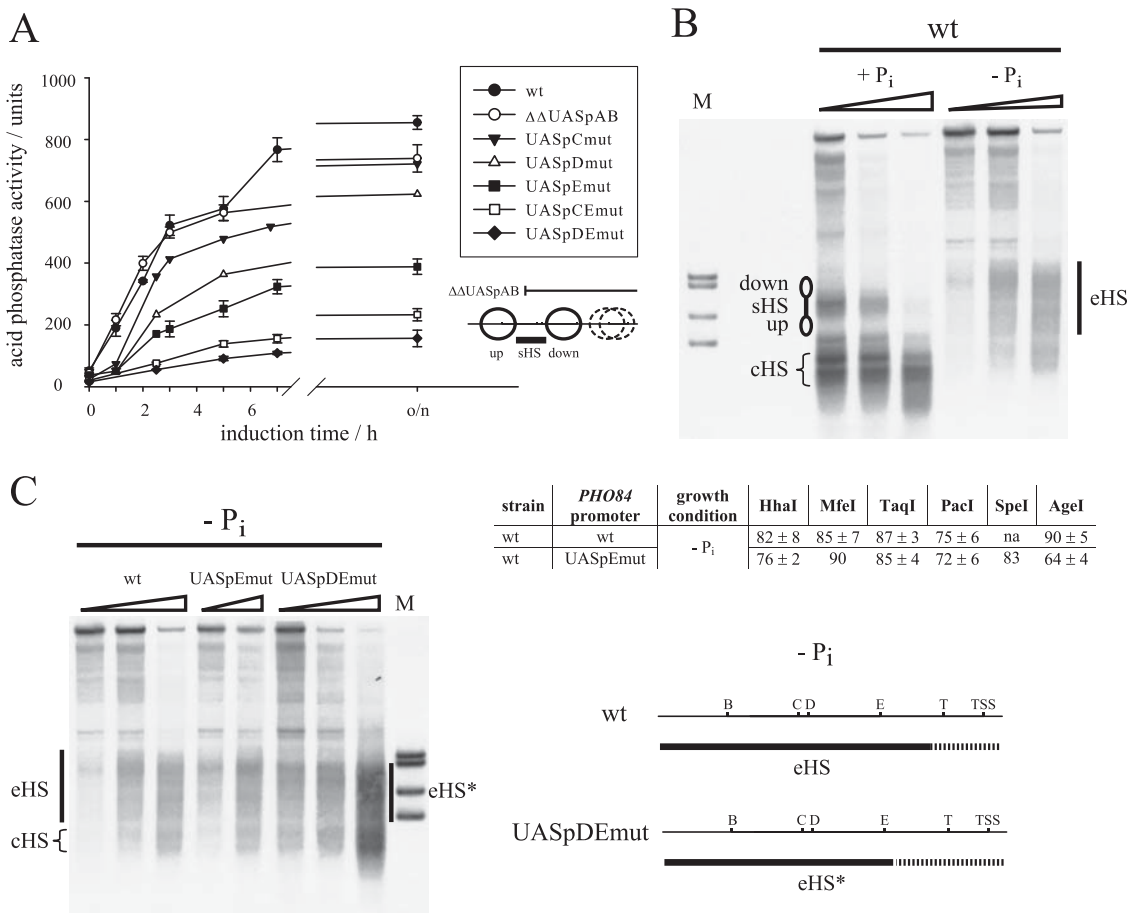

strain	*PHO84* promoter	growth condition	HhaI	MfeI	TaqI	PacI	SpeI	AgeI
wt	wt	- P_i	82 ± 8	85 ± 7	87 ± 3	75 ± 6	na	90 ± 5
wt	UASpEmut		76 ± 2	90	85 ± 4	72 ± 6	83	64 ± 4

FIG. 3. Effects of Pho4 binding site deletions on *PHO84* promoter induction kinetics and chromatin remodeling. (A) The *PHO84* promoter induction kinetics after shift to phosphate-free medium was monitored in a *pho5* strain (CY339) bearing reporter plasmids where either the wt *PHO84* promoter (plasmid pCB84a), a truncated *PHO84* promoter leading to the deletion of UASpA and UASpB (ΔΔUASpAB; plasmid pCB84b), or promoter variants with point mutations in Pho4 binding sites (plasmids pCB84a-UASpCmut, -Dmut, -Emut, -CEmut, and -DEmut) were coupled to the *PHO5*-coding region. Thereby, the induction kinetics could be monitored by an acid phosphatase activity assay. Error bars show the standard deviations of at least three biological replicates. o/n, overnight induction. The scheme below the legend corresponds to the scheme in Fig. 1B, and the blunt end of the line above shows the point of truncation in the ΔΔUASpAB variant (plasmid pCB84b). (B) The chromatin transition between the repressed (+P_i) and induced (−P_i) states of the *PHO84* promoter on the pCB84a plasmid locus as monitored by DNase I indirect end labeling. The same blot as in Fig. 1A was stripped and rehybridized with the probe for the plasmid locus. Labeling is as for Fig. 1A, but the marker fragments (lane M) correspond to double digests with HindIII and either AgeI, SpeI, ApaI, or BsrBI (from top to bottom in the lane). The SpeI site was introduced upon mutating UASpE and therefore corresponds to the position of this site. (C) DNase I indirect end labeling and markers as for panel B for the plasmids pCB84a (wt), pCB84a-UASpEmut, and -DEmut, respectively, in strain CY339 under inducing conditions (−P_i). All samples were electrophoresed in the same gel, but for the UASpDE data a stronger exposure is shown. The table shows average accessibility values of the indicated restriction enzymes as in Fig. 1D. The wt data are the same as in Fig. 1D, and data for the UASpEmut promoter variant are derived from two biological replicates if a variation is given. na, not applicable. The schematics are analogous to Fig. 1B. eHS*, the less-extended hypersensitive region of *PHO84* promoter variants with mutated UASpE.

mid pCB84a, for which the *PHO84* promoter was coupled to the *PHO5* coding gene. Thereby we avoided possible chromatin structure artifacts due to the close presence of the bacterial *lac*Z DNA sequence (unpublished observations). The enzymatic activity of the secreted acid phosphatase Pho5 can be measured easily with intact cells and *PHO5* transcriptional activity fully correlates with acid phosphatase activity, indicating no significant posttranscriptional regulation of *PHO5* expression (8). Importantly, the endogenous copy of *PHO5* was always deleted in strains where *PHO84* reporter constructs were used.

Using the pCB84a construct we observed phosphate-regulated *PHO84* promoter activity with a substantially higher basal and final level of Pho5 acid phosphatase activity than seen with the *PHO5* promoter (Fig. 3A; see also Fig. 9A and B, below). This was expected for the stronger *PHO84* promoter.

The *PHO84* promoter chromatin structure on the plasmid underwent the same regulated transition as the endogenous chromosomal locus (compare Fig. 3B and 1A for DNase I mapping; data not shown for restriction enzyme accessibilities). It should be noted that the region far upstream of the *PHO84* promoter, which is used for probing in indirect end-labeling techniques, was different between the plasmid and the chromosomal locus, thus allowing for a distinction of both loci within the same cell by differential probing and therefore excellent internal control. Due to the different relative position of the secondary cleavage site at the plasmid and chromosomal

locus, the DNase I indirect end-labeling fragments at the plasmid locus were 214 bp smaller, leading to a more stretched out appearance of the plasmid chromatin patterns on the blot. Possible minor changes in nucleosome positions between the chromosomal and the plasmid locus could still be undetected by this low-resolution approach.

Using this reporter plasmid, a set of promoter variants similar to the ones of Ogawa et al. (54) was constructed: a truncated version, plasmid pCB84b, in which effectively the upstream nucleosome and UASpA and UASpB were deleted (ΔΔUASpAB [schematic in Fig. 3A]), and point mutants for either one of the Pho4 binding sites, UASpC, UASpD, and UASpE, or for two sites together, i.e., UASpCEmut or UASpDEmut. For the truncated promoter the proper positioning of the downstream nucleosome in the repressed state and the generation of the corresponding extended hypersensitive region (truncated eHS type) upon induction were confirmed by DNase I indirect end labeling (data not shown).

Induction of the truncated promoter ΔΔUASpAB as monitored by acid phosphatase activity was very similar to the wt promoter (Fig. 3A). Mutation of the accessible high-affinity sites, UASpC or UASpD, affected the final promoter activity rather slightly, with the effect of the UASpD mutation being a bit more pronounced (Fig. 3A). In contrast, the absence of the intranucleosomal low-affinity site, UASpE, had a much stronger effect, reducing the final promoter strength by more than 50%. The combination of mutations in the UASpE and either UASpC or UASpD sites drastically reduced the final promoter activity to about 25% and 15% of the wt activity, respectively. We conclude, in agreement with Ogawa et al. (54), that the contribution of UASpC and UASpD was redundant, whereas UASpE contributed about half the promoter activity by itself. Further, there was some cooperativity between the intranucleosomal UASpE site and the accessible site UASpD and maybe also UASpC, as the effects of the double mutants were larger than the sum of the effects of each single mutant.

Next we examined if the effects on promoter strength were a consequence of inefficient promoter chromatin remodeling or of an effect downstream of chromatin opening. The DNase I indirect end-labeling patterns under inducing conditions of the UASpCmut or UASpDmut promoter variants were the same as for the wt promoter (data not shown), which was in agreement with a rather slight effect of these mutations on promoter activity. The finding that one UASp element in the sHS linker was sufficient for full remodeling of the upstream and downstream nucleosome is similar to the *PHO8* but different from the *PHO5* promoter, where the linker site UASp1 alone was not sufficient for chromatin remodeling (25). This may be because UASp1 at the *PHO5* promoter is a low-affinity binding site, in contrast to the high-affinity linker sites at the *PHO84* and *PHO8* promoters (5, 7, 54).

Any promoter variant lacking UASpE showed a hypersensitive region under inducing conditions that was less extensive in the downstream direction (eHS*) (Fig. 3C, schematic). This was especially clear in the DNase I patterns of the induced UASpCEmut and UASpDEmut promoter variants (Fig. 3C and data not shown), in which the extended hypersensitive region (eHS*) extended only up to about the SpeI marker band (−259 bp) (Fig. 3C), which was introduced with the UASpEmut point mutation and marked therefore the position of UASpE. In contrast, the eHS region of the induced wt promoter pattern reached further downstream beyond the AgeI marker (bp −172) (Fig. 1A and B and 3B). This less-extensive eHS* region was less clearly visible in the DNase I pattern of the UASpEmut variant (Fig. 3C), but less extensive remodeling downstream of the SpeI site was confirmed also for this variant by a reduced final accessibility of the AgeI site (Fig. 3C, table). We concluded that UASpE is essentially required for remodeling of the region between the downstream nucleosome and the TATA box.

Gcn5 is not essential for *PHO84* promoter remodeling, but its absence causes a strong delay in histone eviction kinetics and concomitant promoter induction. Previously, we found that remodeling of the chromatin structure at the weak *PHO8* promoter was critically dependent on Gcn5 and Snf2 (28). At the stronger *PHO5* promoter only the rate of chromatin remodeling was strongly decreased in the absence of Gcn5 or Snf2 (6, 8, 19), but eventually full remodeling was achieved. We wondered if remodeling at the even stronger *PHO84* promoter would be mostly or even fully independent of the presence of these cofactors.

First, we examined induction kinetics of the *PHO84* promoter in *gcn5* cells and found a strong delay in comparison to wt cells, even though the final induction level was unaffected (Fig. 4A). In agreement with this, the DNase I pattern of the fully induced promoter in the *gcn5* mutant was the same as observed in wt cells (Fig. 4B). Therefore, the Gcn5 activity had no essential role for the final opening of the *PHO84* promoter chromatin. This was confirmed further by restriction enzyme analysis of DNA accessibility at the entire promoter region under fully inducing conditions (Fig. 4C and D, $-P_i$).

In analogy to our earlier findings at the *PHO5* promoter (8), we assumed that the kinetic delay on the activity level in the *gcn5* mutant (Fig. 4A) was caused by a delay in the chromatin remodeling step. We quantified chromatin opening for wt and *gcn5* cells by restriction enzyme accessibility at 1.5 h after shift to phosphate-free medium and by histone H3 ChIP during an induction time course. To our surprise, we did not catch much of a delay in the increase of restriction enzyme accessibility at this time point of induction. There was only a slight delay compared to wt in opening at the AgeI site, i.e., in the region between the downstream nucleosome and the TATA box (Fig. 4C and D, 1.5 h, $-P_i$). For comparison, chromatin remodeling at the *PHO5* promoter, as probed by ClaI accessibility, was still strongly delayed after 3 hours of induction in a *gcn5* strain (8). Nonetheless, we did observe a strong delay in histone eviction kinetics as monitored by histone H3 ChIP (Fig. 4E). Even after 2 hours of induction, there was six to seven times more histone H3 still present at the promoter in the *gcn5* mutant than in the wt cells. Therefore, we observed for the first time a large disparity between restriction enzyme accessibility and histone H3 eviction kinetics during induction of a PHO promoter. We conclude that histone eviction, rather than an initial increase of DNA accessibility, appeared to be the rate-limiting step in *PHO84* promoter opening in a *gcn5* mutant.

In the absence of Snf2, remodeling of the *PHO84* promoter chromatin structure is only partial: the downstream nucleosome is fully remodeled but the upstream one is not at all. Second, we examined *PHO84* promoter induction kinetics in a *snf2* mutant and observed a similar delay as with the *gcn5*

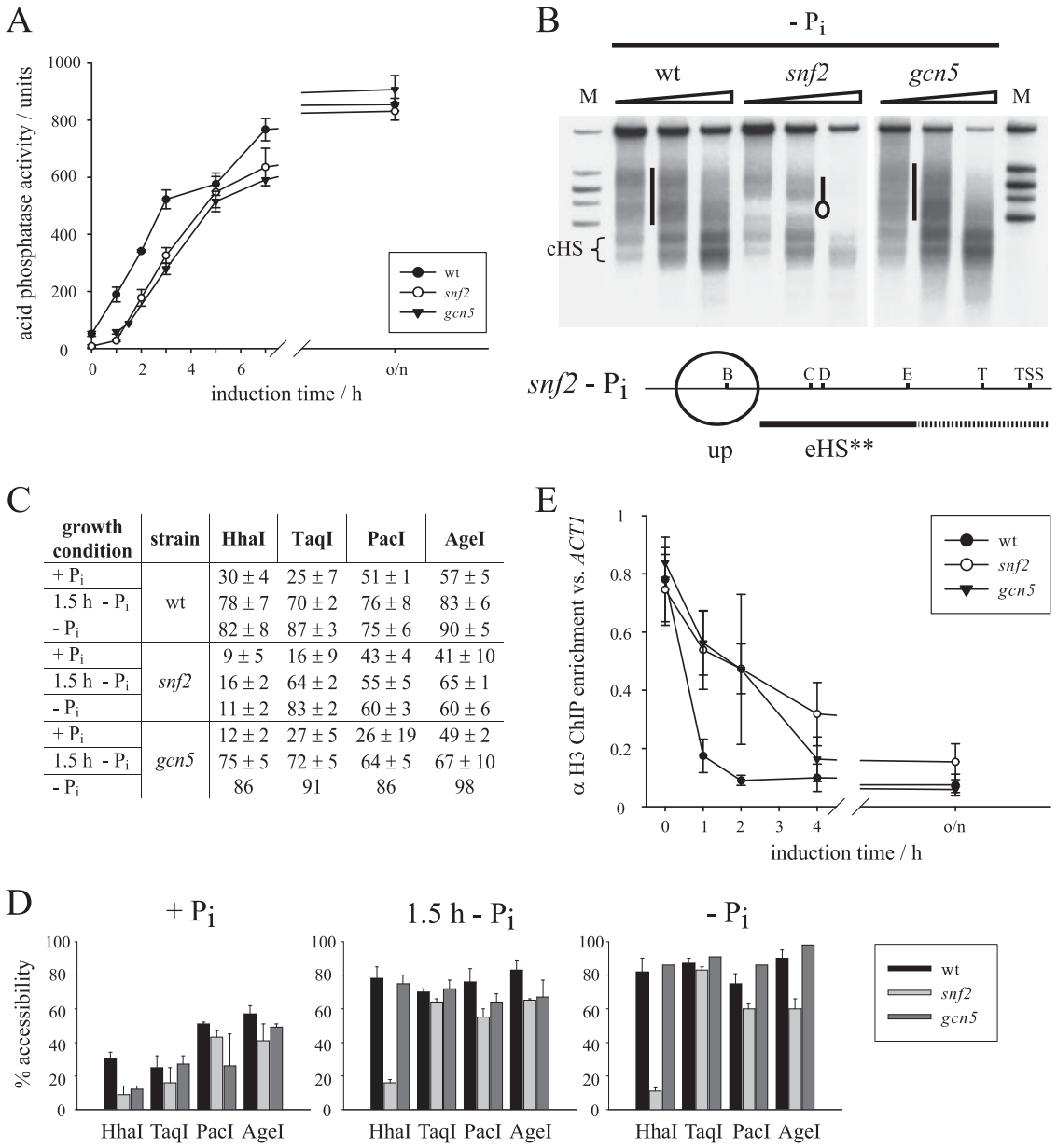

growth condition	strain	HhaI	TaqI	PacI	AgeI
+ P_i	wt	30 ± 4	25 ± 7	51 ± 1	57 ± 5
1.5 h - P_i		78 ± 7	70 ± 2	76 ± 8	83 ± 6
- P_i		82 ± 8	87 ± 3	75 ± 6	90 ± 5
+ P_i	*snf2*	9 ± 5	16 ± 9	43 ± 4	41 ± 10
1.5 h - P_i		16 ± 2	64 ± 2	55 ± 5	65 ± 1
- P_i		11 ± 2	83 ± 2	60 ± 3	60 ± 6
+ P_i	*gcn5*	12 ± 2	27 ± 5	26 ± 19	49 ± 2
1.5 h - P_i		75 ± 5	72 ± 5	64 ± 5	67 ± 10
- P_i		86	91	86	98

FIG. 4. Chromatin remodeling at the *PHO84* promoter is incomplete and delayed in the absence of Snf2 and only delayed in the absence of Gcn5. (A) *PHO84* promoter induction kinetics as in Fig. 3A for wt (CY339 pCB84a), *snf2* (CY409 pCB84a), and *gcn5* (CY53379 *pho5* pCB84a) strains. o/n, overnight induction. (B) DNase I indirect end-labeling analysis of the *PHO84* promoter chromatin structure at the chromosomal locus in the induced state ($-P_i$) for wt (CY339 pCB84a-UASpCEmut), *snf2* (CY409 pCB84a-UASpCEmut), and *gcn5* (CY53379 *pho5* pCB84a) strains. Marker lanes (M) are as described for Fig. 1A (AgeI, MfeI, ApaI, and BsrBI, from top to bottom). The vertical bars between the second and third and between the eighth and ninth lanes mark the eHS (as in Fig. 1A) of the induced wt promoter pattern. The bar and oval between the sixth and seventh lanes corresponds to the schematic below the blot that illustrates the semiremodeled pattern of the induced *PHO84* promoter in a *snf2* strain. eHS** denotes the reduced extended hypersensitive region of this pattern. All other labeling is analogous to that for Fig. 1A and B. All samples were electrophoresed in the same gel, but for the *gcn5* data a stronger exposure is shown. (C) Average accessibility values for the indicated restriction enzymes under conditions of repression ($+P_i$), full induction ($-P_i$), and an early time point of induction (1.5 h $-P_i$) for wt, *snf2* (CY409 pCB84a), and *gcn5* (CY53379 *pho5* pCB84a) strains. The wt $+P_i$ and $-P_i$ data are the same as in Fig. 1D, and the wt 1.5-h $-P_i$ data were generated with strain CY339 pCB84a. Averages are derived from two to four biological replicates if a variation is given. (D) Same data as shown in panel C, but plotted as bar diagrams and grouped according to growth conditions. (E) Histone loss kinetics as in Fig. 2 using the *PHO84* promoter amplicon with wt (CY337), *snf2* (CY407), and *gcn5* (CY53379) strains. Error bars show the standard deviations of three biological replicates. o/n, overnight induction.

mutant, again with hardly any effect on the final level of induction (Fig. 4A). In marked contrast and much to our surprise, this final activity of the *snf2* strain corresponded to an only partially open DNase I pattern of the induced *PHO84* promoter, both on the chromosomal and the plasmid locus (Fig. 4B and data not shown). The downstream nucleosome was remodeled, but the upstream one was not at all. In addition, we noticed that the spreading of the eHS region was less

extensive in the downstream direction than in the wt case (eHS**) (Fig. 4B, schematic) and confirmed this by a reduced final accessibility of the AgeI and PacI sites (Fig. 4C and D, $-P_i$). This reduced downstream spreading of the eHS** region was similar to the reduced spreading of the eHS* region in the UASpEmut variant (Fig. 3C). It was even somewhat more severe, as also the PacI site accessibility was reduced in the eHS** but not in the eHS* region (Fig. 4C and 3C, tables). Even though the eHS** region in the *snf2* mutant was less remodeled than the eHS* region in the UASpEmut variant, it was still compatible with full final activity levels (Fig. 4A). So, we concluded that the lower final activity in the UASpEmut, and even more so in the UASpCEmut and UASpDEmut variants (Fig. 3A), was less due to compromised chromatin remodeling but mainly due to the reduced number of UASp elements (see also reference 41). As the transition from the semiopen to the fully open state in the region between the downstream nucleosome and the TATA box was compromised in both the *snf2* mutant and the UASpEmut variant, we suggest that recruitment of the SWI/SNF complex by UASpE-bound Pho4 was essential for chromatin remodeling in this region.

Restriction enzyme probing of the induced state in the *snf2* mutant also confirmed the lack of remodeling of the upstream nucleosome, i.e., persistently low HhaI accessibility, and full remodeling of the downstream nucleosome, i.e., high TaqI accessibility (Fig. 4C and D, $-P_i$). Altogether, this chromatin pattern constituted a third type of extended hypersensitive region (eHS**) (Fig. 4B, schematic), where the upstream nucleosome was still present, the downstream nucleosome fully remodeled, and the region between the downstream nucleosome and the TATA box not fully remodeled.

The same partially remodeled DNase I pattern was also observed in the *snf2K798A* strain, which bears a point mutation in the Snf2 ATPase domain (Fig. 5A), confirming that the ATPase activity of Snf2 rather than some other feature of the SWI/SNF complex was responsible for the observed effect.

In analogy to the *gcn5* mutant, we examined whether the kinetic delay of *PHO84* promoter induction in the *snf2* mutant (Fig. 4A) corresponded not only to the aforementioned reduction in the final extent of remodeling but also to a kinetic delay of chromatin opening, for example, at the TaqI site in the downstream nucleosome. After 1.5 h of induction there was not much delay in opening of the TaqI or any other site, based on the 1.5-h values for the *snf2* strain compared to wt and normalized to their respective $-P_i$ values (Fig. 4C and D). However, histone eviction kinetics measured by histone H3 ChIP in *snf2* cells showed a strong delay (Fig. 4E). At present we are unsure why the final level of histone occupancy at the induced *PHO84* promoter in *snf2* cells as measured by histone H3 ChIP was not much higher than for the wt and *gcn5* strains. This would be expected due to the continued presence of the upstream nucleosome in the *snf2* strain. The resolution of our ChIP analysis (about 500 bp) cannot distinguish between the upstream and the downstream nucleosome, because the amplicon used (Fig. 2, schematic) will score fragments from both nucleosome regions. However, as the upstream nucleosome was not remodeled at all and as the downstream region close to the TATA box was remodeled to a lesser extent than in the wt (see above), we assume that histone H3 ChIP mainly monitored remodeling of the downstream nucleosome. Therefore, the delayed histone eviction in the *snf2* mutant argues for a role of Snf2 in remodeling of the downstream nucleosome. Similar to the case of the *gcn5* mutant, also here histone eviction seemed to be the rate-limiting step.

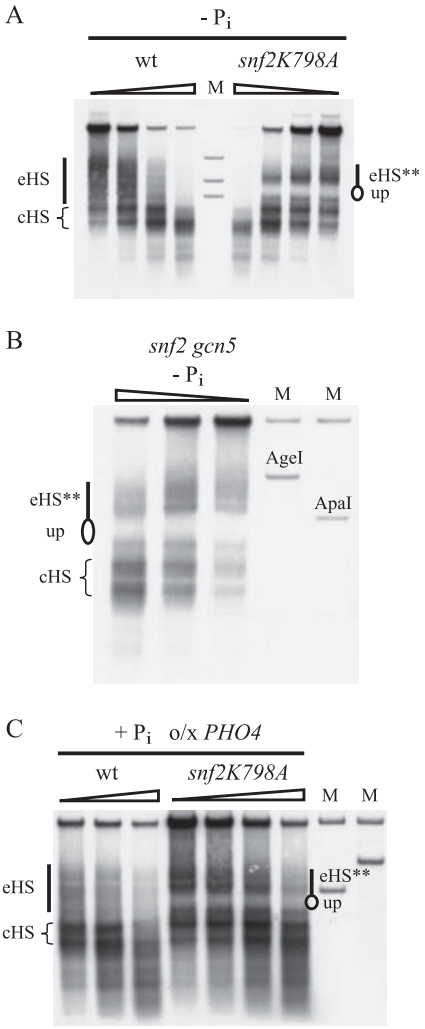

FIG. 5. The Snf2 ATPase domain point mutant as well as a *snf2 gcn5* double mutant show the same *PHO84* promoter chromatin organization in the induced state as the *snf2* deletion mutant. (A) DNase I indirect end labeling of the induced *PHO84* promoter chromatin structure in wt (CY396) and *snf2K798A* (CY397) strains. Labeling is analogous to that used in Fig. 1A and 4B. Marker fragments (lane M) correspond to double digests with HindIII and either AgeI, ApaI, or BsrBI (from top to bottom in the lane). (B) DNase I indirect end labeling of the induced *PHO84* promoter chromatin structure in a *snf2 gcn5* strain (FY1352). Labeling is as for panel A. Marker fragments correspond to double digests with HindIII/AgeI (left lane M) and HindIII/ApaI (right lane M). (C) DNase I indirect end labeling of the *PHO84* promoter chromatin structure under conditions of *PHO4* overexpression (o/x *PHO4*) in phosphate-containing medium ($+P_i$) for wt (CY396 pP4-70l) and *snf2K798A* (CY397 pP4-70l) strains. Labeling is as for panel A. Marker fragments correspond to double digests with HindIII/ApaI (left lane M) and HindIII/AgeI (right lane M).

As remodeling of the downstream nucleosome was eventually complete but kinetically delayed at the histone eviction step in both the *snf2* and *gcn5* single mutants, we wondered if the downstream nucleosome may not open up at all in a *snf2*

gcn5 double mutant. This was not the case, as the DNase I pattern of the fully induced *PHO84* promoter in the *snf2 gcn5* double mutant was indistinguishable from that found in *snf2* cells (Fig. 5B).

Previously, it was shown by us and others that submaximal induction conditions can exacerbate the dependency of *PHO5* promoter chromatin remodeling on chromatin cofactors (19, 38). Such submaximal induction conditions may be achieved by using low-phosphate rather than phosphate-free medium (19) or by overexpression of Pho4 in high-phosphate medium (25). We tested under the latter conditions whether the differential requirement of Snf2 for remodeling of the downstream and the upstream nucleosome still persisted at submaximal induction. DNase I indirect end-labeling analysis under these submaximal induction conditions showed the same pattern as under fully inducing conditions, for both the wt as well as the *snf2K798A* mutant (Fig. 5C). So, even at such low induction levels the downstream nucleosome could be remodeled without Snf2 activity, demonstrating further the different degree of Snf2 requirement for remodeling of the upstream and downstream nucleosome.

The semiopen chromatin structure close to the TATA box is not sufficient, and basal remodeling of the upstream nucleosome is not necessary for substantial basal *PHO84* transcription. The *pho4*, *snf2*, and *gcn5* mutants all had a decreased basal level of transcription (Fig. 4A and data not shown) (69). In all these three mutants the semiopen less-organized chromatin structure between the downstream nucleosome and the TATA box was not affected in the repressed state. Therefore, this semiopen structure was not sufficient for sustaining substantial basal transcription under repressing conditions.

Nonetheless, in all three mutants the accessibility of the HhaI site under repressing conditions was reduced in comparison to wt, in *snf2* and *gcn5* cells even more so than in the *pho4* mutant (Fig. 4C and D, $+P_i$, and 1D, table). The reduced HhaI accessibility might have been responsible for the reduced basal transcription. In the wt, the targeted recruitment of Snf2 and Gcn5 by Pho4 could keep the upstream nucleosome in a partially remodeled state, which would allow partial access to UASpB and lead to even more remodeling of the upstream nucleosome and high basal transcription. To test this, we introduced a point mutation in UASpB and found indeed that the HhaI site accessibility under $+P_i$ conditions ($19 \pm 2\%$) was significantly lower than at the wt promoter and similar to that of the wt promoter in the *pho4* mutant ($17 \pm 2\%$) (Fig. 1D). However, despite this lower HhaI accessibility there was hardly any effect on the basal level of activity for the UASpBmut construct (data not shown), arguing that UASpB and basal remodeling of the upstream nucleosome were not necessary for the substantial basal transcription. In addition, mutation of the other intranucleosomal site, UASpE, which analogously may have been involved in basal remodeling of the downstream nucleosome, did not affect basal transcription either (Fig. 3A).

Ino80 is not essential for chromatin opening at the entire *PHO84* promoter, neither in wt nor in *snf2* cells, but its absence causes a strong delay in chromatin opening kinetics. As we had already observed a cooperation between Snf2 and Ino80 for chromatin remodeling at the *PHO5* and *PHO8* promoters (6), and as others have shown a recruitment of both Snf2 and Ino80 to the *PHO84* promoter upon induction (23, 36, 72), we investigated the role of Ino80 for *PHO84* promoter opening. In particular, there was the possibility that Ino80 would be the alternative remodeler for remodeling of the downstream nucleosome in the absence of Snf2.

The absence of Ino80 by itself did not prevent full remodeling of the *PHO84* promoter chromatin structure, i.e., the DNase I pattern of an *ino80* mutant under fully inducing conditions corresponded to the eHS type of the wt (Fig. 6A) and the accessibility of restriction enzymes along the promoter region increased to almost-wt levels (Fig. 6C). Further, the DNase I pattern of the induced promoter in the *snf2 ino80* double mutant was indistinguishable from the pattern of the *snf2* single mutant (Fig. 6B). Together, these results argue that Ino80 was neither essentially required for remodeling under fully inducing conditions in the wt strain nor for remodeling of the downstream nucleosome in the absence of Snf2. Nonetheless, the chromatin opening kinetics in the *ino80* strain was strongly delayed over the entire promoter region after 1.5 h of induction as examined by restriction enzyme accessibility (Fig. 6C). Therefore, Ino80 is clearly involved in the wt chromatin remodeling pathway at the *PHO84* promoter.

In contrast to Snf2 and Gcn5, Ino80 was not involved in keeping the upstream nucleosome in a partially remodeled state under repressing conditions ($+P_i$), as the HhaI accessibility was not affected in the *ino80* mutant (Fig. 6C, table, $+P_i$). A slight decrease in PacI accessibility may indicate that Ino80 has a minor role in positioning the downstream nucleosome under repressing conditions.

As presented above for the case of Snf2, we checked if *PHO84* promoter opening became more dependent on Ino80 under submaximal conditions. Strikingly, the DNase I patterns of the *snf2K798A* and the *ino80* mutants at submaximal induction were indistinguishable, i.e., under these conditions the upstream nucleosome became strictly dependent also on Ino80 (Fig. 6D).

The stricter cofactor requirements for remodeling of the upstream nucleosome correlates with higher intrinsic stability as measured in vitro and predicted in silico. As shown above, remodeling of the upstream nucleosome was strictly dependent on Snf2, whereas remodeling of the downstream nucleosome was not (Fig. 4B and 5A). In addition, remodeling of the upstream nucleosome was more dependent on Ino80 than remodeling of the downstream nucleosome (Fig. 6D). This constitutes a case of differential cofactor requirements for nucleosome remodeling within one and the same promoter.

We found earlier that the differential cofactor requirements for chromatin remodeling at the *PHO5* and *PHO8* promoters correlated with differential intrinsic stabilities of the positioned nucleosomes (31). These stabilities were measured using our yeast extract chromatin assembly system that is able to generate the proper in vivo nucleosome positioning de novo in vitro (31, 39). In this system, plasmids bearing the yeast locus of interest are assembled by salt gradient dialysis into a chromatin structure with a specific but usually not proper, i.e., not in vivo-like, nucleosome positioning pattern. The in vivo-like pattern is induced in the next step by the addition of yeast whole-cell extract in the presence of energy. A so-far-unidentified energy-dependent activity in the yeast extract apparently constitutes the thermodynamic conditions for in vivo-like nucleo-

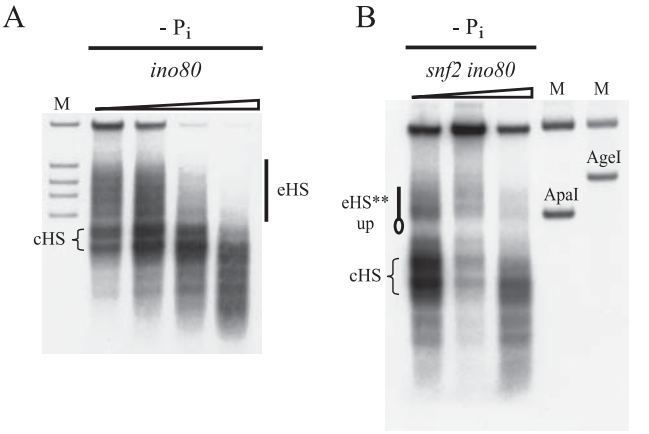

C

strain	growth condition	HhaI	TaqI	PacI	AgeI
wt	+ P_i	30 ± 4	25 ± 7	51 ± 1	57 ± 5
ino80		28 ± 1	26 ± 1	43 ± 1	57 ± 1
wt	1.5 h - P_i	73 ± 1	86 ± 3	81 ± 6	78 ± 4
ino80		31 ± 4	46 ± 1	45 ± 3	57 ± 4
wt	- P_i	79 ± 8	90 ± 4	89 ± 5	91 ± 2
ino80		69	84	86	79

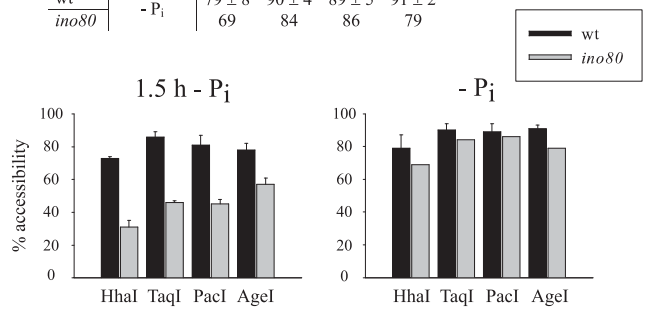

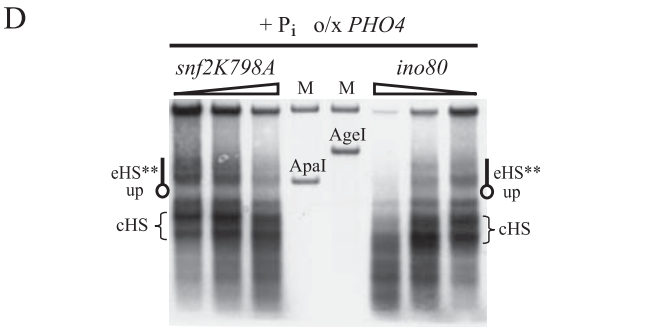

FIG. 6. Chromatin remodeling at the *PHO84* promoter is delayed in the absence of Ino80. (A) DNase I indirect end-labeling analysis of the induced *PHO84* promoter chromatin structure for an *ino80* strain (BY4741-1). Labeling is as for Fig. 1A and 4B. Marker in lane M is as in Fig. 1A (AgeI, MfeI, ApaI, and BsrBI, from top to bottom). (B) DNase I mapping as for panel A, but for the *snf2 ino80* double mutant (CY407 *ino80*). Marker fragments correspond to double digests with HindIII/ApaI (left lane M) and HindIII/AgeI (right lane M). Labeling is as for Fig. 1A and 5B. (C) Restriction enzyme accessibility data are as for Fig. 4C and D for wt (BY4741) and *ino80* (BY4741-1) strains. Averages are derived from two to three biological replicates if a variation is given. The wt + P_i data are the same as those in Fig. 1D. (D) DNase I mapping of the *PHO84* promoter under submaximal induction conditions as in Fig. 5C for *snf2K798A* (CY397 pP4-70l) and *ino80* (BY4741-1 pP4-70l) strains. The left five lanes are the same as the right five lanes in Fig. 5C. Labeling and markers as in Fig. 5C.

some positioning. In a next step, it is possible to compare the intrinsic stability of properly positioned nucleosomes by titrating the histone concentration. Under conditions of limiting histones (underassembled chromatin) there are fewer nucleosomes deposited onto the DNA than there are nucleosome positions available. Therefore, the multitude of alternative and mostly overlapping nucleosome positions will compete for nucleosome occupancy. Positions that are already occupied in equilibrium in underassembled chromatin are more stable than those that are occupied only in fully assembled chromatin (for a full discussion of this methodology see reference 31). Using this approach, we observed previously that the proper positioning over the *PHO5* promoter region could only be generated in fully assembled chromatin, whereas the proper *PHO8* promoter pattern was also achieved in underassembled chromatin. Therefore, the intrinsic stability of the *PHO8* promoter nucleosomes was higher than the stability of the *PHO5* promoter nucleosomes.

With the same methodology we compared the intrinsic stability of the upstream and downstream nucleosome at the *PHO84* promoter (Fig. 7A and B). First, we prepared fully assembled salt gradient dialysis chromatin (histone octamer: DNA mass ratio set as 100%) using a plasmid with a 3.5-kb *PHO84* insert as template and tested if the yeast extract would generate the in vivo pattern. Much to our surprise, we observed that the DNase I pattern of the salt gradient dialysis chromatin was already very similar to the in vivo pattern (Fig. 7A, compare SGD and in vivo). This pattern was clearly different from a digest of free DNA and did not change much, as expected (31), with the addition of yeast extract in the absence of energy. This was the first case out of 14 tested yeast loci (C. Wippo and P. Korber, unpublished results) where salt gradient dialysis by itself was already able to generate a very in vivo-like chromatin structure. This suggests that rather strong nucleosome positioning sequence elements in the *PHO84* promoter lead to in vivo-like nucleosome positioning already under pure salt gradient dialysis conditions. Nonetheless, incubation with yeast extract and energy did make the pattern more similar to the in vivo pattern, especially regarding the relative band intensities and the upper part of the lane, i.e., the coding region (Fig. 7A, compare SGD +Yex/ATP with in vivo). Therefore, the *PHO84* promoter is one more example where our yeast extract in vitro assembly system constitutes conditions more similar to in vivo conditions for nucleosome positioning than salt gradient dialysis alone.

Second, we repeated the salt gradient dialysis chromatin assembly with limiting histones (histone octamer:DNA mass ratio of 60%) and still obtained a rather in vivo-like pattern (Fig. 7B). This in vivo-like pattern again did not change upon the addition of yeast extract without energy. However, incubation with yeast extract in the presence of energy, i.e., conditions that should be closer to the in vivo conditions, had a differential effect on the regions upstream and downstream of the sHS region. The upstream nucleosome and the cHS region again became even more like the in vivo pattern, but the sHS region was so much extended further downstream that the position of the downstream nucleosome was compromised. The sHS region was always somewhat sharper in the pure salt gradient dialysis chromatin pattern and became fuzzier upon addition of yeast extract and energy, also with fully assembled chroma-

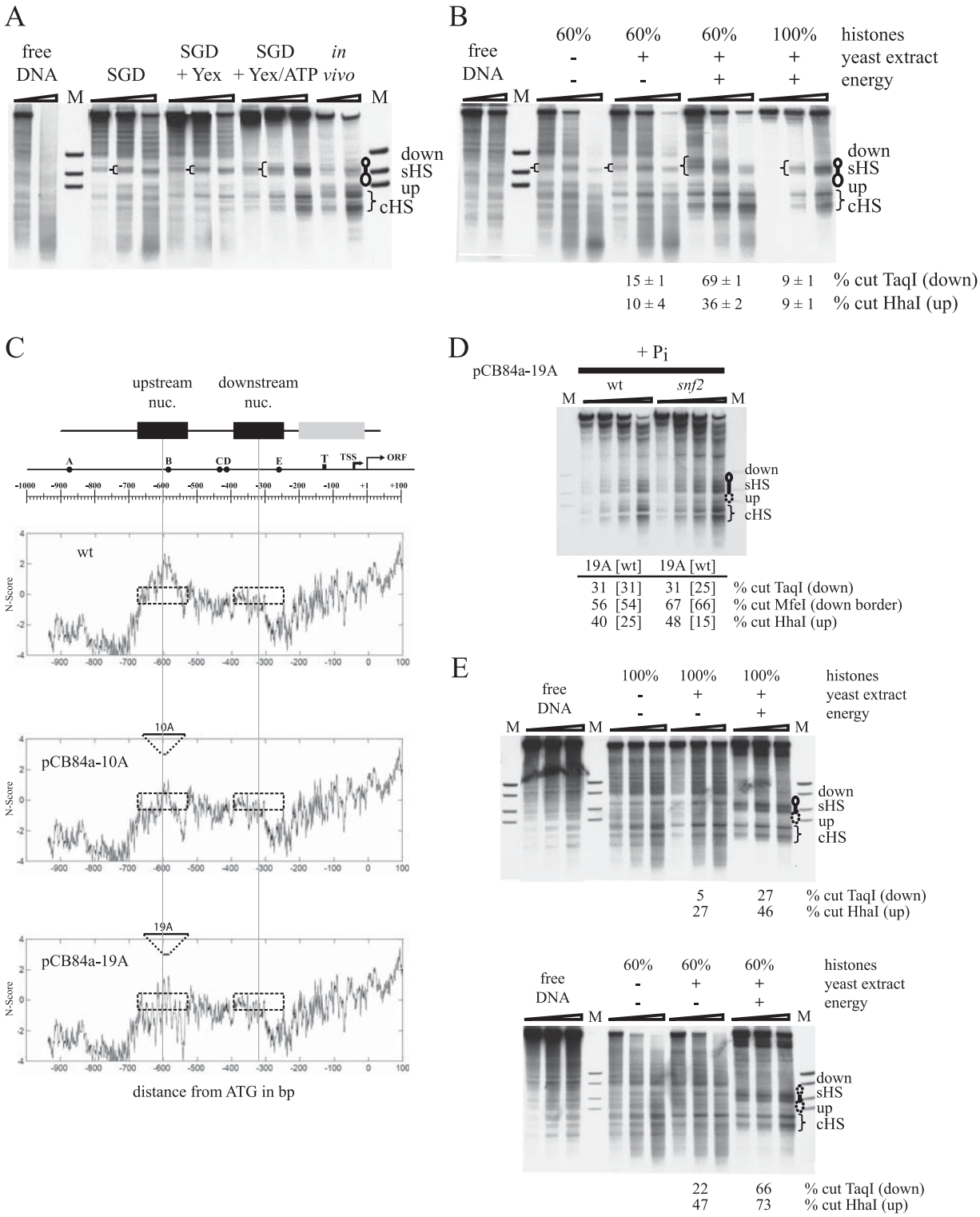

FIG. 7. The nucleosome upstream of the short hypersensitive site at the *PHO84* promoter has higher intrinsic stability than the downstream nucleosome and can be destabilized by introducing poly(dA) stretches. (A) DNase I indirect end-labeling analysis of the *PHO84* promoter region on plasmid pUC19-PHO84 in vitro either as free DNA or after chromatin assembly by salt gradient dialysis (SGD) and further incubation with yeast extract in the absence (SGD +Yex) or presence of energy (SGD +Yex/ATP). The *PHO84* promoter chromatin pattern of the repressed state in vivo is shown for comparison. Marker fragments (lanes M) correspond to double digests with SspI and either AgeI, ApaI, or BsrBI (from top to bottom in the lanes). Schematics next to the blot are as described for Fig. 1A. Brackets in the lanes highlight the extent of the sHS region. (B) DNase I indirect end labeling and markers (lane M) as for panel A but with either underassembled (60% histones) or fully assembled (100% histones; the same degree of assembly as in panel A) salt gradient dialysis chromatin on plasmid pUC19-PHO84 and incubation with yeast extract and energy as indicated. Brackets in the lanes mark the extent of the sHS under the different chromatin assembly conditions. The accessibilities

tin templates (Fig. 7A; compare widths of brackets). But whereas the more fuzzy sHS region in the fully assembled chromatin (100%) resembled more the in vivo case, it was stretched too far downstream to be compatible with a proper positioning of the downstream nucleosome for the underassembled chromatin templates (60%) (Fig. 7B; compare widths of brackets). We stress that the more extensive sHS region under underassembled conditions compared to fully assembled conditions (Fig. 7B) was not due to the use of different degrees of DNase I digestion, as we saw such a difference significantly and repeatedly over a wider range of DNase I digestions (data not shown).

This differential effect on the upstream and downstream nucleosome was confirmed by restriction enzyme accessibility assays. The accessibility of the TaqI site in the downstream nucleosome increased much more (from 15% to 69%) (Fig. 7B) upon addition of extract and energy to underassembled chromatin than the accessibility of the HhaI site in the upstream nucleosome (from 10% to 36%). The overall lower accessibilities in the fully assembled chromatin compared to the in vivo situation probably reflected here a subpopulation of aggregated, i.e., indigestible, templates in vitro, which may form especially at such high histone concentration. Altogether, these results suggested that the downstream nucleosome was intrinsically less stably positioned in vivo than the upstream nucleosome. This correlated with its more relaxed cofactor requirements.

The finding of higher intrinsic stability of the upstream nucleosome also correlated strikingly with the prediction of the *N*-score algorithm (84) (Fig. 7C). The *N*-score algorithm was trained on in vivo yeast nucleosome positioning data and used to predict the probability for nucleosome occupancy (positive values) or depletion (negative values) rather than exact positions. It showed a positive peak right in the middle of the upstream nucleosome, maybe suggesting an especially stable nucleosome here in vivo. In contrast, the DNA sequence underlying the downstream nucleosome was rather neutral, or even negative at its 3′ end, with regard to the propensity for nucleosome occupancy.

Introduction of destabilizing mutations into the DNA sequence of the upstream nucleosome relieves the Snf2 dependency for its remodeling in vivo. So far, we correlated, in this and our previous study (31), intrinsic nucleosome stability and the cofactor requirement. Next we wished to test directly if stability was causative for requirement. Extended stretches of poly(dA-dT) are known to be unfavorable for nucleosome formation in vivo and in vitro (4, 33, 57). So we replaced a stretch of 10 or 19 consecutive bases with adenine deoxynucleotides (plasmids pCB84a-10A and −19A, respectively) in the middle of the upstream nucleosome region (Fig. 7C). As expected, such replacements led to increasingly more negative *N*-scores for the region that was occupied by the upstream nucleosome in the wt promoter (Fig. 7C).

We needed to check if the upstream nucleosome would still form in vivo on these mutated DNA templates. DNase I mapping confirmed the presence of the upstream nucleosome for both variants in the wt and *snf2* backgrounds (Fig. 7D and data not shown). Restriction enzyme accessibility assays showed that there was no increase in HhaI site accessibility for the 10A replacement compared to the wt promoter (data not shown) but an increase for the 19A variant (from 25 to 40% in wt and from 15 to 48% in the *snf2* background) was observed (Fig. 7D). This suggested a destabilized upstream nucleosome for the 19A variant already under repressive conditions. There was also a subtle shift in positioning as the sHS region extended more upstream beyond the ApaI marker (compare Fig. 7D and 3B). This region of additional hypersensitivity at the 3′ border of the upstream nucleosome correlated with the region of the most negative *N*-score at about −550 (Fig. 7C).

The reduced stability of the 19A variant was directly assessed in our in vitro chromatin assembly assay (Fig. 7E). First, the upstream nucleosome formed neither with a limiting (60%) nor with the full (100%) complement of histones during salt gradient dialysis, but the DNase I pattern in this region was similar to that of the free DNA digest. This speaks for the lower nucleosome positioning power of the mutated DNA sequence under these conditions. Second, the addition of yeast extract and energy induced a more in vivo-like chromatin structure in the fully assembled (100%) chromatin template, with accessibilities for the HhaI and TaqI sites that were very similar to the in vivo values (Fig. 7D and E; compare 19A in the wt background [D] and 100% with yeast extract and energy [E]). This confirmed again that the unidentified energy-depen-

of the respective chromatin states to HhaI and TaqI (monitoring the accessibility of the upstream and downstream nucleosome, respectively, by the same assay as shown in Fig. 1C) are given underneath the blot. Average values and variations are derived from two independent treatments of a given salt gradient dialysis chromatin preparation. DNase I mapping data were reproduced with two independent salt gradient chromatin preparations. (C) The scheme on top shows the *PHO84* promoter chromatin organization, with black boxes indicating the positioned upstream and downstream nucleosomes and the gray box representing the less-organized structure close to the TATA box. The positions of five UASp elements (A to E), of the TATA box (T), transcription start site (TSS), and the ORF are indicated on top of the scale that plots the distance in base pairs from the ATG (+1). The three graphs show the *N*-score (84) plotted against the distance from the ATG in base pairs for the wt *PHO84* promoter and for promoter variants where stretches of 10 or 19 bases were replaced with homopolymeric deoxyadenylate at the indicated positions in the plasmids pCB84a-10A and pCB84a-19A, respectively. Stippled boxes show the positions of the upstream and downstream nucleosomes as in the schematic above, and thin gray lines mark the center of these nucleosomes. (D) DNase I indirect end-labeling analysis of the *PHO84* promoter chromatin structure at the plasmid locus in wt (CY339 pCB84a-19A) and *snf2* (CY409 pCB84a-19A) strains under repressive conditions ($+P_i$). Markers (lanes M) are as for panels A and B (AgeI, ApaI, and BsrBI, from top to bottom). Labeling is as in Fig. 1A, but the oval representing the upstream nucleosome in the *snf2* strain is stippled to indicate the partially open state. Accessibilities for the indicated restriction enzymes are indicated underneath the blot, as for panel B. MfeI monitors the border of the downstream nucleosome toward the sHS region (down border). Values in brackets show the respective accessibilities of the endogenous chromosomal wt promoter in the same cells. (E) DNase I indirect end-labeling and restriction enzyme accessibility assays analogous to those in panel B but with plasmid pUC19-PHO84-19A. Stippled ovals in the schematics indicate destabilized nucleosomes. Marker fragments (M lanes) correspond to double digests with SspI and either ClaI, AgeI, ApaI, or BsrBI (from top to bottom in the lane). All DNase I indirect end-labeling samples in each panel of the entire figure were electrophoresed on the same gel, but images from different film exposure times were combined using Adobe Photoshop CS2.

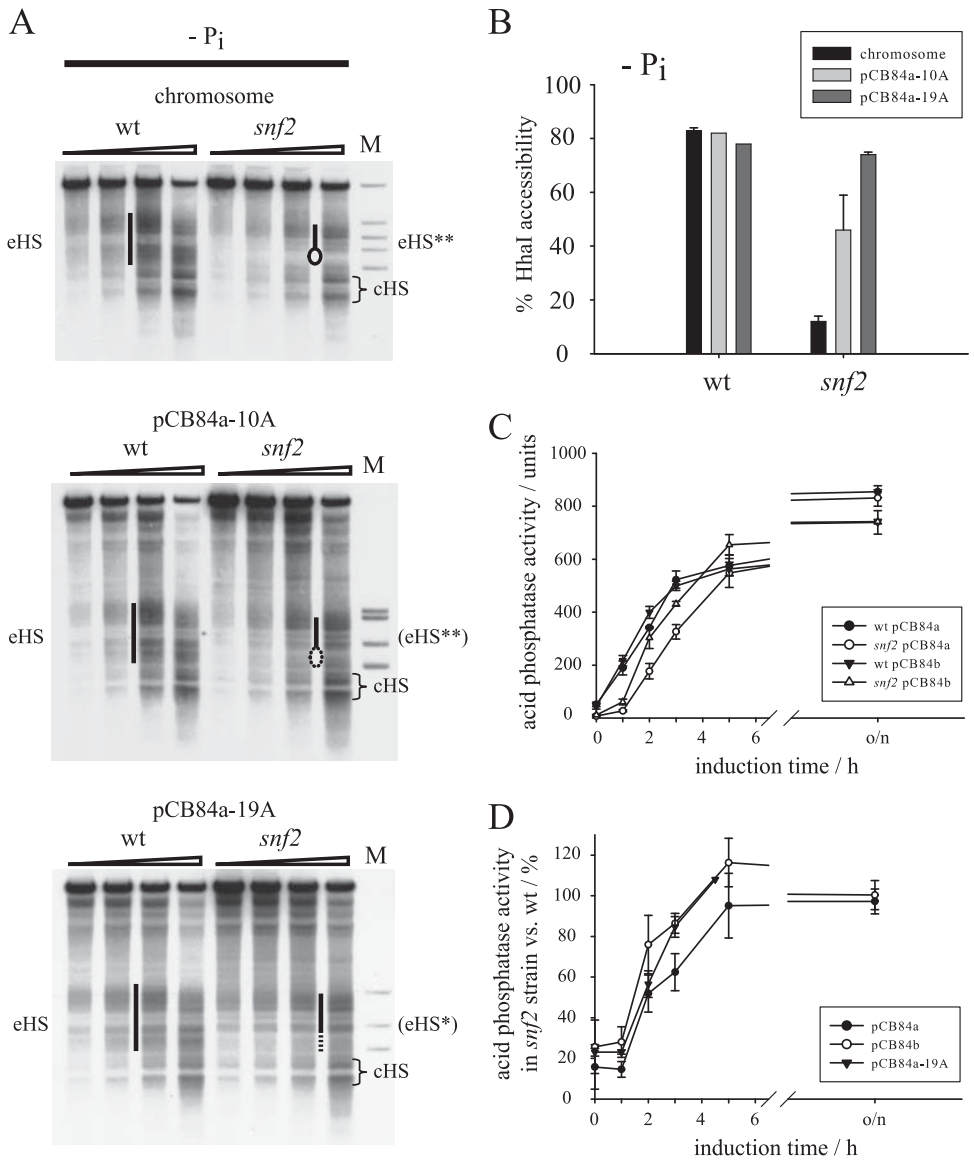

FIG. 8. Mutations that progressively destabilize the upstream nucleosome also progressively relieve its Snf2 dependency of remodeling, but destabilization or complete removal of the upstream nucleosome has only a small effect on the Snf2 dependency of overall promoter induction. (A) DNase I indirect end-labeling analysis as in Fig. 1A for wt (CY339 pCB84a-10A or pCB84a-19A) and *snf2* (CY409 pCB84a-10A or pCB84a-19A) strains under inducing ($-P_i$) conditions, probed for either the chromosomal or the plasmid locus. The top panel shows the chromosome locus of the strains bearing plasmid pCB84a-10A. The pattern was the same for the strains with plasmid pCB84a-19A (not shown). The middle and bottom panels show the plasmid locus of the indicated plasmids. Labeling is as for Fig. 1A and 5A, but (eHS**) stands for a somewhat more remodeled eHS** (stippled oval representing a partially remodeled upstream nucleosome), and (eHS*) indicates a somewhat less remodeled eHS* (stippled line denoting a not completely remodeled upstream nucleosome) type of extended hypersensitive region. Marker lane M of the top panel is as in Fig. 1A (AgeI, MfeI, ApaI, and BsrBI, from top to bottom), of the middle panel as in Fig. 3B (AgeI, SpeI, ApaI, and BsrBI, from top to bottom), and of the bottom panel as in Fig. 5A (AgeI, ApaI, and BsrBI, from top to bottom). (B) HhaI accessibility for the conditions shown in panel A. Error bars show the variations of two biological replicates (four replicates in the case of the chromosome locus in the *snf2* background). (C) *PHO84* promoter induction kinetics as in Fig. 3A for wt (CY339) and *snf2* (CY409) strains carrying either a reporter plasmid with the full-length *PHO84* promoter (pCB84a) or with a *PHO84* promoter lacking the upstream nucleosome (pCB84b). o/n, overnight induction. (D) Same data as in panel C and additional data for the *snf2* strain with plasmid pCB84a-19A, normalized at each time point to the values of the wt carrying the same respective plasmid.

dent activity in the yeast extract constitutes conditions for more in vivo-like nucleosome positioning. Third, addition of yeast extract and energy to the underassembled (60%) chromatin templates increased not only the TaqI site accessibility (from 22 to 66%) (Fig. 7E), similar as seen before for the wt promoter (from 15 to 69%) (Fig. 7B) but now also the HhaI site accessibility (from 47 to 73%). This argued for a low stability of both the upstream and downstream nucleosome.

Finally, both variants showed remodeling of the upstream nucleosome upon induction in a *snf2* strain. The extent of remodeling as judged by DNase I indirect end labeling was substantial for both variants in comparison to the internal

control of the wt promoter at the chromosome locus (Fig. 8A) and to the plasmid locus (data not shown). HhaI site accessibility assays confirmed a partial remodeling for the 10A variant and almost full remodeling for the 19A replacement variant (Fig. 8B). Altogether, these results argue strongly that the intrinsic stability of the upstream nucleosome in the wt promoter caused its strict Snf2 requirement for remodeling.

The destabilization or complete absence of the upstream nucleosome relieves the Snf2 dependency of promoter induction only partially. In addition to the mechanistically interesting relationship between intrinsic stability and Snf2 dependency of remodeling of the upstream nucleosome, we asked further if the critical Snf2 dependency of remodeling the upstream nucleosome was the main cause for the Snf2 effect on overall *PHO84* promoter induction kinetics (Fig. 4A). If so, the kinetic delay in a *snf2* background should be reduced if the upstream nucleosome is destabilized (19A variant, plasmid pCB84a-19A) or absent (ΔΔUASpAB variant, plasmid pCB84b). We followed induction kinetics for both variants in the wt and *snf2* backgrounds by acid phosphatase assay and compared them to the kinetics of the wt promoter in both backgrounds (Fig. 8C and D). For both variants the delay of induction in the *snf2* mutant compared to the wt background was somewhat diminished, more so in the case of the truncated promoter and only very slightly in the case of the mutated promoter. This was more apparent after normalization of the phosphatase activity in the *snf2* strains to the respective activity in the wt background at the same time points (Fig. 8D). Nonetheless, as the delay in the *snf2* strains was still substantial in both cases, we reasoned that there was a significant Snf2 dependency of other parts of the *PHO84* promoter besides the upstream nucleosome. For example, we showed specifically that the kinetics of remodeling the downstream nucleosome was dependent on Snf2, as histone eviction of the wt promoter was delayed in the *snf2* mutant (Fig. 4E) (see above).

Since the HhaI accessibility of the *PHO84* promoter variant in pCB84a-19A was considerably increased under repressive conditions in a *snf2* strain (Fig. 7D) but did not result in a higher basal level of transcription (data not shown), it seemed again (see above) that Snf2 had an effect on basal transcription that was not necessarily linked to basal remodeling of the upstream nucleosome.

The histone acetyltransferase Rtt109 has a role for induction of both the *PHO84* and the *PHO5* promoters. We and others found that the histone chaperone Asf1 is involved in the induction of the coregulated *PHO5* and *PHO8* promoters (1, 38). Recently, several groups reported the critical requirement of Asf1 for the activity of the histone acetyltransferase Rtt109, which acetylates histone H3 at lysine 56 (18, 21, 30, 64, 78). This finding raised the question of whether an involvement of Asf1 reflects its role solely as histone chaperone or rather a role of Rtt109. We checked this for induction of the *PHO5* promoter and observed that the delay in induction was virtually the same in the *asf1* and *rtt109* mutants and that there was no further delay in an *asf1 rtt109* double mutant (Fig. 9A). This argued strongly that Asf1 and Rtt109 function together in the same pathway during *PHO5* induction. We also noted that for both the *asf1* mutant as well as the *rtt109* mutant the basal *PHO5* activity levels were slightly but significantly elevated.

In contrast, induction of *PHO84* was significantly delayed only in the *rtt109* but hardly at all in the *asf1* mutant (Fig. 9B). The induction delay in the *rtt109* mutant was due to a delay on the level of chromatin remodeling as monitored by restriction enzyme accessibility and histone ChIP assays (Fig. 9C, D, and E). However, the effects were much less severe than those in the *snf2*, *gcn5*, or *ino80* mutants (compare to Fig. 4E and 6C), especially as they were rather limited to an early time of induction (45 min). There was hardly any effect on the level of restriction enzyme accessibilities for the *asf1* mutant, and only at 45 min of induction was there a slight delay in histone eviction. This may constitute a weaker pendant to the effects in the *gcn5* and *snf2* strains, i.e., histone eviction being the rate-limiting step.

There was no differential Rtt109 requirement of the upstream and downstream nucleosome discernible, as the kinetics of restriction enzyme site accessibility were similarly delayed for the HhaI and the TaqI sites in the *rtt109* mutant (Fig. 9C). We also checked the effects of the *asf1* and *rtt109* deletions on induction of the truncated pCB84b construct and got similar results as with the full-length pCB84a plasmid (Fig. 9F), speaking for a role of Rtt109 in remodeling of the downstream nucleosome but not excluding a role for remodeling of the upstream nucleosome as well.

The effects of the *asf1* and *rtt109* deletions on *PHO5* and *PHO84* induction showed some dependency on the strain background. In the BY4741 background, the *rtt109* mutant showed a weaker delay for *PHO5* induction than the *asf1* mutant (data not shown). In the W303 background, the *rtt109* mutant had a similar effect on *PHO84* induction as in the BY4741 background, but here also the *asf1* mutant had an appreciable effect, similar to that of the *rtt109* mutant (data not shown).

It was shown that Rtt109 exists in a complex with another histone chaperone, Vps75 (78); however, the absence of Vps75 caused hardly any effect on *PHO5* and *PHO84* induction (data not shown).

DISCUSSION

The induction of the *PHO84* promoter is coupled to a prominent Pho4-dependent chromatin structure transition. In this study we present a characterization of *PHO84* promoter regulation on the level of chromatin structure. The *PHO84* promoter in its repressed state harbored an sHS region flanked by two positioned nucleosomes (upstream and downstream nucleosome) and a semiopen and less-organized chromatin structure close to the TATA box. This chromatin organization became extensively remodeled upon induction, leading to an extended hypersensitive region of about 500 bp and the eviction of histones.

At the outset of our study no data on the nucleosomal structure of the *PHO84* promoter were available. However, during recent years several groups have undertaken genome-wide nucleosome positioning studies in yeast (45, 49, 67, 82, 85). Very recently, during the preparation of the manuscript, Lam et al. (41) mapped the promoter chromatin structures of PHO regulon genes by tiled PCR amplicons with mononucleosomal DNA as template. Their analysis of the *PHO84* nucleosome organization agrees remarkably well with our mapping (Fig. 10A). Even the less-organized structure between the downstream nucleosome and the TATA box region was reflected by a reduced PCR product peak in this

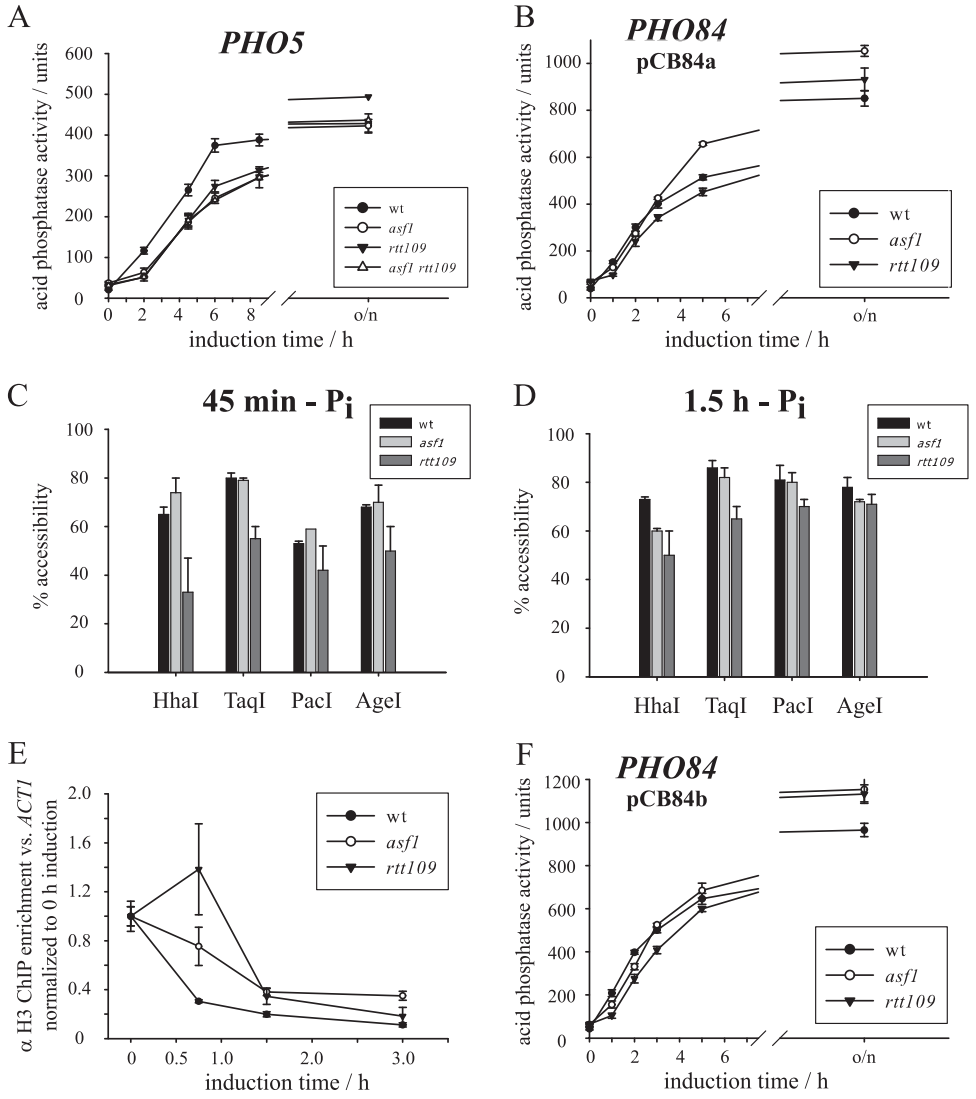

FIG. 9. Induction of the *PHO84* and *PHO5* promoters is delayed in the absence of Rtt109, but the effect is weaker for *PHO84* induction and not as pronounced there in an *asf1* strain. (A) *PHO5* promoter induction kinetics as in Fig. 3A but for wt (W303a), *asf1* (W303a *asf1*), *rtt109* (PKY4170), and *asf1 rtt109* (PKY4182) strains. (B) *PHO84* promoter induction kinetics as in panel A for wt (Y00000 pCB84a), *asf1* (Y01310 pCB84a), and *rtt109* (Y01490 pCB84a) strains. (C and D) Restriction enzyme accessibility assays at the chromosomal *PHO84* promoter as in Fig. 1C for the wt (Y00000), *asf1* (Y01310), and *rtt109* (Y01490) strains after 45 min (C) or 1.5 h (D) of induction. Error bars show the variations of two biological replicates. (E) Histone loss kinetics as in Fig. 2 for the same strains as in panels C and D using the *PHO84* promoter amplicon. ChIP data were normalized to input DNA, the *ACT1* amplicon, and to the 0-h values of each strain. Error bars show the variations of two biological replicates. (F) Same experiment as in panel B but with strains carrying plasmid pCB84b.

region. They also found the same extensive nucleosome-free region in the induced state.

In contrast to this congruence of two locus-specific nucleosome mapping studies using different methods, there is less agreement with the genome-wide approaches. The experiments of Lee et al. (45) did not reveal any nucleosomes in the extended *PHO84* promoter region, Whitehouse et al. (82) mapped nucleosomes right in the cHS and sHS regions, and Mavrich et al. (49) correctly assigned the position of the upstream nucleosome and of the cHS and sHS regions but not of the downstream nucleosome. Both our own mapping and that of Lam et al. (41) employed medium with added phosphate to ensure complete repression, whereas the mentioned genome-wide studies used YPD medium, which can lead to a significant level of *PHO84* transcription (23, 53). These differences in growth conditions could explain at least the lack of nucleosome detection.

We did the analogous comparison of nucleosome positioning data for the *PHO5* and *PHO8* promoter regions and found significant disparities as well, especially for the *PHO8* promoter (Fig. 10B and C). These differences can be less well explained by differences in growth conditions, as both *PHO5* and *PHO8* are largely repressed in YPD medium (3, 5, 53). So, it seems that genome-wide nucleosome positioning data, even though they are extremely valuable for detecting genome-wide trends of nucleosomal organization, may need to be verified by locus-specific mapping techniques.

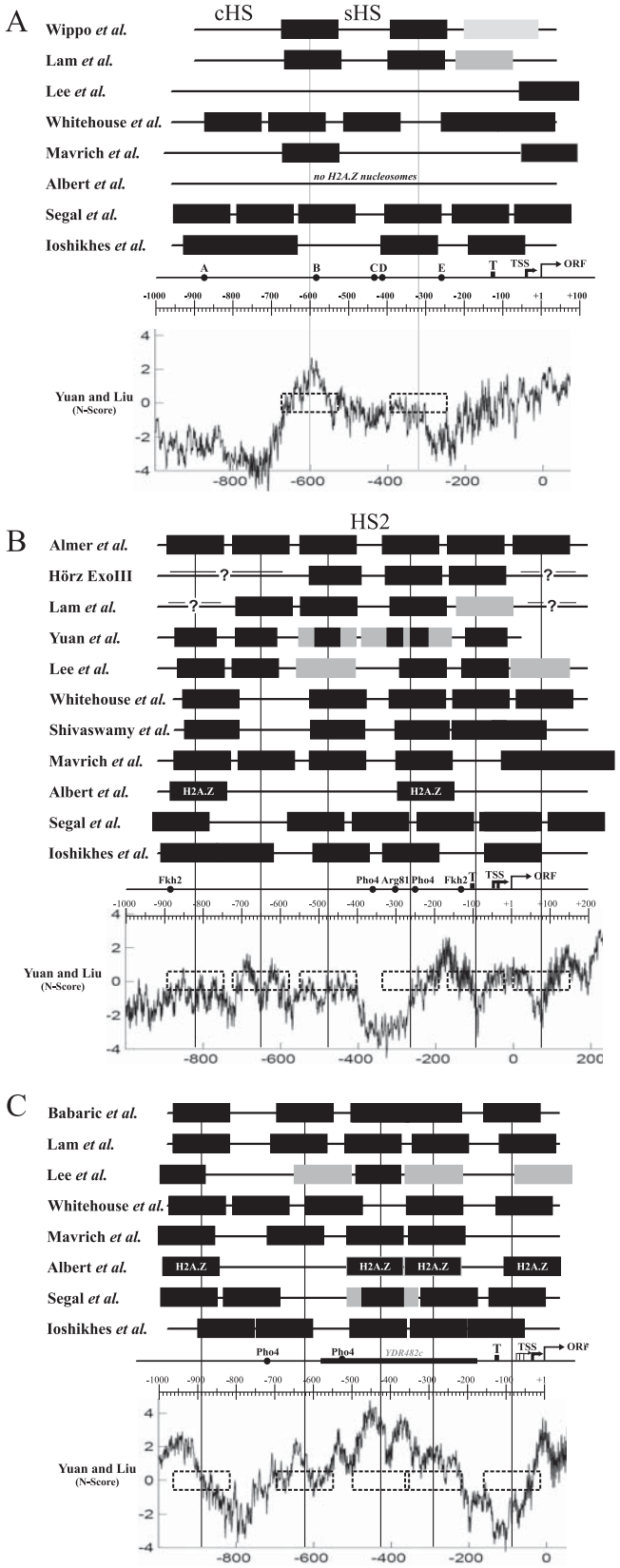

FIG. 10. Comparison of nucleosome positions (filled black rectangles) at the repressed *PHO84* (A), *PHO5* (B), and *PHO8* (C) promoters as measured by (i) individual assays (this study; same positions as in Fig. 1B), Lam et al. (41); Almer et al. (3); Hörz (unpublished data, obtained by ExoIII mapping in the Hörz laboratory), and Barbaric et al. (5) (ii) with positions as determined in genome-wide studies reported by Lee et al. (45), Whitehouse et al. (82), Mavrich et al. (49) (fit threshold of 2 was used), Albert et al. (2) (those authors mapped only H2A.Z-containing nucleosomes; fit threshold of 2), and Shivaswamy et al. (67), and (iii) as predicted by bioinformatic algorithms of Segal et al. (65) and Ioshikhes et al. (32). The shown *N*-score algorithm of Yuan and Liu (84) is predictive for local nucleosome enrichment or depletion (positive or negative values) (Fig. 7C). Gray rectangles denote fuzzy mapping of nucleosome positioning. The midpoints of positioned nucleosomes as mapped by our own group are marked by vertical lines for orientation and their positions are denoted as stippled boxes within the *N*-score plots. For regions marked with -?-, we had no information on nucleosome positions. The positions of promoter features are labeled as in Fig. 1B and the graded horizontal line shows base pair positions relative to the ATG start codon (+1). Positions of the TSS were taken from reference 50, and positions of TATA boxes were taken from reference 9. The sHS and cHS regions of the *PHO84* promoter and hypersensitive region 2 (HS2) at the *PHO5* promoter (3) are labeled.

The need for experimental verification is also very important with regard to the prediction of nucleosome positions by DNA sequence-based algorithms. For example, the algorithms of Segal et al. (65) and Ioshikhes et al. (32) predicted the downstream nucleosome and the extended linker at the sHS region rather well (Fig. 10A). However, the upstream nucleosome was not met and the cHS region was missed. As mentioned above, the *N*-score algorithm of Yuan and Liu (84) accurately predicts low nucleosome occupancy for the cHS region and a peak of high nucleosome occupancy just at the center of the upstream nucleosome. This prediction agrees well with our data that showed a higher intrinsic stability of the upstream nucleosome than for the downstream nucleosome.

Different intrinsic stabilities of the two positioned nucleosomes at the *PHO84* promoter determine their differential cofactor requirement for remodeling. The *PHO84* promoter appears like a hybrid between the *PHO5* and *PHO8* promoters with regard to the cofactor dependency for chromatin remodeling upon induction. On one hand, it has a similar degree of cofactor dependency as the *PHO5* promoter, because the remodeling of the downstream nucleosome and the overall promoter activation were not essentially dependent on Snf2, Ino80, Gcn5, and Rtt109. It was not even abolished in the *snf2 ino80* or *snf2 gcn5* double mutants. Nonetheless, all these factors have a more or less important role in remodeling kinetics of the downstream nucleosome. Steger et al. (72) also reported a defect in *PHO84* mRNA induction in *snf6* (subunit of the SWI/SNF complex) and *arp8* (subunit of the Ino80 complex) strains, which corresponds nicely to the promoter-opening delays reported here for the *snf2* and *ino80* mutants. On the other hand, remodeling of the upstream nucleosome was reminiscent of the *PHO8* promoter, as it was strictly dependent on Snf2. In addition, it became critically dependent on Ino80 under submaximal induction conditions, while the downstream nucleosome was still remodeled, i.e., remodeling of the upstream nucleosome appeared to be more dependent on Ino80 than remodeling of the downstream nucleosome.

Therefore, the *PHO84* promoter presents an example of a differential cofactor requirement for histone eviction from two neighboring nucleosomes at the same promoter. This differen-

tial cofactor requirement poses even more poignantly the question that was raised earlier after the observation of the differential cofactor requirements at the *PHO5* and *PHO8* promoters: what makes remodeling of one nucleosome strictly dependent on a certain cofactor, for example, Snf2, while remodeling of another nucleosome is not dependent on this cofactor? In order to answer this question, the two neighboring nucleosomes at the *PHO84* promoter constitute a system that is very well internally controlled for the influence of any external factors, like cofactor recruitment, higher-order structure, or nuclear location.

One possible answer to the above question could relate to the presence of a functionally important intranucleosomal activator binding site in nucleosomes that show less cofactor dependency, like the UASpE site in the downstream nucleosome at the *PHO84* promoter or the UASp2 site in the −2 nucleosome at the *PHO5* promoter (26). However, we tested the UASpEmut, UASpCEmut, and UASpDEmut *PHO84* promoter variants in the *snf2* background under inducing conditions and saw the same sHS**-type region as for the wt *PHO84* promoter in *snf2* cells (unpublished results). Therefore, the presence of the intranucleosomal UASpE element did not influence the differential cofactor dependency for remodeling of the upstream and downstream nucleosome.

As an alternative explanation, Dhasarathy and Kladde (19) showed that the stringency of cofactor requirements for chromatin remodeling at the *PHO5* promoter was dependent on the amount of Pho4 recruited to the promoter. We found this relationship also at the *PHO84* promoter, as the upstream nucleosome became critically dependent on Ino80 if less Pho4 was recruited, i.e., under submaximal inducing conditions. However, this effect is unlikely to explain the promoter-internal difference in cofactor requirements at the *PHO84* promoter under the same induction conditions. Here both the upstream and downstream nucleosome should be exposed simultaneously to the same degree of Pho4 recruitment, unless, for example, the higher-order structure makes a difference for the two nucleosomes. But this seems unlikely, as the differential Snf2 dependencies of both nucleosomes were equally observed at the plasmid and the chromosomal locus (Fig. 4B and our unpublished data), which probably differ in higher-order structures.

In this study we provide strong evidence for a hypothesis that we raised previously (31) as an answer to the above question: different intrinsic stabilities of positioned nucleosomes cause different cofactor requirements for their remodeling. We showed previously, using our yeast extract in vitro chromatin assembly system, that the nucleosomes at the *PHO8* promoter were intrinsically more stable than those at the *PHO5* promoter, thus providing a correlation of nucleosome stability and dependency on cofactors. By the same methodology we measured now a similar, although more subtle, trend while comparing the stabilities of the upstream and downstream nucleosome at the *PHO84* promoter. The former was more stably positioned than the latter. This correlated well with the prediction by the *N*-score algorithm for the *PHO84* promoter. Analogously, most of the *PHO8* promoter region had a positive prediction for nucleosome occupancy and most of the *PHO5* promoter region showed either mildly or strongly negative nucleosome propensity and the only positive peak was located in a linker region in vivo (Fig. 10B and C). This is in agreement with our earlier notion that the nucleosomes at the repressed *PHO5* promoter adopt positions in a "loaded spring-like state" (31, 39). Altogether, it appears that nucleosomes that are positioned over DNA regions with more positive *N*-scores are more strictly dependent on chromatin cofactors for remodeling, and nucleosomes over less favorable DNA sequences according to the *N*-score can be remodeled by multiple redundant pathways.

We tested this directly for the case of the *PHO84* promoter by introducing stretches of homopolymeric poly(dA) at the position of the upstream nucleosome. This progressively lowered the *N*-score for this region. Indeed, we confirmed in the in vitro assay that the upstream nucleosome was destabilized and observed in vivo that a progressively lower stability of the upstream nucleosome allowed progressively more remodeling of this nucleosome in the absence of Snf2. Importantly, our in vitro assay was an independent measure of nucleosome stability; therefore, we needed not to invoke Snf2 dependency itself as an indicator of stability. A similar approach was undertaken at the *RNR3* promoter, where insertion of one or even two 34A stretches close to the TATA box prevented the formation of a positioned nucleosome and relieved the Snf2 dependency of *RNR3* induction (86).

We conclude that promoter strength is not necessarily correlated with the degree of cofactor requirement for chromatin remodeling but rather that intrinsic properties of individual promoter nucleosomes determine the cofactor dependency for their remodeling.

Histone eviction at the *PHO84* promoter seems to be the rate-limiting step in the absence of Gcn5 or Snf2. We and others showed previously for the *PHO5* and *PHO8* promoters that chromatin remodeling led to the eviction of histones from the promoter region (1, 14, 38). Genome-wide studies confirmed that histone-depleted regions are a common property of promoters of active genes (13, 43). As discussed earlier (14, 24, 58, 59), there is a significant mechanistic difference if remodeling of nucleosomes leads to increased DNA accessibility while histones are still present or as histones are evicted. Importantly, this distinction cannot be made by techniques based on nuclease digestion, as DNA accessibility and therefore nuclease digestibility changes in both cases. Therefore, it is not necessarily to be expected that chromatin remodeling kinetics as followed by nucleases, e.g., restriction enzyme accessibility, and by histone ChIP will coincide. Even though such kinetic measurements were congruent so far for remodeling at the *PHO5* and *PHO8* promoters (6, 8), we now observed slower kinetics of histone eviction compared to restriction enzyme accessibility kinetics during induction of the *PHO84* promoter in the *gcn5* mutant and also specifically for remodeling of the downstream nucleosome in the *snf2* mutant. This may argue for an initial phase of nucleosome remodeling leading to altered nucleosomal states that allow more restriction enzyme accessibility but still retain histones associated with DNA. This initial phase may precede the actual, rate-limiting histone eviction phase. For the *gcn5* mutation this interpretation is concordant with reports on the stimulatory effect of histone acetylation on histone eviction (17).

Rtt109 increases the rate of *PHO5* and more weakly also of *PHO84* promoter activation. The mechanism of histone evic-

tion raises the question of the histone acceptor. We and others suggested in the past that histone chaperones may be the most promising candidates as histone acceptors and showed a role for Asf1 in increasing the rate of opening of the *PHO5* and *PHO8* promoters (1, 38). However, the recognition of Asf1 as an essential cofactor for the activity of the histone H3 lysine 56-specific histone acetyltransferase Rtt109 (18, 21, 22, 30, 64, 78) raised the alternative possibility that Asf1 functions through the H3 K56ac modification rather than solely as histone acceptor. Indeed, the *PHO5* induction kinetics was equally delayed in *asf1* and *rtt109* strains, and the *asf1 rtt109* double mutant showed no synthetic effect. Very recently, just before submitting the manuscript, equivalent result were published by Williams et al. (83). So, Asf1 appears to function in histone eviction at the *PHO5* promoter mainly through H3 K56ac, and it is currently unclear if it also serves directly as a histone acceptor.

Surprisingly, in the BY4741 strain background Asf1 seemed to be hardly involved at all in *PHO84* induction despite the considerable role for Rtt109. This suggested that Rtt109 may have other targets than H3 K56. This is not unlikely, as Rtt109 exists in a complex with another histone chaperone, Vps75, that seems to be less important for acetylation of H3 K56 in vivo (12, 30, 78). The absence of Vps75 caused only a slight effect on *PHO5* induction, much weaker than that observed in the absence of Asf1, and had no significant effect on *PHO84* induction (unpublished data). Therefore, Rtt109 could function in *PHO84* induction through a so-far-unidentified target that may be acetylated by Rtt109 independently of both Asf1 and Vps75.

Chromatin cofactors have a direct effect on *PHO84* promoter regulation. All mutants used in this study (besides *rtt109*) were controlled for causing direct effects on the coregulated *PHO5* and *PHO8* promoters rather than causing side effects on PHO regulon induction (6, 8, 38). In addition, we observed decreased chromatin remodeling in the *snf2K798A* and the *ino80* mutants under steady-state conditions (overexpression of *PHO4* in $+P_i$ medium), under which effects on growth rate should not matter, which otherwise is a concern for effects on PHO induction (6, 38). Other groups have shown a direct role for Snf2, Ino80, and Gcn5 at the *PHO84* promoter in ChIP assays (23, 36, 68, 69, 72).

Remodeling of the downstream nucleosome seems to be more important for *PHO84* promoter regulation through chromatin than remodeling of the upstream nucleosome. Even though the stable upstream nucleosome poses a very interesting case for the mechanistic study of nucleosome remodeling, it seems to have a rather minor role in the overall regulation of the *PHO84* promoter. Given its higher stability and occlusion of the UASpB site, it might play a repressive or fine-tuning role for *PHO84* regulation. However, its absence in the pCB84b construct only had a very slight effect on the promoter induction kinetics and on their Snf2 dependence. Further, full final promoter activity was achieved in the *snf2* mutant without remodeling of the upstream nucleosome. Finally, the destabilization of the upstream nucleosome in the 19A variant did relieve the Snf2 dependency for remodeling of the upstream nucleosome but had no effect on the basal level of transcription and only mild effects on the promoter induction kinetics. On the other hand, full *PHO84* promoter activity was always concomitant with complete remodeling of the downstream nucleosome and every delay in induction kinetics went together with a delay in its remodeling. As its intranucleosomal UASpE site was especially important for *PHO84* induction, it seems that controlling the accessibility to UASpE through remodeling of the downstream nucleosome is key to regulating *PHO84* promoter induction.

ACKNOWLEDGMENTS

We are grateful to P. D. Kaufman, C. L. Peterson, X. Shen, A. Verreault, and F. Winston for the gifts of yeast strains and to A. Schmid and to V. Fajdetic for technical assistance.

This work was supported by the German Research Community (Transregio 05), the 6th Framework Programme of the European Union (Network of Excellence The Epigenome), and the Ministry of Education, Science, and Technology of the Republic of Croatia, grant 058-0580477-0247 (to S.B.).

This paper is dedicated by P.K. to his wife Marion Rouette, who became indirectly involved enough during the preparation of the manuscript to earn her an honorary coauthorship.

REFERENCES

1. **Adkins, M. W., S. R. Howar, and J. K. Tyler.** 2004. Chromatin disassembly mediated by the histone chaperone Asf1 is essential for transcriptional activation of the yeast PHO5 and PHO8 genes. Mol. Cell **14:**657–666.
2. **Albert, I., T. N. Mavrich, L. P. Tomsho, J. Qi, S. J. Zanton, S. C. Schuster, and B. F. Pugh.** 2007. Translational and rotational settings of H2A.Z nucleosomes across the Saccharomyces cerevisiae genome. Nature **446:**572–576.
3. **Almer, A., H. Rudolph, A. Hinnen, and W. Hörz.** 1986. Removal of positioned nucleosomes from the yeast *PHO5* promoter upon *PHO5* induction releases additional upstream activating DNA elements. EMBO J. **5:**2689–2696.
4. **Anderson, J. D., and J. Widom.** 2001. Poly(dA-dT) promoter elements increase the equilibrium accessibility of nucleosomal DNA target sites. Mol. Cell. Biol. **21:**3830–3839.
5. **Barbaric, S., K. D. Fascher, and W. Hörz.** 1992. Activation of the weakly regulated *PHO8* promoter in *S. cerevisiae*: chromatin transition and binding sites for the positive regulator protein Pho4. Nucleic Acids Res. **20:**1031–1038.
6. **Barbaric, S., T. Luckenbach, A. Schmid, D. Blaschke, W. Hörz, and P. Korber.** 2007. Redundancy of chromatin remodeling pathways for the induction of the yeast PHO5 promoter in vivo. J. Biol. Chem. **282:**27610–27621.
7. **Barbaric, S., M. Münsterkötter, C. Goding, and W. Hörz.** 1998. Cooperative Pho2-Pho4 interactions at the *PHO5* promoter are critical for binding of Pho4 to UASp1 and for efficient transactivation by Pho4 at UASp2. Mol. Cell. Biol. **18:**2629–2639.
8. **Barbaric, S., J. Walker, A. Schmid, J. Q. Svejstrup, and W. Hörz.** 2001. Increasing the rate of chromatin remodeling and gene activation - a novel role for the histone acetyltransferase Gcn5. EMBO J. **20:**4944–4951.
9. **Basehoar, A. D., S. J. Zanton, and B. F. Pugh.** 2004. Identification and distinct regulation of yeast TATA box-containing genes. Cell **116:**699–709.
10. **Becker, P. B., and W. Hörz.** 2002. ATP-dependent nucleosome remodeling. Annu. Rev. Biochem. **71:**247–273.
11. **Berger, S. L.** 2007. The complex language of chromatin regulation during transcription. Nature **447:**407–412.
12. **Berndsen, C. E., T. Tsubota, S. E. Lindner, S. Lee, J. M. Holton, P. D. Kaufman, J. L. Keck, and J. M. Denu.** 2008. Molecular functions of the histone acetyltransferase chaperone complex Rtt109-Vps75. Nat. Struct. Mol. Biol. **15:**948–956.
13. **Bernstein, B. E., C. L. Liu, E. L. Humphrey, E. O. Perlstein, and S. L. Schreiber.** 2004. Global nucleosome occupancy in yeast. Genome Biol. **5:**R62.
14. **Boeger, H., J. Griesenbeck, J. S. Strattan, and R. D. Kornberg.** 2003. Nucleosomes unfold completely at a transcriptionally active promoter. Mol. Cell **11:**1587–1598.
15. **Bun Ya, M., M. Nishimura, S. Harashima, and Y. Oshima.** 1991. The PHO84 gene of *Saccharomyces cerevisiae* encodes an inorganic phosphate transporter. Mol. Cell. Biol. **11:**3229–3238.
16. **Carvin, C. D., and M. P. Kladde.** 2004. Effectors of lysine 4 methylation of histone H3 in Saccharomyces cerevisiae are negative regulators of PHO5 and GAL1-10. J. Biol. Chem. **279:**33057–33062.
17. **Chandy, M., J. L. Gutierrez, P. Prochasson, and J. L. Workman.** 2006. SWI/SNF displaces SAGA-acetylated nucleosomes. Eukaryot. Cell **5:**1738–1747.

18. **Collins, S. R., K. M. Miller, N. L. Maas, A. Roguev, J. Fillingham, C. S. Chu, M. Schuldiner, M. Gebbia, J. Recht, M. Shales, H. Ding, H. Xu, J. Han, K. Ingvarsdottir, B. Cheng, B. Andrews, C. Boone, S. L. Berger, P. Hieter, Z. Zhang, G. W. Brown, C. J. Ingles, A. Emili, C. D. Allis, D. P. Toczyski, J. S. Weissman, J. F. Greenblatt, and N. J. Krogan.** 2007. Functional dissection of protein complexes involved in yeast chromosome biology using a genetic interaction map. Nature **446:**806–810.
19. **Dhasarathy, A., and M. P. Kladde.** 2005. Promoter occupancy is a major determinant of chromatin remodeling enzyme requirements. Mol. Cell. Biol. **25:**2698–2707.
20. **Dion, M. F., T. Kaplan, M. Kim, S. Buratowski, N. Friedman, and O. J. Rando.** 2007. Dynamics of replication-independent histone turnover in budding yeast. Science **315:**1405–1408.
21. **Driscoll, R., A. Hudson, and S. P. Jackson.** 2007. Yeast Rtt109 promotes genome stability by acetylating histone H3 on lysine 56. Science **315:**649–652.
22. **Drogaris, P., H. Wurtele, H. Masumoto, A. Verreault, and P. Thibault.** 2008. Comprehensive profiling of histone modifications using a label-free approach and its applications in determining structure-function relationships. Anal. Chem. **80:**6698–6707.
23. **Duina, A. A., and F. Winston.** 2004. Analysis of a mutant histone H3 that perturbs the association of Swi/Snf with chromatin. Mol. Cell. Biol. **24:**561–572.
24. **Eberharter, A., and P. B. Becker.** 2004. ATP-dependent nucleosome remodelling: factors and functions. J. Cell Sci. **117:**3707–3711.
25. **Fascher, K. D., J. Schmitz, and W. Hörz.** 1990. Role of trans-activating proteins in the generation of active chromatin at the *PHO5* promoter in *S. cerevisiae*. EMBO J. **9:**2523–2528.
26. **Fascher, K. D., J. Schmitz, and W. Hörz.** 1993. Structural and functional requirements for the chromatin transition at the *PHO5* promoter in *Saccharomyces cerevisiae* upon *PHO5* activation. J. Mol. Biol. **231:**658–667.
27. **Gregory, P. D., S. Barbaric, and W. Hörz.** 1999. Restriction nucleases as probes for chromatin structure. Methods Mol. Biol. **119:**417–425.
28. **Gregory, P. D., A. Schmid, M. Zavari, M. Münsterkötter, and W. Hörz.** 1999. Chromatin remodelling at the *PHO8* promoter requires SWI-SNF and SAGA at a step subsequent to activator binding. EMBO J. **18:**6407–6414.
29. **Haguenauer-Tsapis, R., and A. Hinnen.** 1984. A deletion that includes the signal peptidase cleavage site impairs processing, glycosylation, and secretion of cell surface yeast acid phosphatase. Mol. Cell. Biol. **4:**2668–2675.
30. **Han, J., H. Zhou, B. Horazdovsky, K. Zhang, R. M. Xu, and Z. Zhang.** 2007. Rtt109 acetylates histone H3 lysine 56 and functions in DNA replication. Science **315:**653–655.
31. **Hertel, C. B., G. Längst, W. Hörz, and P. Korber.** 2005. Nucleosome stability at the yeast PHO5 and PHO8 promoters correlates with differential cofactor requirements for chromatin opening. Mol. Cell. Biol. **25:**10755–10767.
32. **Ioshikhes, I. P., I. Albert, S. J. Zanton, and B. F. Pugh.** 2006. Nucleosome positions predicted through comparative genomics. Nat. Genet. **38:**1210–1215.
33. **Iyer, V., and K. Struhl.** 1995. Poly(dA:dT), a ubiquitous promoter element that stimulates transcription via its intrinsic DNA structure. EMBO J. **14:**2570–2579.
34. **Jamai, A., R. M. Imoberdorf, and M. Strubin.** 2007. Continuous histone H2B and transcription-dependent histone H3 exchange in yeast cells outside of replication. Mol. Cell **25:**345–355.
35. **Jeffery, D. A., M. Springer, D. S. King, and E. K. O'Shea.** 2001. Multi-site phosphorylation of Pho4 by the cyclin-CDK Pho80-Pho85 is semi-processive with site preference. J. Mol. Biol. **306:**997–1010.
36. **Jonsson, Z. O., S. Jha, J. A. Wohlschlegel, and A. Dutta.** 2004. Rvb1p/Rvb2p recruit Arp5p and assemble a functional Ino80 chromatin remodeling complex. Mol. Cell **16:**465–477.
37. **Kaffman, A., I. Herskowitz, R. Tjian, and E. K. O'Shea.** 1994. Phosphorylation of the transcription factor Pho4 by a cyclin-CDK complex, Pho80-Pho85. Science **263:**1153–1156.
38. **Korber, P., S. Barbaric, T. Luckenbach, A. Schmid, U. J. Schermer, D. Blaschke, and W. Hörz.** 2006. The histone chaperone Asf1 increases the rate of histone eviction at the yeast PHO5 and PHO8 promoters. J. Biol. Chem. **281:**5539–5545.
39. **Korber, P., and W. Hörz.** 2004. In vitro assembly of the characteristic chromatin organization at the yeast PHO5 promoter by a replication-independent extract system. J. Biol. Chem. **279:**35113–35120.
40. **Kouzarides, T.** 2007. Chromatin modifications and their function. Cell **128:**693–705.
41. **Lam, F. H., D. J. Steger, and E. K. O'Shea.** 2008. Chromatin decouples promoter threshold from dynamic range. Nature **453:**246–250.
42. **Längst, G., E. J. Bonte, D. F. Corona, and P. B. Becker.** 1999. Nucleosome movement by CHRAC and ISWI without disruption or trans-displacement of the histone octamer. Cell **97:**843–852.
43. **Lee, C. K., Y. Shibata, B. Rao, B. D. Strahl, and J. D. Lieb.** 2004. Evidence for nucleosome depletion at active regulatory regions genome-wide. Nat. Genet. **36:**900–905.
44. **Lee, T. I., H. C. Causton, F. C. Holstege, W. C. Shen, N. Hannett, E. G. Jennings, F. Winston, M. R. Green, and R. A. Young.** 2000. Redundant roles for the TFIID and SAGA complexes in global transcription. Nature **405:**701–704.
45. **Lee, W., D. Tillo, N. Bray, R. H. Morse, R. W. Davis, T. R. Hughes, and C. Nislow.** 2007. A high-resolution atlas of nucleosome occupancy in yeast. Nat. Genet. **39:**1235–1244.
46. **Li, B., M. Carey, and J. L. Workman.** 2007. The role of chromatin during transcription. Cell **128:**707–719.
47. **Liu, X., C. K. Lee, J. A. Granek, N. D. Clarke, and J. D. Lieb.** 2006. Whole-genome comparison of Leu3 binding in vitro and in vivo reveals the importance of nucleosome occupancy in target site selection. Genome Res. **16:**1517–1528.
48. **Luger, K., A. W. Mader, R. K. Richmond, D. F. Sargent, and T. J. Richmond.** 1997. Crystal structure of the nucleosome core particle at 2.8 Å resolution. Nature **389:**251–260.
49. **Mavrich, T. N., I. P. Ioshikhes, B. J. Venters, C. Jiang, L. P. Tomsho, J. Qi, S. C. Schuster, I. Albert, and B. F. Pugh.** 2008. A barrier nucleosome model for statistical positioning of nucleosomes throughout the yeast genome. Genome Res. **18:**1073–1083.
50. **Miura, F., N. Kawaguchi, J. Sese, A. Toyoda, M. Hattori, S. Morishita, and T. Ito.** 2006. A large-scale full-length cDNA analysis to explore the budding yeast transcriptome. Proc. Natl. Acad. Sci. USA **103:**17846–17851.
51. **Morse, R. H.** 2007. Transcription factor access to promoter elements. J. Cell. Biochem. **102:**560–570.
52. **Münsterkötter, M., S. Barbaric, and W. Hörz.** 2000. Transcriptional regulation of the yeast *PHO8* promoter in comparison to the coregulated *PHO5* promoter. J. Biol. Chem. **275:**22678–22685.
53. **Neef, D. W., and M. P. Kladde.** 2003. Polyphosphate loss promotes SNF/SWI- and Gcn5-dependent mitotic induction of PHO5. Mol. Cell. Biol. **23:**3788–3797.
54. **Ogawa, N., H. Saitoh, K. Miura, J. P. V. Magbanua, M. Bunya, S. Harashima, and Y. Oshima.** 1995. Structure and distribution of specific cis-elements for transcriptional regulation of PHO84 in Saccharomyces cerevisiae. Mol. Gen. Genet. **249:**406–416.
55. **Oshima, Y.** 1997. The phosphatase system in Saccharomyces cerevisiae. Genes Genet. Syst. **72:**323–334.
56. **Park, Y. J., and K. Luger.** 2008. Histone chaperones in nucleosome eviction and histone exchange. Curr. Opin. Struct. Biol. **18:**282–289.
57. **Prunell, A.** 1982. Nucleosome reconstitution on plasmid-inserted poly(dA)·poly(dT). EMBO J. **1:**173–179.
58. **Reinke, H., and W. Hörz.** 2003. Histones are first hyperacetylated and then lose contact with the activated *PHO5* promoter. Mol. Cell **11:**1599–1607.
59. **Reinke, H., and W. Hörz.** 2004. Anatomy of a hypersensitive site. Biochim. Biophys. Acta **1677:**24–29.
60. **Richmond, E., and C. L. Peterson.** 1996. Functional analysis of the DNA-stimulated ATPase domain of yeast SWI2/SNF2. Nucleic Acids Res. **24:**3685–3692.
61. **Roberts, S. M., and F. Winston.** 1997. Essential functional interactions of SAGA, a *Saccharomyces cerevisiae* complex of Spt, Ada, and Gcn5 proteins, with the Snf-Swi and Srb-mediator complexes. Genetics. **147:**451–465.
62. **Rufiange, A., P. E. Jacques, W. Bhat, F. Robert, and A. Nourani.** 2007. Genome-wide replication-independent histone H3 exchange occurs predominantly at promoters and implicates H3 K56 acetylation and Asf1. Mol. Cell **27:**393–405.
63. **Sarkar, G., and S. S. Sommer.** 1990. The "megaprimer" method of site-directed mutagenesis. BioTechniques **8:**404–407.
64. **Schneider, J., P. Bajwa, F. C. Johnson, S. R. Bhaumik, and A. Shilatifard.** 2006. Rtt109 is required for proper H3K56 acetylation: a chromatin mark associated with the elongating RNA polymerase II. J. Biol. Chem. **281:**37270–37274.
65. **Segal, E., Y. Fondufe-Mittendorf, L. Chen, A. Thastrom, Y. Field, I. K. Moore, J. P. Wang, and J. Widom.** 2006. A genomic code for nucleosome positioning. Nature **442:**772–778.
66. **Shen, X., G. Mizuguchi, A. Hamiche, and C. Wu.** 2000. A chromatin remodelling complex involved in transcription and DNA processing. Nature **406:**541–544.
67. **Shivaswamy, S., A. Bhinge, Y. Zhao, S. Jones, M. Hirst, and V. R. Iyer.** 2008. Dynamic remodeling of individual nucleosomes across a eukaryotic genome in response to transcriptional perturbation. PLoS Biol. **6:**e65.
68. **Shukla, A., P. Bajwa, and S. R. Bhaumik.** 2006. SAGA-associated Sgf73p facilitates formation of the preinitiation complex assembly at the promoters either in a HAT-dependent or independent manner in vivo. Nucleic Acids Res. **34:**6225–6232.
69. **Shukla, A., N. Stanojevic, Z. Duan, P. Sen, and S. R. Bhaumik.** 2006. Ubp8p, a histone deubiquitinase whose association with SAGA is mediated by Sgf11p, differentially regulates lysine 4 methylation of histone H3 in vivo. Mol. Cell. Biol. **26:**3339–3352.
70. **Simon, R. H., and G. Felsenfeld.** 1979. A new procedure for purifying histone pairs H2A + H2B and H3 + H4 from chromatin using hydroxylapatite. Nucleic Acids Res. **6:**689–696.
71. **Springer, M., D. D. Wykoff, N. Miller, and E. K. O'Shea.** 2003. Partially phosphorylated Pho4 activates transcription of a subset of phosphate-responsive genes. PLoS Biol. **1:**e28.

72. **Steger, D. J., E. S. Haswell, A. L. Miller, S. R. Wente, and E. K. O'Shea.** 2003. Regulation of chromatin remodeling by inositol polyphosphates. Science **299:**114–116.
73. **Strahl-Bolsinger, S., A. Hecht, K. Luo, and M. Grunstein.** 1997. SIR2 and SIR4 interactions differ in core and extended telomeric heterochromatin in yeast. Genes Dev. **11:**83–93.
74. **Svaren, J., and W. Hörz.** 1997. Transcription factors vs nucleosomes: regulation of the *PHO5* promoter in yeast. Trends Biochem. Sci. **22:**93–97.
75. **Svaren, J., J. Schmitz, and W. Hörz.** 1994. The transactivation domain of Pho4 is required for nucleosome disruption at the *PHO5* promoter. EMBO J. **13:**4856–4862.
76. **Svaren, J., U. Venter, and W. Hörz.** 1995. *In vivo* analysis of nucleosome structure and transcription factor binding in *Saccharomyces cerevisiae*. Microb. Gene Tech. **6:**153–167.
77. **Thomas, M. R., and E. K. O'Shea.** 2005. An intracellular phosphate buffer filters transient fluctuations in extracellular phosphate levels. Proc. Natl. Acad. Sci. USA **102:**9565–9570.
78. **Tsubota, T., C. E. Berndsen, J. A. Erkmann, C. L. Smith, L. Yang, M. A. Freitas, J. M. Denu, and P. D. Kaufman.** 2007. Histone H3-K56 acetylation is catalyzed by histone chaperone-dependent complexes. Mol. Cell **25:**703–712.
79. **Tsukiyama, T.** 2002. The in vivo functions of ATP-dependent chromatin-remodelling factors. Nat. Rev. Mol. Cell Biol. **3:**422–429.
80. **Venter, U., J. Svaren, J. Schmitz, A. Schmid, and W. Hörz.** 1994. A nucleosome precludes binding of the transcription factor Pho4 in vivo to a critical target site in the *PHO5* promoter. EMBO J. **13:**4848–4855.
81. **Wechser, M. A., M. P. Kladde, J. A. Alfieri, and C. L. Peterson.** 1997. Effects of Sin- versions of histone H4 on yeast chromatin structure and function. EMBO J. **16:**2086–2095.
82. **Whitehouse, I., O. J. Rando, J. Delrow, and T. Tsukiyama.** 2007. Chromatin remodelling at promoters suppresses antisense transcription. Nature **450:** 1031–1035.
83. **Williams, S. K., D. Truong, and J. K. Tyler.** 2008. Acetylation in the globular core of histone H3 on lysine-56 promotes chromatin disassembly during transcriptional activation. Proc. Natl. Acad. Sci. USA **105:**9000–9005.
84. **Yuan, G. C., and J. S. Liu.** 2008. Genomic sequence is highly predictive of local nucleosome depletion. PLoS Comput. Biol. **4:**e13.
85. **Yuan, G. C., Y. J. Liu, M. F. Dion, M. D. Slack, L. F. Wu, S. J. Altschuler, and O. J. Rando.** 2005. Genome-scale identification of nucleosome positions in S. cerevisiae. Science **309:**626–630.
86. **Zhang, H., and J. C. Reese.** 2007. Exposing the core promoter is sufficient to activate transcription and alter coactivator requirement at RNR3. Proc. Natl. Acad. Sci. USA **104:**8833–8838.